Improving the Performance of Sensors for Electronic Noses Using Zeolites as Selectivity Modifiers

A Thesis Submitted To The
University College London
For the Degree Of
Doctor of Philosophy (Chemistry)

by

Themis C. Paraskeva

Supervised By

Prof David E. Williams

Dr Dewi W. Lewis

Department of Chemistry

University College London

ProQuest LLC
789 East Eisenhower Parkway
P.O. Box 1346
Ann Arbor, MI 48106-1346

Abstract

The demanding problem of lack of selectivity in semiconducting oxide gas sensors was addressed by the combination of different technologies: shape and size selective catalysts (zeolites), chromium-titanium oxide sensing material and multi-electrode sensor arrays. Sensor devices were fabricated with additional shape and size selective catalysts (zeolites) of three different types (ZSM-5, β and Y) either printed over the top of the sensing material or admixed with it.

The shape and size selectivity of the zeolite sensors has been demonstrated in their ability to discriminate a range of volatile organic, flavour and fragrance compounds of different molecular size and shape. To promote the selective catalytic activity of the sensors the zeolites were catalytically modified (ion exchanged) by the controlled addition of chromium catalysts. The modification increased their catalytic activity in a controlled way allowing them to selectively crack longer species into smaller ones without resulting in complete combustion of the analytes.

Arrays of these sensors have been used in an electronic nose with small number of sensors and a sufficiently large variance in the response for reliable and repeatable discrimination of gases. The discrimination was as good as, and in some cases better than, that achieved using much larger sensor arrays, while also allowing additional discrimination of gases on the basis of their reactivity.

Investigation of different parameters such as the chromium loading of the zeolites, the thickness of the zeolite layer, and the sensor operating temperature, allowed further improvements in the discrimination between the different tested compounds.
Computational simulations of the interactions of a range of volatile organic molecules with different zeolites were performed using a commercially available software to select promising zeolite catalyst materials for the construction of new sensors and to compare computational predictions with experimental results.

Acknowledgments

Initially, I would like to thank Prof David E. Williams who gave me the chance to undertake this interesting research work and fulfill my PhD. I am extremely grateful to him for his support, advice, nice ideas and supervision throughout these years.

I would also like to particularly thank Dr Keith F. E. Pratt for his numerous discussions over the years and his valuable support at the very early and latest stage of my work.

In addition, I would like to thank Dr Dewi W. Lewis for his supervision and guidance for the computational part of my project.

I am grateful to Prof Ivan P. Parkin for his assistance and support especially at the latest stage of my work and submission of the final thesis.

A special thanks to all my friends and colleagues in the University for creating an enjoyable place to work. Also, I would like to thank the technical staff of Chemistry Department for their help.

Last but not least I would like to thank my family for all their support; without them I would not have been able to complete this thesis.

This project was sponsored by the Overseas Research Student Awards Scheme (ORS Awards) and the European Commission.

Table of Contents

Table of Figures

Figures in Chapter 2

Figures in Chapter 3

Figures in Chapter 4

Figures in Chapter 5

Figures in Chapter 6

Figures in Chapter 7

Figures in Chapter 8

List of Tables

Tables in Chapter 6

Tables in Chapter 7

Tables in Chapter 8

Table of Symbols

m	Meters (Length)
mm	Millimetres (Length)
μm	Micrometers (Length)
nm	Nanometers
ppm	Parts per million (Concentration measure)
^oC	Degrees Celsius (Temperature)
rpm	Revolutions per minute
$\AA$	Angstroms
E_g	Band gap (Semiconductors)
n_i	Intrinsic carrier concentration
n	The concentration of electrons in the conduction band (Semiconductors)
p	The concentration of holes in the valence (Semiconductors)
k	Constant
T	Temperature
D	Debye length
L	Crystallite size
C_g	Concentration of gas
R_g	Resistance in dry gas
R_o	Baseline Resistance in dry air in the absence of the target gas
β	Response power (exponent)
A_g	Sensitivity in dry gas (prefactor)
R	Resistance
R_1	Gas-Independent Resistance
R_2	Resistance of gas-sensitive element
P_{rel}	Relative Pressure
S'	Network parameters gas-insensitive series element (Model)
Q	Network parameters gas-insensitive shunt element (Model)
K_T	Dimensionless ratio
h	Porous oxide layer thickness
R_i	Resistance of gas i
$R_{o,i}$	Resistance in clean air
$A_{g,i}$	Response coefficient of the material to the i'th gas

C_i	Gas Concentration
$a_{i,j}$	Response coefficient
θ	Angle
W	Thickness of the crystal in $\AA$
λ	X-ray wavelength
θ_B	Bragg angle
Θ	Line width in degrees at half peak maximum
RL	Resistance of Large Electrode Gap Sensor
Rs	Resistance of Small Electrode Gap Sensor
R_s	Gas Sensor resistance
V_s	Sensor voltage
R_m	Measuring resistance
V_{app}	Voltage given on the electronic boards
P	Pressure expressed in Torrs
K	Temperature in degrees Kelvin
C_l	Concentration of the testing compound in ppm
C	Vapour phase concentration of the testing compound in ppm
vl	Sample injection speed (from syringe) in ml/min
v	Flow rate of carrier gas (dry air) in ml/min
E_{FF}	Force-field energy
E_{str}	Energy function for stretching a bond between two atoms
E_{bend}	Energy required for bending an angle
E_{tors}	Torsional energy for rotation around a bond
E_{vdw}	Van der Waals energy describing the repulsion or attraction between atoms that are not directly bonded
E_{el}	Electrostatic energy between non-bonded atoms. The electrostatic term most often used is the Coulombs law term for the energy of attraction or repulsion between charged centres.
E_{cross}	Coupling between the first three bonded terms. Modern force-fields generally achieve higher accuracy by including cross terms to account for such factors as bond or angle distortions caused by nearby atoms. Cross terms can include the following: stretch-stretch, stretch-bend-stretch, bend-bend, torsion-stretch, torsion-bend-bend, bend-torsion-bend, and stretch-torsion-stretch.
l	Bond length
θ	Bond angle

A, B	Constants particular to the elements in a certain hybridization state
γ	Integer
r	Non bonded distance
q	Charge of an atom
E_{BIND}	Binding Energy (BE) of guest molecule (kJ/mol)
E (M-Z)	Energy of the guest molecule in zeolite
E (Z)	Energy of zeolite
E (M)	Energy of guest molecule in the gas phase

Abbreviations

GC	Gas Chromatography
MS	Mass Spectroscopy
MOS	Metal Oxide Semiconductors
MOSFET	Metal Oxide Semiconductor Field Effect Transistors
CP	Conducting Organic Polymers
BAW	Bulk Acoustic Wave
QCM	Quartz Crystal Microbalances
FOX 4000	ALFA M.O.S. (France) Electronic Nose Model
FOX 2000	ALFA M.O.S. (France) Electronic Nose Model
PCA	Principal Component Analysis
LDA	Linear Discriminant Analysis
CTO	Chromium Titanium Oxide
A/F	Air to Fuel Ratio
SEMDEC	Semiconductors Multi-Electrode Design
IZA	International Zeolite Association
IPA	Propan-2-ol
ESL400	Commercial Chemical Vehicle
XRD	X-Ray Powder Diffraction
SEM	Scanning Electron Microscopy
EDAX	Energy Dispersive Analysis of X-rays
RPM	Revolutions Per Minute
PTFE	A type of Polymer Material
ADC16	Analogue to Digital Converter
SOLGEL	Sol-Emulsion Gelation Method
HS100	Static Headspace Autosampler
VOC	Volatile Organic Compounds
MR	Member Ring
BE	Binding Energy
MD	Molecular Dynamic Calculation
JCPDS	Joint Committee on Powder Diffraction Standards

Chapter 1

Introduction

1.1 Definition of the Problem

Gas-sensitive resistors based on semiconducting metal oxides have been successfully employed as sensing devices for the detection of a wide range of reactive gases in air. Their main advantages are low cost, small size, high sensitivity, and physical robustness with applications in a wide range of industrial and environmental sectors. Some operating problems such as the lack of selectivity, humidity dependency and the poisoning of such devices by many species (i.e. silicones, H_2S and SO_2) have been overcome to a certain degree with the development of new sensor materials.

Small improvements in the selectivity of sensors have been achieved by varying the sensors' operating temperature, the use of alternative sensor materials as well as by adding catalysts and promoters of various kinds. However, the complex response mechanism of such devices makes it difficult to predict how the effects of such modifications will influence the response to different analytes. Despite these improvements, the lack of selectivity is still a fundamental problem that plagues semiconducting oxide gas sensor devices.

Another strategy proposed to deal with the demanding problem of lack of selectivity is based on the use of array of different sensors (electronic noses) with partial specificity and an appropriate pattern-recognition system, capable of recognising simple or complex odours. Given that electronic noses comprise a number of sensors presenting various levels of sensitivity and selectivity, the combined sensors signals yield more information about a given odour than an individual sensor signal would.

Although, the use of electronic noses has indeed succeeded in delivering a degree of selectivity, the disadvantage of the current technology is that the variance in behaviour across a typical sensor array is too small for reliable and repeatable discrimination of

complex odours. The usual approach is to add more and more sensors in the array (for example, ten or more), but this leads to problems regarding the calibration stability and reproducibility of the array, the poisoning of the devices and the domination of the array by the response of a few sensor devices.

Accordingly, another technique has been proposed for obtaining an improved and controlled selectivity using a single sensor device having an array of electrodes of different geometry underneath the sensing layer. In such a configuration, gases differing in their reactivity give different signals on electrodes of different spacing. As a consequence, a single sensing device having an array of electrodes of different spacing (multi-electrode sensor device) is functionally equivalent to a sensor array. The interesting additional benefit of such devices is that certain failure modes (e.g. poisoning of the device) can be recognised by the way in which the pattern of responses is varying on the different electrodes.

1.2 Innovation of the Present Research Work

The present research work goes one step beyond the above-mentioned technologies by making an innovative connection between them. The new element of innovation is based on the combination of the technology of shape and size selective catalysts (zeolites), as a means of introducing variance of response pattern across an array of sensors, with the chromium-titanium oxide (CTO) sensing material and the multi-electrode sensor arrays.
It is suggested that the combination of these advances in sensor technology could lead to the establishment of a sound theoretical basis for the control and tailoring of the microstructure and catalytic activity of semiconducting oxides multi-electrode array devices. Furthermore, it is expected that the developed novel gas sensors with improved selectivity towards specific analytes will reinforce their suitability for a wide range of electronic nose applications.

The desirable variance of response pattern is proposed to be achieved by the chemical cracking of a variety of headspace vapours using a range of zeolite catalysts with well-defined cavity shapes and sizes. The vapour presented to the sensor material is modified from the headspace vapour, but the modification is done in such a way as to preserve a well-defined relation between the 'sensor vapour' and the headspace. This relation depends on the headspace composition in a chemically well-defined way.

Different variations of the 'sensor vapour' in different devices is the primary means to achieve variance in the array; different cracking patterns are expected to give different sensor signals.

1.3 Project Objectives

The main objectives of this work were as follows:

- To study and modify the surface reactivity of the CTO sensor device as a means to improve variance in the behaviour of an array of sensors.
- To develop methods for controlling and tailoring the microstructure of sensor devices.
- To establish and demonstrate a sound theoretical basis for the optimisation of the design and fabrication procedures for multi-electrode array devices.
- To provide novel gas sensors with increased shape and size selectivity to a wide range of volatile organics and flavour compounds.
- To demonstrate the suitability of the newly developed multi-sensors array devices for electronic nose applications.

1.4 Work Methodology

Different sensor devices were fabricated using chromium titanium oxide (CTO) as the gas sensing material, with zeolite layers of three different types (ZSM-5, β, Y) added both as additional layers over the sensing material and admixed with it. The microstructure of both the sensing material and catalyst material -that play an important role in the gas selectivity of the sensors- were controlled and tailored accordingly.

Additional sensors were also produced where the different zeolite types were catalytically modified (ion exchanged) by the addition of chromium catalysts to promote selective catalytic activity.

Multiple electrode SEMDEC substrates were used for all fabricated sensor devices as these allow discrimination of gases on the basis of their reactivity with the catalyst material.

The newly developed sensors were tested in the presence of a wide range of volatile organic and flavour compounds using custom built testing rings and a commercial electronic nose.

Investigation of different parameters, which affect the behaviour of sensors in a well defined and useful way (i.e. changes in the physical dimensions of the sensor and catalyst layer as well as changes in sensor's operating temperature) were examined to allow further possibilities for improvements in the discrimination between various tested analytes for the different sensor arrays.

Computational simulations of the interactions of a range of volatile organic molecules with different zeolites were performed using a commercially available software package in order to examine suitable zeolite catalyst materials for the construction of new sensors. The computational results were then compared with the experimental results in an effort to build the trust on computational simulations to be used as the basis for new material selection for the development of novel gas sensors.

1.5 Structure of Thesis

As the objective of this project was to develop and study semiconducting oxide gas sensors with additional zeolite materials for electronic noses, the first three chapters of the thesis are based on the theoretical background of these mentioned technologies.
The concept of electronic noses and their applications is analysed in ***Chapter 2***.
The theory and applications of semiconducting metal oxide sensors and an introduction to zeolite materials are described in ***Chapter 3*** **and** ***4*** respectively.
The experimental results of this research work are presented in ***Chapters 5, 6*** **and** ***7.***
The fabrication methodology of the newly developed sensor array and the experimental study of their response to carbon monoxide and ethanol gases are described in ***Chapter 5.*** ***Chapter 6*** gives an account of the testing of a range of CTO sensors to the presence of a range of volatile organic and flavour compounds using a newly developed rig.
The suitability of the newly developed gas sensor arrays to be used in electronic nose applications for the discrimination of a wide range of volatile organic and flavour compounds is presented by the experimental study in ***Chapter 7.***

The computational part of the project is given in ***Chapter 8*** where a series of simulations (computational modelling) of the adsorption and transport of a range of organic species in zeolites are presented.

Chapter 9 summarises the main conclusions of this research work with particular reference to proposals for future work.

Chapter 2

Electronic Noses and Their Applications

2.1 Introduction

The perception of volatile compounds by the human nose is of great importance in evaluating the quality of foods, air, cosmetics and numerous other items of everyday life. Therefore, it is not surprising that repeated efforts have been made over the years to introduce cheap and small instruments for fast imaging of specific chemicals (odours, or toxic substances) operating on a similar principle as the human nose. In most cases these systems would not replace but compliment conventional analyses of volatile compounds based on sensory methods and traditional analytical techniques.

2.2 Odorous Molecules

Odorant molecules are typically small, partly hydrophobic volatile organic molecules with relative molecular masses in the range of 30 to 300 Dalton. They tend to have one or at most two polar functional groups, which frequently contain an oxygen moiety, although nitrogen and sulphur moieties can also be found.[1] ***Table 2.1*** lists the common simple functional groups that can be found in a range of different types of odorous molecules. Many different types of aromatic molecules are of particular importance in odour, fragrance, and flavour chemistry.

Naturally occurring odours from foodstuffs, beverages, plants and the odours of perfumes are not due to single molecular species but are the results of complex mixtures of molecules made up of tens, hundreds, or even thousands of separate compounds. The odour, which is perceived, is the result of the combined impact of the mixture.

Despite the importance of odour there is lack of a suitable vocabulary to describe odours. Plato[2] suggested that, "the varieties of smell have no name, and they have not many, or

definite and simple kinds; but they are distinguished only as painful and pleasant". As a consequence, odours can only be described by relative terms and in relation to other odorous materials.

Table 2.1 The structure and stereochemistry of some simple functional groups found in odorous molecules

[J. W. Gardner and P. N. Bartlett, in *Electronic Noses Principles and Applications*, ed. Oxford University Press, Inc., New York, 1999, p.13.]

FUNCTIONAL GROUP	STRUCTURE	FUNCTIONAL GROUP	STRUCTURE
Alcohol	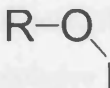	Lactone	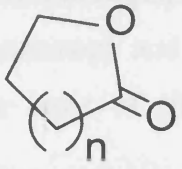
Ether	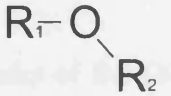	Amine	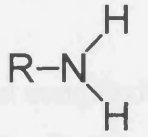
Aldehyde	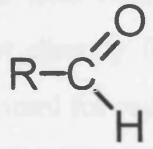	Nitrile	
Ketone	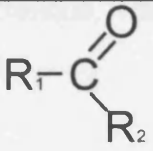	Isonitrile	
Acid	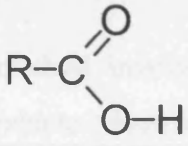	Thiol	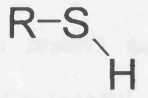
Ester	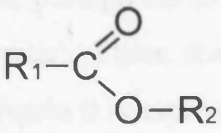	Amide	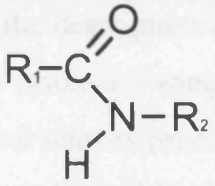

2.3 Instrumental and Sensory Analysis

Nowadays, two different kinds of technique are used in the evaluation of the odour and flavour of commercial products: the instrumental analytical methods and methods using sensory evaluation by panels of human testers.

2.3.1 Instrumental Techniques

The most commonly used methods for the instrumental analysis of the chemical composition of substances generally use the chromatographic separation of the chemical components (e.g. liquid or gas chromatography) in a mixture, followed by the detection and quantification of these components. In most cases spectroscopic techniques are then used to identify the individual components. These techniques are used to characterise the chemical compositions of materials and also to identify sources of malodour, taint, or off-flavour[3]. The combination of Gas Chromatography and Mass Spectroscopy (GC-MS) is the most popular technique for the identification of volatile compounds in foods and beverages.[4] This is because the excellent separation achieved by the gas chromatographic technique is ideally complemented by the high sensitivity of mass spectroscopy and its ability to identify the molecules eluting from the column on the basis of their fragmentation patterns.

However, the main drawbacks of the GC-MS approaches are the cost and complexity of the instrumentation and the time required to fully analyse each sample. Further, the experimental results are not directly linked with an odour characterisation. For these reasons the technique is not used for routine evaluation, but rather it should be considered as a powerful analytical technique, which can determine the sources of taints and also help in product development.

2.3.2 Sensory Evaluation

The sensory evaluation method involves the use of panel of human testers as the analytical instrument to evaluate odour or flavour. The procedure includes a careful cross check of individual odour perceptions to achieve some objectivity in the description of features in an 'odour space'. These features are used to determine prices of wines, perfumes, or foodstuff.[5] Again it is expensive to train and maintain skilled sensory panels, and the numbers of replicate samples that can be evaluated at any time is limited by the onset of olfactory fatigue. Furthermore, they are unsuited for use in aggressive environments and with toxic odours. Yet, despite the importance of expert perception of odour and flavour there is a real problem in comparing a person's experience of smell with that of another (i.e. the risk of subjective responses from the involved 'human

sensors') and in quantifying odour.[6] What comprises pleasant and unpleasant gustatory and olfactory experiences differs between individuals, tribes, races and nations.

Consequently, an alternative approach for creating an odour sensing system is highly desired in a large variety of technological fields such as food analysis, drink analysis, cosmetics industry, environmental monitoring, products quality control, chemistry process control, medical appliances. Many researches have demonstrated the use of chemical sensor systems called electronic noses, which can complement or in some cases replace the available existing methods.

2.4 Definition of an Electronic Nose

The concept of an electronic nose as an intelligent, chemical array sensor system for odour classification was proposed in 1982 by Persaud and Dodd[7] and thereafter by Ikegami et al.[8] By this time developments in electronics, sensors, and computing had combined to reach a stage where an electronic nose had become genuine possibility. As a consequence, at the beginning of the 1990s the term 'artificial' or 'electronic nose' appeared, and several commercial instruments that could mimic the human sense became available.

Gardner and Bartlett[9] defined the electronic nose as 'an instrument, which comprises an array of electronic chemical sensors with partial specificity and an appropriate pattern-recognition system, capable of recognising simple or complex odours'. In theory, such systems have to rely on gas sensors, devices that respond to a particular analyte in a selective way through a chemical reaction.

Electronic noses are composed of several gas sensors, presenting various levels of sensitivity and selectivity. Like the mammalian nose, they detect gases by means of sensors (sensor organ), which send signals to the computer (recognition organ). Each chemical vapour presented to the sensor array produces a signature, fingerprint or pattern characteristic of the vapour. This is then analysed by an appropriate pattern recognition system to identify the odour through comparison with a reference library of previously obtained measurements of known samples. The extraction of information is based on the requirement that all the sensors in the array have different selectivity properties.

2.5 Advantages of Electronic Noses

The principal advantage of electronic noses is that they can be used for obtaining quite different kinds of information and thus have many applications. These include monitoring of domestic, residential and environmental air quality or toxicity, odour characterisation, the classification of foods (meat, fish), beverages (wine, beers and spirits), gas mixtures, and the quality control of industrial products.[10]

The main advantage of an electronic nose over an expert sensory panel is, besides the smaller cost and simplicity of use, that the signals are in principle very reproducible (at least in the short term). The results obtained with such instruments are further highly correlated with the composition of the volatile compounds of the samples investigated. It further happens that typical changes of the gas phase of a certain product are related to specific odour changes. There might even exist a strong correlation between the electronic nose data and the product's aroma. In these cases, electronic noses could be useful in the production control of chemicals or foodstuff.

The advantages of an electronic nose over a classical GC instrument are its simpler use and higher speed. The greatest disadvantage is that the compounds present cannot be analytically identified.

2.6 Overview of Sensor Types

All chemical sensors comprise an appropriate, chemically sensitive material interfaced to a transducer ***(See Figure 2.1)***[1]. The analyte molecules interact with the chemically sensitive material and generate some physical change that is sensed by the transducer and converted into an output signal, *z(t)*. A wide variety of physical signals can be measured according to the transducer type. The most common are electrical measurements (current, capacitance, resistance and voltage) and the measurement of mass changes, heat generation and optical changes (absorption, fluorescence, and reflectivity).

It can be said that electronic noses contain many different components, which have to be optimised for each individual application. They can generate a huge amount of independent chemical information (features) by the variations of sensor active materials, types of signal transduction to convert chemical to electronic information and modes of operation of the sensor.[11] Even for a given sensor material and transducer principle a

variety of structural modifications may lead to new information in the chemical sensing process.

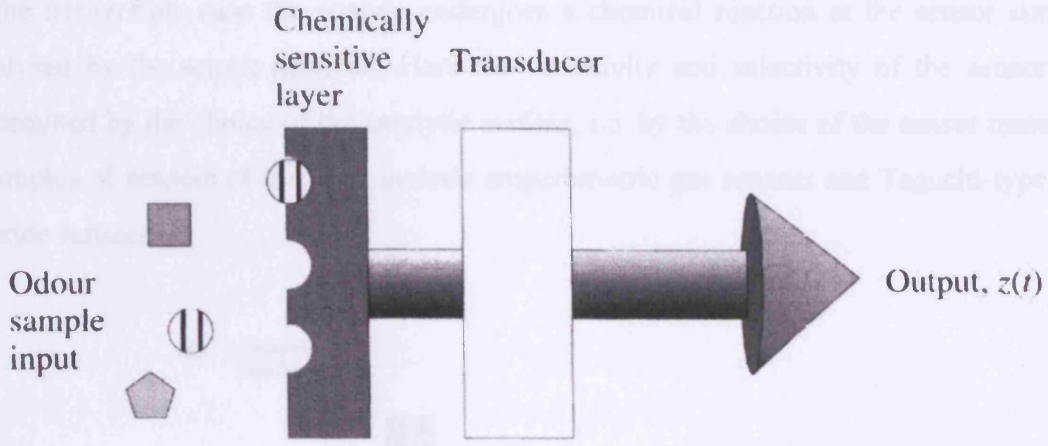

Figure 2.1 The basic components of a chemical sensor
[J. W. Gardner and P. N. Bartlett, in *Electronic Noses Principles and Applications,* ed. Oxford University Press, Inc., New York, 1999, p.72.]

2.6.1 Chemical Sensor Materials

The range of gas-sensitive materials is very broad and can be divided up in a number of ways, either by material type or by the nature of the interaction with the analyte.

Three different categories of chemical sensor materials have been reported according to the type of material used.[10] The first category involves a range of inorganic crystalline or polycrystalline materials. These include semiconductors, metal oxides, zeolite absorbent materials, and metallic catalysts. These types of materials when they are operated at elevated temperatures function as catalytic materials in irreversible, or chemically reactive, sensors.

The second category of chemical sensor materials includes the polymers and a range of organic materials. These materials when they are operated at room temperature function as reversible sensor materials. Biologically derived materials such as proteins, enzymes, and antibodies comprise the third class of chemical sensor materials.

The interaction between the analyte and the sensor material can be either reversible or irreversible. ***Figure 2.2*** illustrates the two types of sensor mechanism. In the reversible case the analyte molecules dissociate from the sensor material when the external concentration is removed and overall they undergo no net change. Examples of this type

include the adsorption of gases into polymer films and the interaction of gases with conducting polymers.

In the irreversible case the analyte undergoes a chemical reaction at the sensor surface catalysed by the sensor material. Here the sensitivity and selectivity of the sensor are determined by the choice of the catalytic surface, i.e. by the choice of the sensor material. Examples of sensors of this type include amperometric gas sensors and Taguchi-type tin-dioxide sensors.[1]

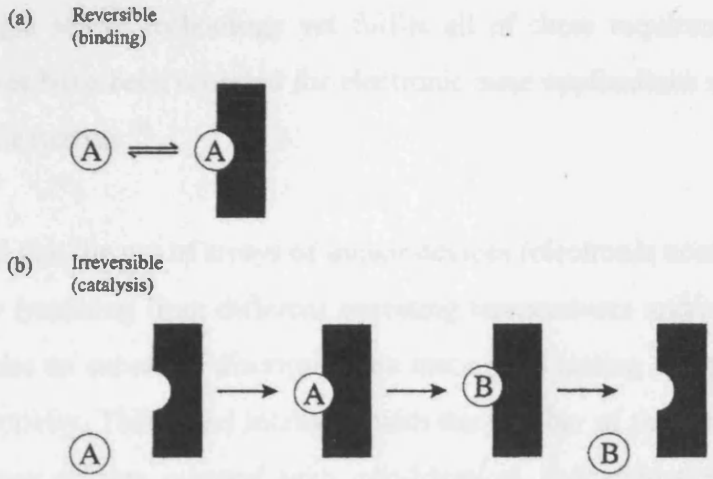

Figure 2.2 The two fundamental mechanisms of operation exhibited by chemical sensors: (a) reversible (binding) and (b) irreversible (catalysis)
[J. W. Gardner and P. N. Bartlett, in *Electronic Noses Principles and Applications,* ed. Oxford University Press, Inc., New York, 1999, p.73.]

2.6.2 Sensor Arrays

In many ways, the sensor array is the heart of an electronic nose system. For a sensor array to be successful in providing a sufficiently large variance in behaviour, in response to a range of gases, a careful selection of the individual gas sensors should be made. The ideal sensors to be integrated in an electronic nose should fulfil the following criteria:

- Manufactured at minimal cost
- Operate at minimal power drain
- High selectivity
- High sensitivity towards chemical compounds (in the ppm to ppb range)
- High stability

- Quick response in the presence of the gas of interest
- Rapid recovery time
- Robust
- High repeatability (the ability to obtain the same pattern for a sample on the same array over short intervals of time)
- High reproducibility (the ability of different sensor batches to produce the same pattern for the same odour or chemical)
- Low sensitivity to environmental variables such as temperature and humidity
- Easy calibration

Although no single sensor technology yet fulfils all of these requirements, a range of sensor technologies have been reported for electronic nose applications and some of them are also used in the market.[12]

It should be noted that the use of arrays of sensor devices (electronic noses), each having a partial specificity (resulting from different operating temperatures and/or different sensor materials), provides an enhanced discrimination among the testing compounds as well as an increased selectivity. This effect increases with the number of the sensors in the array, provided that these sensors respond with non-identical characteristics and low cross-sensitivity to the range of odours.

However, the disadvantage of electronic noses is that the variance of response patterns across a typical sensor array is usually too small for reliable and repeatable discrimination of complex gas mixtures.

The usual approach is to add more and more sensors (for example, ten or more) in the array creating problems in relation to the calibration stability and reproducibility of the array, the poisoning of devices and the domination of the array by the response of a few sensor devices.

It should be noted that advances in the technology of electronic noses are presented continuously with an effort to overcome their problems and introduce new applications.

2.6.3 Gas Sensor Technologies

Various kinds of gas sensors are available, but only four technologies are currently used in commercialised electronic noses: metal oxide semiconductors (MOS),[13,14] metal oxide

semiconductor field effect transistors (MOSFET),[15] conducting organic polymers (CP)[9,16,17] and acoustic wave devices (Bulk Acoustic Wave (BAW)) often referred to as Quartz Crystal Microbalances (QCM).[18,19,20] Other devices such as fibre-optic[21,22] electrochemical,[23,24] and bi-metal sensors are still in the developmental stage and may be integrated in the next generation of electronic noses.

2.7 Applications of Electronic Noses

Currently, the biggest market for electronic noses is the food industry. Applications include quality control of foods, such as meat,[25] fish[1], edible oil,[26] or blueberries[27]. Other authors proposed electronic noses to supervise the quality of beer,[28] wine,[29] cork stoppers[30] and alcoholic beverages[31] or perfumes[32]. Other applications include the use of electronic noses for the quality control of industrial products (such as the paper), the classification of different cigarette brands,[33] cosmetics and the monitoring of environmental air quality. An overview of electronic noses applications is given in ***Table 2.2***.

Table 2.2 Various applications of electronic noses

APPLICATION	TEST	INSTRUMENTAL SYSTEM / SENSOR TECHNOLOGY	REFERENCE
COFFEE	Discrimination between blend and roasting level	12 MOS	Ref. 34
	Discrimination between varieties	12CP	Ref. 35
	Discrimination between varieties	12MOS	Ref. 36
	Discrimination of different types of coffee	FOX 4000 (18 MOS)	Ref. 32
BEER	Presence of Diacetyl taint in synthetic beer	18 CP	Ref. 37
	Discrimination between different commercial beers	12 CP	Ref. 38
	Discrimination between two types of malt	6 MOS	Ref. 39

WINE	Discrimination between different varieties and vintages of same wine	4 MOS	Ref. 29
PERFUMES	Discriminate between different perfume odours	8 lipid-coated BAW	Ref. 55
	Discrimination of seven different perfumes	4 MOS	Ref. 32
FISH	Spoilage in three different fish species	4 MOS	Ref. 47
MILK	Milk ageing anal.	4 MOS	Ref. 42
ENVIRONMENT	Discrimination of five air pollutants	4 MOS	Ref. 42
	Measurement of olfactive annoyance	12 MOS	Ref. 51
FUELS	Distinction of 20 diesel fuels	FOX 4000 (18 MOS) Smart Nose GA200 (Mass spectrometer)	Ref. 54
OIL	Classify and recognize different oils	4 MOS	Ref. 42
	Classification of olive oils and seed oils	4 MOS	Ref. 48
FOOD	Classify different kinds of foods (tomato, coffee, wine, sunflower oil, olive oil)	4 MOS	Ref. 42
CHEESE	Discrimination between different cheese types	Aroma Scan A205 20CP	Ref. 1
MEAT	Off flavour and contamination of meat products	Fox 3000 12 MOS	Ref. 25

System: **MOS**=Metal Oxide Semiconductor; **CP**=Conducting Polymer; **BAW**=Bulk Acoustic Wave
Suppliers: **FOX**=Alpha M.O.S, F-Toulouse, **Aroma Scan**= AromaScan plc, UK-Crewe

2.7.1 Discrimination of Food and Drinks

A prime requirement of the food industry is a sensitive method of assessing volatiles, for identification, authentication, process control and product blending or formulation.

2.7.1.1 Coffee

Coffee quality is assessed by expert coffee tasters, largely on the basis of its aroma and flavour, and the highest quality beans command a considerable premium. Coffee volatiles

are numerous and varied in their aroma quality, potency and concentration. The final composition of volatiles depends on a number of factors, such as species/variety of bean, climatic and soil conditions during growth and storage, time and temperature of roasting, as well as the roasting equipment used.

An investigation has been carried out, by Gardner et al.[34] into the response of an array of twelve different commercial tin oxide gas sensors (with partially overlapping sensitivities) to the headspace of coffee packs. Three commercial coffees covering two different blends and two roasts, as well as one coffee which has been subjected to a range of six roasting times were tested. A success rate of 89.9% was achieved in classifying the three commercial coffee odours directly from the response (change in sensor conductance) of the array.
The effect of the set of six roasting times on the specific coffee odour was also investigated and confirmed the expected conductivity increase with roasting time. This study showed that it is possible to discriminate between both the blend and roasting level of coffee using an array of tin oxide gas sensors.

Other researchers[35,36] confirmed the ability of MOS and CP noses to discriminate between the same coffee beans species grown in two different geographical locations (i.e. Colombian and Brazilian roasted coffee beans).

2.7.1.2 Beer

Beer is a complex substance consisting of a large number of components. Any change in the concentration of one or more of these components result in the development of faults (i.e. off-flavour).
Gardner et al.[37] analysed the presence of low-level diacetyl taint in synthetic beer using an array of 24 conducting polymers. Similarly, a laboratory-manufactured system based on 12 CP was able to discriminate between three commercial beers.[38]

Zimmermann and Leclercq[39] investigated the discrimination of two types of malt and the detection of false manufactured batches using a FOX 2000 instrumental system. They concluded that the electronic nose could be used as a tool to improve both the product quality and to develop new beer products.

2.7.1.3 Wine

Di Natalie et al.[29] studied the discrimination of two wines with the same denomination (Groppello red wine) but produced in different vineyards, using an array of metal-oxide semiconductor gas sensors. Wines with the same denomination share some similar features such as the kind of grape from which they are produced and their organoleptic properties. From a chemical point of view the differences are very small and their effects on wine taste can be appreciated only by well trained people. However, some subtle differences among wines produced in different vineyards exist. These are important to evaluate, since wines originating from particular places show different aptitudes, e.g., to be aged. This study, in agreement with other authors,[40] showed that an electronic nose could even identify different varieties of the same wine and its year of vintage.

The performance of the array was compared with that of the standard chemical analytical approach adopted by the wines authority (e.g. pH meters for acidity determination). The electronic nose was found to be superior to the standard chemical analysis. The success of the electronic nose approach is due to the fact that the number of chemical species which contributes to the sensor outputs is greater than those considered in any standard chemical analysis approach. Therefore, the amount of information that can be extracted from a sensor array is expected to be larger and the classification to be more accurate.

2.7.1.4 Other Beverages

Nanto et al.[41] investigated the use of a novel chemical system using Japanese-lacquer-coated quartz resonator chemical sensors together with pattern recognition analysis to discriminate among aromas from several kinds of alcohols (Fruit Liquor, Japanese Sake, Brandy, Rum and Vodka). The shape of the transient response curves depended on the ethanol concentration of alcohols. Quantitative differences among aromas from different kind of alcohols were demonstrated. These results strongly suggest that it is possible to discriminate among aromas using these kinds of sensors in conjunction with pattern recognition technique such as principal component analysis (PCA). This is a powerful, linear, supervised pattern recognition technique that can be used to explore the nature of the electronic nose data and determine the linear reparability of the response vectors by reducing the number of variables that need to be considered (i.e. n sensors) to a smaller number of indices (principal components). For more details about PCA see ***Appendix B***.

2.7.1.5 Milk Ageing Analysis

An array based on four pure SnO_2 sol-gel sensors with the same sensing layer (undoped SnO_2) but with different configurations of the electrodes, was used to analyse milk flavour compounds and to test the capability of the array to recognise and classify the milk as a function of storage time when its rancidity becomes relevant. Measurements were performed by sampling the headspace of a commercially available UHT whole milk day by day for a week. The results of the PCA plot ***(Figure 2.3)***[42] suggest that the array could follow the evolution of rancidity of milk.

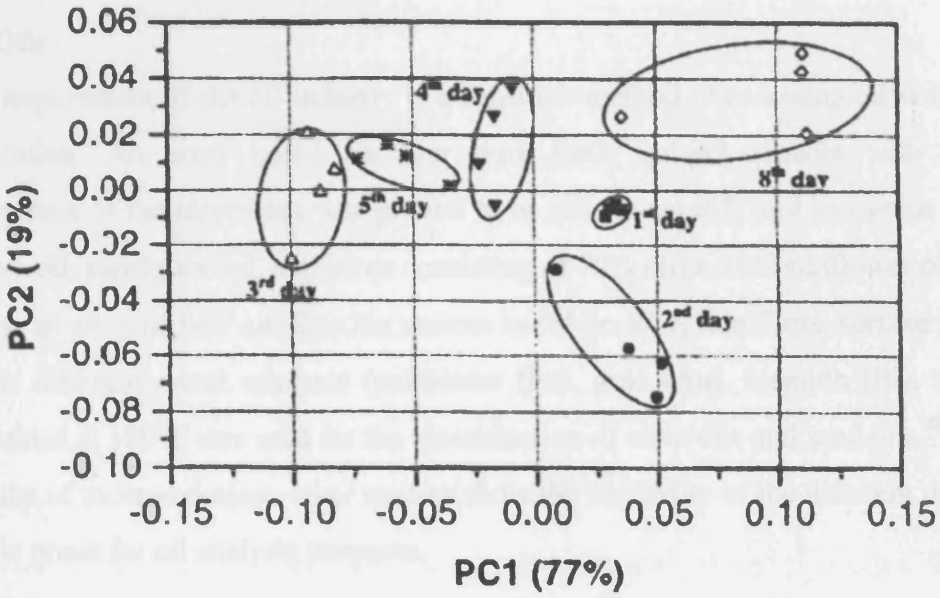

Figure 2.3 PCA results in the PC1-PC2 plane for the milk analysis during a week of ageing

[S. Capone, P. Siciliano, F. Quaranta, R. Rella, M. Epifani and L. Vasanelli, *Sensors and Actuators B.*, 2000, **69**, 230]

2.7.1.6 Analysis of Biological Specimens

In recent years chemical multisensor arrays have been shown to be powerful tools for the analysis of biological specimens. Successful applications were reported for the analysis of fermented food samples,[43] classification of bacterial strains[44] fermentation monitoring[45] and fermentation state visualisation.

Mandenius et al.[46] reported the suitability of an array of sensors (MOSFET, MOS, CP) to predict the fermentation performance of wood hydrolyzates prepared from four different kinds of wood.

2.7.1.7 Fish

The control of food freshness is of increasing importance to industry because of the growing quality expectation by consumers. This consequently places greater demands on industry to both monitor the storage or packaging process and to extend the storage.
Olafsson et al.[47] followed the spoilage in three different fish species (haddock, cod and redfish) using an array of 4 MOS sensors. The electronic nose was trained to learn the characteristic off-flavours of fish or other seafood as they spoil. These results again showed that it is possible to estimate and monitor the freshness of fish using an electronic nose.

2.7.1.8 Oils

A main requirement of the oil industry is a sensitive method of assessing oil volatiles for authentication. An array based on four pure SnO_2 sol-gel sensors with different configurations of the electrodes was proved to be able to classify and recognise different oils (olive-oil, sunflower-oil, a mixture consisting of 70% olive-30% sunflower oil).[42]
Similarly, an array of four metal oxide sensors based on WO_3 thin films, surface activated with four different metal catalysts (palladium (Pd), gold (Au), bismuth (Bi), antimony (Sb) operated at 180°C was used for the classification of olive oils and seed oils.[48]
The results of these and many other studies show the feasibility of the different developed electronic noses for oil analysis purposes.

2.7.2 Environmental Monitoring

One of the most demanding application areas of electronic noses is the monitoring of our environment. There is an increasing interest in the detection and quantification of gaseous air pollutants by using low cost and simple experimental devices for environmental control and air quality analysis in indoor ambient. But this is not the only application of these devices. Other environmental applications of electronic noses include analysis of fuel mixtures,[49] testing ground water for odours, and identification of household odours.[50]
Potential applications include identification of toxic wastes, air quality monitoring, and monitoring factory emissions.

2.7.2.1 Air Pollutants

Capone et al.[42] studied the discrimination of five air pollutants (CO, NO_2, CH_4, C_2H_5OH and CH_3OH) using an array consisting of four sensors based on pure and Pd, Pt, Os doped SnO_2 sol-gel thin films. Recognition of the different air contaminants was achieved by the use of principal component analysis (PCA). ***Figure 2.4*** shows the results of the PCA for five air contaminants. These results confirm that the use of an electronic nose even with a limited number of sensors is a powerful tool for rapidly classifying air contaminants.

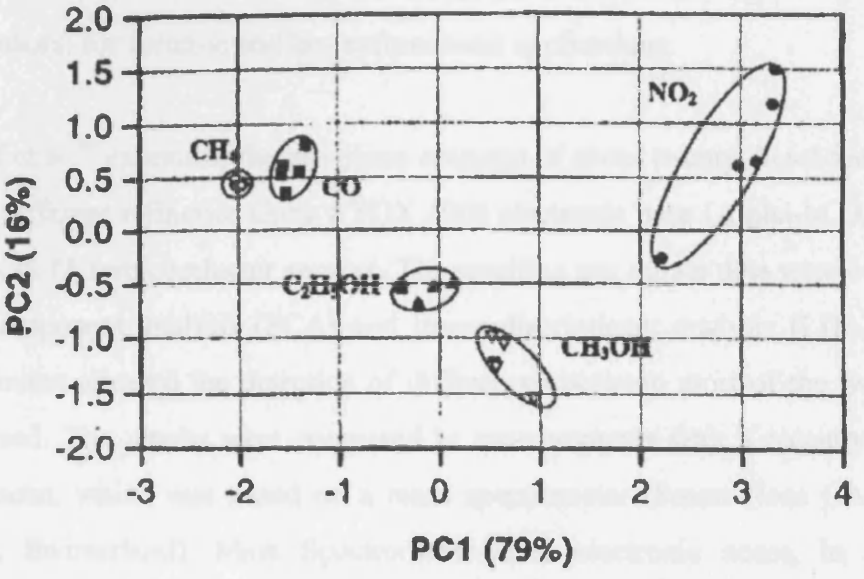

Figure 2.4 Score plot in the PC1-PC2 plane of the principal component analysis for some contaminants

[S. Capone, P. Siciliano, F.Quaranta, R. Rella, M. Epifani and L. Vasanelli, *Sensors and Actuators .*, 2000, 69, 230]

2.7.2.2 Olfactive Annoyance

A laboratory-made malodour sensing array system consisting of twelve commercial tin oxide sensors was developed by Romain et al.[51] to identify five typical sources of olfactive annoyance (printing houses, paint shop in a coach building, wastewater treatment plant, urban waste composting facilities and rendering plant) collected in the field. This study demonstrated that the identification of real malodours is feasible with a simple sensor array and suitable data processing methods. Further these findings are promising in the development of a portable detector for the objective measurement of olfactive annoyance.

2.7.2.3 Fuels

Fuels are mixtures with a strongly varying composition depending on the crude source and refining process. This is accompanied by variations in the composition of the volatiles. A fast and reliable method to determine the odour quality of fuels could be the analysis of their headspace with an electronic nose.

It is interesting to note the work undertaken by B. S. Hoffheins et al.[52] Their study showed the qualitative distinction of several automotive fuels (with different octane values) and aviation fuels by aid of an array of Taguchi-sensors. Another study performed by S. A. Barshick[53] demonstrated the use of an electronic nose (consisting of 32 conducting polymer sensors) for forensic and law enforcement applications.

R. Feldhoff et al.[54] examined the gas phase contents of about twenty diesel fuels obtained from three different refineries using a FOX 4000 electronic nose (Alpha-M.O.S., France) equipped with 18 semiconductor sensors. The resulting gas sensor data were evaluated by principal component analysis (PCA) and linear discriminant analysis (LDA). The Fox 4000 instrument allowed the detection of differences between most of the twenty diesel fuels analysed. The results were compared to measurements with a recently developed electronic nose, which was based on a mass spectrometer (Smart Nose GA 200, LDZ Laboratory, Switzerland). Mass Spectrometer-based electronic noses, in contrast to classical mass spectrometers, use statistical data treatment to compare and to classify an unknown sample with respect to an earlier defined statistical data model. A good correlation was found between the data measured with both types of instrument.

2.7.3 Electronic Noses for Medicine

Because the sense of smell is an important sense to the physician, an electronic nose has applicability as a diagnostic tool. An electronic nose can examine odours from the body (e.g., breath, wounds, body fluids, etc.) and identify possible problems. Odours in the breath can be indicative of gastrointestinal problems, sinus problems, infections, diabetes, and liver problems. Infected wounds and tissues emit distinctive odours that can be detected by an electronic nose. Also, odours coming from body fluids can indicate liver and bladder problems.

2.7.4 Perfumes

Nakamoto et al.[55] studied a set of five different perfumes (citrus, floral, chypre, modern bouquet, oriental) using an array of eight lipid-coated BAW sensors. A principal component analysis of the resulting normalised data set showed five separate clusters corresponding to the five different tested samples ***(See Figure 2.5)***. This study shows that it is possible to use an electronic nose instrument for the automatic testing of perfume products on a factory production line.

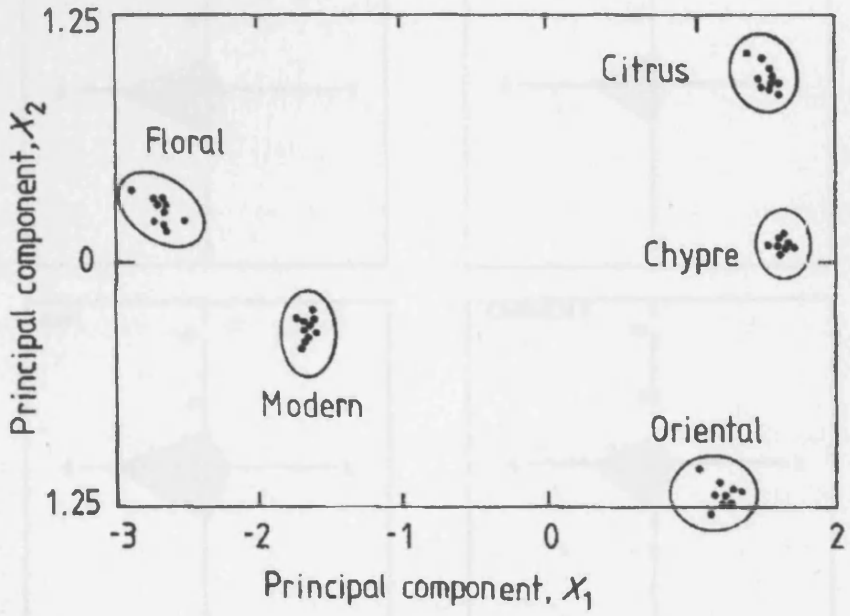

Figure 2.5 Principal components plots of five dissimilar perfumes using an array of eight lipid-coated BAW sensors with 10 replicate samples of each
[N. Nakamoto, A. Fukuda and T. Moriizumi, *Sensors and Actuators B.*, 1993, **10**, 85]

Penza et al.[48] studied the discrimination of seven different perfumes (Sergio Tacchini, Caractere, Gian Marco Venturi, Chanel N.5, Iceberg Twin, Axe, PatrichsNoir) using an array of four WO_3 thin film sensors catalysed by Pd, Au, Bi and Sb. ***Figure 2.6*** illustrates the radar plots of the seven perfumes tested. The radial parameter is the response (R_o/R) of each array sensor shown along a determined axis. The final result is a specific feature characteristic for each flavour by providing a typical fingerprint as chemical imaging of a given flavour. This study also suggests that the electronic nose could be exploited to validate the primary flavours in the cosmetics industry.

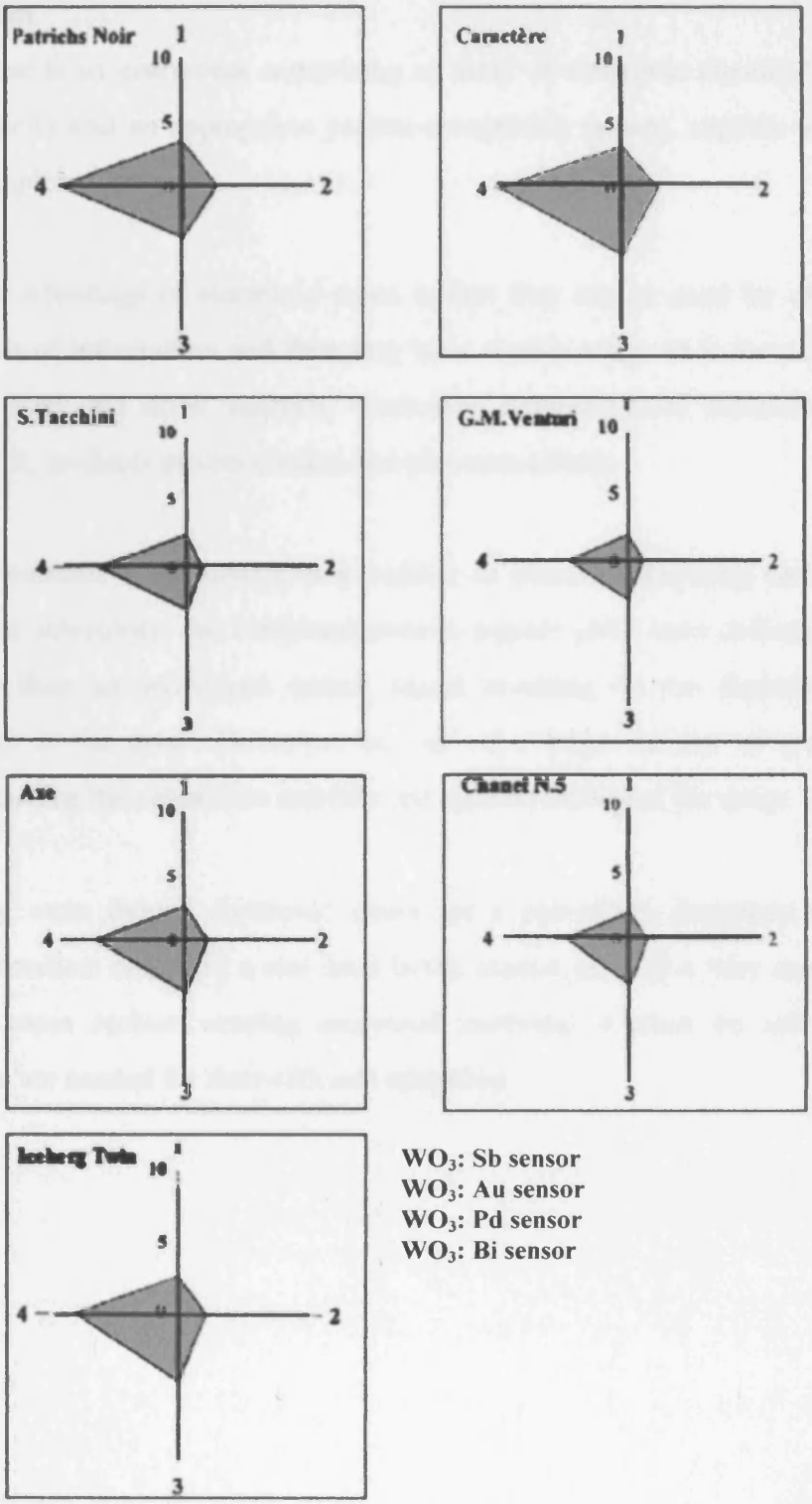

Figure 2.6 Radar plots of seven perfumes using patterns by an array of four sensors
[M. Penza, G. Cassano, F. Tortorella and G. Zaccaria, *Sensors and Actuators B.*, 2001, 73, 76]

2.8 Conclusion

Electronic nose is an instrument comprising an array of electronic chemical sensors with partial specificity and an appropriate pattern-recognition system, capable of recognising simple or complex odours.

The principal advantage of electronic noses is that they can be used for obtaining quite different kinds of information and thus they have a wide range of industrial applications such as the food and drink analysis, cosmetics, environmental monitoring, chemical process control, products quality control and pharmaceuticals.

Given that electronic noses comprise a number of sensors presenting various levels of sensitivity and selectivity, the combined sensors signals yield more information about a given odour than an individual sensor signal resulting in the desirable selectivity improvements in the array. However, the use of a large number of sensors created problems regarding the calibration stability and reproducibility of the array.

Consequently, even though electronic noses are a potentially important new class of analytical instrument and fulfil a real need in the market place (i.e. they can complement or in some cases replace existing analytical methods) it must be said that further developments are needed for their efficient operation.

Chapter 2

References

1. J. W. Gardner and P. N. Bartlett, in *Electronic Noses Principles and Applications,* ed. Oxford University Press, Inc., New York, 1999.

2. T. Plato in *The Dialogues of Plato Vol III,* ed. B. Jowett, Clarendon Press., Oxford, 1892.

3. H. Maarse, in *Food Taints and Off-flavours,* ed. M. J. Saxby, Blackie., London, 1993, p.63.

4. F. A. Mellon, in *Spectroscopic Techniques for Food Analysis,* ed. R. H. Wilson, VCH Publishers., New York, 1994, p.181.

5. D. Pal, S. Sachdeva and S. Singh, *J. Food Sci. Technol.*, 1995, **32**, 357.

6. N. Neuner-Jehle and F. Etzweiler, in *Art, Science and Technology*, ed. P. M. Muller and D. Lamparsky, Elsevier., 1991.

7. K. Persaud and G. H. Dodd, *Nature.*, 1982, **299**, 352.

8. A. Ikegami and M. Kaneyasu, Olfactory detection using integrated sensors, *Proceedings of the 3rd International Conference on Solid-State Sensors and Actuators (Transducers 85),* ed. IEEE Press., New York, 1985, 136.

9. J. W. Gardner and P. N. Bartlett, *Sensors Actuators B.*, 1994, **18**, 21.

10. C. Di Natale, F. A. M. Davide, *Proc. 1st Eur. School Sensors,* ed. Word Scientific., Singapore, 1995.

11. W. Gopel, *Sensors Actuators B.*, 1998, **52**, 125.

12. D. J. Strike, M. G. H. Meijerink and M. K. Hep, *Fresenius J. Anal Chem.*, 1999, **364**, 499.

13. M. Benady, J. E. Simon, D. J. Charles and G. E. Miles, *Transaction of the ASAE.*, 1995, **38**(1), 251.

14. S. Roussel, G. Forsberg, P. Grenier and V. B. Maurel, *Journal of Food Engineering.*, 1999, **39**, 9.

15. M. Holmberg, F. Winquist, I. Lundstrom, J. W. Garrdner and E. L. Hines, *Sensors and Actuators B.*, 1999, **26**, 246.

16. J. W. Gardner and P. N. Bartlett, *Sensors Actuators A.*, 1995, **51**, 57.

17. J. W. Gardner, P. N. Bartlett and K. F. E. Pratt, *IEE proceedings-Circuits Devices Syst.*, 1995, **142**(5), 321.

18. C. Di Natale, A. Macagnano, A. D'amico and F. Davide, *Measurement Science and Technology.*, 1997, **8** (11), 1236.

19. N. Nakamoto, A. Fukuda and T. Moriizumi, *Sensors Actuators B.*, 1993, **10**, 85.

20. Z. Deng, D. C. Stone and M. Thompson, *Analyst.*, 1996, **121**, 671.

21. J. M. Sutter and P. C. Jurs, *Analytical Chemistry.*, 1997, **69**, 856.

22. T. A. Dickinson, J. White, J. S. Kauer and D. R. Walt, *Nature.*, 1996, **382**, 697.

23. C. M. Mari and G. B. Barbi, in *Gas Sensors*, ed. G. Sberveglieri, Dor-drecht Kluwer Academic Publishers., 1992, p. 329.

24. H. Baltruschat, I. Kamphausen, R. Oelgeklaus, J. Rose and M. Wahlkamp, *Analytical Chemistry.*, 1997, **69**, 743.

25. F. Winquist, E.G. Hornstein, H. Sundgren and I. Lundstrom, *Meas. Sci. Technol.*, 1993, **4**, 1493.

26. S. Bazzo, F. Loubet, T. Tan, J. D. Hewett-Jones, C. E. M. Engelen-Cornax and J. F. A. Quadt, *Semin. Food Anal.*, 1998, **3**(1), 15.

27. J. E. Simon, A. Hetzroni, B. Bordelon, G. E. Miles and D. J. Charles, *J. Food Sci.*, 1996, **61**(5), 967.

28. T. C. Pearce, J. W. Gardner, S. Friel, P. N. Bartlett and N. Blair, *Analyst.*, 1993, **118**, 371.

29. C. Di Natale, F. A. M. Davide, A. Amico, P. Nelli, S. Gropelli and G. Sberveglieri, *Sensors Actuators B.*, 1996, **33**(1-3), 83.

30. S. Rocha, I. Delgadillo, A. J. Ferrer Correia, A. Barros and P. Wells, *J. Agric. Food Chem.*, 1998, **46**, 145.

31. H. Nanto, K. Kondo, M. Habara, Y. Douguchii, R. I. Waite and H. Nakazumi, *Sensors Actuators B.*, 1996, **35-36**, 183.

32. D. H. Pybus and C. S. Sell, in *The Chemistry of Fragrances*, ed. Royal Society of Chemistry., Kent, 1999.

33. H. V. Shurmer, J. W. Gardner and H. T. Chan, *Sensors Actuators B.,* 1989, **18**, 361.

34. J. W. Gardner, H. V. Shurmer and T. T. Tan, *Sensors Actuators B.,* 1992, **6**, 71.

35. J. W. Gardner, T. C. Pearce, S. Friel, P. N. Barlett and N. Blair, *Sensors Actuators B.,* 1994, **18**, 240.

36. T. Tan, Q. Lucas, L. Moy, J. W Gardner and P. N. Bartlett, *LC-GC International., 1995,* **8**, 218.

37. J. W. Gardner, T. C. Pearce, S. Friel, P. N. Barlett and N. Blair, *Sensors Actuators B.,* 1994, **18**, 240.

38. T. C. Pearce, J. W. Gardner, S. Friel, P. N. Bartlett and N. Blair, *Analyst.,*1993, **118**, 371.

39. D. Zimmermann and C. Leclercq, Olfaction and Electronic Nose, *2nd International Symposium.*, Toulouse, 1995.

40. C. Di Natale, F. Davide, A. D' Amico, P. Nelli and G. Sberveglieri, *Sensors Actuators B.*, 1995, **25**, 801.

41. H. Nanto, K. Kondo, M. Habara, Y. Douguchi, R. I. Waite and H. Nakazumi, *Sensors Actuators B.,* 1996, **35**, 183.

42. S. Capone, P. Siciliano, F. Quaranta, R. Rella, M. Epifani and L. Vasanelli, *Sensors Actuators B.,* 2000, **69**, 230.

43. C. F. Mandenius, T. Eklov and I. Lundstrom, *Biotechnol. Bioeng.,* 1997, **55**, 427.

44. T. D. Gibson, O. Prosser, J. N. Hulbert, R. W. Marshall, P. Corcoran, P. Lowery, E. A. Ruck-Keene and S. Heron, *Sensors Actuators B.,* 1997, **44**, 413.

45. T. Eklov, G. Johansson, F. Winquist and I. Lundstrom, *J. Sci. Food Agric.*, 1997, **76**, 525.

46. C. F. Mandenius, H. Liden, T. Eklov, M. J. Taherzadeh and G. Liden, *Biotechnol. Prog.*, 1999, **15**, 617.

47. R. Olafsson, E. Martinsdottir, G. Olafsdottir, P. I. Sigfusson and J. W. Gardner, in *Sensors and Sensory Systems for an Electronic Nose*, ed. J. W. Gardner and P. N. Bartlett, Dordrecht Kluwer Academic Publishers., 1992, p. 257.

48. M. Penza, G. Cassano, F. Tortorella and G. Zaccaria, *Sensors Actuators B.,* 2001, **73**, 76.

49. R. J. Lauf and B. S. Hoffheins, *Fuel.*, 1991, **70**, 935.

50. P. E. Keller, R. T. Kouzes, and L. J. Kangas, Three Neural Network Based Sensor Systems for Environmental Monitoring, *IEEE Electro 94 Conference Proceedings.*, MA, Boston, 1994, p. 377.

51. A. C. Romain, J. Nicolas, V. Wiertz, J. Maternova and P. Andre, *Sensors Actuators B.*, 2000, **62,** 73.

52. B. S. Hoffheins and R. J. Lauf, *Analusis.*, 1992, **20**, 201.

53. S. A. Barshick, W. H. Griest and A. A. Vass, *SPIE.*, 1997, **63**, 2941.

54. R. Feldhoff, C. A. Saby and P. Bernadet, *Analyst.*, 1999, **124**, 1167.

55. N. Nakamoto, A. Fukuda and T. Moriizumi, *Sensors Actuators B.*, 1993, **10**, 85.

Chapter 3

Metal Oxide Semiconductor Sensors

3.1 Introduction

Work in the field of semiconducting oxide sensors first started in the early 60s by Seiyama et al. in Japan,[1] where they found that thin films of ZnO, heated to ~300°C in air, had an electrical conductivity that was very sensitive to the presence of traces of reactive gases in the air. Taguchi, in 1962[2] found similar properties for sintered SnO_2, with the added advantage of greater stability.

Metal oxide semiconductors have been successfully employed as sensing devices, primarily for the detection and metering of combustible gases such as hydrocarbons and carbon monoxide, with varying degree of commercial success (such as industrial and domestic health and safety monitoring). Semiconducting oxides have also been shown to be very promising for the detection of H_2S,[3] NH_3,[4] PH_3, Cl_2[5] and NO_x[6]. Also, they are the most widely used sensor technology for odour measurement in electronic nose applications.

Since their invention, they have been the subject of extensive research, directed both at understanding the mechanism of response and improving their performance particularly in terms of selectivity, long-term stability, humidity dependency and the poisoning of the devices by different species (i.e. silicones, H_2S and SO_2)[7].

3.2 Sensor Fabrication

Figure 3.1 shows the basic construction of a semiconducting oxide sensor. The sensor is based on a ceramic substrate, which carries a set of electrodes on one side and a heater track on the other. A sensing element that usually consists of a semiconducting material

presenting a high surface-to-bulk ratio (i.e. a porous thick film) is deposited on the two metallic electrodes.

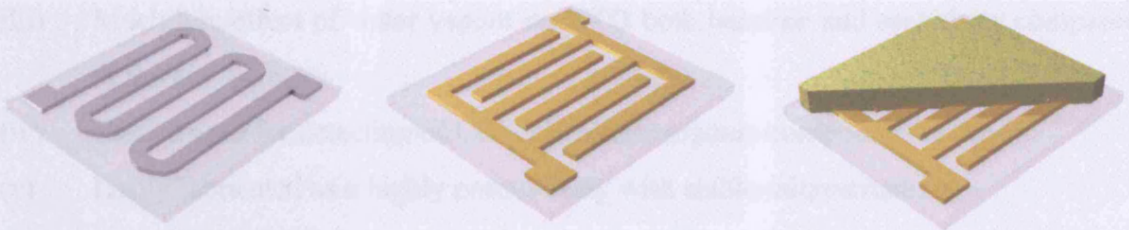

Screen printed platinum heater track on alumina substrate

Screen printed gold electrode structure

Sensing oxide deposited onto electrode structure

Figure 3.1 Semiconducting oxide sensor fabrication
[Capteur Sensors and Analysers Ltd, UK]

3.3 The Development of New Materials for Semiconductor Gas Sensors

Previously, the majority of semiconductor gas sensors have used tin dioxide as their reactive element. One of the main problems with tin oxide as well as other gas sensors is their lack of selectivity; they appear to respond to a wide spectrum of reducing gases, thereby making it difficult to assign the signal to a particular gas of interest in a mixture of several.

A degree of selectivity to different gases was shown to be achieved by the adjustment of sensors' operating temperatures, the use of catalyst and promoters of various kinds, and the exploration of alternative sensor materials.[8]

3.3.1 Titanium-Substituted Chromium Oxide

A material of prime interest in gas sensor technology is the titanium-substituted chromium oxide (CTO) such as $Cr_{2-x}Ti_xO_{3+y}$ with $0.01 \leq x \leq 0.5$ (i.e. with low titanium content). Within this range, the material retains a solid solution of TiO_2 in Cr_2O_3 with corundum crystal structure of the unsubstituted chromium oxide, with charge balanced by chromium vacancies. CTO is a single-phase material that exhibits p-type semi-conducting behaviour therefore the resistance will increase in the presence of reducing gases.[9]

A list of advantages of CTO is given below:

(i) High chemical stability at the operating temperature.

(ii) High selectivity towards the reducing gases H_2S and NH_3

(iii) Much less effect of water vapour on CTO both baseline and sensitivity compared to SnO_2

(iv) Can be used for detection of CO and volatile organic compounds in the air

(v) Easily fabricated as a highly porous body with stable microstructure

(vi) CTO is sensitive to higher hydrocarbons, CO, H_2S, NH_3 and a wide range of solvents but is not sensitive to methane

A wide range of materials, which tend to prove almost as advantageous and useful as CTO, have been investigated for use in the detection and monitoring of gases in air.[10] Examples of promising new materials include Ga_2O_3 for methane detection,[11] WO_3 for nitrogen oxide monitoring[12] and $BaSnO_3$ for nitric oxide sensing[13].

3.4 Semiconductors

A semiconductor is a crystalline material whose electrical conductivity, unlike in metals, increases with temperature. The highest occupied and lowest unoccupied energy levels are separated by a band gap that is significant with respect to thermal energy.

3.4.1 Intrinsic Semiconductor

In the case of pure semiconductors (intrinsic semiconductor) conduction takes place by thermal excitation of electrons from the valence band, across the band gap (E_g), to the conduction band, leaving behind unoccupied states in the valence band, which may be regarded as free positively charged carriers, called p-holes ***(See Figure 3.2)***. The intrinsic carrier concentration in the pure semiconductor is referred as n_i ($n_i = p = n$; where p and n denote the concentration of holes in the valence and the concentration of electrons in the conduction band respectively). The electronic excitation can be regarded as a type of defect generation. The conductivity is proportional to $n + p$ and it was found to depend exponentially on E_g/kT by the following expression:[14]

$$\sigma = \sigma_o e^{-Eg/2kT} \qquad \textbf{[3.1]}$$

3.4.2 Extrinsic Semiconductor

The majority of semiconductors are impure and possess defects in their crystal lattice. Consequently, this results in the formation of supplementary charge carriers in addition to the intrinsic electron-hole pairs generated thermally.

If for example arsenic atoms are introduced into a silicon crystal, then one additional electron will be available for each dopant atom that is substituted. This extra electron is only weakly bound to the donor atom and is represented as a donor bound level just below the conduction band. Thermal excitation will lead to the transfer of electrons from the donor band (i.e. energy levels that are associated with defects or impurities) into the empty conduction band. This process gives rise to *n*-type semiconductivity where *n* implies that the charge carriers are negative electrons ***(See Figure 3.3a)***.[15]

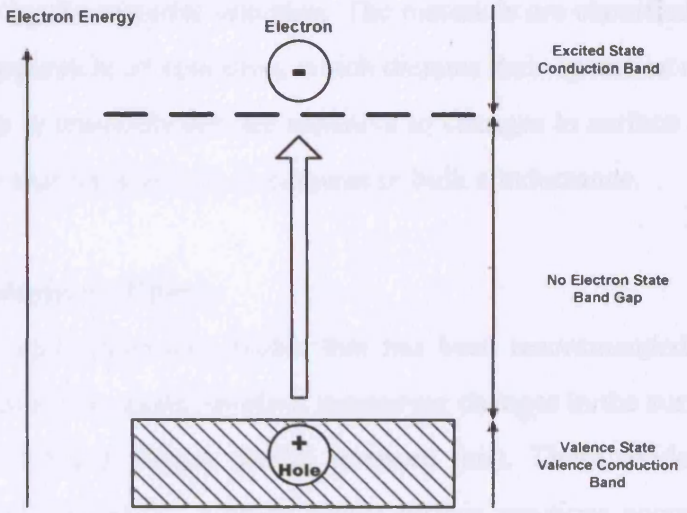

Figure 3.2 Energy band characterizing a semiconductor

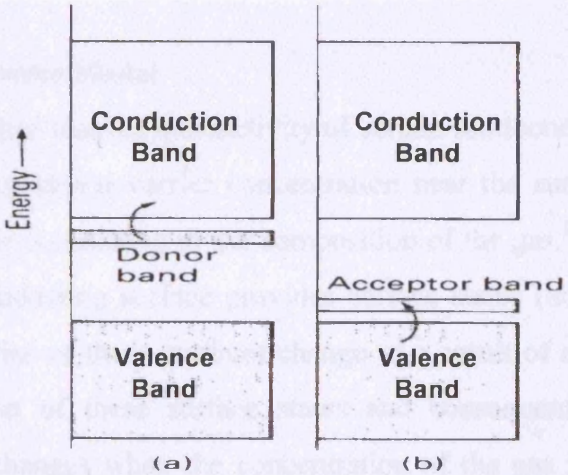

Figure 3.3 The band structure in (a) an *n*-type semiconductor and (b) a *p*-type semiconductor

On the other hand, doping with atoms of an element having fewer valence electrons per atom (i.e. gallium) introduces holes into the solid or the so-called acceptor levels, which are situated just above the valence band. When the temperature is zero the acceptor band is empty, but at higher temperatures electrons may be excited from the valence band to the acceptor band, so that the hole concentration in the valence band is much higher than that arising from the intrinsic electron-hole production. This process gives rise to *p*-type semiconductivity since the charge carriers are now effectively positive holes in the lower band ***(See Figure 3.3b)***.[15]

3.5 Materials and Mechanisms of Operation of Semiconducting Oxide Gas Sensors

It is generally established that the characteristics of semiconducting gas sensors are strongly influenced by the material selection. The materials are classified into two groups according to the temperature of operation, which dictates their operation mechanisms.
The first type refers to materials that are sensitive to changes in surface conductance; the second one to those that are sensitive to changes in bulk conductance.

3.5.1 Surface Conductance Effects

The first group of semiconducting oxides that has been recommended to detect minor concentrations of hazardous gases involves measuring changes in the surface conductivity in an atmosphere of fixed oxygen partial pressure (air). These oxides operate in the temperature range of 300-500°C, a range where surface reactions occurs at an adequate rate.

3.5.1.1 Gas Response Model

It is well established that the conductivity of certain semiconductors is sensitive to certain gases and that the charge-carrier concentration near the surface of a semiconductor in contact with a gas is sensitive to the composition of the gas.[16,17] Adsorption of a foreign gas on a semiconducting surface provides surface states (donors or acceptors), and the electrical properties of these surfaces change as a result of adsorption and/or reaction.[18] The concentration of these surface states and consequently the conductivity of the semiconductor, changes when the concentration of the gas in the ambient environment changes.

Gas sensitivity and consequent changes in electronic conductivity was found to be a common phenomenon for metal oxides, implying a reactive surface species common to all of these systems. This observation implies the existence of oxide surface states, which are the same on all semiconducting oxides regardless of composition and it is with these oxide surface states that the gas reacts[19]. Thus, a change in the surface state concentration is formulated as due to oxygen adsorption on the surface of the semiconductor.

The accepted mechanism is that the oxygen adsorbed from the air acts as an electron acceptor state from the bulk of the solid, lying within the band gap of the oxide but situated at the surface of the material. The fractional surface coverage of this acceptor state (O_2^-, O^- and O^{2-}) is changed as a consequence of the reactions at the surface and hence a change in conductivity is observed. Typical sensor response is illustrated in ***Figure 3.4*** and rationalised by a model such as that shown in ***Scheme 3.1***. It should be noted that this process requires only electron transport within the bulk and no vacancy transport.

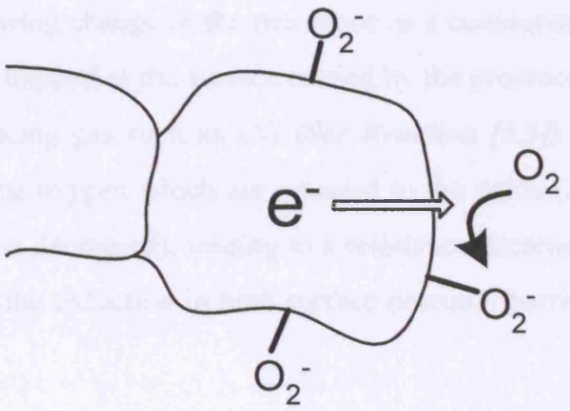

Figure 3.4 Typical sensor response (charge exchange on the surface of a grain)

Williams and Pratt[20] described the response of CTO to CO, acetone, ethanol and toluene in air, and assumed a response mechanism involving reaction of the gas with doubly occupied oxygen surface states (O^{2-}_{ads}). In the first reaction, atmospheric oxygen adsorbed from the air becomes chemisorbed to the surface, consuming the electron.

$$1/2O_2 + 2e \rightarrow O^{2-}_{ads} \qquad [3.2]$$

$$CO + O^{2-}_{ads} \rightarrow CO_2 + 2e^- \qquad [3.3]$$

Scheme 3.1. Simple formal model for sensor response

The conductivity is decreased as a result of this ionosorption of oxygen. The change in conductivity is dependent upon the rate constants for the surface reactions **[3.2]** and **[3.3]**.

In the case of an *n*-type semiconductor (i.e. SnO_2, ZnO, TiO_2, WO_3) ***(See Figure 3.5a)***, electrons come from ionised donors via the conduction band and therefore, the charge carrier concentration at the interface is reduced and an electrical potential barrier to charge transport, ΔG, is developed. As the surface charge grows, the adsorption of further oxygen is prohibited, the adsorption rate slows down because the charge must be transferred from the conduction band to the adsorbate over the developing surface barrier, and the coverage saturates at a rather low value.[21] Finally, the adsorption comes to a stop as the charge transferred to an adsorbate encounters a surface barrier.[22] At the junctions between the grains of the solid, the depletion layer and related potential barrier give rise to high resistance contacts, which control the resistance of the solid ***(See Figure 3.5c)***.[21]

Based on the above description, it can be said that, semiconducting oxides act as gas sensitive resistors showing change in the resistance as a consequence of any alteration of the quantity of charge trapped at the surface caused by the presence of a reactive gas. The introduction of a reducing gas such as CO ***(See Reaction [3.3])*** leads to the release of electrons trapped on the oxygen which are returned to the oxide (i.e. surface coverage of adsorbed oxygen ions is decreased), leading to a resistance decrease in *n*-type oxides; this is the consequence of the reduction in both surface potential barrier height and depletion length.

In a *p*-type semiconducting oxide, ***(See Figure 3.5b)*** the adsorbed oxygen forms an acceptor state at the surface that is able to remove electrons from the valence band resulting to an increase in the charge-carrier (hole) concentration at the interface. In this case the introduction of a reducing gas (i.e. by reaction **[3.3]**) decreases the surface coverage of oxygen ions and the charge carrier concentration and thus leads to an increase in the resistance of the material.

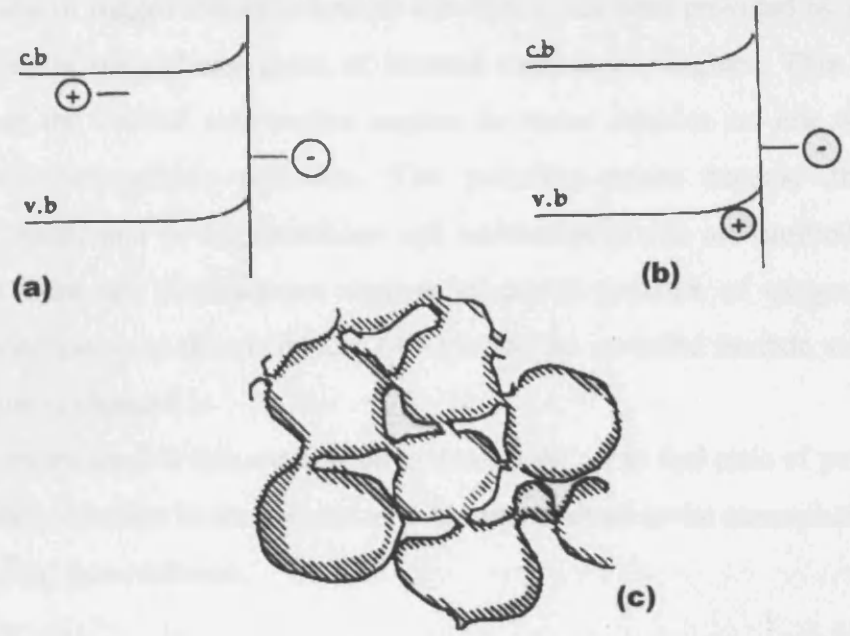

Figure 3.5 (a) n-type oxide: adsorption decreases the charge carrier density at the interface. The surface charge is balanced by the charge carried on the ionised donors. (b) p-type oxide: adsorption increases the charge carrier density at the interface. The charge is balanced by additional holes in the valence band. (c) Schematic representation of grain structure in a porous solid. In an n-type oxide the shaded areas represent the zones depleted of charge carriers. The grain junctions represent either higher resistance paths or Schottky barriers. In a p-type oxide, the shaded areas represent zones which the charge carrier (hole) concentration is higher. The grain junctions may still control the resistance of the solid, but by virtue of their small size.

[P. T. Moseley and A. M. Stoneham, in *Techniques and Mechanisms in Gas Sensing*, ed. P. T. Moseley, J. O. W. Norris and D. E. Williams, Adam Hilger., Bristol, 1991, p.120]

Therefore, materials can be classified as *n*-type or *p*-type according to their resistance response in the presence of a reducing or an oxidising gas in an atmosphere of fixed oxygen partial pressure as shown in ***Table 2.4***.[23]

Table 3.1 Resistance responses expected for reducing and oxidising gases on *n*-type and *p*-type semiconducting oxides

MATERIAL	REDUCING GASES	OXIDISING GASES
n-type	Resistance falls	Resistance rises
p-type	Resistance rises	Resistance falls

3.5.2 Bulk Conductance Effects

Another type of application of oxides is the monitoring of atmospheres in which the fundamental parameter of interest is the partial pressure of oxygen. The main impetus for

the development of rugged low-cost sensors for oxygen has been provided by the need to monitor oxygen in the exhaust gases of internal combustion engines. This is because emissions from the internal combustion engines in motor vehicles are one of the main contributors to atmospheric pollution. The pollution arises because the fuel is incompletely burnt, and so hydrocarbons and carbon monoxide are emitted. In such environments there are simultaneous changes of partial pressure of oxygen and of a number of other gases, as the air to fuel (*A/F*) ratio (the so-called lambda value) in the ignition mixture is changed.

Oxygen sensors are used in this application to control the air to fuel ratio of petrol fuelled engines. A huge reduction in the amount of pollutants emitted to the atmosphere has been obtained by using these sensors.

Materials that respond to changes in oxygen partial pressure in the temperature range of 700°C and above are reflecting the equilibrium between the composition of the atmosphere and their bulk stoichiometry. The first material studied for use as a bulk equilibration sensor oxygen was titanium dioxide (*n*-type).[19] In addition, several other oxides with perovskite crystal structure (eg. doped barium and strontium ferrates) have been found to exhibit sufficient oxygen sensitivity of conductance and activation energy near to zero that are useful in the construction of oxygen sensors.[24]

3.6 Microstructure Effect on Response of Gas Sensitive Resistors

The previous section has explained how a gas molecule present in the ambient environment in small concentrations interacts with a semiconductor gas surface leading to surface physical processes (i.e. sensor resistivity) that give rise to a change in the electrical resistance of the semiconductor. These alterations in the surface physical processes are believed to be affected by the microstructure and the semiconductive properties of the oxide.

An overview of the literature in terms of the effects of sensor microstructure on gas response is given below:[25,26]

- The behaviour of the devices is determined by the effect of the gas on the dimension and conductance of a thin layer of altered conductivity at the interface between the individual particles and the gas. Thus, one set of interpretation has

been in terms of the relative dimension of crystallites, or necks between crystallites, and the Debye length in the solid ***(Section 3.6.1)***.

- Similarly, the conductance of an array of overlapping particles of variable size is determined by the connectivity of the network of particles. A porous particle network remains sensitive to changes of conductivity in a thin surface layer even when the thickness of this layer is very small relative to the particle size and even when the porosity is relatively small ***(Section 3.6.2)***.

- Another formulation has considered the effects of the reaction and diffusion within the porous microstructure: the gas causing the change of conductivity could be catalytically burnt on the particle surface, so that a gradient of gas composition and hence conductivity could exist through the sensor layer. This is reflected in the measured conductance in a complex way dependant on the geometry of the electrodes ***(Section 3.7)***.

3.6.1 Particle Size and Design of Gas Sensitive Resistors

The grain size of the solid and the geometry of the connection between the particles affect the surface physical processes. Many models accounting the effects of grain sizes have been proposed in the literature.[27,28] Different mechanisms of conduction control arise, depending on whether the grains are partially or completely depleted of carriers, and on the relative Debye length (D), compared with twice the size of the crystallite, $2L$. The depletion layer describes the region where the positively charged donor ions in the semiconductor are uncompensated. Debye length (D) is the region over which the depletion layer extends.

Due to the granular structure of porous solids, there will be lower resistance paths through the bulk of the crystallite, with higher resistance constrictions at the points of contact of the grains. Beekmans[28] suggested the idea that the conduction of electrons through an oxide powder could be limited by the presence of necks between grains. A model has been formulated by Tamaki et al.[29] that takes into account the necks and grain boundary contacts. Their model consists of a 1-D chain of SnO_2 particles with a large number of necks and a small number of grain boundary contacts. Three cases can be distinguished

according to the relative magnitude of the crystallite size, *L*, and the Debye length, D. ***Figure 3.6*** illustrates three models accounting for grain size effects.[30]

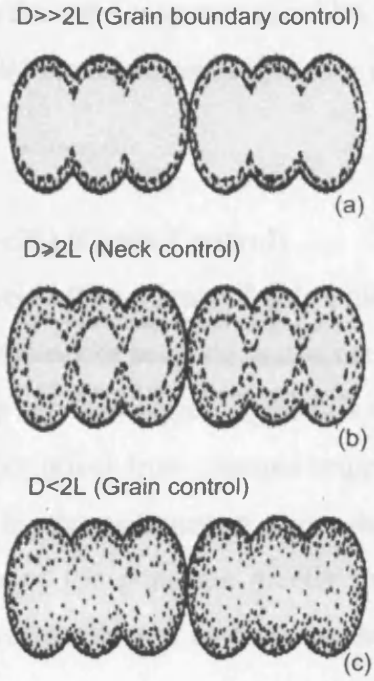

Figure 3.6 A comprehensive model accounting for grain size effects. Shaded parts show core region (low resistivity), while unshaded parts indicate space charge region (high resistivity)

[N. Yamazoe and N. Mivra, in *Chemical Sensor Technology.*, ed. S. Yamanchi, Kodansha Ltd and Elsevier Science Publishers, Amsterdam, 1992, Vol 4, p. 19.]

3.6.1.1 Well Sintered (*D>>2L*) (Grain Boundary Control)

This situation applies to systems that have been well sintered. In this case ***(See Figure 3.6a)*** the neck between adjacent grains is wide enough that an undepleted layer is available between the grains. In this case the conductivity is controlled by the undepleted layer (electron channel) in the centre of the neck.

3.6.1.2 Closed Neck (*D≥2L*) (Neck Control)

The depletion layer from the two surfaces is larger in comparison to the crystal size and therefore they overlap, leaving a high resistance path between grains ***(See Figure 3.6b)***. This situation arises from less complete sintering which causes narrow necks, or it can arise from an open neck being constricted by changes in the composition of gaseous atmosphere, which leads to a change in the depletion layer thickness and thus the neck width. The number of necks in the chain is greater than the number of grain boundary

contacts, so the resistances of the necks in the chain determine the resistance of the entire element.

The situations described in ***Figure 3.6a*** (open) and ***Figure 3.6b*** (close) imply that a porous body would respond in the same way as a thin film gas sensor, where ***Figure 3.6c*** (Schottky Barrier) shows a third situation applicable in a porous mass, but not in a thin film sensor.

3.6.1.3 Schottky Barrier ($D<<2L$) (Grain Control)

The final model Schottky Barrier ***(See Figure 3.6c)*** applies to porous bodies only and studies the situation in which the necks between grains become shorter and narrower and the formation of contact points between adjacent grains is also followed by the formation of Schottky barriers. The barrier arises from charged trapped in the surface states. Here, conductivity would be limited by charge transport across the barrier. In this case D is very small so the resistance values of the grain are greater than the resistance of the neck region and thus the electrical resistance and both the gas sensitivity are controlled by the grain size.

All these different cases mentioned above lead to a difference in the sensitivity of the semiconducting oxides to the gas. Optimum sensitivity of the oxide to the gas is achieved when L is less than or equal to the space charge thickness (D). It should be noted that, it is implausible that any real material will contain one type of intergranular contact exclusively.

3.6.2 A Simple Equivalent Circuit Model of Microstructure

In the literature, it has been noted that the conductivity response of a semiconducting oxide to the presence of a reactive gas, could be described in the form of power law, with the response power being an irrational decimal, varying from one sensor to another.

The sensor response law gives the relation between the local conductivity and the local gas concentration; in general, for devices with resistance increase:

$$R_g / R_o = 1 + A_g C_g^{\beta} \qquad [3.4]$$

where, R_g is the resistance in dry gas of concentration C_g, R_o is the baseline resistance in dry air in the absence of the target gas, β is the response power (exponent) and A_g denotes the sensitivity in dry gas.

The sensor response is characterised by the sensitivity (prefactor), A_g, and the response power, β. Both A_g and β vary widely between different preparations of a given material in response to a given gas, and their relative value for different gases can also be changed dramatically by change of the sensor microstructure.

Chabanis et al.[26] studied a simple three-element resistance network model to simulate effects of microstructure on response using sensors prepared with deliberately different, widely varying microstructure. Their study showed that it is possible to understand the observed wide range of variations in β, to distinguish specific effects due to the gas, to distinguish the effects of microstructure variations through the thickness of the sensor layer, and to differentiate the consequence of reaction-diffusion effects from those of variable microstructure. They showed experimentally that, for a given gas, whilst A_g and β in equation change drastically with alteration of the microstructure, A_g and β are correlated in a way which depends upon the gas. Their study involved the use of a simple series-parallel equivalent circuit model for the sensor in which only one of the elements is gas-sensitive. They showed that the gas-sensitive resistance elements follow equation **[3.4]** with β a rational fraction, and that the model's behaviour approximates equation **[3.4]** with β irrational. If the relative values of the circuit elements were changed, then a correlated variation of A_g and β was found. The form of this correlation was explored and its dependence on the parameters of the equivalent circuit used to deduce some conclusions concerning the sensor microstructure and the interaction of the gas with the solid.

3.6.2.1 Simulation of Sensor Behaviour where the Gas Response is a Resistance Increase

The modelling approach was based on the modelling of the sensor as an array of 'domains' (which might be single particles or particle agglomerates) separated by 'connections'.

Figure 3.7 shows the result of fitting equation **[3.4]** to the computed gas response of a three-element circuit, shown in ***Figure 3.7***, in which the 'connections' are represented by a gas-independent resistance (R_1) whilst the 'domains' are represented as a parallel combination of a gas-sensitive and a gas insensitive resistance. The gas-sensitive element

has resistance $R_2 = R_2^0(1+P_{rel})$. The correlation of response exponent, β, and prefactor, A_g, and its dependence on conductance ratios, which would vary with variation of the microstructure, is shown in ***Figure 3.7.*** The behaviour is determined by the two parameters $S' = \sigma_3/\sigma_1$ (describing the relative importance of the gas-insensitive series element) and $Q=\sigma_3/\sigma_2^0$ (describing the relative importance of the gas-insensitive parallel element). The response exponent is determined by Q and the prefactor is determined by S'. The conclusion from ***Figure 3.7*** is that the prefactor (A_g) and exponent (β) are correlated in a way which depends upon the network parameters S' and Q. The effects of the two parameters are interlinked. Low values of β are associated with high values of Q (i.e. with high values of the gas-insensitive parallel conductance). Low values of A_g are associated with high values of S' (i.e. with low relative values of gas-insensitive series resistance).[26]

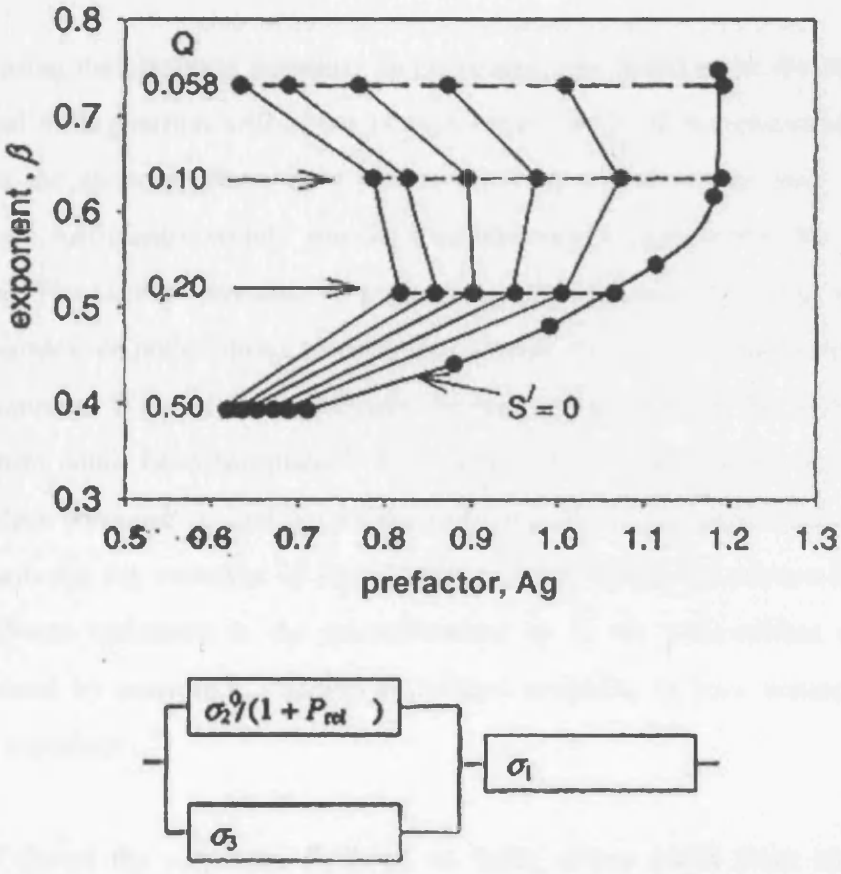

Figure 3.7: Gas response, represented according to equation 3.4, of the series-parallel circuit shown with conductance, σ, decrease (resistance, R, increase). Fitted parameters A_g and β as a function of the conductance ratios $S' = \sigma_3/\sigma_1$ and $Q = \sigma_3/\sigma_2^0$. Points are for $S' = 0, 0.01, 0.02, 0.03, 0.04, 0.05$

[G. Chabanis, I. P. Parkin and D. E.Williams, *Meas. Sci. Technol.*, 2003, **14**, 76]

3.7 Reaction-Diffusion Effects: Multi-Electrode Arrays

This section describes the effect of reaction and diffusion within the porous microstructure and proposes another way of dealing with the increased demand of selectivity enhancement with the use of a single device with an array of electrodes of different geometry. [4]

Semiconducting oxide sensors are fabricated as finely porous ceramic bodies. The target gas, being in air, diffuses through the body of the oxide and decomposes on the heated sensor surface as a consequence of the detection mechanism ***(Scheme 3.1)***. Under these circumstances the concentration of oxygen is considered to be constant, but the concentrations of the target gas and its decomposition products vary with position inside the sensor body. If the sensor material has a conductivity which changes in response to changes in the concentration of the target gas or of its decomposition products, then the conductivity of the material will vary with position within the oxide layer. [30]

Therefore, using the electrode geometry as the means, one could probe the variation of the sensor signal with position within the porous sensor body. If the electrodes are closely spaced then the electrons flow, only probes the base of the sensor layer, whilst if the electrodes are sufficiently widely spaced, then the current flow probes the whole of the sensor layer. The current can also be pushed out into the layer by using widely spaced (large) electrodes, or pulled down towards the base of the layer by using narrowly spaced (small) electrodes. With this measurement the rate constant (k) for the surface-catalysed decomposition could be determined.[30] This should be a characteristic parameter of the gas, the surface composition and the temperature, and therefore can be used to identify the gas. Alternatively, the variation of signal with position within the porous body could be used to indicate variations in the microstructure or in the composition of the sensor surface (caused by poisoning, changes in relative humidity or as a consequence of the fabrication technique). [4]

Figure 3.8 shows the response, R_o/R, of an SnO_2 sensor (with three electrode gaps) operated at 625°C as a function of CH_4 concentration. The graph demonstrates that the response increases with electrode gap as a consequence of the concentration gradient of the gas within the porous sensor body.

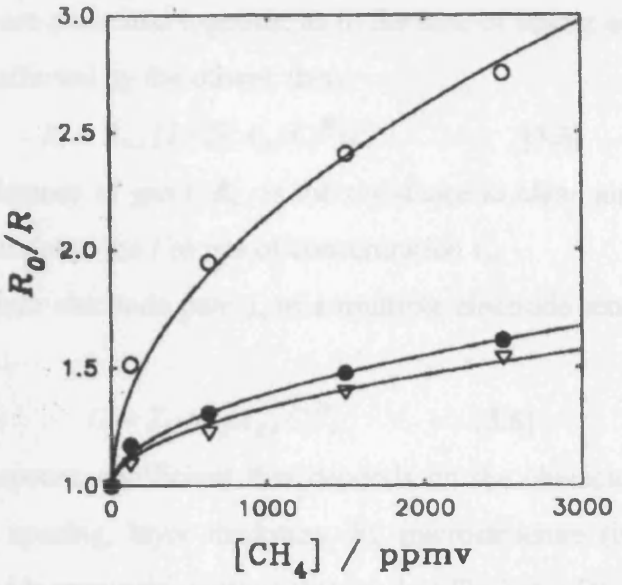

Figure 3.8 The response, R_o/R, of an SnO_2 sensor operated at 625°C as a function of CH_4 concentration. The response of the three electrode gaps, wide (O), medium (•) and narrow (▼) are fitted to Eq. (3.4) as shown by the solid lines. The response increases with electrode gap as a consequence of the concentration gradient of the gas within the porous sensor body.

[D. E. Williams, *Sensors and Actuators B.*, 1999, 57, 1]

3.7.1 Theory to Describe the Measured Conductivity of Multiple Electrode Devices

Williams and Pratt[31] developed a simple model for multiple electrode devices, in which the porous sensor layer was treated as a homogeneous medium. The general principle of this model is that the target gas diffuses into the porous sensor structure and is decomposed by a surface catalysed oxidation. If the gas decomposition is of first order in the target gas with apparent rate constant (k) then, the concentration profile is characterised by the dimensionless ratio $K_T = kh^2/D$. Here, h is the porous oxide layer thickness, k denotes combustion rate constant, and D denotes the gas diffusivity within the porous layer. The parameter D is dependent on the microstructure and k upon the internal surface area.

Based on the treatment of the oxide layer as an effective medium of spatially variable conductivity, the measured resistance for various assumed geometries of the sensor and electrodes can be calculated.

Jones et al.[32] in 1989, proposed the idea that a single device, having an array of electrodes of different geometry was functionally equivalent to an array of different sensors.

If a number of gases are presented together, as in the case of sensor arrays, the response to each is linear and unaffected by the others, then:

$$R_i = R_{o,i}\,[1+\Sigma(A_{g,i}\,C_i^{\beta i})] \qquad \textbf{[3.5]}$$

Here, R_i denotes resistance of gas i, $R_{o,i}$ is the resistance in clean air, $A_{g,i}$ is the response coefficient of the material to the i*'th* gas of concentration C_i.

The response from each electrode pair, j, of a multiple electrode sensor can be written in the form:[31]

$$G_j = \Sigma_{ij}\,(a_{i,j}\,A_{g,i}\,C_i^{\beta i}) \qquad \textbf{[3.6]}$$

In which, $a_{i,j}$ is a response coefficient that depends on the characteristics of the sensor geometry (electrode spacing, layer thickness, h), microstructure (internal surface area, porosity) and the gas (decomposition rate constant, k, diffusivity, D).

Equation **[3.6]** demonstrates that the multi-electrode sensor behaves just like a sensor array, with the important difference that the response coefficients of the different electrode pairs in the multi-electrode device, $a_{i,j}$, can be tailored by adjustment of the geometry and combustion kinetics, and are, furthermore, related to one another. The device is self-diagnostic in that temporal or spatial variations of $a_{i,j}$ can, in certain circumstances, be detected.

The detection of sensor poisoning by this means has been demonstrated several times.[3,5,33,34] For example, ***Figure 3.9a*** shows a diagram of the conductance measured using the narrow electrode spacing plotted against the conductance measured with the wide electrode spacing for a clean and a poisoned sensor. In this case, the wide (large) gap is configured to detect conductance changes through the whole of the sensor thickness where the narrow (small) gap is configured just to detect changes at the base of the sensor layer, near the electrodes. For a given value of the target gas concentration, the resulting point on the diagram could be called the operating point for the sensor. Thus, the signals from the two different gaps define an operating line for the sensor; this is the line along which the operating point defined by the two signals moves if the only variable is the target gas concentration.[31]

If the response is the same on the two gaps, as would be the case if there is no concentration gradient of gas within the sensing structure, then the operating line will be at an angle of 45° to the axes. If there is a concentration gradient of gas due to reaction

within the layer, then the gas concentration seen by the small electrode gap will be less than that seen by the large gap. In this case an operating line steeper than 45°C will be observed. Then, the angle of the operating line effectively gives a measure of the reactivity of the gas within the sensing layer (i.e. the concentration gradient).

If there were to be some variation, other than variation of the target gas concentration (as in this case sensor poisoning), affecting the conductivity of the sensor material, the operating point would move off the operating line. As ***Figure 3.9b*** demonstrates, the effect of poisoning is to shift the operating line. This condition could therefore be detected and distinguished from a variation of target gas concentration and therefore a fault could be indicated. The same idea can be used to distinguish the effects of variation of relative humidity from the effects of variation of target gas concentration. ***Figure 3.10*** represents the operating lines for wet and dry conditions. The operating line is shifted by a change in relative humidity.[31] Since the relative responses of the two electrode gaps are different for different gases, it should be possible to distinguish pairs of gases. An example of this is shown in ***Figure 3.11*** for a CTO ($Cr_{1.8}Ti_{0.2}O_3$) sensor. In this case, all three operating lines are different hence all gases can be distinguished.[7]

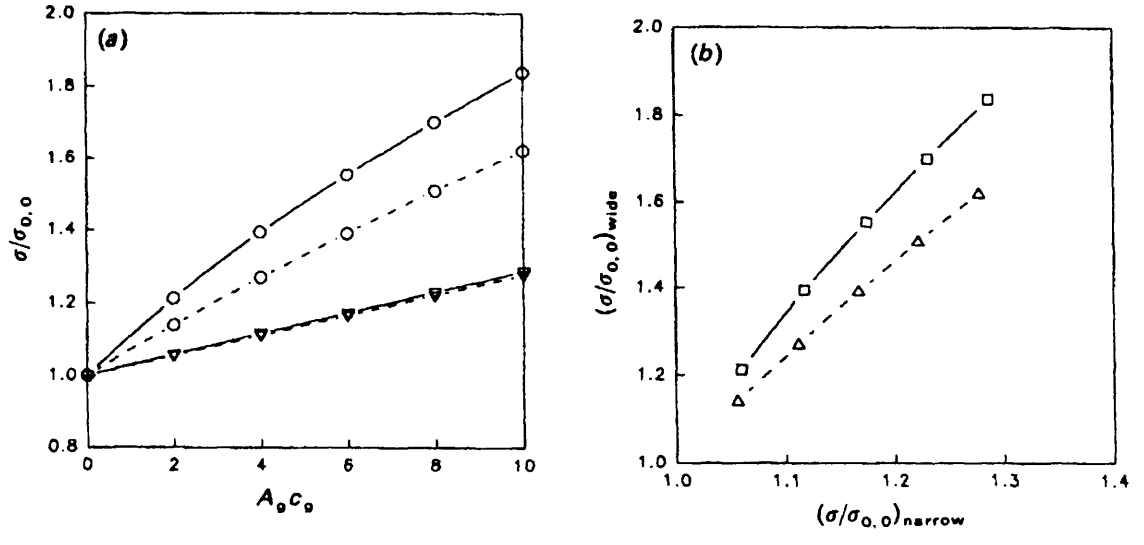

Figure 3.9 (a) Concentration dependence of the normalized conductance $\sigma/\sigma_{0,0}$, for clean (—) and poisoned (----) sensors, for the kinetic parameter $kh^2/D=20$ and $\beta=1$. a/h; (∇) 0.2, (O) 1; the outer 10% of the sensor layer is considered "poisoned". (b) Operating lines plotted as the normalized conductance for the wide electrode spacing *vs.* that of the narrow spacing

[D. E. Williams and K. F. E. Pratt, *J. Chem. Soc. Faraday Trans.*, 1995, **91**(13), 1961]

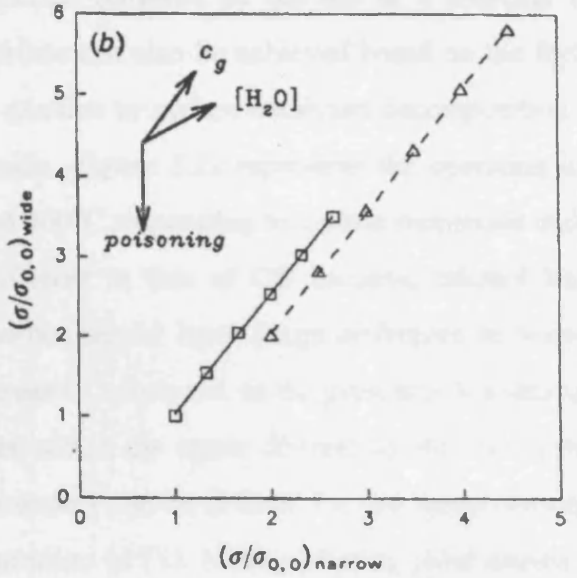

Figure 3.10 Operating lines plotted as the normalized conductance for a wide electrode spacing Vs that of the narrow spacing. The inset "signpost" shows the directions of movement caused by gas concentration, humidity and poisoning
[D. E. Williams and K. F. E. Pratt, *J. Chem. Soc. Faraday Trans.*, 1995, **91**(13), 1961]

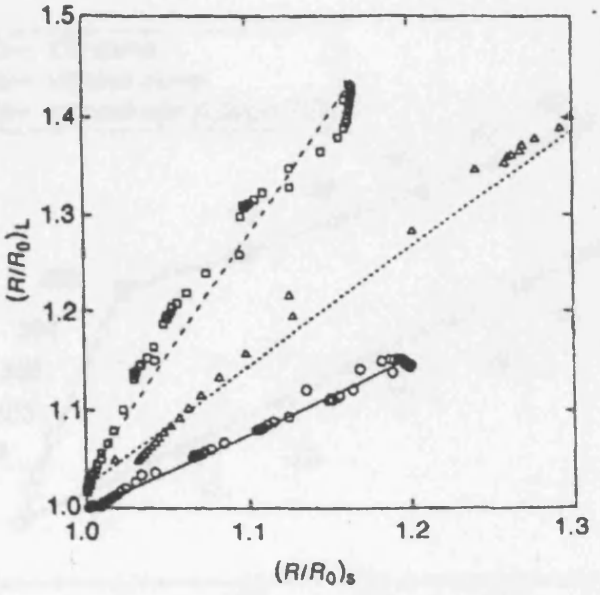

Figure 3.11 Operating lines for CO (—O—), acetone (--□--) and toluene (--△--) on platinised $Cr_{1.8}Ti_{0.2}O_{3+y}$, showing the possibility of distinguishing all three gases.
[D. E. Williams and K. F. E. Pratt, *J. Chem. Soc. Faraday Trans.*, 1996, **92**(22), 4497]

A potential widespread application of semiconducting oxide sensors with multiple electrodes, is the detection of dangerous levels of carbon monoxide in domestic applications. In this type of application the major interferences, apart from the effect of relative humidity changes, come from volatile organics such as ethanol and solvents.

These interferences can be removed by the use of a charcoal filter above the sensor. Resolution of the interface can also be achieved based on the fact that ethanol and many solvents are far more reactive to surface-catalysed decomposition at elevated temperature than is carbon monoxide. ***Figure 3.12*** represents the operating lines for multi-gap CTO ($Cr_{1.8}Ti_{0.2}O_3$) sensor at 400°C responding to carbon monoxide and ethanol. The operating line for ethanol is different to that of CO because, ethanol has a large concentration gradient within the porous sensor layer (large difference in response between large and small electrodes) whereas CO does not. In the presence of a mixture of the two gases, the operating point moves within the space defined by the two lines (the CO line and the ethanol line), and a boundary can be defined for this space corresponding to the presence of a hazardous concentration of CO. If the operating point moves above this line, then an alarm should sound. If the operating point should moves across either of the two boundaries (the CO line and the ethanol line) then the sensor indication would not be reliable, and a warning could be given.[7]

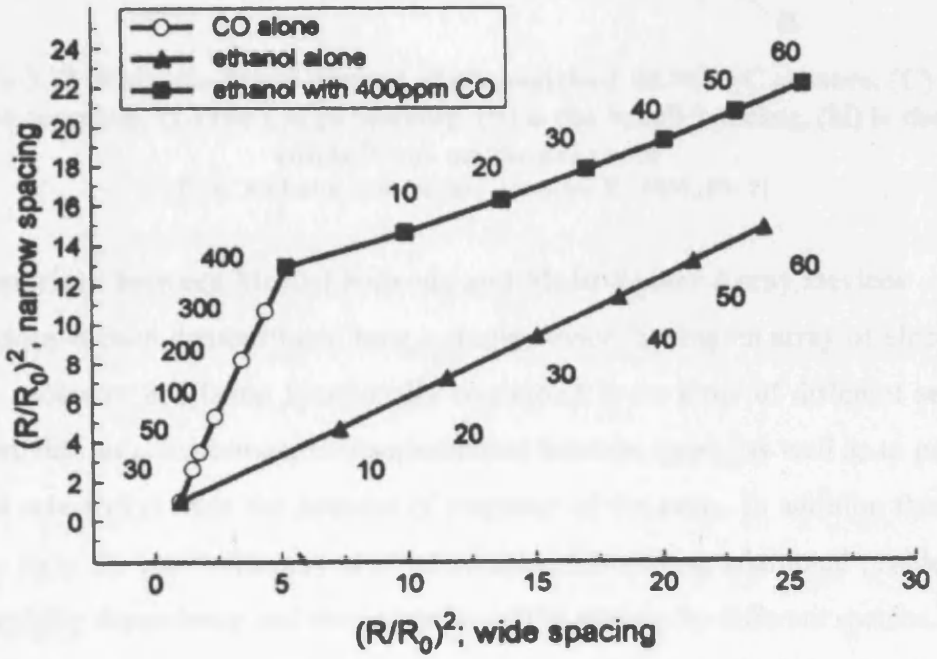

Figure 3.12 Operating lines for multi-gap CTO devices at 400°C to ethanol and carbon monoxide. Labels: gas concentration ppm^{-1}.
[D. E. Williams, *Sensors Actuators B.*, 1999, 57, 1]

Williams et al.[3,7,31] have described various designs for devices with multiple electrode spacing. One example is a SEMDEC device, which has a common electrode and two sets of electrode gaps (small, large) all on one sensor ***(See Figure 3.13)***. The SEMDEC

substrates were photoetched by Capteur Sensors and Analysers Ltd. A typical SEMDEC device has an array of electrodes of different geometry i.e. 30 μm narrow (small) gap and 200μm wide (large) gap electrodes.

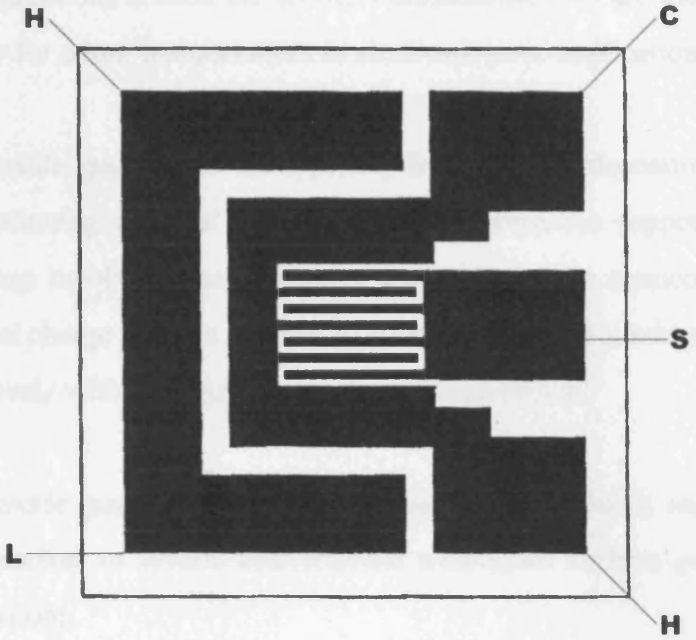

Figure 3.13 Multi-electrode designs of photoetched SEMDEC sensors. (C) is the Common terminal, (L) the Large Spacing, (S) is the Small Spacing, (H) is the Heater connections on the near side

[D. E. Williams, *Sensors and Actuators B.*, 1999, **57**, 1]

3.8 Comparison between Multi-Electrode and Multi-Sensor Array Devices

The previous section demonstrated how a single device, having an array of electrodes of different geometry and being functionally equivalent to an array of different sensors, is able to provide an enhancement in discrimination between gases (as well as to provide an increased selectivity) from the patterns of response of the array. In addition these multi-electrode array devices were proved to be valuable for solving additional problems such as the humidity dependency and the poisoning of the devices by different species.

Taking all the above issues into account, it can be said that multi-electrode sensor array devices (with reduced number of sensors) are more suitable for use in electronic nose applications instead of multi-sensor array devices. This is because, they provide an enhanced selectivity, calibration stability, manufacturing reproducibility (due to the effects of microstructure on the response), and can detect the humidity dependency problem and the poisoning of the devices by different species.

3.9 Conclusion

Gas sensors based on the conductivity change in semiconducting oxides play a critical role in many important industrial and domestic applications. They are used constantly in monitoring and controlling air pollution in the environment as well as in various domestic and industrial installations around the world. Furthermore, they are the most widely used sensor technology for odour measurement in electronic nose applications.

Semiconducting oxide gas sensors are typically fabricated by depositing a highly porous layer of semiconducting material across a pair of electrodes supported on a ceramic substrate. Reactions involving gas molecules take place at the semiconductor surface to alter the density of charge carriers that are available. Thus, the conductance of the device changes progressively with changing atmospheric composition.

Semiconducting oxide gas sensors are easy to use, highly durable and inexpensive and offer viable alternatives to several conventional techniques such as gas chromatography and infrared absorption.

However, there are a number of problems associated with most of the devices that are based on one pair of electrodes. They generally tend to be sensitive to too many gases, suffer from slow baseline drift and they are affected by variations in humidity and can be poisoned by many species. The development of new sensing materials and the use of multi-electrode sensing devices have showed valuable improvements in selectivity and solved many operating problems regarding these sensors.

Although extensive advances have been made in the sensor technology, further developments are needed to optimise the performance of metal oxide semiconductor sensors, especially with regards to selectivity improvements.

Chapter 3

References

1. T. Seiyama, A. Kato, K. Fulishi and M. Nagatani, *Anal. Chem.*, 1962, **34,** 1502.

2. A. Chiba, in *Chemical Sensor Technology,* ed. S. Yamauchi, Kodansha., Tokyo, 1992, Vol. 4, p.1.

3. D. E. Williams, G. S. Henshaw and K. F. E. Pratt, *J. Chem. Soc., Faraday Trans.*, 1995, **91**(18), 3307.

4. D. E. Williams, *Sensors Actuators B.*, 1999, **57,** 1.

5. K. F. Pratt and D. E. Williams, *Sensors Actuators B.*, 1997, **45,** 147.

6. H. Bosch, and F. Janssen, *Catal. Today.*, 1988, **2**, 369.

7. D. E. Williams, G. S. Henshaw, K. F. E. Pratt and R. Peat, *J. Chem. Soc., Faraday Trans.*, 1995, **91**, 4299.

8. D. E. Williams and K. F. Pratt, *J. Chem. Soc. Faraday Trans.*, 1996, **92**(22), 4497.

9. D. H. Dawson, G. S. Henshaw and D. E. Williams, *Sensors Actuators B.*, 1995, **26,** 76.

10. P. T. Moseley, *Sensors Actuators B.*, 1992, **6**, 149.

11. M. Fleischer and H. Meixner, *Sensors Actuators B.*, 1995, **26,** 81.

12. G. Sberveglieri, L. Depero, Gropelli and P. Nelli, *Sensors Actuators B.*, 1995, **26,** 89.

13. U. Lampe, J. Gerblinger and H. Meixner, *Sensors Actuators B.*, 1995, **26,** 97.

14. D. F. Shriver, P. W. Atkins and C. H. Langford, in *Inorganic Chemistry*, ed. Oxford University Press., Oxford, 1994, p.98.

15. H. Nanto, T. Minami and S. Tanaka, *J. Appl. Phys.*, 1986, **60**, 482.

16. R. Morrison, *Sensors and Actuators.*, 1987, **11**, 283.

17. T. Moseley, Material Selection for Semiconductor Gas Sensors, *Eurosensors Conference.*, Rome, Italy, 1991.

18. A. M. Azad, S. A. Akbar, S. G. Mhaisalkar, L. D. Birkefeld and K. S. Goto, *Electrochem. Soc.*, 1992, **139**, 12.

19. P. McGeehin, P. T. Moseley and D. E. Williams, *Sensor Review.*, 1994, **14**(1), 13.

20. D. E. Williams and K. F. E. Pratt, *Sensors Actuators B.*, 2000, **70,** 214.

21. P. T. Moseley and A. M. Stoneham, in *Techniques and Mechanisms in Gas Sensing*, ed. P. T. Moseley, J. O. W. Norris and D. E. Williams, Adam Hilger., Bristol, 1991, p.120.

22. B. Weisz, *J. Chem. Phys.*, 1953, **21**, 153.

23. A. M. Stoneham, in *Solid State Gas Sensors*, ed. P. T. Moseley and B. C. Tofield, Adam Hilger., Bristol, 1987, p.151.

24. P. Kofstad, in *Non-stoichiomertry, Diffusion and Electrical Conductivity in Binary Metal Oxides*, ed. Wiley Interscience., New York, 1972.

25. D. E. Williams and K. F. E. Pratt, *Sensors Actuators B.*, 2000, **70,** 214.

26. G. Chabanis, I. P. Parkin and D. E. Williams, *Meas. Sci. Technol.*, 2003, **14**, 76.

27. N. Barsan, *Sensors and Actuators.*, 1994, **17**, 241.

28. N. M. Beekmans, *J. Chem. Soc. Faraday Trans. I.*, 1978, **74,** 31.

29. C. Xu, J. Tamaki, N. Miura, and N. Yamazoe, *Sensors and Actuators.*, 1994, **17**, 241.

30. A. M. Stoneham, in *Solid State Gas Sensors*, ed. P. T. Moseley and B. C. Tofield, Adam Hilger., Bristol, 1987, p.93.

31. D. E. Williams and K. F. Pratt, *J. Chem. Soc. Faraday Trans.*, 1995, **91**(13), 1961.

32. C. P. Jones, P. T. Moseley and D. E. Williams, *UK Pat.*, 2 218 523, 1989.

33. J. W. Gardner, *Sensors Actuators B.*, 1995, **27**, 261.

34. D. E. Williams, *UK Pat.*, 92 21018, 1992.

Chapter 4

Introduction to Zeolites

4.1 Introduction

Microporous solids (pore diameter $\leq$ 2nm), typically based on aluminosilicate or aluminophosphate frameworks, are crystalline materials, which possess a 3-D open framework structure with molecular sized cavities.

Zeolites are a well-defined class of open-framework crystalline aluminosilicates, which are both naturally occurring and synthetic. They have 3-D structures arising from a framework of $[SiO_4]^{4-}$ and $[AlO_4]^{5-}$ polyhedra linked by all their corners. The frameworks are generally very open and contain channels and cavities, of regular and molecular dimensions, in which cations and water molecules are located. A representative empirical formula of a zeolite is:

$$M_{2/n}O \,.\, Al_2O_3 \,.\, x\, SiO_2 \,.\, yH_2O \qquad \textbf{[4.1]}$$

where *M* represents the exchangeable cation of valence *n*. *M* is generally a Group *I* or *II* ion, although other metal, non-metal and organic cations may also balance the negative charge created by the presence of Al in the structure.[1]

Most zeolites are synthesized by dissolving a source of alumina and a source of silica in a strongly basic aqueous solution. Ultimately, the solubility, the SiO_2 /Al_2O_3 ratio, the nature of the cation and the synthesis temperature of the resultant gel determine what structure is formed.

4.2 The Structure and Pore Size of Zeolites

As stated earlier all zeolites have 3-D structures constructed by joining together $[SiO_4]^{4-}$ and $[AlO_4]^{5-}$ polyhedra. These tetrahedra are assembled together in such a way that the

oxygen at each tetrahedral corner is shared with that in another tetrahedron. This corner sharing creates infinite lattices comprised of identical unit cells. Since zeolite structures have identical (or very similar) repeating structural sub-units called "secondary building units" (sbus), which are less complex than their repeating unit cells, a classification can be made based on the symmetry of these unit cells. It must be noted that this classification denotes only the aluminosilicate skeleton (i.e. the Si, Al and O positions in space relative to each other) and excludes consideration of the cation and water motieties placed within the cavities and channels of the framework. ***Figure 4.1*** shows some subunits and cages that recur in several framework types.

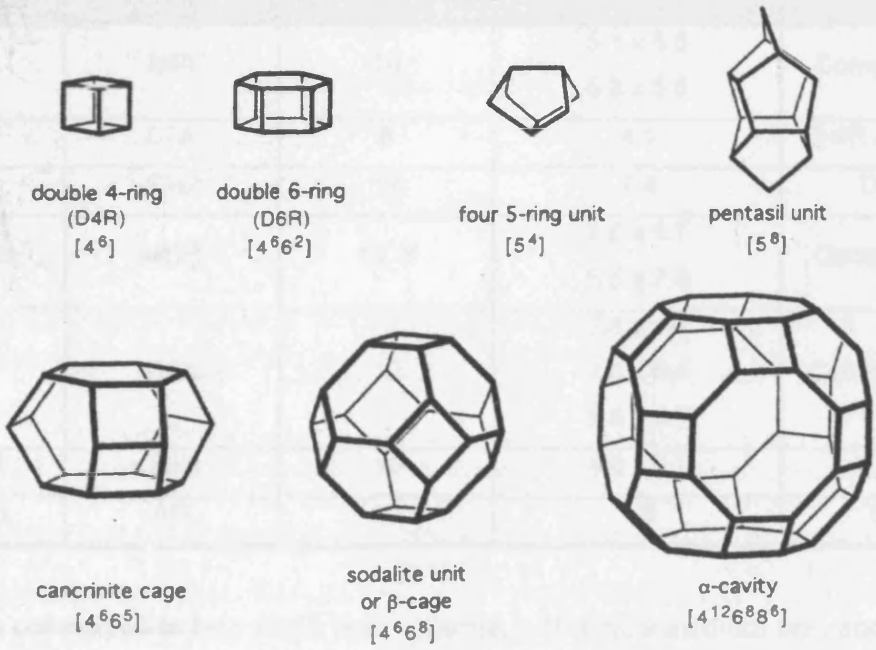

Figure 4.1 Some subunits and cages that occur in several framework types.
[H. Van Bekkum, E. M. Flanigen, P. A. Jacobs and J. C. Jansen, in *Introduction to Zeolite Science and Practice*, ed. Elsevier., Amsterdam, 2001, p.39]

The Structure Commission of the International Zeolite Association has compiled all known zeolites and other molecular sieve structures and has assigned official three letter codes for the known framework topology irrespective of composition.[2,3]

The codes are normally derived from the name of the zeolite or type material, e.g. FAU from the mineral faujasite, LTA from Linde Type A, and MFI from ZSM-5 (Zeolite Socony Mobil–five). Currently this database contains some 140 different structure-types.

As new codes are approved, they are announced on the IZA Structure Commission's web page.

Table 4.1 shows seven different types of zeolites, along with information about their structure type code, the number of oxygens in the aperture of each zeolite, the pore dimensions and the type of secondary unit that describes their structure.

Table 4.1 Zeolites and their pore (aperture) dimensions
[A. Dyer, in *An Introduction to Zeolite Molecular Sieves*, ed. John Wiley and Sons Ltd., New York, 1988, http://www.izastructure.org/databases/]

Zeolite Name	Structure Type (Code)	Number of Oxygens in the Ring	Aperture(pore) Dimensions, Å	Secondary building unit (sbu)
ZSM-5	MFI	10	5.1 x 5.5 5.3 x 5.6	Complex 5-1
A	LTA	8	4.1	D-4R (α-cage)
Y	FAU	12	7.4	D-6R
Mordenite	MOR	12, 8	2.6 x 5.7 6.5 x 7.0	Complex 5-1
Beta	BEA	12	7.6 x 6.4 7.6 x 6.4 5.5 x 5.5	Combinations
Theta-1	TON	10	4.6 x 5.7	6, 5-1
$AlPO_4$-5	AFI	12	7.3	6, 4

An 8-ring is considered to be a small pore opening, a 10-ring a medium one, and a 12-ring a large one, with free diameters (calculated using oxygen radius of 1.35 Å) of approximately 4.1, 5.5 and 7.4 Å, respectively. Of course rings can be distorted considerably so these numbers should only be used as a rough guide.

Figure 4.2 summarises the average channel sizes of some zeolites, along with the sizes of their cavities (supercages) and the critical molecular dimensions of a number of hydrocarbons that are potential reactants in zeolite catalysed reactions.

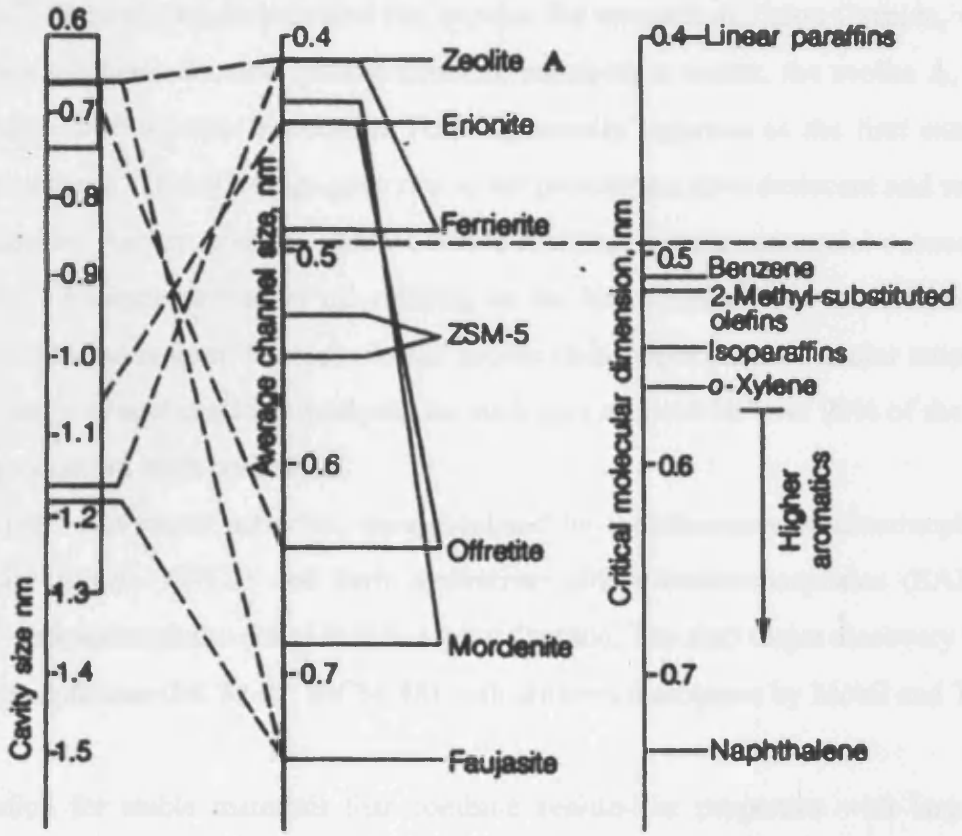

Figure 4.2 Pore dimensions and critical dimensions of some hydrocarbons
[E. G. Derouane, in *Intercalation Chemistry*, ed. M. S. Whittingham and A. J. Jacobson, Academic Press., New York, 1982, p.101]

4.3 Aluminium Content and Acidity

Zeolites are further grouped into families on the basis of composition, namely, the Si/Al ratio. Since the ion exchange capacity is equal to the concentration of Al^{3+} ions in the zeolite, the structures with low Si/Al ratios can have higher concentrations of catalytic sites than others.

Some examples of zeolites with low Si/Al atomic ratio (1-1.5) include Zeolites A and X. Chabazite, Mordenite, and the synthetic Y, MOR have intermediate Si/Al ratio (2-5) where zeolite beta and ZSM-5 have high ratio (~10-∞).

4.4 An Insight to Zeolytes' History and Research

In 1756 minerologists found zeolites in relatively small cavities in rocks of volcanic origin (a classical zeolite occurrence). Jewellery represented just about the only commercial interest in zeolite minerals for nearly 200 years. R.M. Barrer placed zeolite science on a firm physicochemical footing and furnished quantitative and theoretical descriptions of the ion exchange, dehydration and gas-sorptive behaviour of natural

zeolites.[4,5] Barrer's results provided the impetus for research at Union Carbide, where at 1949 they synthesised a new zeolitic structure unknown in nature, the zeolite A, by low-temperature hydrothermal processes. This is generally regarded as the first example of zeolite synthesis. Their findings gave rise to the present lucrative desiccant and molecular sieve market. Further work at Union Carbide resulted in the commercial success of the synthetic FAU-type zeolite in oil refining in the late 1950's.[6] The use of zeolites as catalysts was the biggest discovery in the zeolite field. Since then the major employment of zeolites is as acid cracking catalysts. As such they account for over 99% of the world's petrol production from crude oils.

In the 1980's, research activities were escalated by the discovery of aluminophosphate molecular sieves ($AlPO_4$) and their derivatives silicoaluminophosphates (SAPO) and metal aluminophosphates (MeAPO) by Union Carbide. The next major discovery was that of aluminosilicates (MCM-41, MCM-48) with uniform mesopores by Mobil and Toyota.[7]

The search for stable materials that combine zeolite-like properties with larger pores continues. The latest industrial focus in this area has been on fine chemical synthesis, for which DAF-4, DAF-5, SAPO-34, MAPO-36, MCM-41 all have distinct properties. The latest developments are in the use of organo-metallic chemistry to graft active sites onto the pore surfaces (e.g. Ti onto MCM-41), which changes the reactivity pattern in a very distinctive way, and to design new materials based on a computational approach to selection of templates for the synthesis, which has recently been pioneered.[6,8]

4.5 Properties of Zeolites

Zeolite compounds are materials with unique properties, which have become extremely successful as catalysts for oil refining, petrochemistry, and organic synthesis in the production of fine and speciality chemicals, particularly when dealing with molecules having kinetic diameters below 10 Å. The reason for their success in catalysis is related to the following specific features of these materials:[9,10]

1. They have very high surface area and adsorption capacity. They are used efficiently to adsorb a variety of materials. This includes applications in drying, purification, and separation.

2. The adsorption properties of the zeolites can be controlled, and they can be varied from hydrophobic to hydrophilic type materials.
3. Another characteristic zeolite property arising from their molecular framework structures is that they possess a wide variety of internal channel and cavity assemblages accessed through oxygen windows, which happen to be close in size to the dimensions of common organic and inorganic molecules (5-12 Å).
4. Zeolites are made catalytically active by the introduction of acidic or redox-active sites into their structure on the surface of the molecular cavities; the strength and concentration of these active sites can be tailored for a particular application.
5. Their intricate channel structure allows the zeolites to present different types of shape selectivity i.e. reactant, product and transition state, which can be used to direct a given catalytic reaction towards the desired product avoiding undesired side reactions.
6. All of these properties of zeolites, which are of paramount importance in catalysis, are ultimately dependent on the high thermal and hydrothermal stability of these materials. Such materials can be activated to produce very stable materials not just resistant to heat and steam but also to chemical attacks.

4.5.1 Ion Exchange

The aluminosilicate structure incorporates Si^{4+}, Al^{3+}, and O^{2-} ions. When some of the Si^{4+} ions in the SiO_4 tetrahedra in this framework are replaced by Al^{3+} ions, an excessive negative charge is generated. A compensating source of positive charge, such as cations, must be added. Therefore, zeolites function as ion exchangers by allowing the replacement of cations held in their aluminosilicate anion framework by ions present in the external solutions or melts. They are used as builders i.e. enhance the cleaning efficiency of detergents primarily by removing Ca^{2+} and Mg^{2+} ions present in the water by ion exchange with Na^{+},[11] wastewater treatment (including industrial, agricultural and radioactive)[12] and animal food supplementation (e.g., to regulate ammonia or ammonium levels in the stomach).

Cation exchange in a zeolite is accompanied by an alteration of stability, adsorption behaviour and selectivity, catalytic activity and other properties. In some cases, the

introduction of a larger or smaller cation will decrease or enlarge the pore opening. The location of that cation within the crystal will also contribute to the size of pore opening.

4.6 Zeolites as Shape Selective Catalysts

The most important application of molecular sieves is as catalysts. Zeolites combine high acidity with shape selectivity, high surface area and high thermal stability and are used to catalyse a variety of hydrocarbon reactions, such as cracking, hydrocracking, alkylation and isomerisation. The reactivity and selectivity of zeolites as catalysts are determined by the active sites brought about by a charge imbalance between the silicon and aluminium atoms in the framework. Each framework aluminium atom induces a potential active acid site.

Given that catalysis takes place largely within zeolite frameworks, access to this environment is controlled by the oxygen windows. This is a diffusion-limited process. This means that zeolites have very special practical advantages over the more traditional catalysts, in that they will admit only certain reactant molecules (rejection based on of their effective molecular dimensions) and that this can be potentially tailored to produce selected products. This selectivity, largely unique to zeolites, is known as shape selective catalysis "molecular sieving" and is controlled by configurational diffusion.

4.6.1 Reactant Shape Selectivity

Reactant shape selectivity results from the limited diffusivity of some of the reactants, which cannot effectively enter and diffuse inside the pores. If the diffusion of a bulkier reactant molecule inside the pores is hindered, the less bulky reactant molecule will preferentially react. In the limiting case, one kind of molecule may be too large to fit through the pores. This is the idea of molecular sieving whereby, for example, small molecules in a mixture may enter the pores and be catalytically converted whereas large molecules pass through the reactor unconverted.

A classic example of reactant shape selectivity is the cracking of straight and branched-chain paraffins in zeolite A. ***Figure 4.3(a)*** demonstrates that the straight-chain reactant fit inside the pores of zeolite A and is therefore selectively converted in the presence of this catalyst, whereas the branched-chain homologue is too large to enter the small pore zeolite A.[13]

4.6.2 Product Shape Selectivity

Product shape selectivity occurs when slowly diffusing product molecules cannot rapidly escape from the pores, and undergo secondary reactions.

This is essentially a function of the rates of diffusion of products away from the reactive sites, through the crystal pores and out of the crystallites. If the diffusion of the bulkier product molecule inside the pores is hindered, the less bulky molecule will be formed preferentially. The limiting case is a complete suppression of the formation of the bulkier molecule.

Perhaps the best known example of this type of selectivity is in the preferred alkylation of toluene to *p*-xylene over H-ZSM-5 shown in ***Figure 4.3(b)***. The diffusivity of the *para* isomer, in the zeolite, is much greater than that of the *o*- and *m*-xylene isomers and thus the *p*- isomer is formed preferentially.

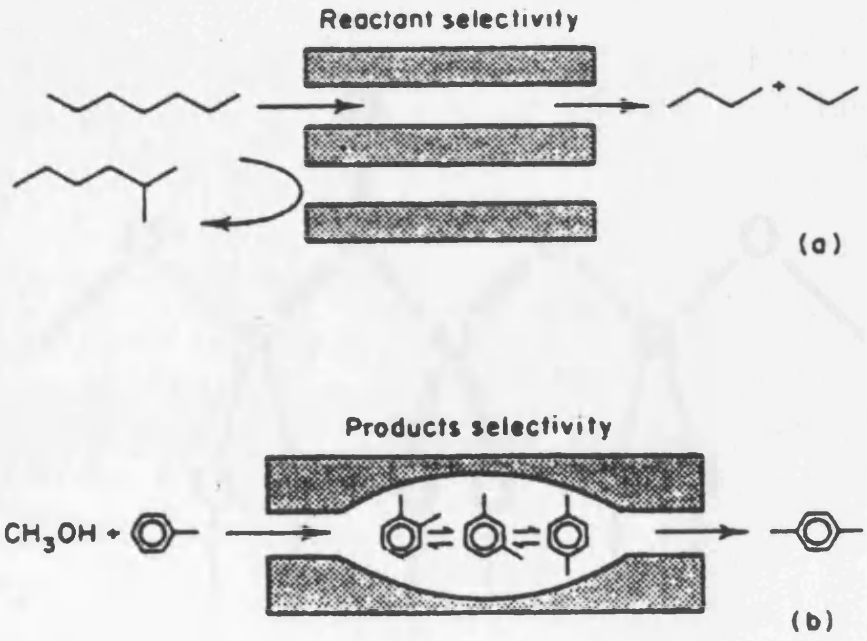

Figure 4.3 Representation of (a) reactant shape selectivity in zeolite channels (rejection of branched chain hydrocarbons) and (b) product shape selectivity (p-xylene diffuses preferentially out of the channels)
[S. M. Csicsery, *Chemistry in Britain.*, May, 1985, p. 473]

4.6.3 Transition State Selectivity

A different kind of restriction related to the steric requirements of the catalysis rather than to the transport of reactants and products: If there is not sufficient space in the zeolite pores to allow formation of the transition state for a step in a catalytic cycle, then

that cycle is suppressed. If it is suppressed at the expense of another cycle, the term *restricted transition state selectivity* is applied.

4.7 Introduction to Acid Catalysis with Zeolites in Hydrocarbon Reactions

Catalytic conversion of hydrocarbons over crystalline microporous acidic aluminosilicate catalysts is applied in large petroleum refining processes including catalytic cracking, hydrocracking, isomerization, alkylation and oligomerisation.

It is generally recognised that the zeolite acid strength is more in line with conventional strong acids rather than with superacids.[14] Both Brønsted and Lewis acids occur in zeolites. The active sites of aluminosilicate zeolites are complex and comprise a hydroxyl group, bridging a Si and an Al atom and having strong Brønsted acid properties, and the oxo bridges, having Lewis base properties ***(Figure 4.4).***[15,16]

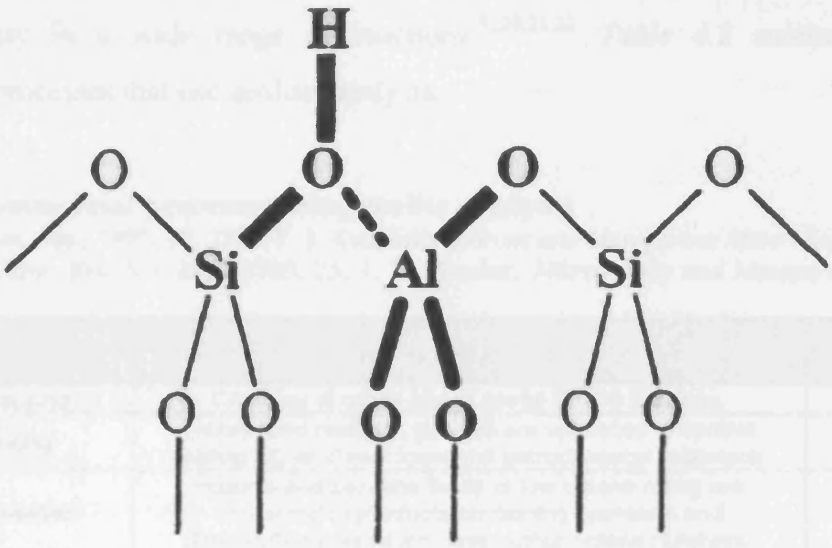

Figure 4.4 Active sites in hydrogen aluminosilicate zeolites. The bridging hydroxyl group and the oxo ligants of the Al-atom act as bifunctional Brønsted acid-Lewis base sites.

[H. Van Bekkum, E. M. Flanigen, P. A. Jacobs and J. C. Jansen, in *Introduction to Zeolite Science and Practice*, ed. Elsevier., Amsterdam, 2001, p.633]

It is generally accepted that the reaction mechanisms of hydrocarbon conversions on acid zeolites involve the formation of carbocations, i.e. carbenium ions ($C_nH^+_{2n+1}$) and/or carbonium ions ($C_nH^+_{2n+3}$) as reaction intermediates. ***Figure 4.5*** summarises the different reactions that can occur during catalytic cracking.[17,18]

Dehydrogenation to alkene

$$R_1CH_2{-}CH_2R_2 \rightarrow R_1CH{=}CHR_2 + H_2$$

Formation of carbenium ion

$$R_1CH = CHR_2 + H^+ \rightarrow R_1CH_2{-}\overset{+}{C}HR_2$$

Methyl group migration

$$CH_3{-}CH_2{-}\overset{+}{C}HR_6 \rightarrow \overset{+}{C}H_2{-}CH(CH_3)R_6 \rightarrow CH_3{-}\overset{+}{C}(CH_3)R_6$$

Hydride transfer

$$R_1CH_2{-}\overset{+}{C}HR_2 + R_3CH(CH_3){-}CH_2R_4 \rightarrow R_1CH_2{-}CH_2R_2 + R_3\overset{+}{C}(CH_3){-}CH_2R_4$$

β-scission

$$R_3\overset{+}{C}(CH_3){-}CH_2{-}CH_2R_5 \rightarrow R_3C(CH_3) = CH_2 + \overset{+}{C}H_2R_5$$

Figure 4.5 Reactions occurring during catalytic cracking
[http://teach.chem.ucl.ac.uk/]

4.8 Applications of Zeolites

Zeolites have found widespread industrial applications as highly selective adsorbents (drying, physical separations of hydrocarbons), ion exchangers (detergents) and, most importantly, catalysts (shape selective and acid catalysts) of exceptionally high activity and selectivity in a wide range of reactions.[9,,20,21,22] ***Table 4.2*** summarises some commercial processes that use zeolite catalysts.

Table 4.2 Commercial processes using zeolite catalysts
[A. Carma, *Chem. Rev.*, 1997, **97**, 2373. F. J. Keil, *Microporous and Mesoporous Materials.*, 1999, **29**, 49. C. D. Chang, *Catal. Rev. Sci. Eng.*, 1983, 25, 1. M. Stocker, *Microporous and Mesoporous Materials.*, 1999, **29**, 3]

Commercial Processes	Details of Process	Zeolite Catalyst Used
Catalytic cracking	Cracking of crude oils to useful C1-C6 fractions.	HY
Hydrocracking	Heavy, and residual, gas oils are upgraded to central heating oil, jet diesel fuels and petrochemical feedstock.	X, Y, MOR, H-ZSM-5
Hydroisomerisation	Hexane and pentane feeds of low octane rating are converted to products containing i-pentane and dimethylbutanes which have higher octane numbers.	Pt MOR
Dewaxing	Lubricating and diesel oils which contain long-chain paraffin are removed by crystallization below 100°C.	Pt MOR, H-ZSM-5, ZSM-23
Benzene Alkylation	The production of ethylbenzene from ethylene and benzene. This is a vital stage for the formation of styrene for polystyrene manufacture.	ZSM-5
Xylene isomerisation	Selective isomerisation of o-xylene to p-xylene.	ZSM-5
Methanol to gasoline conversion (MTG)	The conversion of methanol into gasoline-range hydrocarbons (including aromatics) plus water.	ZSM-5
Methanol to olefin conversion (MTO)	The conversion of methanol into olefin.	ZSM-5
Ion exchange for use in detergents	The replacement of cations held in aluminosilicate anion framework by ions present in the external solutions or melts.	A
NOx reduction	The reduction of the oxides of nitrogen for atmospheric pollution minimization.	H-MOR

Mordenite and clinoptilolite are used in small volume in adsorbent applications including air separation and in drying and purification. Natural zeolites have also found use in bulk applications as filters in paper, in pozzolanic cements and concrete, in fertilizer and soil conditioners and as dietary supplements in animal husbandry.

The highest market value for synthetic zeolites is in catalysis. The synthetic zeolite that is the least expensive FAU-type zeolite, accounts for more than 95% of the catalysis market. Oil refineries consume large quantities of the FAU-type zeolites to manufacture gasoline from crude oil in the Fluid Catalytic Cracking (FCC) process.[23]

Some refineries use additives such as MFI type[24] or less frequently BEA-type zeolites to the FCC process to optimise yield. Due to the shape selective properties of medium pore zeolite ZSM-5 paraffinic components in gasoline are preferentially cracked to light gaseous hydrocarbons. An octane increase is achieved, since the most reactive n-paraffin molecules have the lowest research octane number. Due to this, MFI type zeolites are the second most used zeolite catalyst.[25]

Based on the high activity in zeolite area in the last two decades, we can expect a continuation of the proliferation of new molecular sieve compositions and structures as well as the development of new application areas.

4.9 Conclusion

The combination of many properties such as the microporous character of uniform pore dimensions, the ion exchange properties, the ability to develop internal acidity, the high thermal stability and the high internal surface area, make zeolites unique among inorganic oxides.

Zeolites may be modified in many ways. They can be tuned over a wide range of acidity and basicity, and of hydrophilicity and hydrophobicity and many cations can be introduced by ion exchange. Moreover metal crystallites and metal complexes can be entrapped within the microporous environment. Altogether rich opportunities are provided for designing and employing heterogeneous catalysts that are tailored to suit the reactions desired.

Zeolites have been successfully used in many industrial applications due to their unique architecture; they can be used as sieves to purify water, to separate out molecules of different sizes, to make detergents for the kitchen, to remove radio-active elements from spent nuclear fuel, and as catalysts for many chemical reactions especially in the petro-chemical industry. Hundreds of different zeolite compositions have been prepared, with over 140 unique framework topologies with further materials being prepared every year, both in academic and industrial laboratories.

Chapter 4

References

1. D. W. Breck, in *Zeolite Molecular Sieves: Structure, Chemistry and Use*, ed. John Wiley., London, 1974.

2. W. M. Meier, D. H. Olson, in *IZA Atlas of Zeolite Structure Types,* ed. Butterworth-Heinemann., Boston, 1992.

3. http://www.izastructure.org/databases/

4. R. M. Barrer, *J. Soc. Chem.* Ind., 1945, **64**, 130.

5. R. M. Barrer, *J. Chem. Soc.*, 1948, **21**, 58.

6. H. Van Bekkum, E. M. Flanigen, P. A. Jacobs, J. C. Jansen, in *Introduction to Zeolite Science and Practice*, ed. Elsevier., Amsterdam, 2001, p.633.

7. J. C. Vartuli, W. J. Roth, J. S. Beck, S. B. McCullen and C. T. Kresge, in *Molecular Sieves,* ed. H. G. Karge, J. Weitkamp, Springer., Berlin, 1998, Vol.1, p.97.

8. C. Jones, T. Katsuyuki and M. E. Davis, *Nature.*, 1998, **393**, 52.

9. A. Carma, *Chem. Rev.,* 1997, **97**, 2373.

10. A. Dyer, in *An Introduction to Zeolite Molecular Sieves*, ed. John Wiley and Sons Ltd., New York, 1988.

11. C. J. Adams, A. Araya, S. W. Carr, A. P, Chapple, K. R. Fraklin, P. Graham, A. R. Minihan, T. J. Osinga and J. A. Stuart, *Stud. Surf. Sci. Catal.*, 1997, **105**, 1667.

12. B. W. Mercer and L. L. Ames, in *Natural Zeolites: Occurrence, Properties, Use*, ed. L. B. Sand and F. A. Mumpton, Pergamon Press., 1978, 451.

13. P. B. Weisz, , V. J. Frilette, R. W. Maatman and E. B. Mower, *J. Catal.*, 1962, **1**, 307.

14. J. Sommer, M. Hachoumy, F. Garin and D. Barthomeouf, *J. Am. Chem. Soc.*, 1994, **116**, 5491.

15. V. B. Kazansky, *Stud. Surf. Sci. Catal.*, 1994, **85,** 25.

16. F. Haase and J. Sauer, *J. Am Chem. Soc.*, 1995, **117,** 3780.

17. Bruce C. Gates, in *Catalytic Chemistry*, ed. John Wiley and Sons, Inc., New York, 1992.

18. http://teach.chem.ucl.ac.uk/

19. D. W. Breck, in *Zeolite Molecular Sieves: Structure, Chemistry and Use*, ed. John Wiley., London, 1974.

20. F. J. Keil, *Microporous and Mesoporous Materials.*, 1999, **29**, 49.

21. C. D. Chang, *Catal. Rev. Sci. Eng.*, 1983, **25**, 1.

22. M. Stocker, *Microporous and Mesoporous Materials.*, 1999, **29**, 3.

23. S. Bhatia, *Zeolite Catalysis: Principles and Applications*, ed. CRC Press, Inc., Boca Raton, Florida, 1990.

24. C. D. Chang, *Catal. Rev. Sci. Eng.*, 1983, **25**, 1.

25. K. Tanabe, W. F. Holderich, *Appl.Catal.*, 1999, **181,** 399.

Chapter 5

Study of the Response of Zeolite CTO Gas Sensors to the Presence of Simple Gases

5.1 Introduction

The objective of this Chapter is to demonstrate the suitability of the newly developed multi-electrode zeolite-CTO gas sensor devices with additional shape and size selective catalysts afforded by zeolites to show an improved discrimination between ethanol and carbon monoxide gases compared to a standard CTO sensor.

5.2 Experimental Method

5.2.1 Preparation of CTO Powders

Since the important development in this research study was primarily to increase the variance of response pattern across an array of sensors using shape and size selective catalysts, it was essential to use a consistent, stable, well-defined and reproducible sensing material. Titanium substituted chromium oxide was ideal for this purpose and had been well studied in previous research works.[1,2]

Titanium substituted chromium oxide powder (CTO) with nominal composition $Cr_{1.95}Ti_{0.05}O_3$ was prepared using the following preparation method:

I. Ultra fine powder of chromium oxide (Cr_2O_3) was prepared by careful thermal decomposition of ammonium dichromate $(NH_4)_2Cr_2O_7$ at 300°C, as shown below,

$(NH_4)_2Cr_2O_7 + \text{Heat} \Rightarrow Cr_2O_3 + 4H_2O + N_2$ *(DANGER: EXPLOSION HAZARD)*

(Bright Orange) *(Green)*

[All chemicals were supplied by Aldrich]

It should be emphasised that during the decomposition the temperature was raised slowly to the ignition point, and then the heating was ceased.

II. Chromium oxide (Cr_2O_3) and propan-2-ol (IPA) (500 ml per 20 g of CTO product) were mixed thoroughly together for 5 minutes at 10000 rpm using an industrial blender (Ultra-Turrax T25 supplied by IKA-Labortechnik).

III. The Cr_2O_3 suspension was transferred to 1L rotary evaporator flask and the required weight of titanium isopropoxide was added.

IV. The flask was immersed in an ultrasonic bath and was attached to a rotary evaporator. Then, 50 ml of IPA containing 5 ml water was run in slowly, using a modified burette on the shaft of the rotary evaporator, while sonicating for 15 minutes to ensure complete reaction.

V. The solvent (IPA) was then evaporated on the rotary evaporator whilst continuing sonication and the resulting CTO powder ($Cr_{1.95}Ti_{0.05}O_3$) was fired in the furnace (Carbolite Furnace HTC 1400) to the desired temperature (1000^0C for 4 hours) with up and down ramp rates of 15^0C min^1. The continued sonication prevented size fractionation of the oxide powder during the solvent evaporation.

5.2.2 Fabrication of Sensor Arrays

An object of this research work was to provide gas sensors able to offer increased selectivity and enhancement in sensor response to a wide range of specific gases. This was achieved by the use of particular types of porous materials (zeolites).

Two types of multi-electrode sensor array devices were constructed for this study namely,

(i) The layered zeolite sensors that have a layer of zeolite printed on top of the CTO sensing material ($Cr_{1.95}Ti_{0.05}O_3$), and

(ii) The mixed zeolite sensors where the zeolite was mixed with the sensing material.

Three different types of zeolites (Zeolite Y Powder, Zeolite β Powder and Zeolite ZSM-5 Powder) were used to produce the different sensors. All zeolite powders were supplied by Zeolysts International. The zeolite types used were specifically chosen as they have a range of pore sizes and are all considered to be sufficiently robust to withstand the firing and operating temperatures of the sensors. (Details regarding the zeolite structures can be found in ***Section 8.3***).

In addition to the newly developed zeolite-CTO sensors, a standard (control) CTO gas sensor without zeolite was prepared by screen-printing 8 layers (100 μm) of $Cr_{1.95}Ti_{0.05}O_3$ onto multiple electrode substrates using a DEK1202 hybrid screen printer (supplied by DEK). After screen printing, the device was fired in air at 600°C for 30 minutes, obtained by a temperature ramp of 25°C min^{-1} and bonded using 50 μm platinum wires in order to suspend it in a polyphenylene sulphide housing.

Multiple electrode SEMDEC substrates ***(See Figure 3.13)*** were used for all fabricated sensors. Such double electrode sensors are functionally equivalent to an array of two different sensors, where the differing concentration profiles of gases result in different relative responses on the various pairs of electrodes. A typical SEMDEC device has an array of electrodes of different geometry i.e. 30 μm narrow (small) gap and 200 μm wide (large) gap electrodes. The SEMDEC substrates were photoetched by Capteur Sensors and Analysers Ltd.

5.2.2.1 Sensors with Layered Microstructure

Figure 5.1 is a schematic diagram of sensors with layered microstructure. Chromium titanium oxide powder was mixed with a commercial dual organic vehicle, ESL400 (supplied by Agmet ES Ltd) in appropriate ratios to produce a screen printable ink. The ink was then passed through a triple roll mill to ensure homogeneous dispersion of powder in the vehicle. Eight layers (100 μm) of CTO were then screen-printed onto multiple electrode SEMDEC substrates. Then, eight layers of zeolite were screen-printed on top of the sensing layer. Between each layer of printing, the ink was dried by placing the sensor under an infra-red lamp for 15 minutes. Contacts to the devices were formed by spot welding 100μm diameter platinum wire to the pads. After screen printing, the devices were fired in a furnace at 600°C for 30 minutes, obtained by a temperature ramp of 25°C min^{-1}. This was done in order to remove the organic vehicle and to strengthen the attachment of the sensor material to the gold electrode. It should be noted that great attention was taken to wire bound the sensors onto the heaters without making any significant damage on the zeolite layers.

The following layered sensor types were produced,

Table 5.1 Sensors with layered microstructure

Sensor type	Powder/Vehicle Mass Ratio for Zeolite Layer
Layered Y	0.58
Layered β	0.44
Layered ZSM-5	0.72

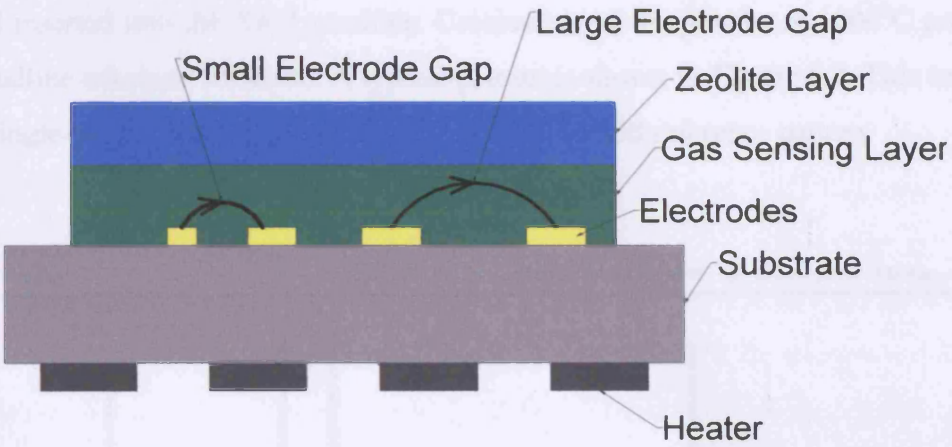

Figure 5.1 Schematic diagram of multi-electrode sensor configuration with added zeolite layer over the gas sensing material (Layered)

5.2.2.2 Sensors with Mixed Microstructure

The second type of sensors was produced by mixing the chromium titanium oxide and zeolite. The chromium titanium oxide was milled and then mixed with zeolite (25% by mass) in IPA for 10 minutes using a homogeniser at 10000 rpm. The solvent was allowed to evaporate and the powder was mixed with the printing vehicle using a triple roll mill. Then, eight layers (100 μm) of powder were screen-printed onto multiple electrode substrates and the devices were fired in air at 600°C for 30 minutes.

The following mixed sensor types were produced,

Table 5.2 Sensors with mixed microstructure

Sensor Type	Powder/Vehicle Mass Ratio
Mixed ZSM-5	1
Mixed Y	1.01
Mixed β	0.86

5.2.3 Characterisation of the CTO Powders

a) X-Ray Powder Diffraction Measurements

X-ray powder diffraction pattern of the $Cr_{1.95}Ti_{0.05}O_3$ powder treated at 1000°C was recorded in the region 2θ =15 ° - 75 ° with a scanning speed of 0.12° min^{-1} on a Siemens D5000 diffractometer in transmition mode using germanium monochromated $CuK_{\alpha 1}$ (λ=1.5046Å) radiation. The sample was prepared by grinding about 20 mg of powder using a mortar and pestle. The powder was then applied between two pieces of Scotch tape and inserted into the XRD machine. Calcination of the powder at 1000°C produced the crystalline eskolaite structure. A typical pattern is shown in ***Figure 5.2***. This indicates a clear single-phase material when compared to the JCPDS reference pattern.

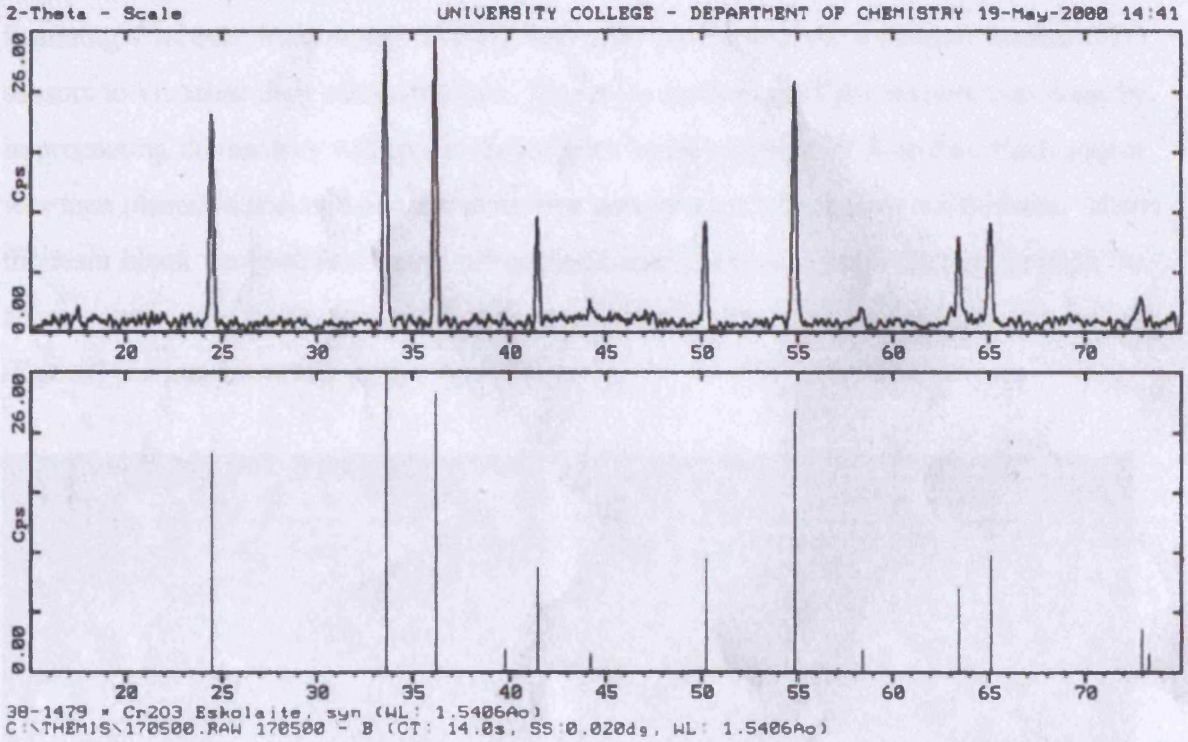

Figure 5.2 X-ray diffraction pattern of the sample CTO ($Cr_{1.95}Ti_{0.05}O_3$) fired at 1000 °C compared to the JCPDS reference pattern

The average crystallite size W was found to be equal to 390 Å determined by additional X-ray line broadening using the well known Scherrer equation:[3]

$$W = 0.9\,\lambda / \Theta \cos\theta_B \qquad [5.1]$$

Where W is the thickness of the crystal in $\AA$, λ is the X-ray wavelength, θ_B is the Bragg angle and Θ is the line width in degrees at half peak maximum.

b) Scanning Electron Microscopy (SEM) and Energy Dispersive Analysis of X-Rays (EDAX)

The morphology of the $Cr_{1.95}Ti_{0.05}O_3$ powder treated at 1000°C was studied using the Hitachi 5570 scanning electron microscope operating at 20 keV. The sample was coated with sputtering gold to reduce charging effects. Selected images are shown in ***Figure 5.3***. Most of the particles were found to be small (0.5 μm) and sintered together, leaving some holes in the structure.

Elemental analysis of the sample was carried out on the Hitachi scanning electron microscope equipped with an energy dispersive X-ray analyser. EDAX analysis of the CTO powder revealed the absence of impurities and confirmed the nominal composition of $Cr_{1.95}Ti_{0.05}O_3$. Cr/Ti elemental ratio (39.2) analysed by broad beam EDAX analysis was very close to the expected Cr/Ti ratio (39).

Scanning Electron Microscopy (SEM) was also performed on sectioned zeolite-CTO sensors to visualise their microstructure. The cross sectioning of the sensors was done by impregnating the sensors with resin (Scandiplex resin supplied by Scandia). Each sensor was then placed in a mould and the resin was poured over it to make a solid block. Then the resin block was polished down using glasspaper to reveal a cross section through the sensor chip, and finally polished with successively finer grades of diamond polish (Kemet) (25 μm down to 1 μm).

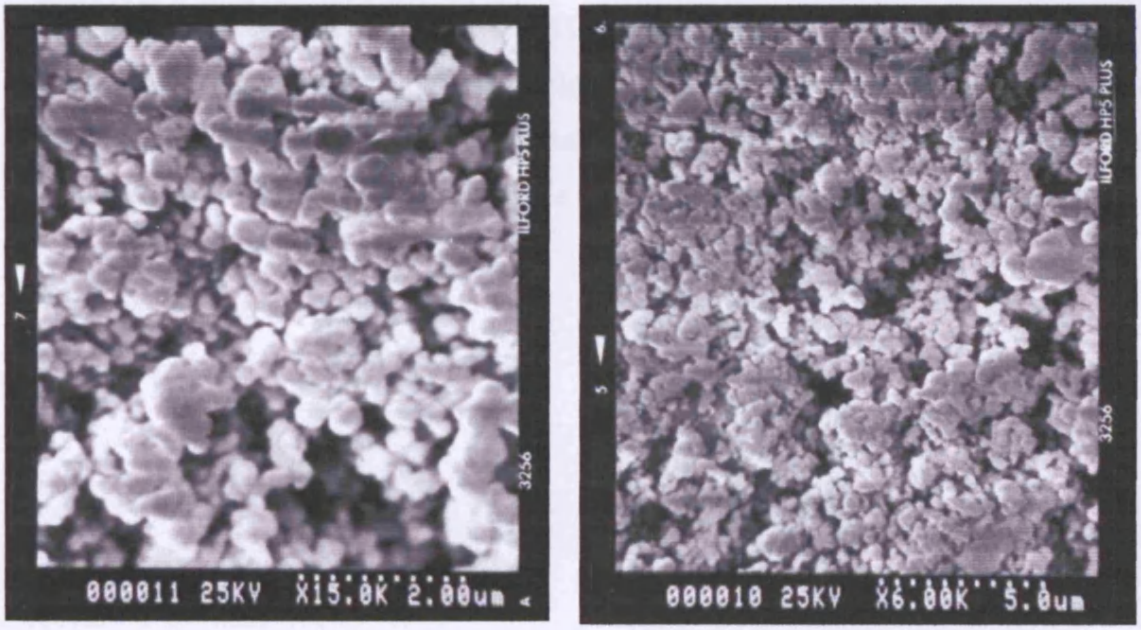

Figure 5.3 Scanning electrode micrographs of CTO powder at different magnifications

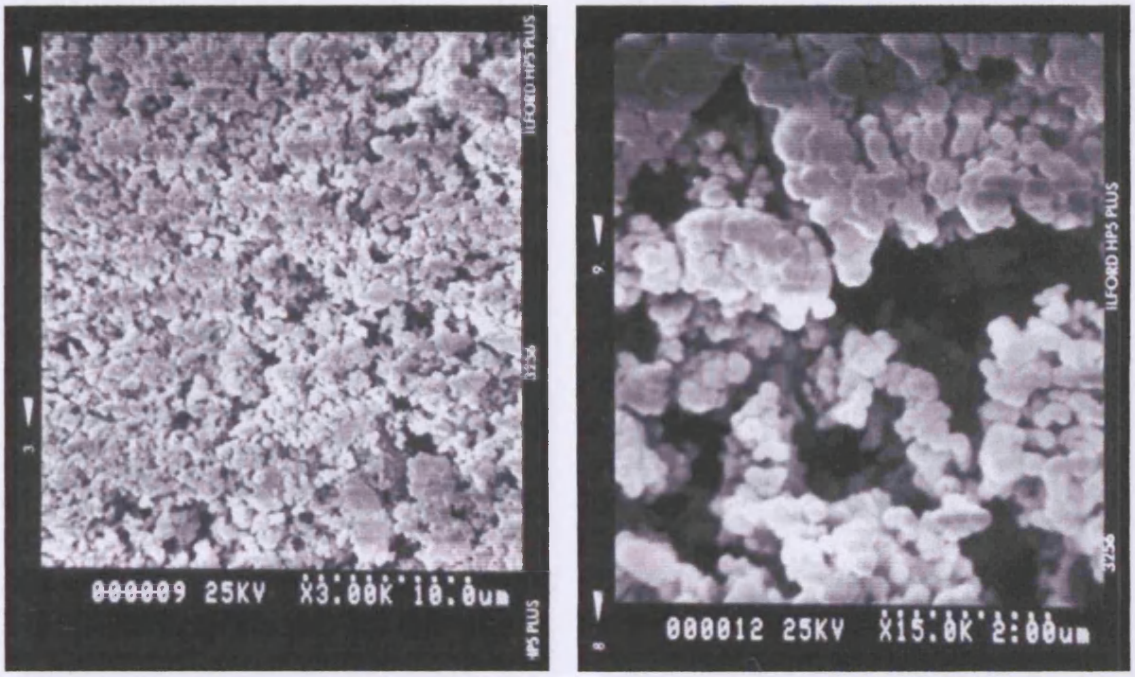

Figure 5.3 Scanning electrode micrographs of CTO powder at different magnifications

Figure 5.4 shows micrographs of layered zeolite-CTO sensors where differences in the microstructure of the different sensors are observed. Zeolite ZSM-5 sensor ***(Figure 5.4 (c))*** has fine particles and good homogeneity whereas zeolite Y sensor ***(Figure 5.4 (a))*** is less homogenous with zeolite β sensor ***(Figure 5.4 (b))*** being the least homogenous with various particle shapes and sizes as illustrated in ***Figure 5.4 (e)***. ***Figure 5.4 (d)*** shows that the interface between the zeolite and the CTO layer is clean.

Comparing the micrographs of layered ***(Figure 5.4)*** and mixed zeolite sensors ***(Figure 5.5)*** differences in the microstructure of the two different types of sensors are observed since mixed zeolite sensors are more porous than their corresponding layered ones.

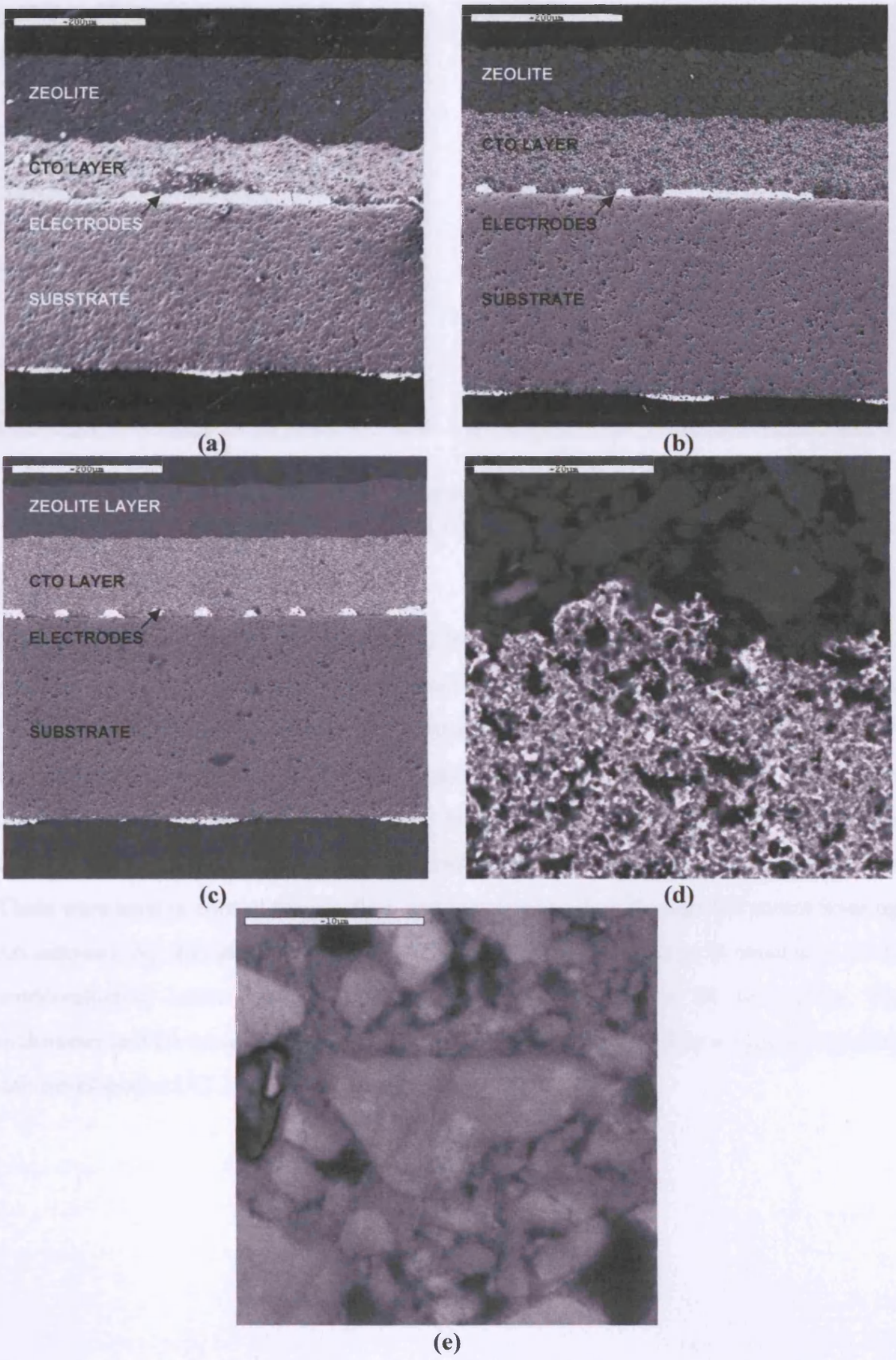

Figure 5.4 Scanning electrode micrographs of cross sections of layered zeolite-CTO sensors. (a) Layered Y (b) Layered β (c) Layered ZSM-5 (d) Interface between CTO and zeolite β, (e) Zeolite layer of Layered β sensor.

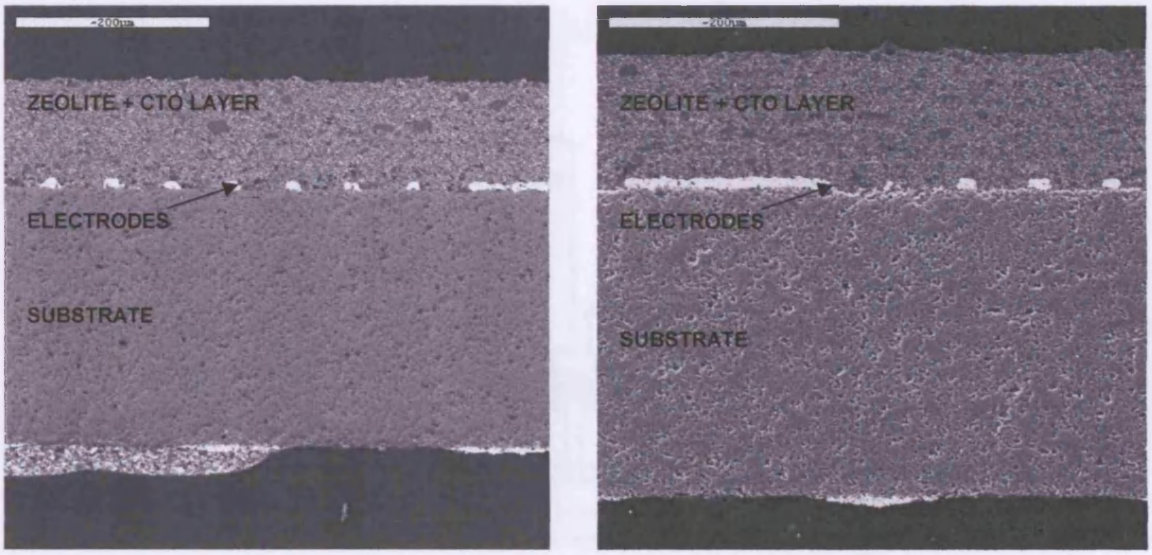

(a) **(b)**

Figure 5.5 Scanning electrode micrographs of cross sections of mixed zeolite-CTO sensors. (a) Mixed ZSM-5 (b) Mixed Y.

5.2.4 Experimental Set-Up

Figure 5.6 is a schematic representation of the testing rig used to perform the resistance measurements. The sensors were maintained at 400°C using a heater driver circuit that maintained the heater track at constant resistance.

The reactant gases from cylinders (100 ppm ethanol in synthetic air and 10000 ppm carbon monoxide in synthetic air supplied by BOC plc.) were mixed with purified and dried laboratory air and supplied to the sensor housing through mass-flow controllers. These were used to control the gas flow and the concentration through the sensor housing. An auto-ranging digital multimeter was used to monitor the change in resistance of the semiconducting oxide powder, between the gold electrodes at 60 sec cycles. The multimeter and the mass flow controllers were computer controlled by a signal-processing unit developed at UCL.

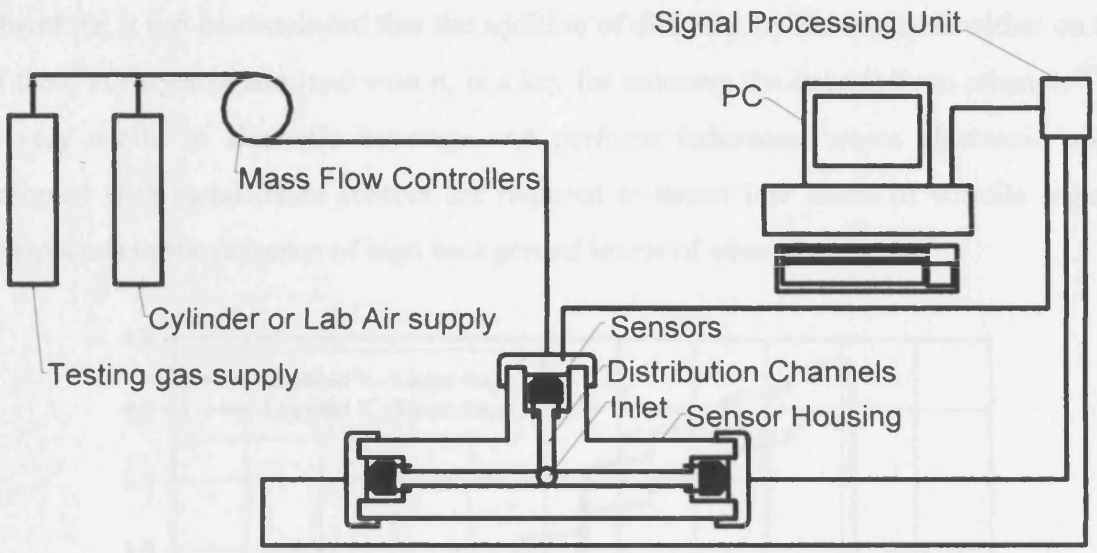

Figure 5.6 Schematic representation of the testing rig

5.3 Experimental Results

The six newly developed zeolite-CTO sensors (with three different zeolite materials and two different arrangements i.e. mixed and layered) and a standard CTO sensor (with no zeolite) were tested in the presence of carbon monoxide and ethanol. Since the characteristic response of the semiconductor sensors is strongly depended on the operation temperature all sensors were operated at 400°C. The resistance response, R_g, (resistance in dry gas) of each sensor to a particular gas was normalised to its baseline resistance, R_o, (resistance in dry air in the absence of the target gas) so as to get the actual magnitude of response to a given gas and thus to be easier to compare responses between different sensors and gases.

5.3.1 Microstructure Effects on the Response

5.3.1.1 Sensitivity to Ethanol and Carbon Monoxide

Figures 5.7-5.12 show the response (normalised resistance, R/R_o Vs *Time*) of the seven sensors to different concentrations of ethanol in dry air. Ethanol gas concentration was progressively increased (0, 5, 10, 20, 30, 50, 60, 70, 80, 0 ppm) to allow the response law operating lines to be derived later ***(Section 5.3.2.1)***.

In all cases the ethanol response of the large gap was found to be higher than that of the small electrode gap. Differences in the sensitivities (R/R_o) to ethanol were observed for different sensors. All zeolite sensors were shown to be less sensitive (i.e. lower R/R_o) to ethanol compared to the standard CTO sensor with the exception of mixed β sensor.

Therefore, it can be concluded that the addition of different zeolite materials either on top of the CTO layer or admixed with it, is a key for reducing the sensitivity to ethanol. This is very useful in alcoholic beverage and perfume industries, where electronic noses designed with metal oxide sensors are required to detect low levels of volatile organic compounds in the presence of high background levels of ethanol.

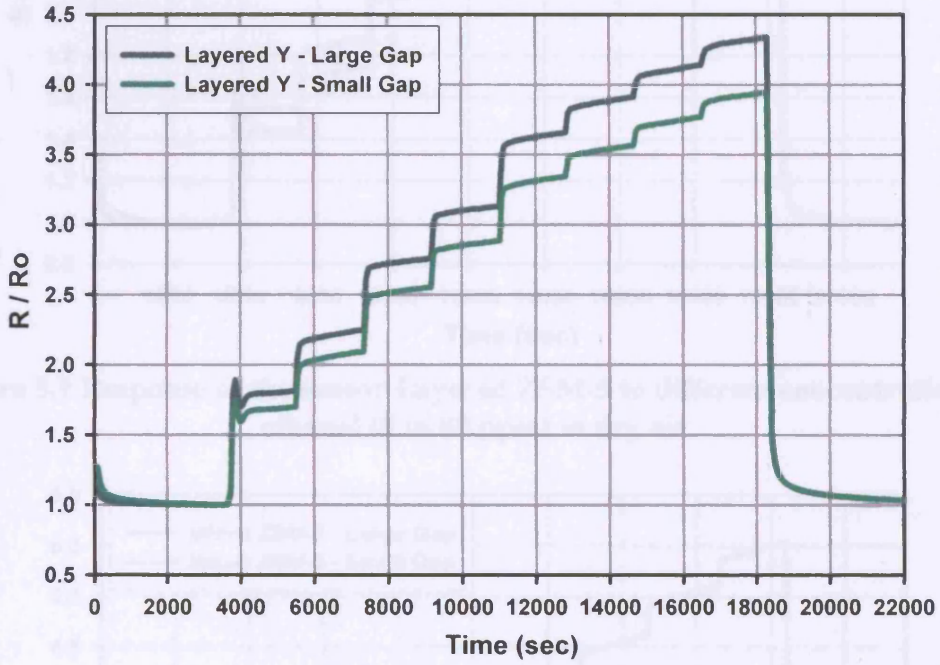

Figure 5.7 Response of the sensor Layered Y to different concentrations of ethanol (0 to 80 ppm) in dry air

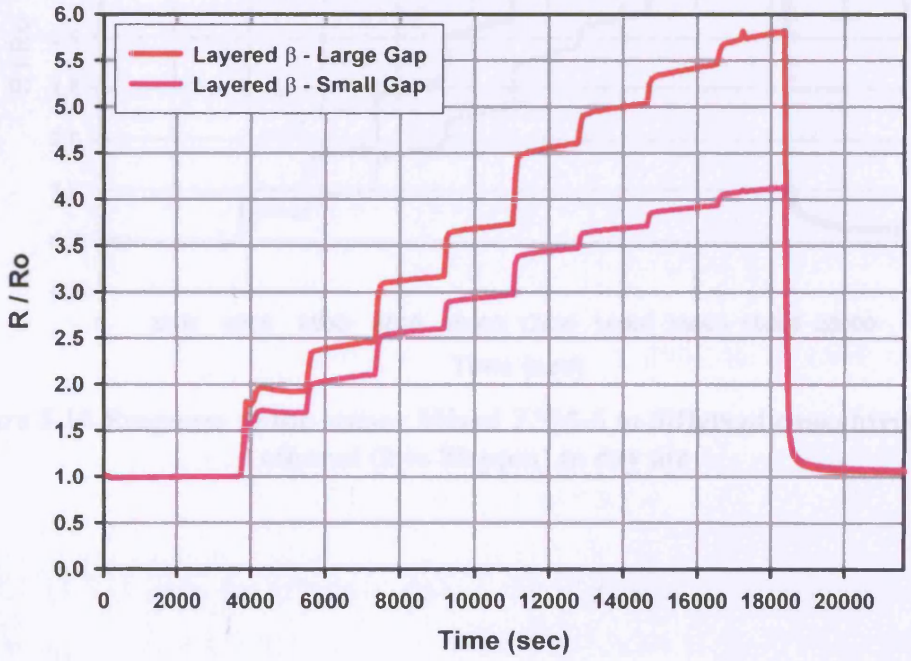

Figure 5.8 Response of the sensor Layered β to different concentrations of ethanol (0 to 80 ppm) in dry air

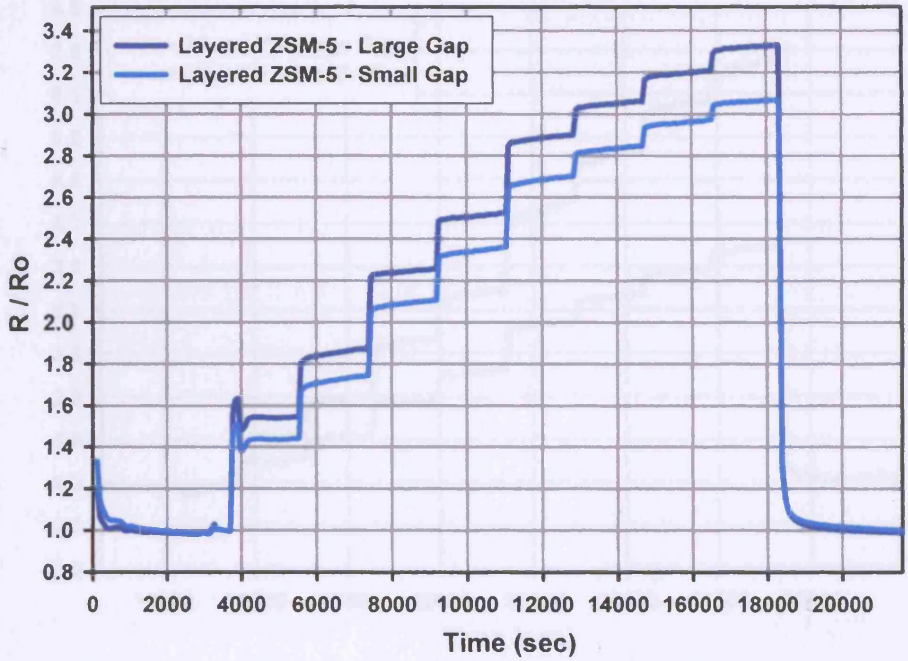

Figure 5.9 Response of the sensor Layered ZSM-5 to different concentrations of ethanol (0 to 80 ppm) in dry air

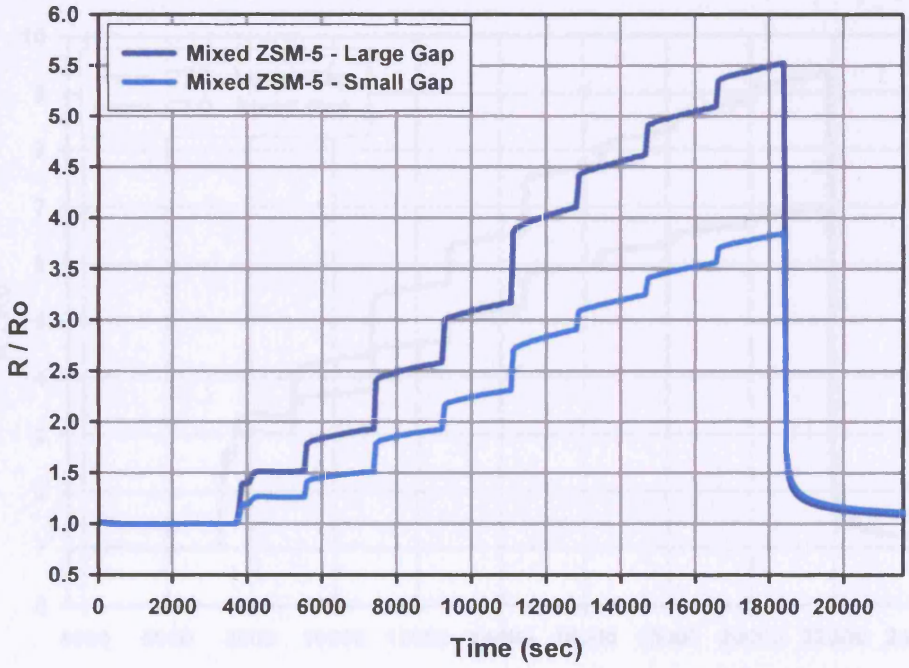

Figure 5.10 Response of the sensor Mixed ZSM-5 to different concentrations of ethanol (0 to 80 ppm) in dry air

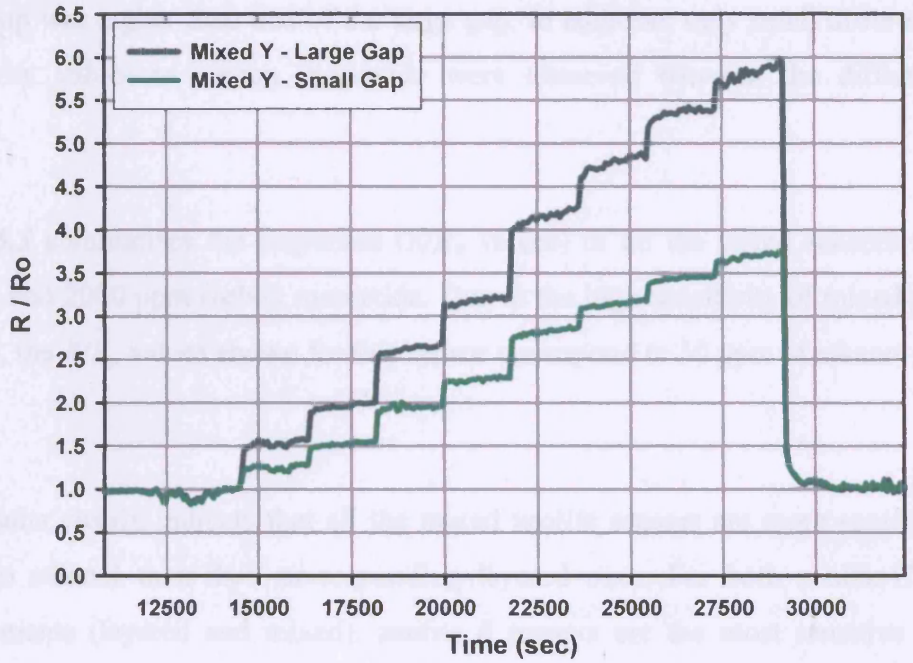

Figure 5.11 Response of the sensor Mixed Y to different concentrations of ethanol (0 to 80 ppm) in dry air

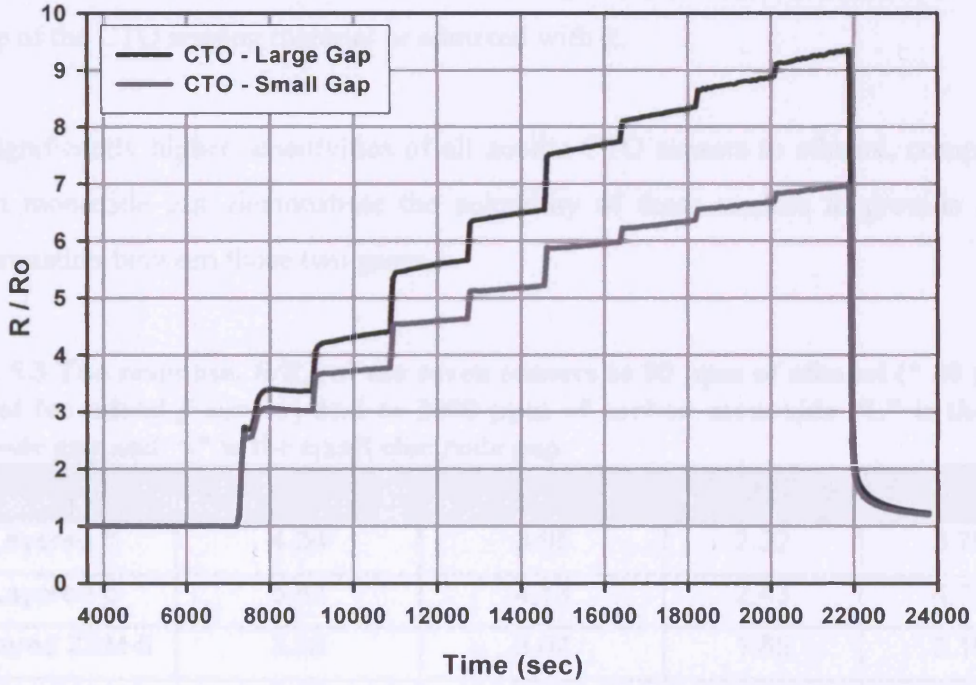

Figure 5.12 Response of the sensor CTO to different concentrations of ethanol (0 to 80 ppm) in dry air

Figures 5.13-5.19 show the response of the different sensors to several concentrations of carbon monoxide (0, 200, 400, 600, 1200, 1600, 1800, 2000, 0 ppm). The principal effect of the microstructure on the response to carbon monoxide was that the response on the

small gap was higher than that of the large gap. In addition, only small differences in the sensitivity values to carbon monoxide were observed between the different zeolite sensors.

Table 5.3 summarises the responses (R/R_o values) of all the tested sensors to 80 ppm ethanol and 2000 ppm carbon monoxide. Due to the high sensitivity of mixed β sensor to ethanol, the R/R_o values shown for this sensor correspond to 30 ppm of ethanol and not 80 ppm.

The results clearly indicate that all the mixed zeolite sensors are more sensitive (higher R/R_o) to ethanol than their corresponding layered ones. For both zeolite-CTO sensor arrangements (layered and mixed), zeolite β sensors are the most sensitive to ethanol followed by zeolite Y and finally zeolite ZSM-5. The different responses of the zeolite-CTO sensors as well as the standard CTO sensor to the same gas (ethanol) suggest that there are differences between the sensors resulting from the addition of zeolites either at the top of the CTO sensing material or admixed with it.

The significantly higher sensitivities of all zeolite-CTO sensors to ethanol, compared to carbon monoxide gas, demonstrate the suitability of these sensors to provide a good discrimination between those two gases.

Table 5.3 The response, R/R_o, of the seven sensors to 80 ppm of ethanol (* 30 ppm of ethanol for mixed β sensor) and to 2000 ppm of carbon monoxide "L" is the large electrode gap and "s" is the small electrode gap

Zeolite Type	Ethanol $[R/R_o]_L$	Ethanol $[R/R_o]_s$	CO $[R/R_o]_L$	CO $[R/R_o]_s$
Layered Y	4.34	3.95	2.32	3.70
Layered β	5.82	4.13	2.43	4.72
Layered ZSM-5	3.33	3.07	1.85	3.15
Mixed ZSM-5	5.52	3.85	3.51	7.77
Mixed Y	5.91	3.73	1.99	2.93
Mixed β	10.95*	5.80*	2.99	6.10
CTO	9.38	6.96	5.51	5.96

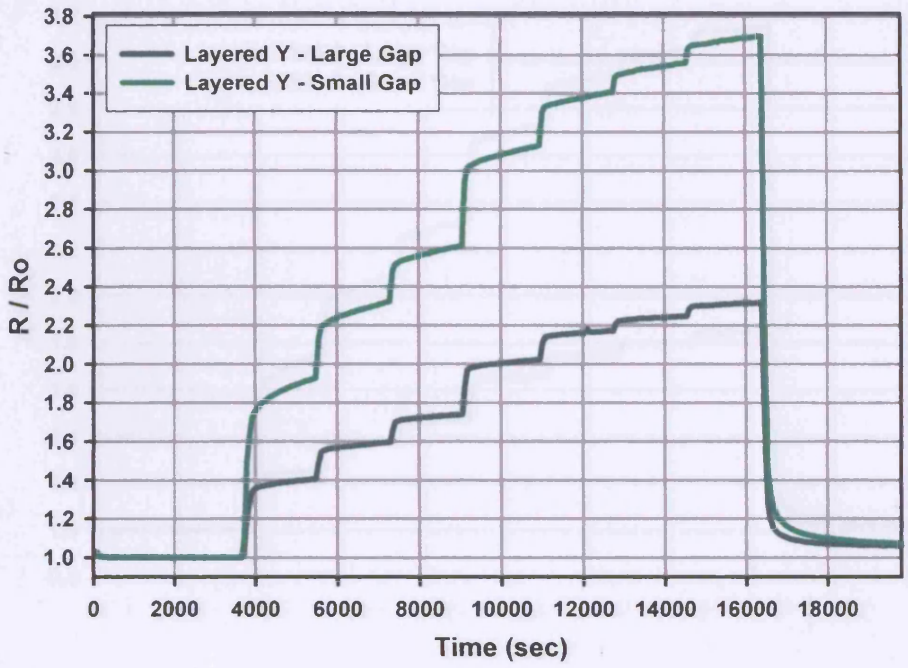

Figure 5.13 Response of the sensor Layered Y to different concentrations of carbon monoxide (0 to 2000 ppm) in dry air

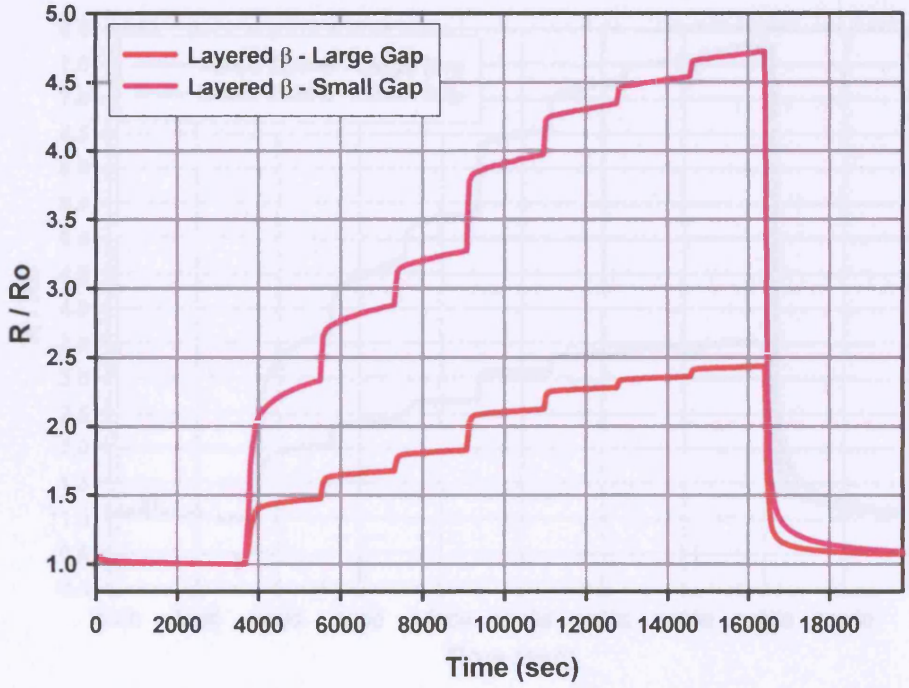

Figure 5.14 Response of the sensor Layered β to different concentrations of carbon monoxide (0 to 2000 ppm) in dry air

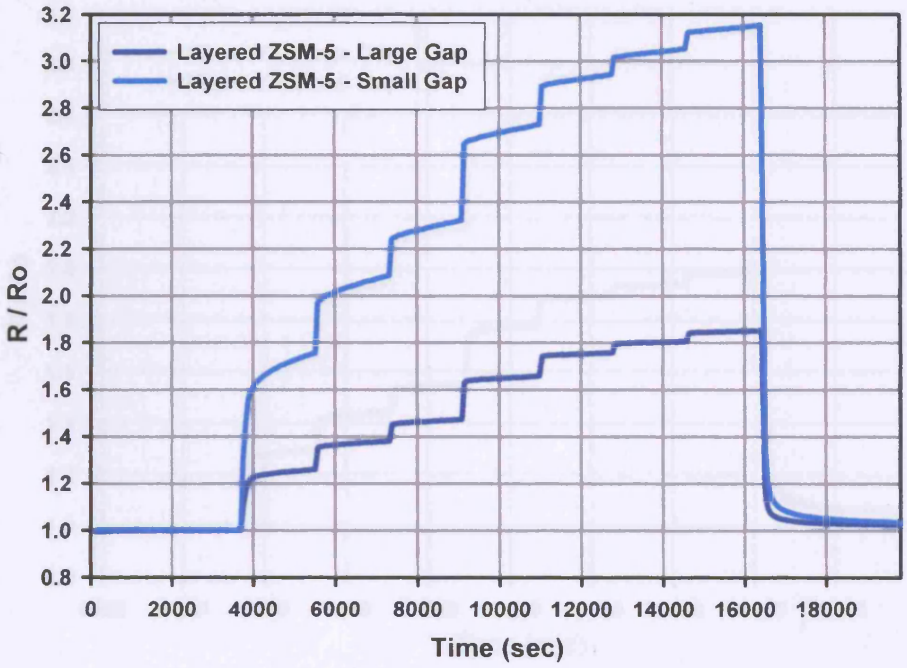

Figure 5.15 Response of the sensor Layered ZSM-5 to different concentrations of carbon monoxide (0 to 2000 ppm) in dry air

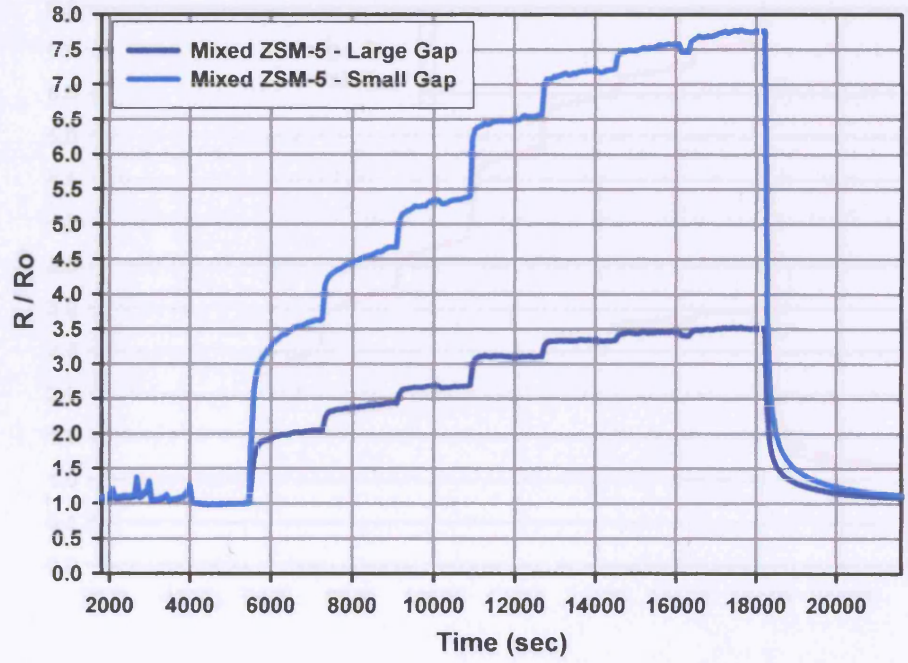

Figure 5.16 Response of the sensor Mixed ZSM-5 to different concentrations of carbon monoxide (0 to 2000 ppm) in dry air

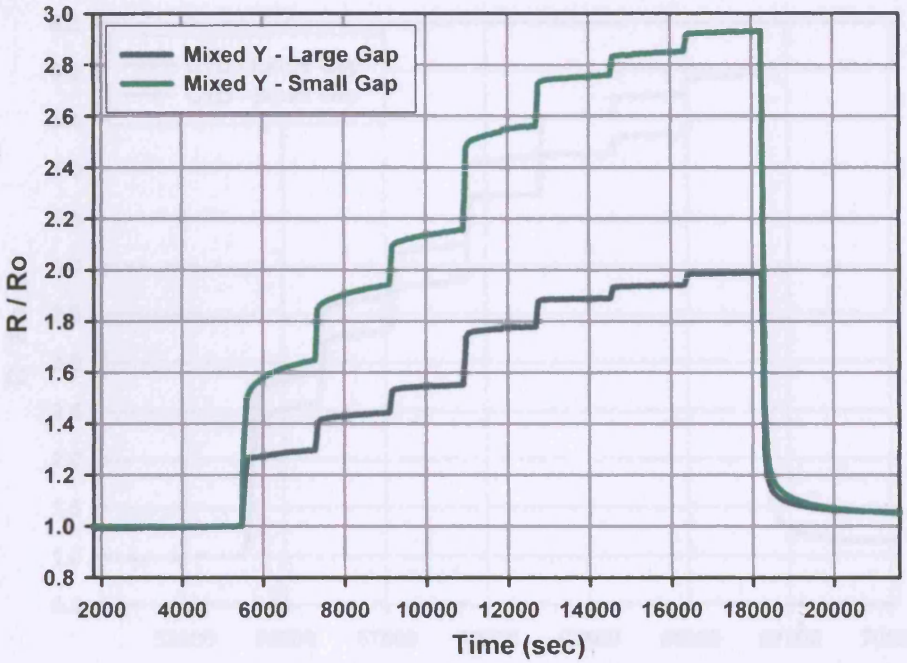

Figure 5.17 Response of the sensor Mixed Y to different concentrations of carbon monoxide (0 to 2000 ppm) in dry air

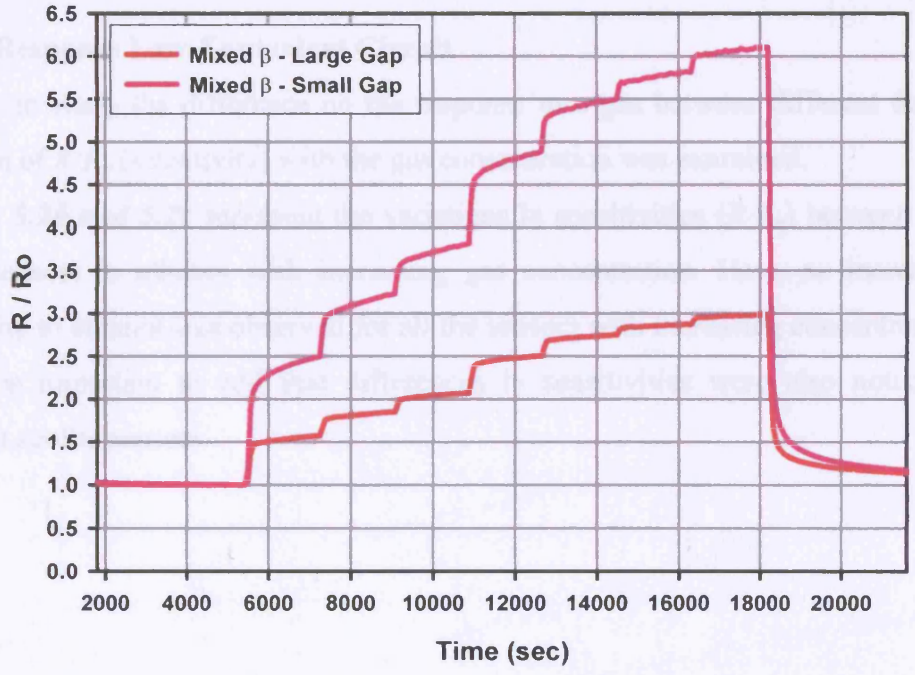

Figure 5.18 Response of the sensor Mixed β to different concentrations of carbon monoxide (0 to 2000 ppm) in dry air

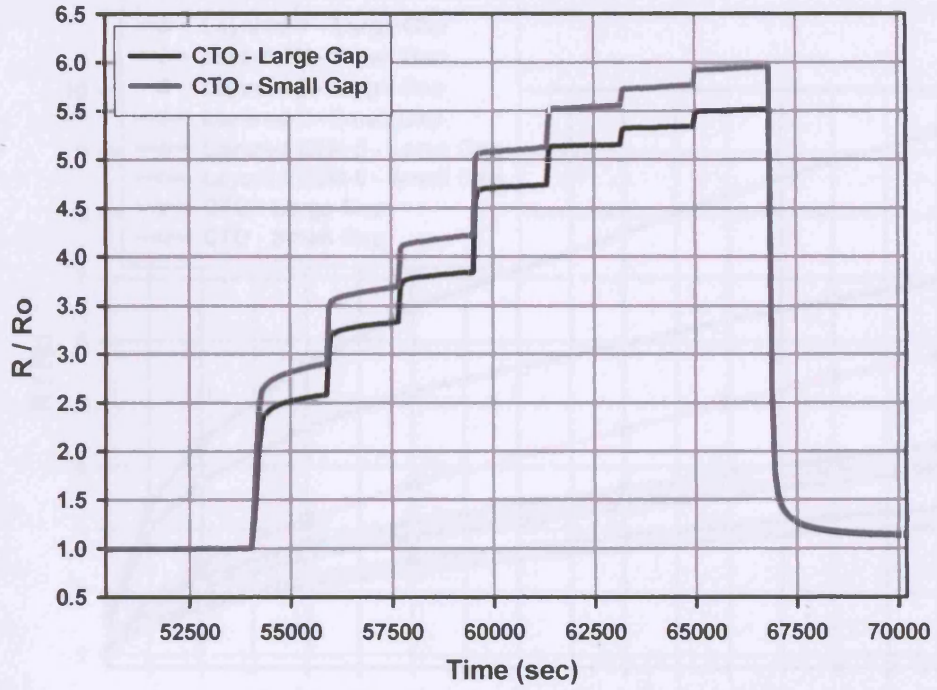

Figure 5.19 Response of the sensor CTO to different concentrations of carbon monoxide (0 to 2000 ppm) in dry air

5.3.1.2 Response Law-Equivalent Circuit

In order to study the difference on the response to a gas between different devices, the variation of R/R_o (sensitivity) with the gas concentration was examined.

Figures 5.20 and 5.21 represent the variations in sensitivities (R/R_o) between the seven tested sensors to ethanol with increasing gas concentration. Here, an increase in the sensitivity to ethanol was observed for all the sensors with increasing concentration of the gas. It is important to add that differences in sensitivities were also noted between different zeolite sensors.

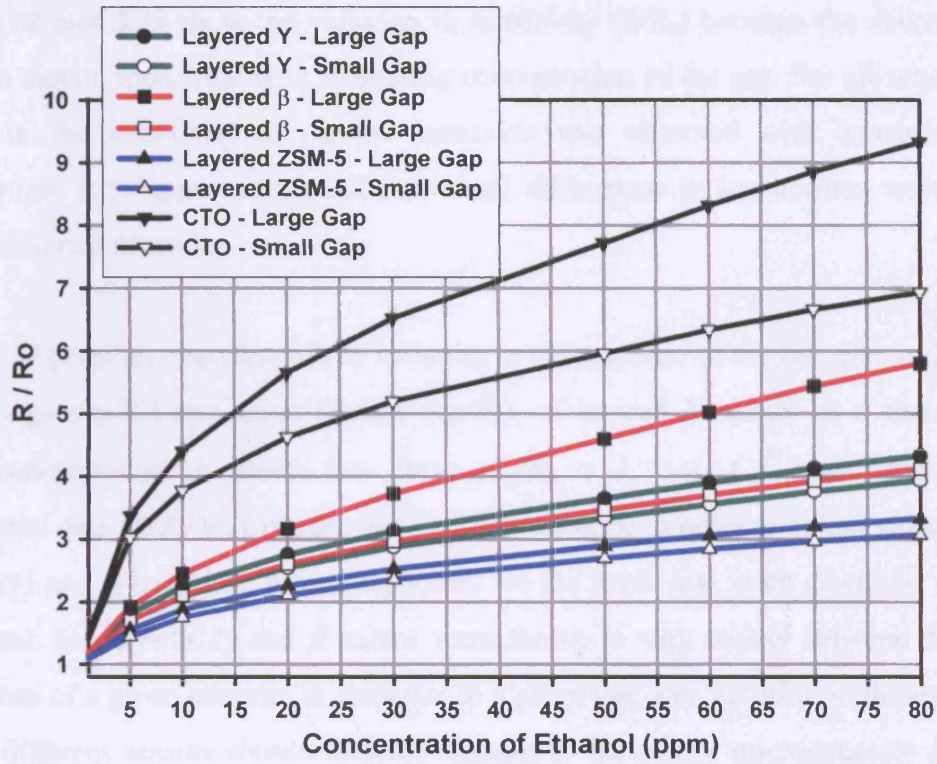

Figure 5.20 The response, R/R_o of the different layered zeolite and CTO sensors as a function of ethanol concentration

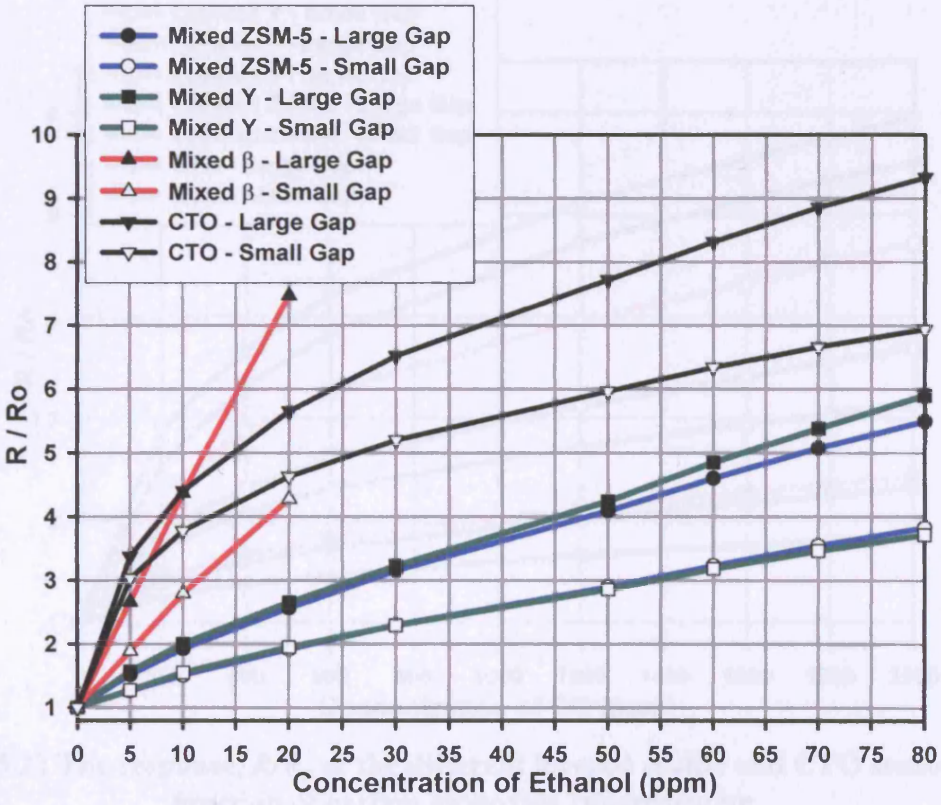

Figure 5.21 The response, R/R_o of the different mixed zeolite and CTO sensors as a function of ethanol concentration

Figure 5.22 and 5.23 show the variation in sensitivity (R/R_o) between the seven tested sensors to carbon monoxide with increasing concentration of the gas. For all sensors, an increase in the sensitivity to carbon monoxide was observed with increasing gas concentration. It is important to add that small differences in sensitivities were noted between different sensors.

Figure 5.24 gives an overview of the variation in the response of the two electrode gaps, large ($RLarge\ Gap/R_o$) and small ($RSmall\ Gap/R_o$), of layered Y sensor as a function of ethanol concentration. A power law curve, $R_g/R_o = 1 + A_g C_g^{\beta}$, was fitted to the experimental data (R/R_o Vs C*oncentration*). This was done in order to obtain values of A_g (sensitivity) and β (response power/exponent) for the small and large electrode gaps of each sensor. Since both A_g and β values were shown to vary widely between different preparations of a given material in response to a given gas, any variation in theses values between different sensors should indicate changes in the sensor microstructure (a more thorough analysis of this issue can be seen in ***Section 3.6.2***).

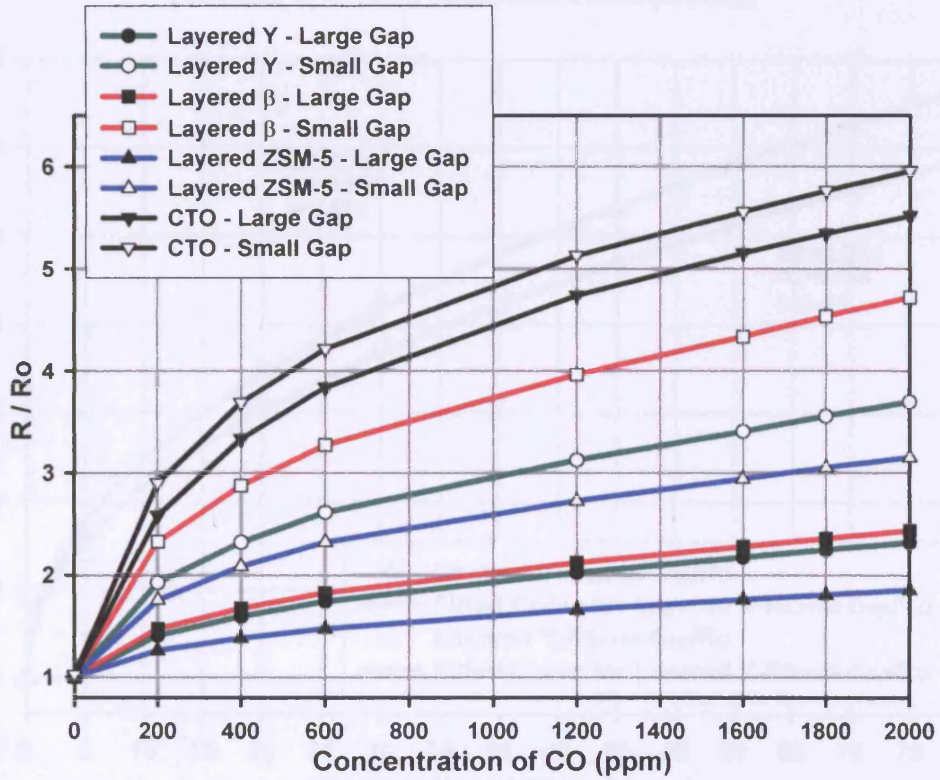

Figure 5.22 The response, R/R_o of the different layered zeolite and CTO sensors as a function of carbon monoxide concentration

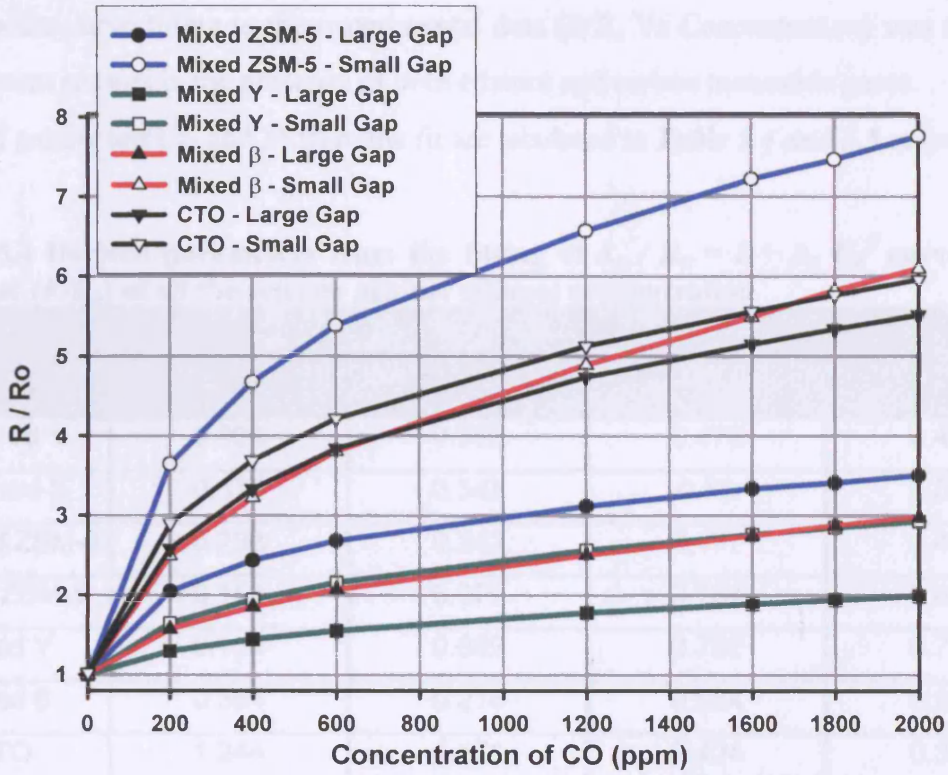

Figure 5.23 The response, R/R_o of the different mixed zeolite and CTO sensors as a function of carbon monoxide concentration

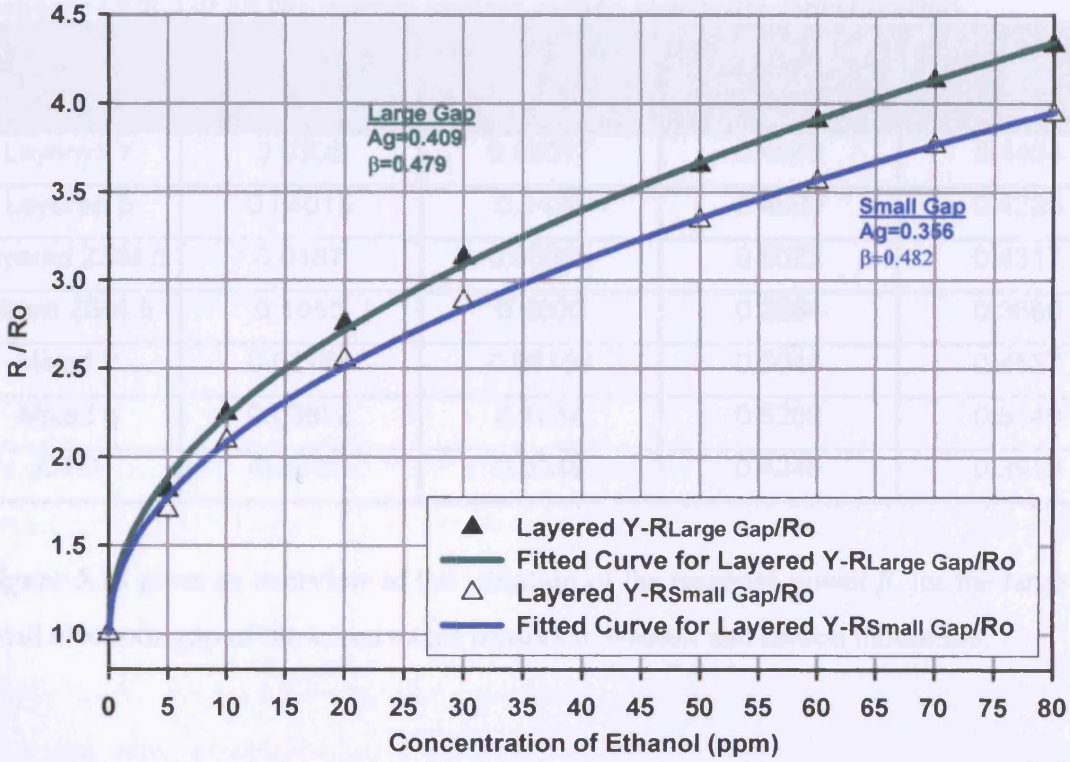

Figure 5.24 The responses of the two electrode gaps, large gap ($R_{Large\ Gap}/R_o$) and small gap ($R_{Small\ Gap}/R_o$) of layered Y sensor as a function of ethanol concentration. A power law curve, $R_g / R_o = 1 + A_g C_g^{\beta}$, where $\beta>0$ was fitted to the data as shown by the solid lines

Appropriate curve fitting to the experimental data (R/R_o Vs *Concentration*) was done for all different sensors in the presence of both ethanol and carbon monoxide gases.

Derived parameters (A_g and β) from the fit are tabulated in ***Table 5.4 and 5.5*** respectively.

Table 5.4 Derived parameters from the fitting of $R_g / R_o = 1 + A_g C_g^{\beta}$ curve to the response (R/R_o) of all the sensors against ethanol concentration

Sensor Type	A_g for Large Gap	A_g for Small Gap	β for Large Gap	β for Small Gap
Layered Y	0.409	0.356	0.479	0.482
Layered β	0.377	0.345	0.58	0.504
Layered ZSM-5	0.292	0.242	0.477	0.494
Mixed ZSM-5	0.158	0.077	0.764	0.821
Mixed Y	0.154	0.092	0.787	0.774
Mixed β	0.361	0.215	0.964	0.910
CTO	1.244	1.171	0.434	0.371

Table 5.5 Derived parameters from the fitting of $R_g / R_o = 1 + A_g C_g^{\beta}$ curve to the response (R/R_o) of all the sensors against carbon monoxide concentration

Sensor Type	A_g for Large Gap	A_g for Small Gap	β for Large Gap	β for Small Gap
Layered Y	0.0306	0.09077	0.4948	0.4454
Layered β	0.04015	0.1426	0.4699	0.4285
Layered ZSM-5	0.0187	0.08085	0.5022	0.4317
Mixed ZSM-5	0.1655	0.3600	0.3584	0.3860
Mixed Y	0.02154	0.06189	0.5044	0.4537
Mixed β	0.03632	0.1014	0.5259	0.5149
CTO	0.1811	0.2548	0.4246	0.3913

Figure 5.25 gives an overview of the variation of the response power β, for the large and small electrode gap of the seven tested sensors to ethanol and carbon monoxide.

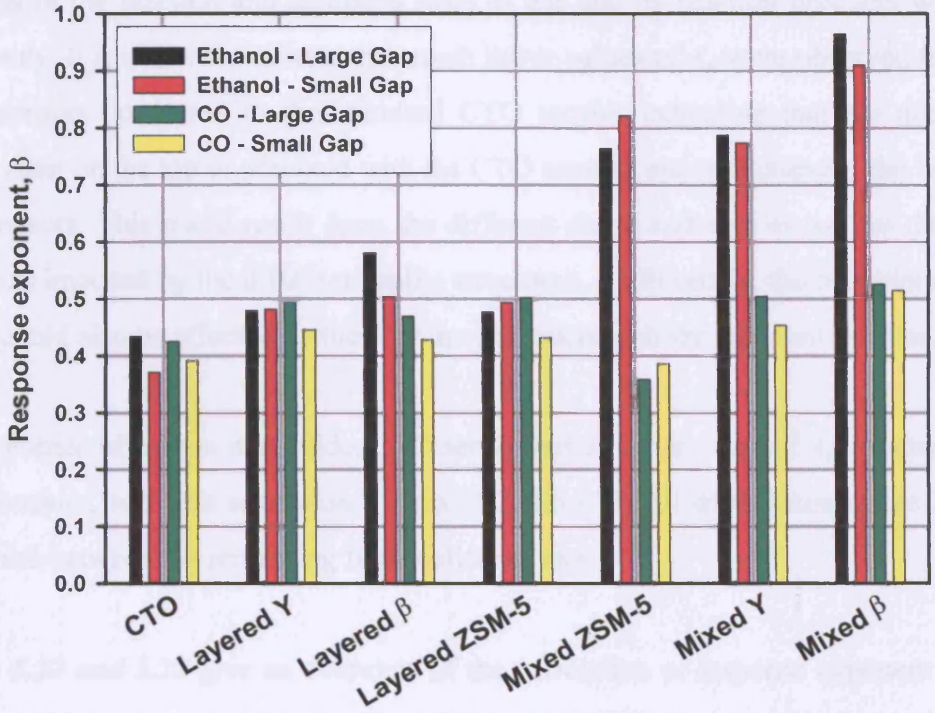

Figure 5.25 Variation of β with the tested sensors to ethanol and carbon monoxide

Large differences in the values of β were observed for the different devices in the presence of ethanol. Three different ranges of β values were obtained; (a) a low value for CTO, (b) a slightly higher value for the layered zeolites and (c) a high value for the mixed zeolite sensors. This proves that the addition of a zeolite material either on top or admixed with the CTO sensing layer modifies the microstructure of the different sensors resulting in different responses.

However, in the presence of carbon monoxide, small variations in β values were observed for all the seven sensors.

Comparing the observed β values for all the sensors in the presence of both ethanol and carbon monoxide, it can be concluded that ethanol has higher β values than carbon monoxide.

Figure 5.26 gives an overview of the variation of A_g (the sensitivity in dry gas) for the large and small electrode gap of the seven sensors to ethanol and carbon monoxide. Different values of A_g were observed for different sensors in the presence of ethanol. In more detail, higher values of A_g were found for the three layered compared to the mixed sensors indicating variations in the microstructure of the tested sensors as well as

variations in the reaction and diffusion rates of gas and its reaction products within the sensor body. It is important to note that much lower values of A_g were observed for all the zeolite sensors compared to the standard CTO sensor, indicating that the addition of zeolites ether on the top or admixed with the CTO sensing material changed the behaviour of the sensors. This could result from the different shape and size as well as diffusional limitations imposed by the different zeolite structures. Additionally, the behaviour of such sensors could also be affected by the way the gas reacts with the different zeolites.

In the presence of carbon monoxide, CTO sensor has a higher value of A_g compared to all zeolite sensors, with the exception of mixed ZSM-5. Small differences in the A_g value were found between the remaining five zeolite sensors.

Figures 5.27 and 5.28 give an overview of the correlation of response exponent (β) with prefactor (A_g), comparing the behaviour of the seven CTO sensors to the presence of two different gases (ethanol and carbon monoxide) and different electrode gaps.

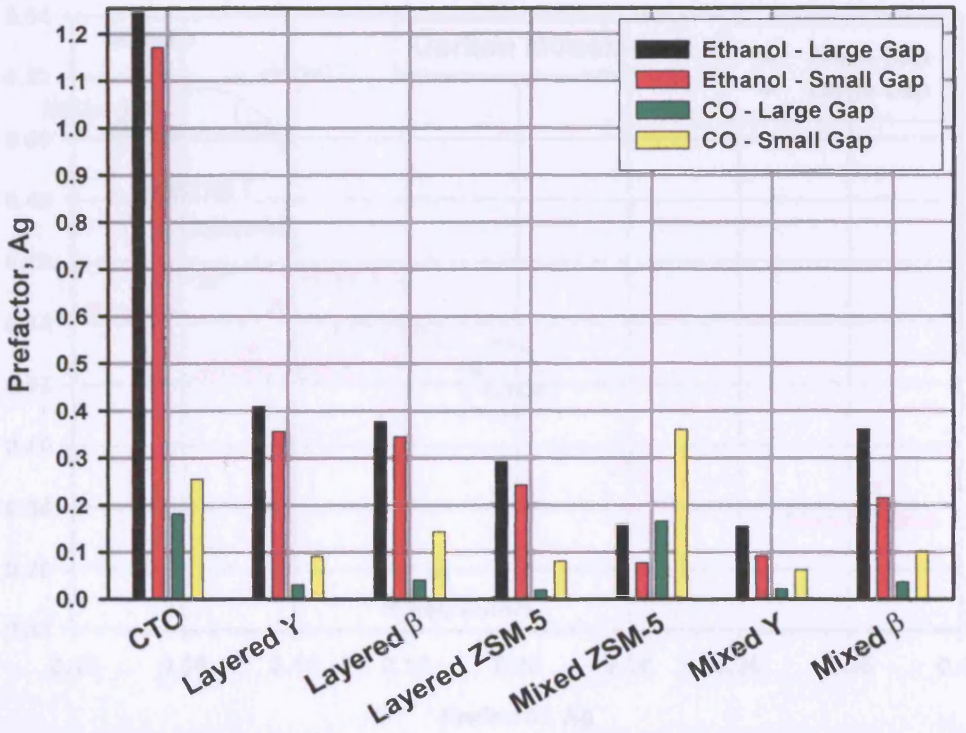

Figure 5.26 Variation of Ag with the tested CTO sensors to ethanol and carbon monoxide

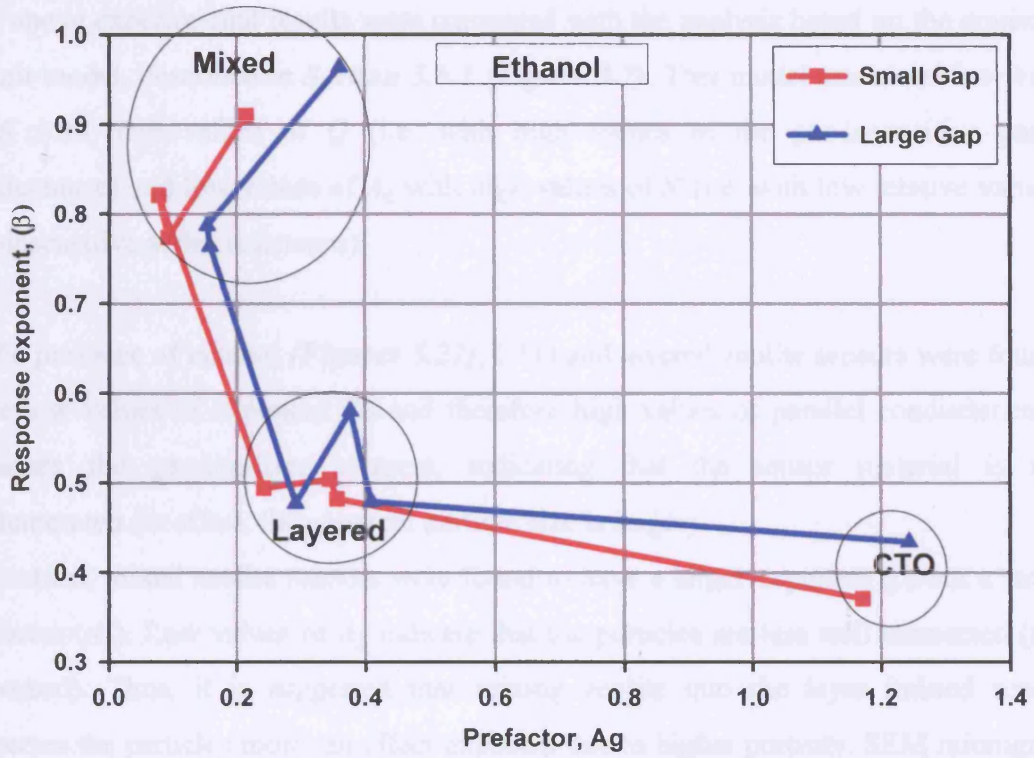

Figure 5.27 Correlation of response exponent with prefactor for the tested CTO sensors in the presence of ethanol

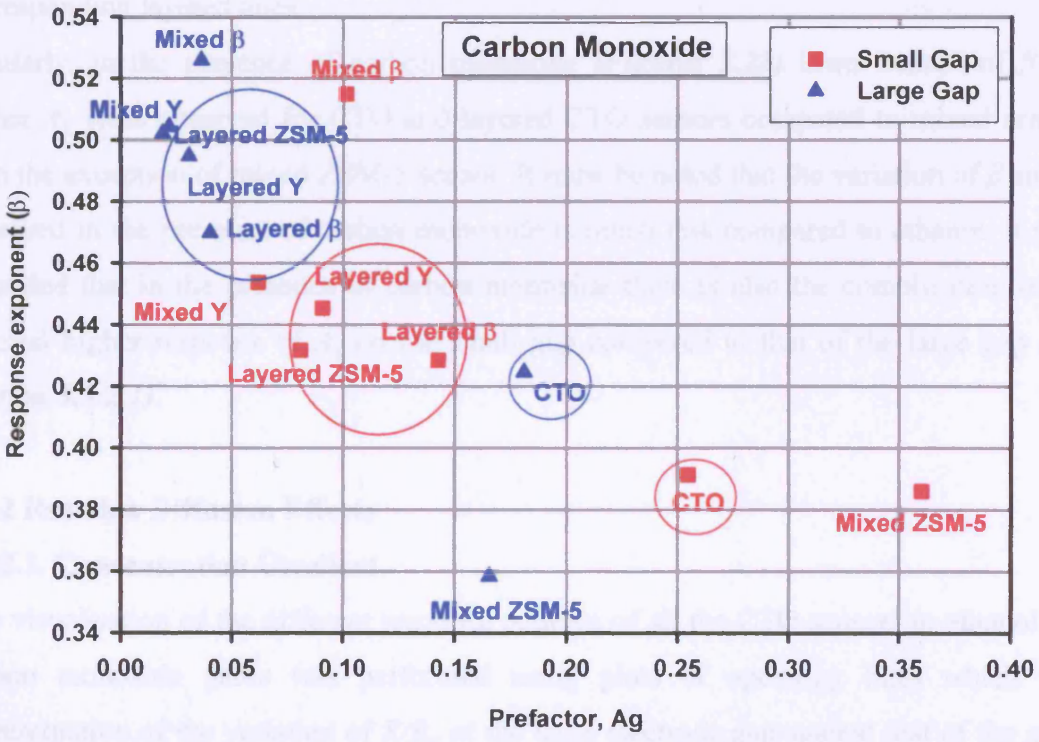

Figure 5.28 Correlation of response exponent with prefactor for the tested CTO sensors in the presence of carbon monoxide

The above experimental results were compared with the analysis based on the equivalent circuit model, described in ***Section 3.6.2 (Figure 3.7)***. This model associates low values of β with high values of Q (i.e. with high values of the gas-insensitive parallel conductance) and low values of A_g with high values of S' (i.e. with low relative values of gas-insensitive series resistance).

In the presence of ethanol ***(Figures 5.27)***, CTO and layered zeolite sensors were found to have low values of exponent *(β)* and therefore high values of parallel conductance that bypasses the gas-sensitive element, indicating that the sensor material is more agglomerated (in effect, the apparent particle size is larger).
In contrast, mixed zeolite sensors were found to have a larger exponent (β) but a smaller prefactor (A_g). Low values of A_g indicate that the particles are less well connected (more dispersed). Thus, it is suggested that mixing zeolite into the layer (mixed sensors) disperses the particles more; an effect expected due to higher porosity. SEM micrographs of layered ***(Figure 5.4)*** and mixed zeolite sensors ***(Figure 5.5)*** confirmed the observed results, showing higher porosity for the mixed zeolite sensors compared to their corresponding layered ones.
Similarly, in the presence of carbon monoxide ***(Figures 5.28)*** lower values of β and higher A_g were observed for CTO and layered CTO sensors compared to mixed sensors with the exception of mixed ZSM-5 sensor. It must be noted that the variation of β and A_g observed in the presence of carbon monoxide is much less compared to ethanol. It must be added that in the presence of carbon monoxide there is also the complication of the unusual higher response of A_g on the small gap compared to that of the large gap ***(See Section 5.3.2.1)***.

5.3.2 Reaction Diffusion Effects

5.3.2.1. Concentration Gradient

The visualisation of the different response patterns of all the CTO sensors to ethanol and carbon monoxide gases was performed using plots of operating lines which is a representation of the variation of R/R_o of the large electrode gap against that of the small electrode gap. The angle of the operating line (i.e. concentration gradient) effectively gives a measure of the reactivity of the gas within the sensing layer.

Figures 5.29-5.35 show operating line plots for all the tested sensors in the presence of carbon monoxide and ethanol. In all cases, the operating line for ethanol was found to be steeper than that of carbon monoxide, indicating that the former has a higher concentration gradient within the porous sensor layer and hence has a higher rate of combustion. This was expected, as carbon monoxide is a smaller molecule than ethanol with relatively higher stability making it less likely to interact with zeolites.

It is interesting to rationalise the unusual "reverse concentration gradient" (i.e. R/R_o of the small electrode gap is larger compared to the R/R_o of the large electrode gap) observed for carbon monoxide. This effect has also been demonstrated by other researchers and it was found to be due to the interaction of the metal oxide layer with electrodes. In more detail, this study revealed that some bonding agents that were added to the gold electrode during manufacturing migrated into the metal oxide layer as the oxide was fired. Cadmium and copper were particularly found in the sensor layer.[4]

The results from ***Figures 5.29-5.35*** demonstrate that a good discrimination between ethanol and CO can be achieved using the tested sensors due to the observed large concentration gradient to ethanol and the inverse gradient to carbon monoxide. The discrimination between the gases is much better for all the zeolite-CTO sensors compared to the standard CTO sensor.

The concentration gradients to ethanol and carbon monoxide (derived from the operating lines) for all the tested devices are tabulated in ***Table 5.6***.

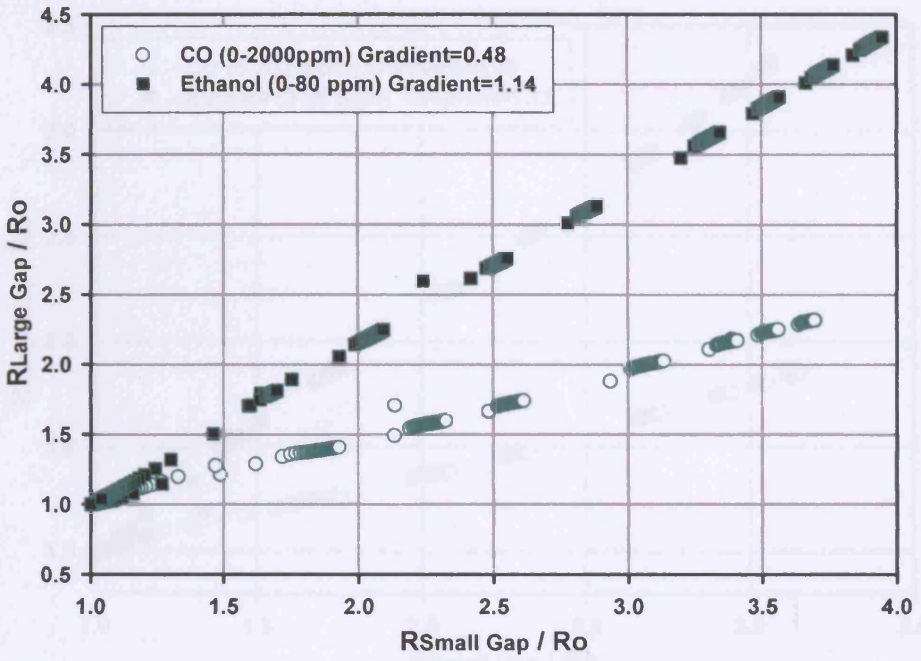

Figure 5.29 Operating lines for ethanol and carbon monoxide on sensor Layered Y

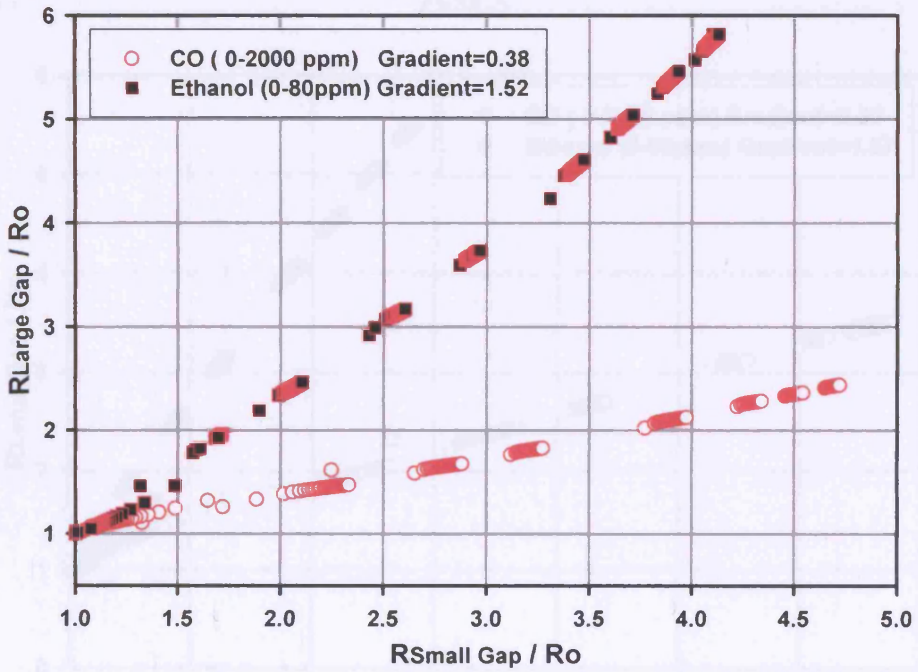

Figure 5.30 Operating lines for ethanol and carbon monoxide on sensor Layered β

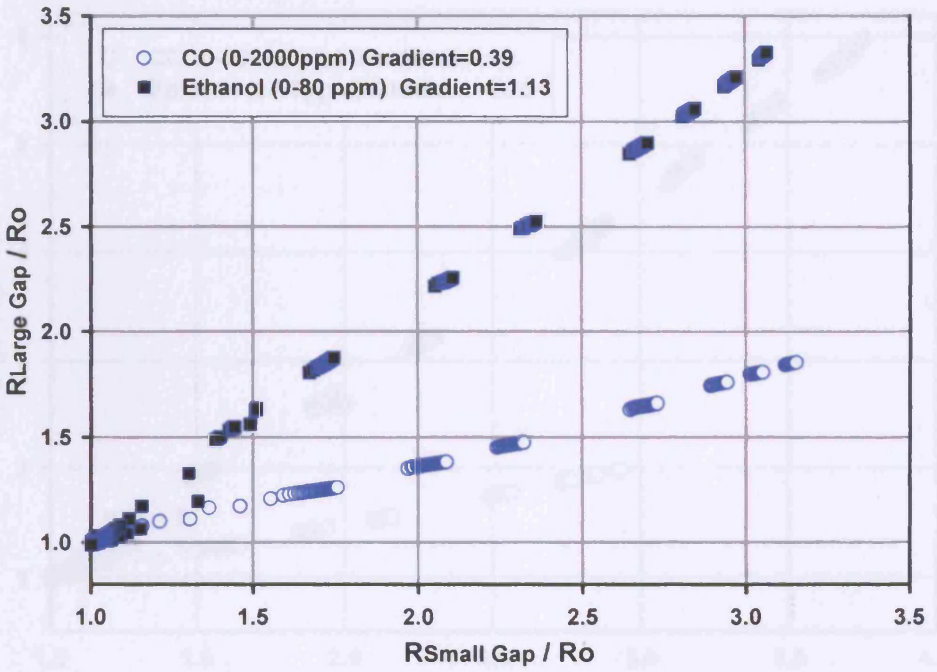

Figure 5.31 Operating lines for ethanol and carbon monoxide on sensor Layered ZSM-5

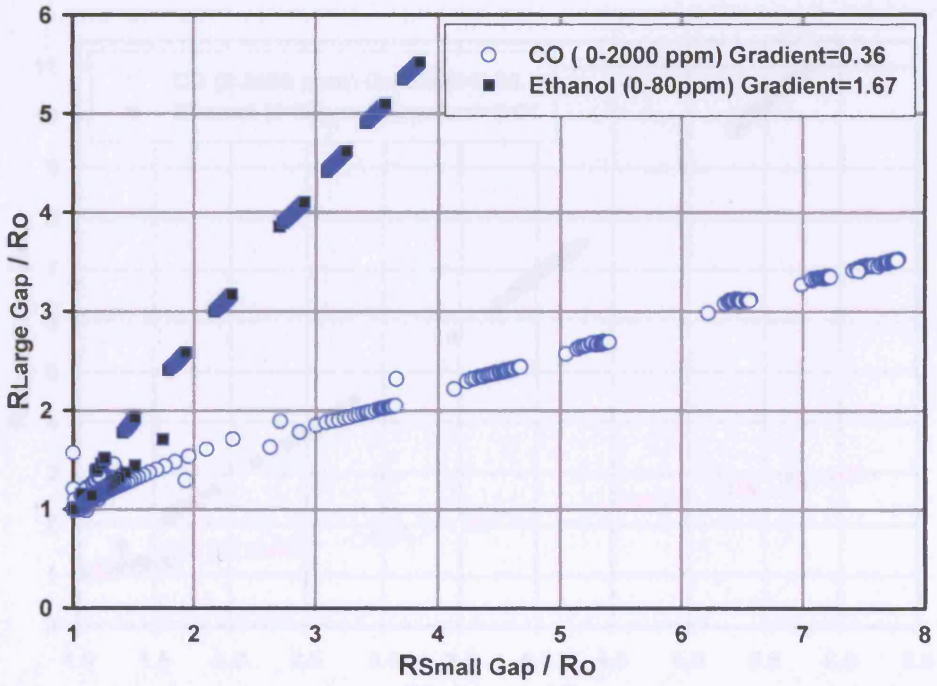

Figure 5.32 Operating lines for ethanol and carbon monoxide on sensor Mixed ZSM-5

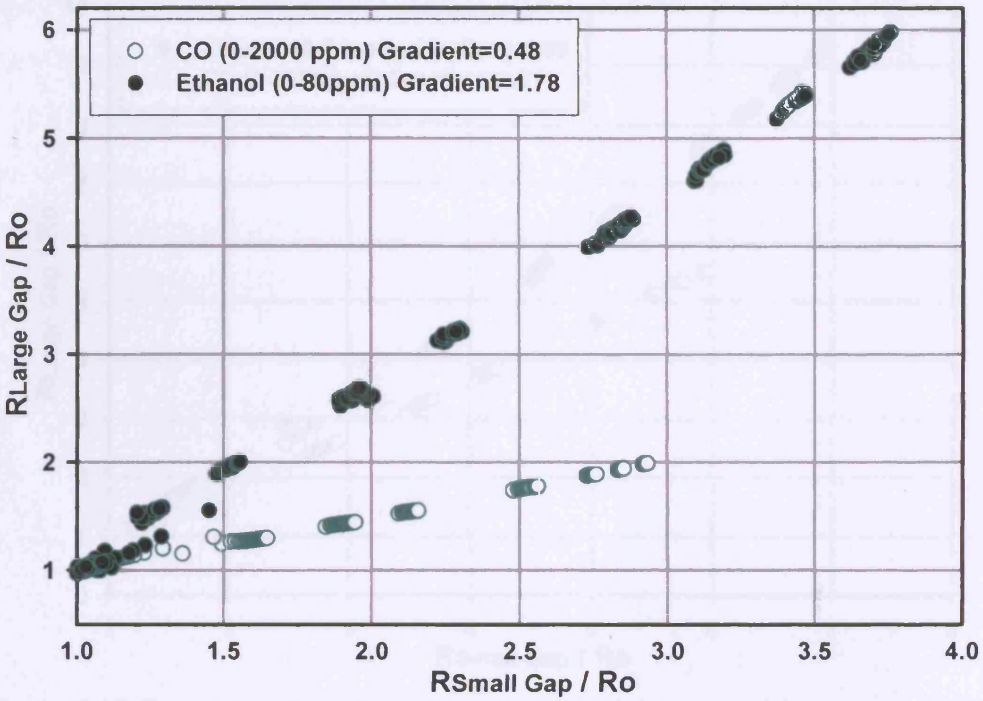

Figure 5.33 Operating lines for ethanol and carbon monoxide on sensor Mixed Y

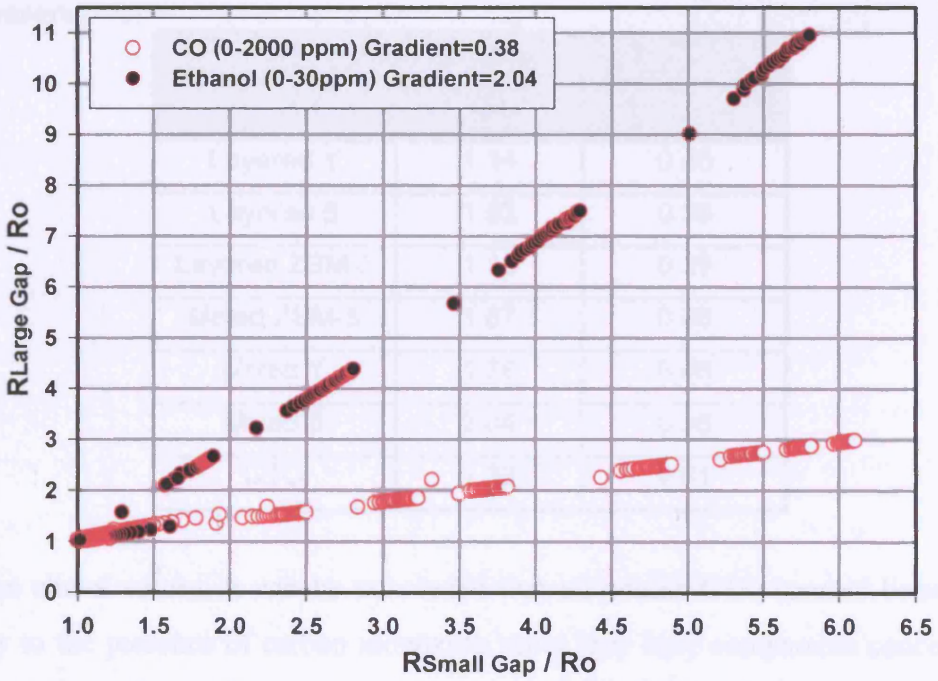

Figure 5.34 Operating lines for ethanol and carbon monoxide on sensor Mixed β

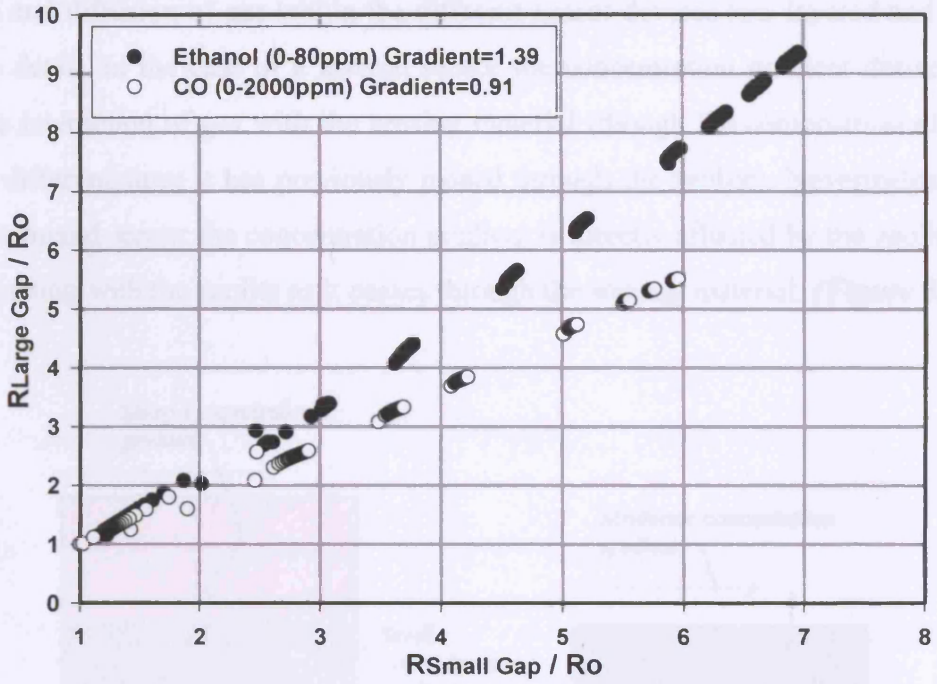

Figure 5.35 Operating lines for ethanol and carbon monoxide on sensor CTO

Table 5.6 Concentration gradients for ethanol and carbon monoxide for the seven CTO sensors

Zeolite Type	Ethanol Gradient	CO Gradient
Layered Y	1.14	0.48
Layered β	1.52	0.38
Layered ZSM-5	1.13	0.39
Mixed ZSM-5	1.67	0.36
Mixed Y	1.78	0.48
Mixed β	2.04	0.38
CTO	1.39	0.91

From the above values, it can be concluded that all zeolite-CTO sensors behave very similarly to the presence of carbon monoxide, since they have comparable concentration gradients. This indicates that CO passes through the zeolites sensors without reacting in contrast to ethanol that is found to react (by combustion) within the sensor device.

It is important to note the higher concentration gradients observed for all mixed zeolite sensors compared to the layered sensors. These differences can be explained based on the

reaction and diffusion of gas within the different sensor devices (i.e. layered and mixed). In more detail, in the case of a layered sensor the concentration gradient derives solely from the interaction of gas with the sensing material (though the composition of the gas may be different since it has previously passed through the zeolite). Nevertheless, in the case of a mixed sensor the concentration gradient is directly affected by the zeolite as the gas is reacting with the zeolite as it passes through the sensing material. ***(Figure 5.3.6)***

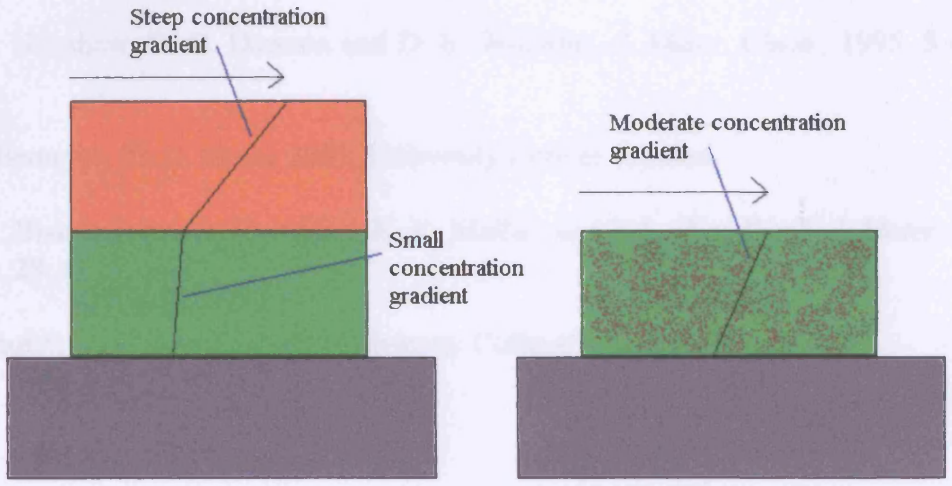

Figure 5.36 Concentration gradients of gas within layered and mixed devices

5.4 Conclusion

Multi-electrode chromium titanium oxide gas sensors with three differently sized porous materials (zeolite Y, β, ZSM-5) and two different configurations (layered and mixed) were successfully produced and tested in the presence of carbon monoxide and ethanol. This experimental study was shown to be successful in providing variations in the sensitivities and concentration gradients of the newly developed sensors to carbon monoxide and ethanol allowing a good discrimination between them. These results are considered to be very important for metal oxide based sensors and indicate a significant step-change for the development of more selective and highly sensitive sensors for a wide range of applications.

Chapter 5

References

1. G. S. Henshaw, D. H. Dawson and D. E. Williams, *J. Mater. Chem.*, 1995, **5** (11), 1791.

2. D. Niemeyer, Ph.D. thesis, 2001, University College London.

3. A. K. Bhattacharya, A. Hartridge, K. K. Mallick and J. L. Woodhead, *J. Mater. Sci.*, 1994, **29**, 6076.

4. K. Shukri, Ph.D. Thesis, 1999, University College London.

Chapter 6

A Study of the Response of Various Chromium Titanium Oxide Sensors to Volatile Organic, Flavour and Fragrance Compounds

6.1 Introduction

In Chapter 5, the newly fabricated zeolite sensors were tested to the presence of carbon monoxide and ethanol, demonstrating the effect of microstructure on their response.

This Chapter examines in more detail the characteristics of the zeolite sensors in combination with a range of chromium titanium oxide sensors using more complex vapours. Experiments have been performed with a number of volatile organic, flavour and fragrance compounds investigating additional effects on the sensor response due to cracking. The aim of this part of the work was to select sets of sensors with optimum discrimination between the tested compounds, and hence produce a sensor array that would show enhanced sensitivity and discrimination compared to conventional sensor arrays for electronic nose applications.

6.2 Experimental Method

6.2.1 Experimental Set-Up

Figure 6.a-c shows the schematic diagram of a newly developed (custom build) testing rig that was build specifically to evaluate the performance of sensor arrays in the presence of various volatile organic and flavour compounds. The rig allowed sensors to be exposed both to gases from cylinders and also from headspace injections in a similar manner to the FOX electronic nose.

As with the case of a generalised electronic nose instrument for odour monitoring, the rig composed of an odour delivery system, which was designed to transfer the odour from the source material to the sensor chamber. Then, a data acquisition system was used to record and forward the response signals from the sensors into the computer.

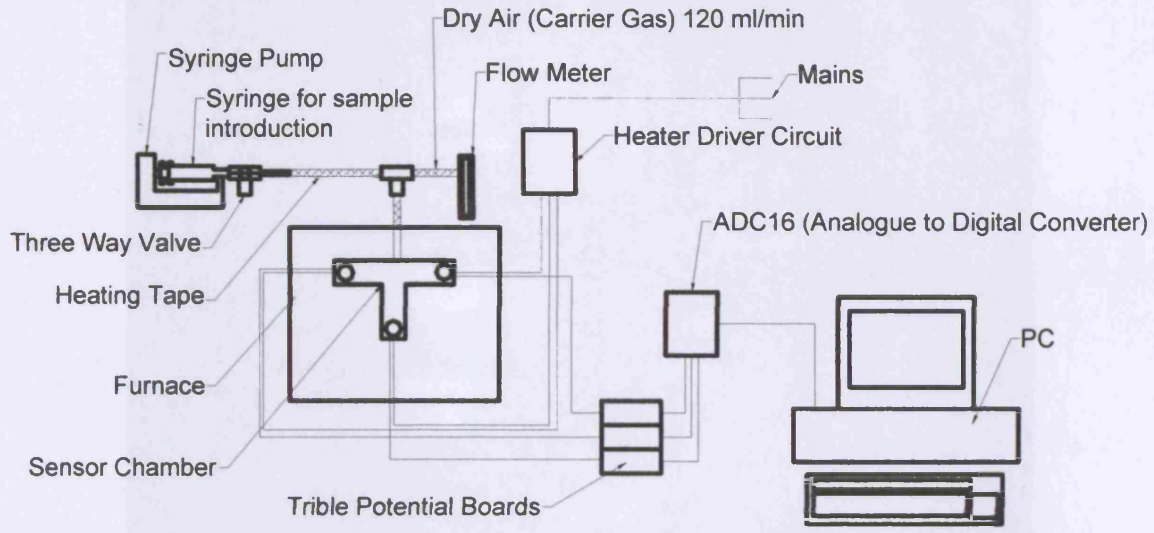

Figure 6.a Schematic diagram of the newly developed testing rig

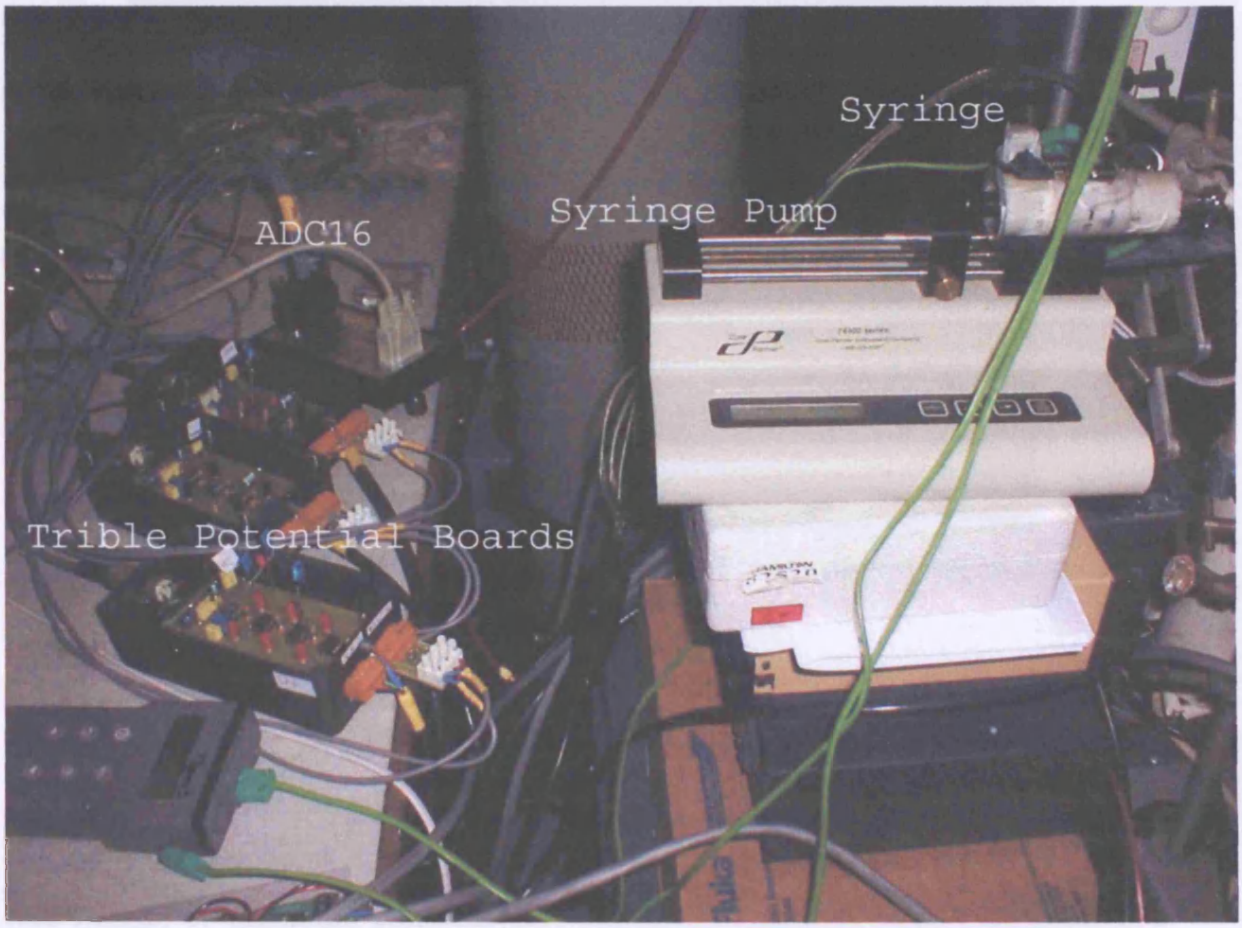

Figure 6.b The sensors electronics and odour delivering system of the newly developed testing rig

Figure 6.c The arrangement of the sensor chamber of the newly developed testing rig in the furnace

6.2.2 Headspace Injection

Generally, an odour can be delivered to the sensor chamber by a headspace or flow injection. In the headspace injection, the headspace of an odorant material is physically removed from a sample vial and inserted into the sensor chamber using either a manual (i.e. syringe) or automated procedure (i.e. commercial sampling unit). Alternatively, a carrier gas can be used to carry the odorant from the sample vessel into the sensor chamber by a method called flow injection.

In the present experiments the headspace injection method was used,

- Initially, a 10 ml sealed sample vial containing 2 ml of a testing compound was heated and agitated at a specific temperature to create a headspace vapour of a particular concentration.
- The headspace vapour was taken out from the sample vial using a glass syringe.
- Then, it was mixed with 120 ml/min of carrier gas (dry air), which was supplied to the sensor chamber through a flow meter.
- Finally, it was introduced into the gas stream (using a syringe pump).
- The sampled headspace for each different compound was introduced into the air stream through a three-way valve.
- The use of a syringe pump for vapour introduction allowed accurate control of the flow rate and the volume of the compound.

6.2.3 Sensor Chamber

A T-shaped PTFE sensor chamber was designed and constructed for these experiments. The design proved to be advantageous since it allowed the positioning of three SEMDEC sensors at equal distance from each other and from the inlet flow, avoiding variations in the response time of each sensor. The sensor chamber was placed into a furnace of constant temperature (60°C) to prevent adsorption of the vapours onto the chamber. For the same reason, a heating tape (operated at 70°C) was placed around the syringe and the stainless steel-pipe connecting the sensor chamber and the three-way valve from where the vapours were introduced into the sensor chamber.

6.2.4 Electronic Interfacing and Data Acquisition

The sensor electronics consisted of three triple potentiostat boards, which applied a fixed potential difference of 100 mV across the sensor and delivered a voltage output proportional to the resulting current. This current allowed the simultaneous measurements of three double gap SEMDEC sensors. The electronic boards (sensor electronics), used for the amplification and signal conditioning of the analogue signal, were connected with a high accuracy Analogue to Digital Converter (ADC16) for PC interfacing. Six output channels of the ADC16 were used as PC inputs (two channels for each triple potential board). Sampling rate of 1 sec was obtained for all three sensors. Because of the different

voltage range (maximum input voltage range) of the ADC16 (±2.5V) and the triple potentiostat boards (±10V), a voltage divider was placed just before the ADC input.

A data logging software from PicoLog based on the following equation was used to convert the acquisition file into real data for the sensors,

$$Rs = \frac{(V_{app} \times R_m)}{V_s \times Voltage\ Divider\ Factor} \qquad [6.1]$$

Where,

R_s is the sensor resistance and V_s is the sensor voltage which correspond to the sensor response. R_m corresponds to the measuring resistance (i.e. the resistance given on the electronic diagram). V_{app} corresponds to the voltage given on the electronic boards (0.1V)

6.2.5 Vapour Pressure and Concentration Calculations

The vapour pressure of the testing compounds was calculated according to the following equation,

$$Log_{10} P = (-0.2185\ M/K) + B \qquad [6.2]$$

Where,

P is the pressure expressed in Torr

K is the temperature in degrees Kelvin

M is the molar heat of vaporisation in calories per gram mole

B is a constant

Values of M, K and B were obtained from the Handbook of Chemistry and Physics.[2]

The concentration of each sample was calculated using the following equation:

$$C_1 = C\ x\ [v_1 / (v_1+v)] \qquad [6.3]$$

Where,

C_1 is the concentration of the testing compound in ppm

C is the vapour phase concentration of the testing compound in ppm

$v1$ is the sample injection speed (from syringe) in ml/min

v is the flow rate of carrier gas (dry air) in ml/min

6.3 Experimental Results

6.3.1 Normalisation Method

Preliminary experiments investigating the response of sensors to various compounds showed difficulties in obtaining repeatable results between injections of the same compound due to variations in headspace concentration. Therefore, a linearisation procedure was developed to eliminate the effects of concentration variation and to avoid their confusion with variations in the patterns of response.

The response of each sensor was therefore linearised (converted to $(R/R_o)^2-1$) and then normalised to the sensor with the highest response$(R_{max}/R_o)^2-1$) in each experiment.

6.3.2 Experiments with Sol-Gel CTO Sensors

Initially, experiments were performed using a range of chromium titanium oxide sensors prepared using a sol-gel method. The objective was to determine the performance of these sensors and to allow true evaluation of the improvements achieved by the new sensors.

6.3.2.1 Preparation of CTO Powders Using Sol-Emulsion-Gel Route

Titanium substituted chromium oxide spherical particles of controlled particle size were synthesised by Gilles Chabanis[1] using the sol-emulsion-gel route. Chromia and titania sols were mixed at the appropriate molar proportions in order to get different CTO compositions (i.e. $Cr_{1.95}Ti_{0.05}O_3$ and $Cr_{1.9}Ti_{0.1}O_3$) and were then gelled. Two differently sized microspheres of 2 and 0.7 μm were produced depending on the stirring condition ***(See Table 6.1)***.

Table 6.1 Summary of the prepared CTO-SOLGEL sensors with different microstructure and composition

CTO Sensor Name	Nominal Composition	Mean Particle Size (μm)
CTO-SOLGEL1	$Cr_{1.95}Ti_{0.05}O_3$	2
CTO-SOLGEL2	$Cr_{1.95}Ti_{0.05}O_3$	0.7
CTO-SOLGEL3	$Cr_{1.9}Ti_{0.1}O_3$	0.7

6.3.2.2 Fabrication of CTO Sensor Arrays

The CTO-SOLGEL powders were screen-printed onto alumina tiles containing 2 mm x2 mm chips with a gold electrode pattern that has both a small (S) and large (L) electrode gap

(SEMDEC) ***(See Figure 3.13)***. Following the screen-printing the devices were fired at 800°C for 2 h, obtained by a temperature ramp of 15°C min^{-1} to remove the organic vehicle and leave the CTO oxide.

6.3.2.3 Results Analysis for CTO Sol-Gel Sensors

The three CTO-SOLGEL sensors (operated at 400°C) with different microstructures were tested for responses to seven compounds (amyl acetate, benzyl acetate, benzyl benzoate, cineole, ethanol, linalool and toluene). The compounds used in these experiments were at least 99.9% pure as obtained from 'Aldrich'. Details regarding their structure are given in ***Appendix A***.

Figures 6.1-6.7 show the normalised response signals of the three CTO-SOLGEL sensors to the seven compounds. Different sensitivities were observed for different sensors when exposed to a particular compound. These results demonstrate that the microstructure of a sensor affects its response behaviour. Additional variances in sensor responses were observed for different sensors and compounds.

From ***Figures 6.1-6.7***, it is clear that both CTO-SOLGEL2 and CTO-SOLGEL3 ***(Table 6.1)*** sensors have a significantly larger (~double) response on the large gap compared to the small gap, for all the compounds. This indicates that the tested gases develop a significant concentration gradient due to combustion of the gas within the sensing layer of these sensors. However, for CTO-SOLGEL1 sensor the response on the two gaps was found to be of similar magnitude.

6.3.2.4 Repeatability of Measurements

- The repeatability of the CTO-SOLGEL sensor responses to each compound was examined using two repeated injections of the same headspace.
- Each compound was heated to a particular temperature to create a headspace vapour of a particular concentration.
- Then, the syringe was filled once with the headspace vapour produced.
- Two consecutive injections of the headspace vapour were performed
- Between each injection the sample injection speed (from syringe), and the flow rate of the air were kept constant.

- The concentration of each compound was therefore the same for the 2 injections.
- For each headspace injection, the gas syringe was flushed by carrier gas (dry air) to avoid cross-contamination.

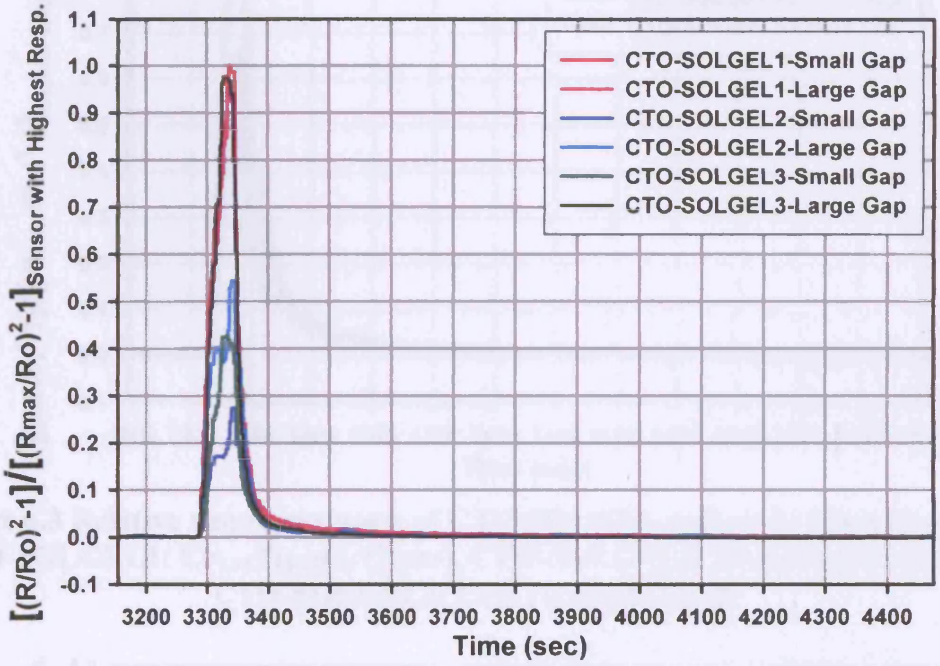

Figure 6.1 Relative response signals of CTO-SOLGEL sensors to amyl acetate CTO-SOLGEL1: $Cr_{1.95}Ti_{0.05}O_3$ (2 µm), CTO-SOLGEL2: $Cr_{1.95}Ti_{0.05}O_3$ (0. 7 µm) CTO-SOLGEL3: $Cr_{1.9}Ti_{0.1}O_3$ (0.7 µm)

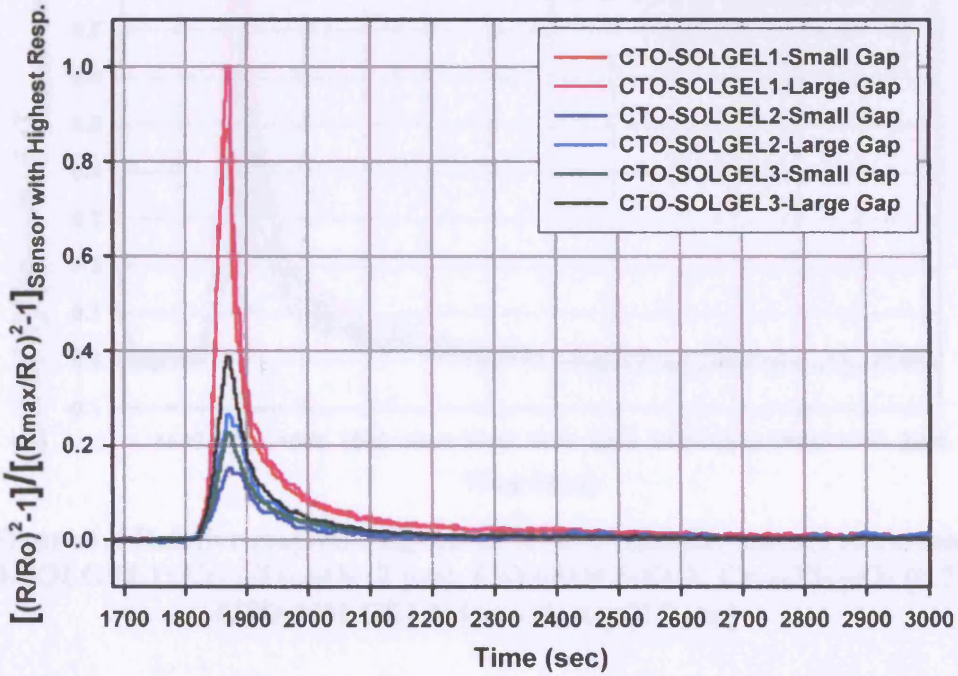

Figure 6.2 Relative response signals of CTO-SOLGEL sensors to benzyl acetate CTO-SOLGEL1: $Cr_{1.95}Ti_{0.05}O_3$ (2 µm), CTO-SOLGEL2: $Cr_{1.95}Ti_{0.05}O_3$ (0.7 µm) CTO-SOLGEL3: $Cr_{1.9}Ti_{0.1}O_3$ (0.7 µm)

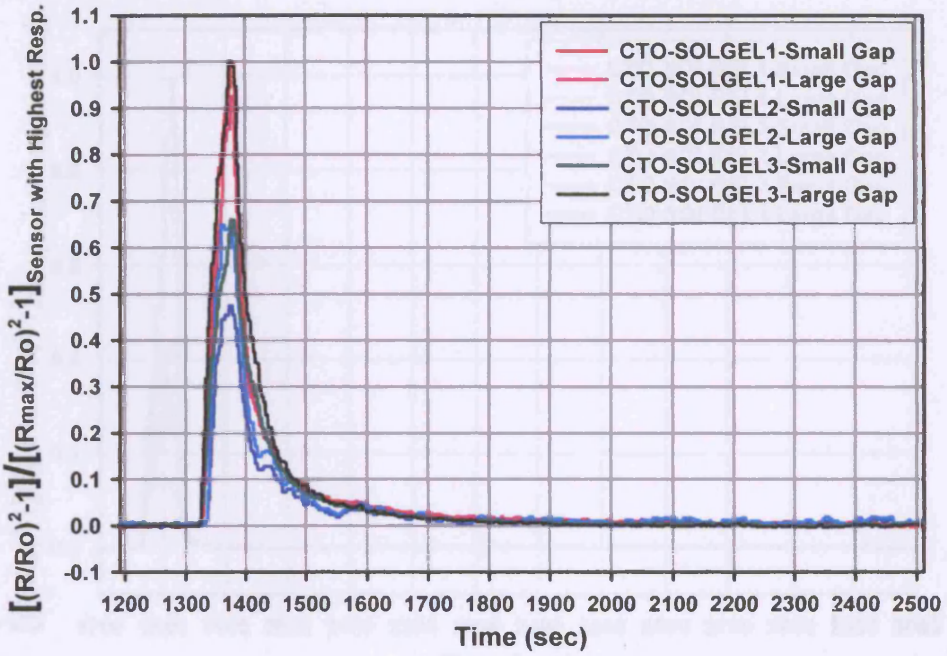

Figure 6.3 Relative response signals of CTO-SOLGEL sensors to benzyl benzoate CTO-SOLGEL1: $Cr_{1.95}Ti_{0.05}O_3$ (2 µm), CTO-SOLGEL2: $Cr_{1.95}Ti_{0.05}O_3$ (0.7 µm) CTO-SOLGEL3: $Cr_{1.9}Ti_{0.1}O_3$ (0.7 µm)

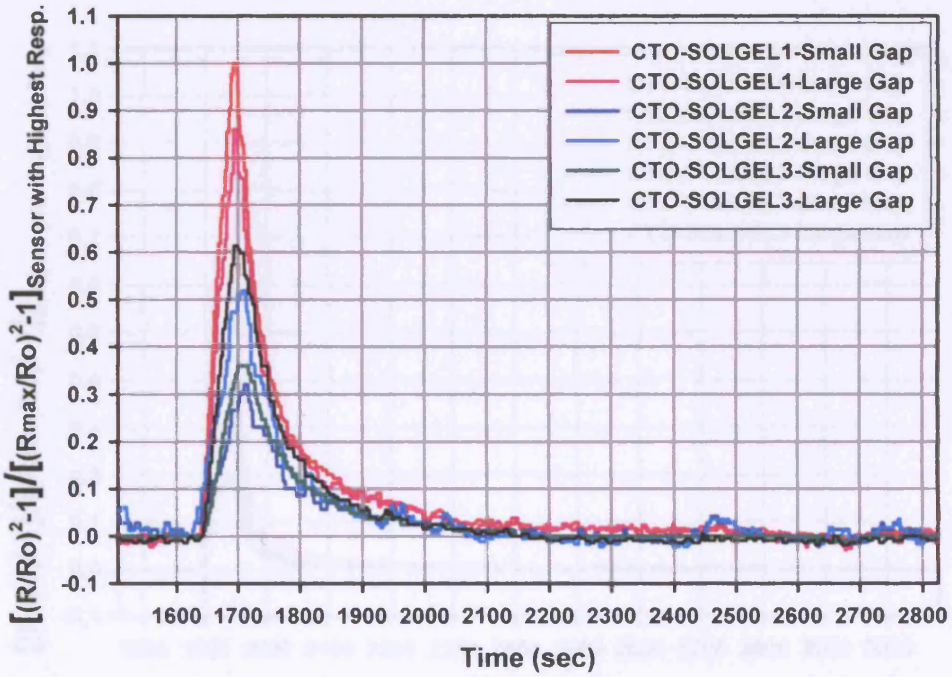

Figure 6.4 Relative response signals of CTO-SOLGEL sensors to cineole CTO-SOLGEL1: $Cr_{1.95}Ti_{0.05}O_3$ (2 µm), CTO-SOLGEL2: $Cr_{1.95}Ti_{0.05}O_3$ (0.7 µm) CTO-SOLGEL3: $Cr_{1.9}Ti_{0.1}O_3$ (0.7 µm)

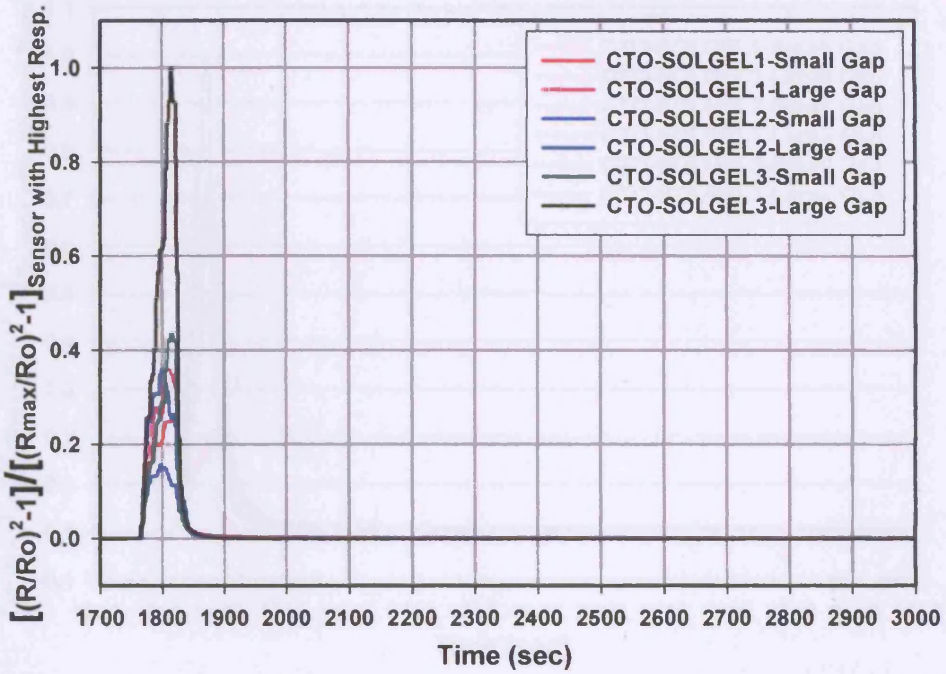

Figure 6.5 Relative response signals of CTO-SOLGEL sensors to ethanol CTO-SOLGEL1: $Cr_{1.95}Ti_{0.05}O_3$ (2 µm), CTO-SOLGEL2: $Cr_{1.95}Ti_{0.05}O_3$ (0.7 µm) CTO-SOLGEL3: $Cr_{1.9}Ti_{0.1}O_3$ (0.7 µm)

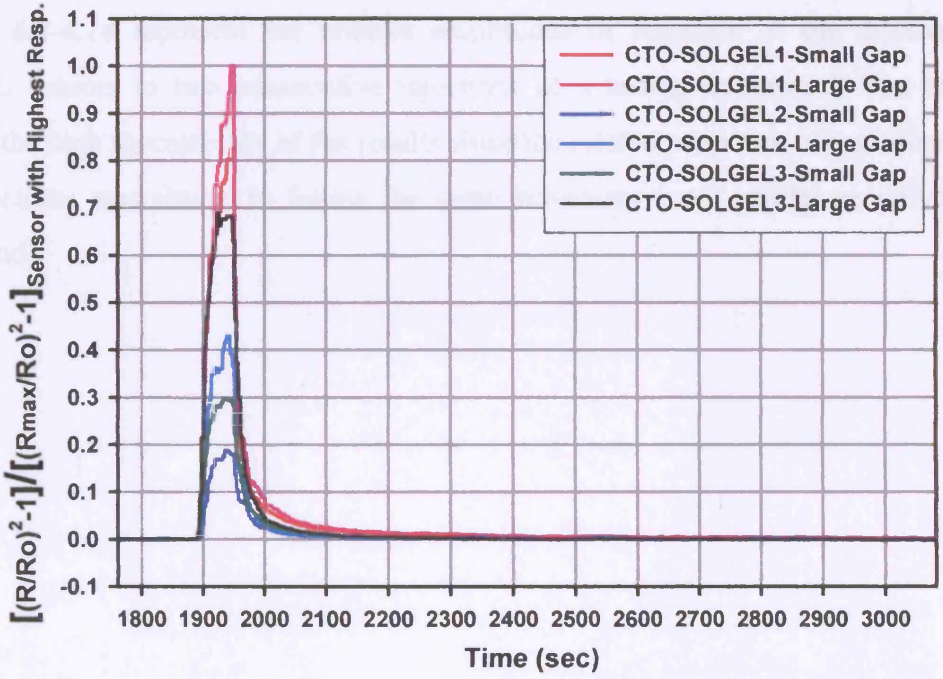

Figure 6.6 Relative response signals of CTO-SOLGEL sensors to linalool CTO-SOLGEL1: $Cr_{1.95}Ti_{0.05}O_3$ (2 µm), CTO-SOLGEL2: $Cr_{1.95}Ti_{0.05}O_3$ (0.7 µm) CTO-SOLGEL3: $Cr_{1.9}Ti_{0.1}O_3$ (0.7 µm)

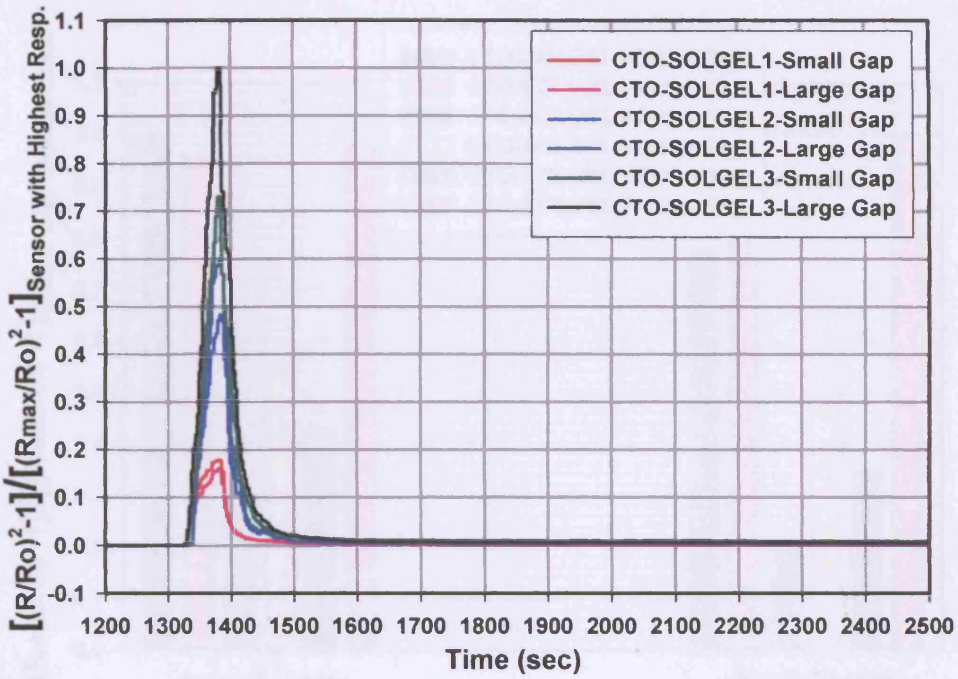

Figure 6.7 Relative response signals of CTO-SOLGEL sensors to toluene CTO-SOLGEL1: $Cr_{1.95}Ti_{0.05}O_3$ (2 µm), CTO-SOLGEL2: $Cr_{1.95}Ti_{0.05}O_3$ (0.7 µm) CTO-SOLGEL3: $Cr_{1.9}Ti_{0.1}O_3$ (0.7 µm)

Figures 6.8-6.14 represent the relative amplitudes of response of the different CTO-SOLGEL sensors to two consecutive injections of a testing compound. The bar charts indicate the high repeatability of the results since the relative response of each sensor to the two injections was shown to follow the same behaviour (very similar sensitivity to the compound).

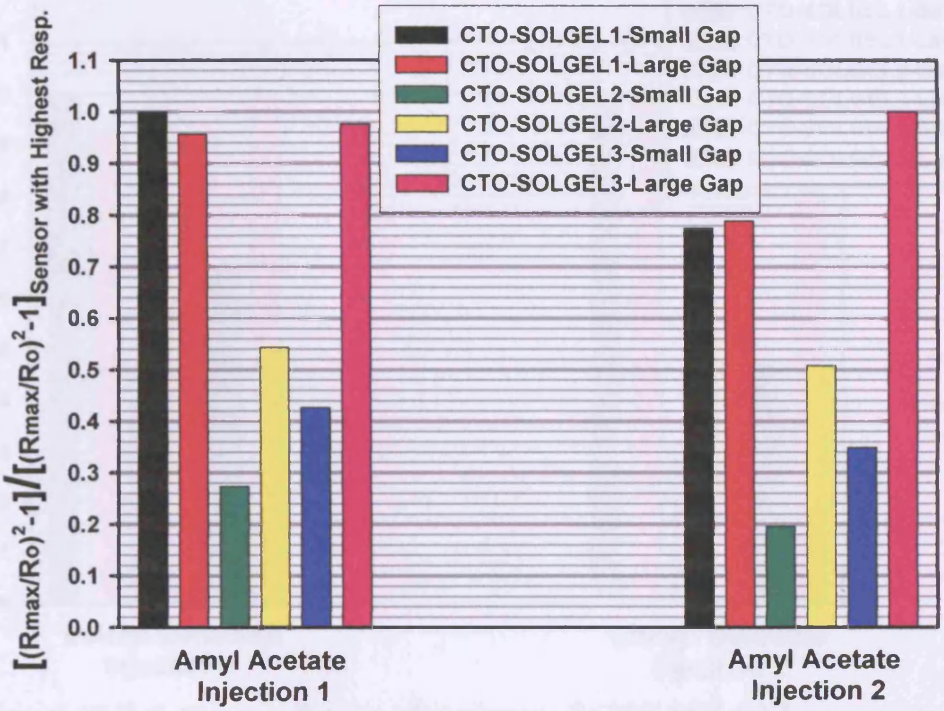

Figure 6.8 Relative amplitudes of response of CTO-SOLGEL sensors to two consecutive injections of amyl acetate
CTO-SOLGEL1: $Cr_{1.95}Ti_{0.05}O_3$ (2 µm), CTO-SOLGEL2: $Cr_{1.95}Ti_{0.05}O_3$ (0.7 µm)
CTO-SOLGEL3: $Cr_{1.9}Ti_{0.1}O_3$ (0.7 µm)

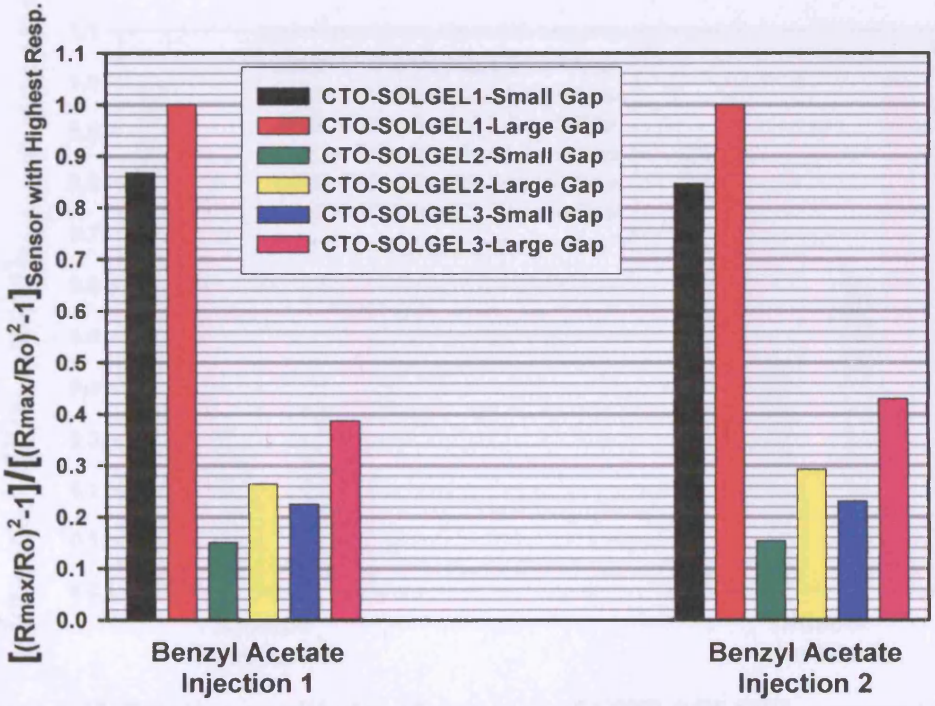

Figure 6.9 Relative amplitudes of response of CTO-SOLGEL sensors to two consecutive injections of benzyl acetate
CTO-SOLGEL1: $Cr_{1.95}Ti_{0.05}O_3$ (2 µm), CTO-SOLGEL2: $Cr_{1.95}Ti_{0.05}O_3$ (0.7 µm)
CTO-SOLGEL3: $Cr_{1.9}Ti_{0.1}O_3$ (0.7 µm)

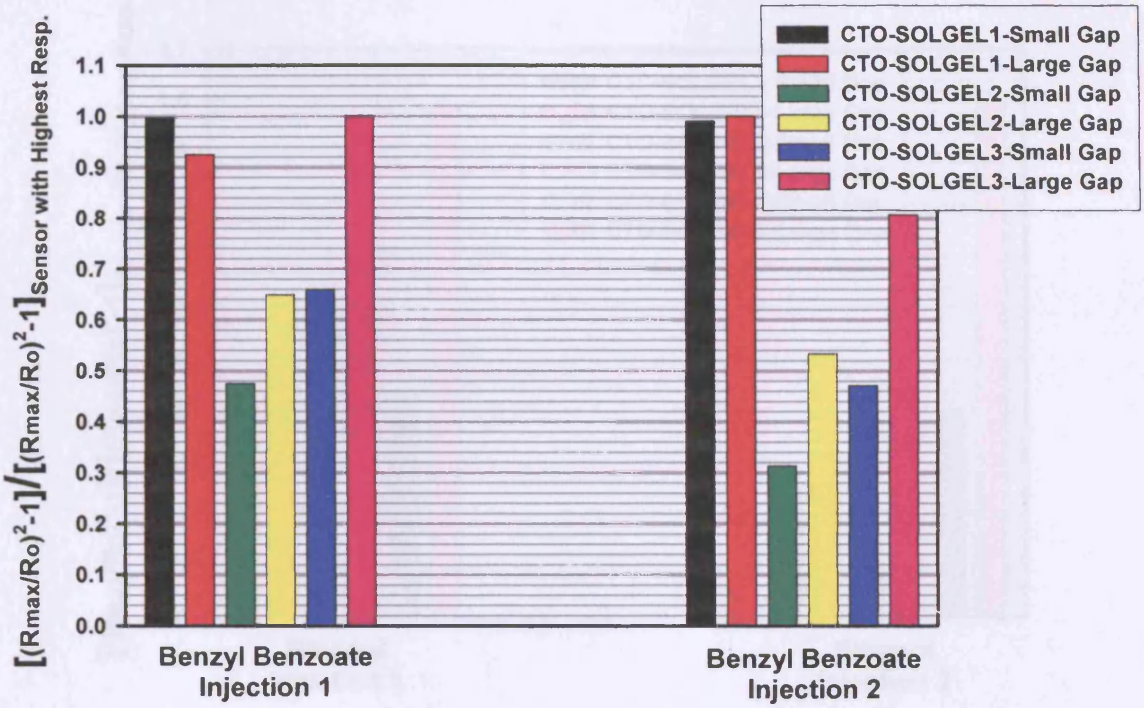

Figure 6.10 Relative amplitudes of response of CTO-SOLGEL sensors to two consecutive injections of benzyl benzoate
CTO-SOLGEL1: $Cr_{1.95}Ti_{0.05}O_3$ (2 µm), CTO-SOLGEL2: $Cr_{1.95}Ti_{0.05}O_3$ (0.7 µm)
CTO-SOLGEL3: $Cr_{1.9}Ti_{0.1}O_3$ (0.7 µm)

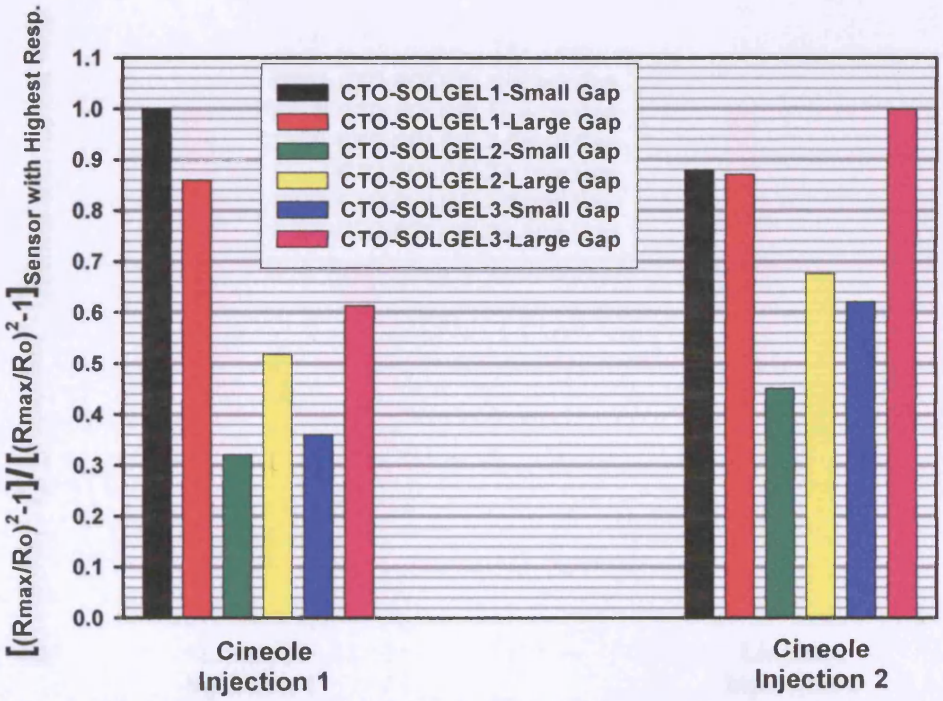

Figure 6.11 Relative amplitudes of response of CTO-SOLGEL sensors to two consecutive injections of cineole
CTO-SOLGEL1: $Cr_{1.95}Ti_{0.05}O_3$ (2 µm), CTO-SOLGEL2: $Cr_{1.95}Ti_{0.05}O_3$ (0.7 µm)
CTO-SOLGEL3: $Cr_{1.9}Ti_{0.1}O_3$ (0.7 µm)

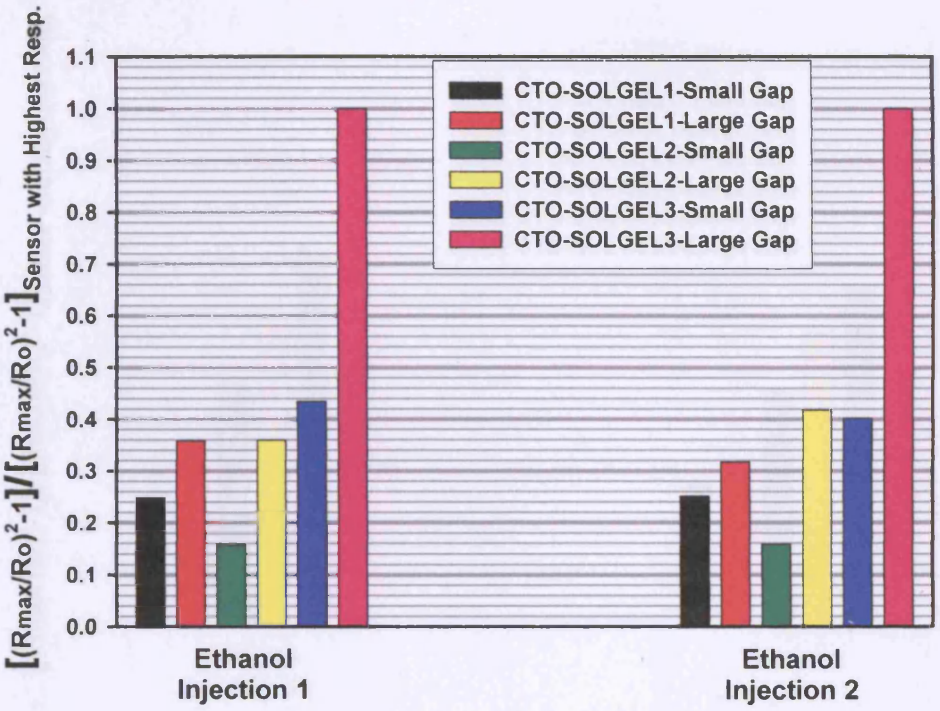

Figure 6.12 Relative amplitudes of response of CTO-SOLGEL sensors to two consecutive injections of ethanol
CTO-SOLGEL1: $Cr_{1.95}Ti_{0.05}O_3$ (2 µm), CTO-SOLGEL2: $Cr_{1.95}Ti_{0.05}O_3$ (0.7 µm)
CTO-SOLGEL3: $Cr_{1.9}Ti_{0.1}O_3$ (0.7 µm)

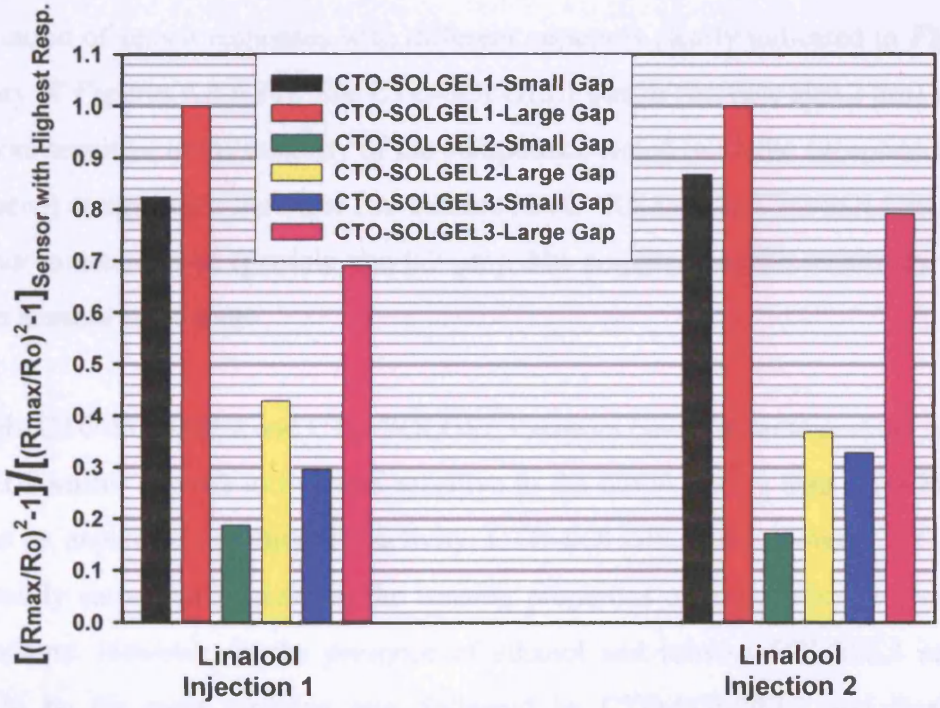

Figure 6.13 Relative amplitudes of response of CTO-SOLGEL sensors to two consecutive injections of linalool
CTO-SOLGEL1: $Cr_{1.95}Ti_{0.05}O_3$ (2 µm), CTO-SOLGEL2: $Cr_{1.95}Ti_{0.05}O_3$ (0.7 µm)
CTO-SOLGEL3: $Cr_{1.9}Ti_{0.1}O_3$ (0.7 µm)

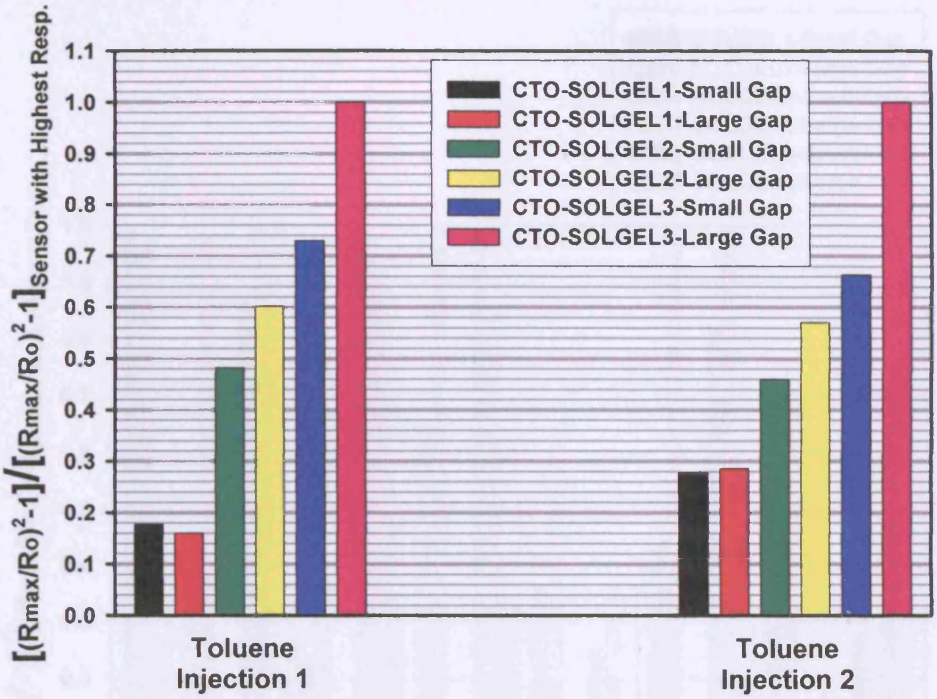

Figure 6.14 Relative amplitudes of response of CTO-SOLGEL sensors to two consecutive injections of toluene
CTO-SOLGEL1: $Cr_{1.95}Ti_{0.05}O_3$ (2 μm), CTO-SOLGEL2: $Cr_{1.95}Ti_{0.05}O_3$ (0.7 μm)
CTO-SOLGEL3: $Cr_{1.9}Ti_{0.1}O_3$ (0.7 μm)

The variation of sensor responses with different odours is clearly indicated in ***Figure 6.15*** (summary of ***Figures 6.8-6.14***). The CTO-SOLGEL1 sensor (particle size 2 μm) was found to be more sensitive to the majority of the compounds tested (with the exception of ethanol and toluene) compared to the other two sensors (CTO-SOLGEL2, CTO-SOLGEL3), which have finer microstructure (particle size 0.7 μm). The amplitude of the sensitivity varies for different sensors and odours.

Although, CTO-SOLGEL2 and CTO-SOLGEL3 sensors have the same particle size, CTO-SOLGEL3 sensor appears to be more sensitive to the tested odours than CTO-SOLGEL2. This can be explained in terms of reactivity; CTO-SOLGEL3 has a lower Cr/Ti ratio and that possibly causes an increase in the sensing properties of this particular sensor to the tested odours. However, in the presence of ethanol and toluene SOLGEL3 sensor was shown to be the most sensitive one, followed by CTO-SOLGEL2 and finally CTO-SOLGEL1. As before, the amplitude of the response was found to vary with sensor and odour type.

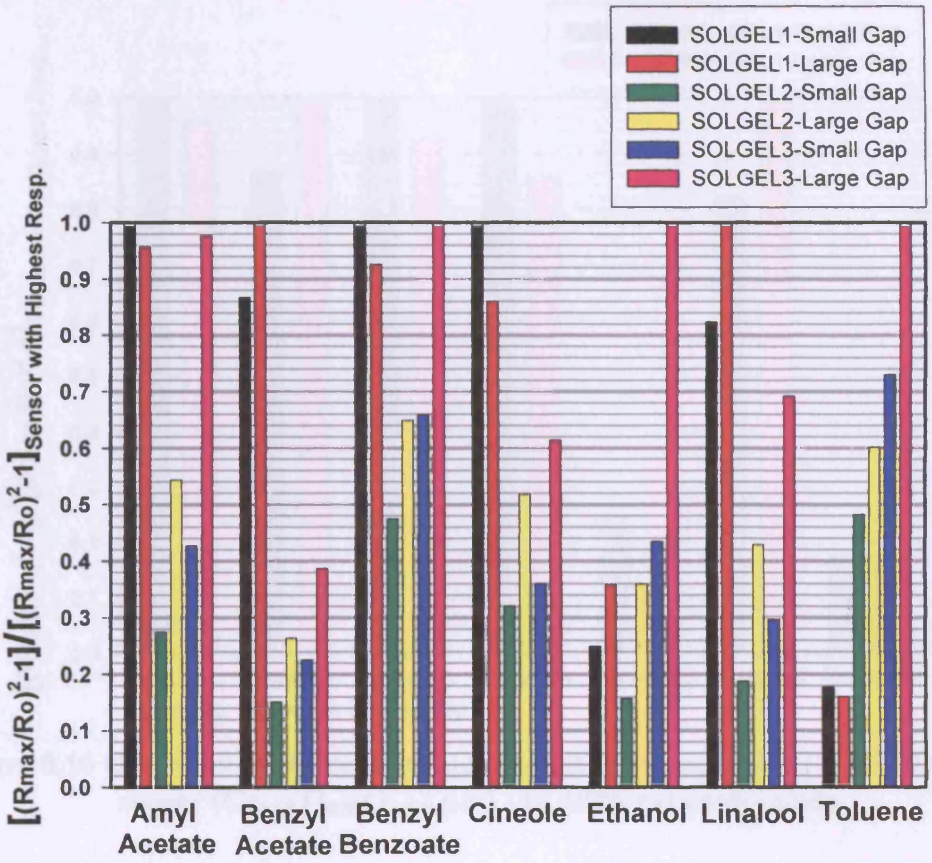

Figure 6.15 Overview of the relative amplitudes of response of CTO-SOLGEL sensors to different compounds
CTO-SOLGEL1: $Cr_{1.95}Ti_{0.05}O_3$ (2 µm), CTO-SOLGEL2: $Cr_{1.95}Ti_{0.05}O_3$ (0.7 µm)
CTO-SOLGEL3: $Cr_{1.9}Ti_{0.1}O_3$ (0.7 µm)

Figures 6.16-6.18 give an overview of the relative amplitude of response (small and large gap) of each sensor separately, to the presence of all odour compounds tested. Figures show clearly that each sensor array reacts differently according to odour type.

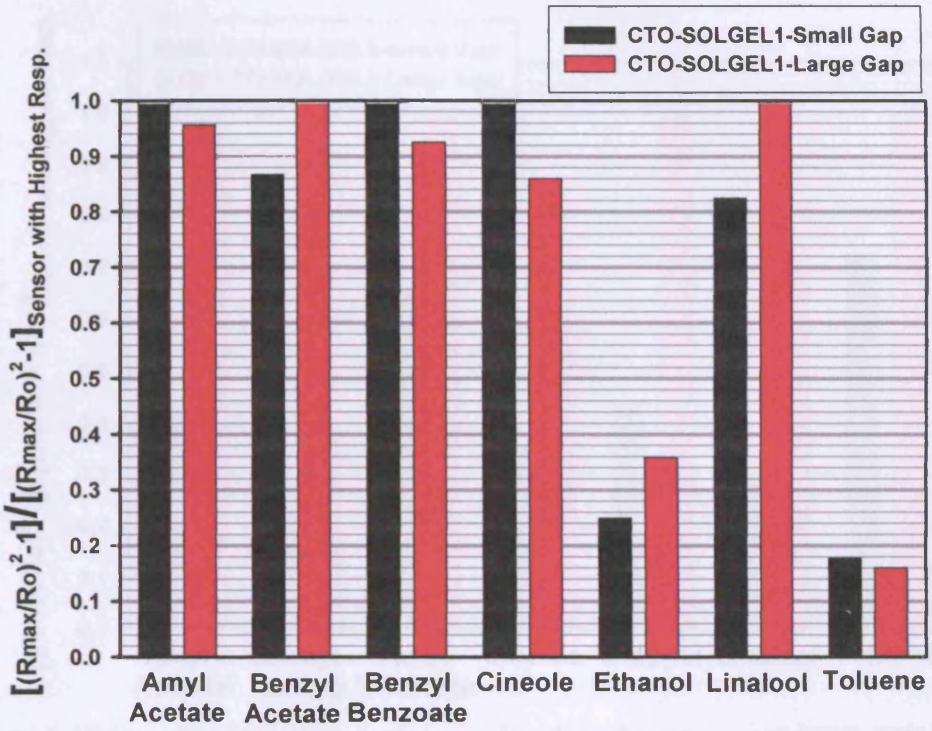

Figure 6.16 Overview of the relative amplitudes of response of CTO-SOLGEL1 sensor ($Cr_{1.95}Ti_{0.05}O_3$ (2 µm)) to different compounds

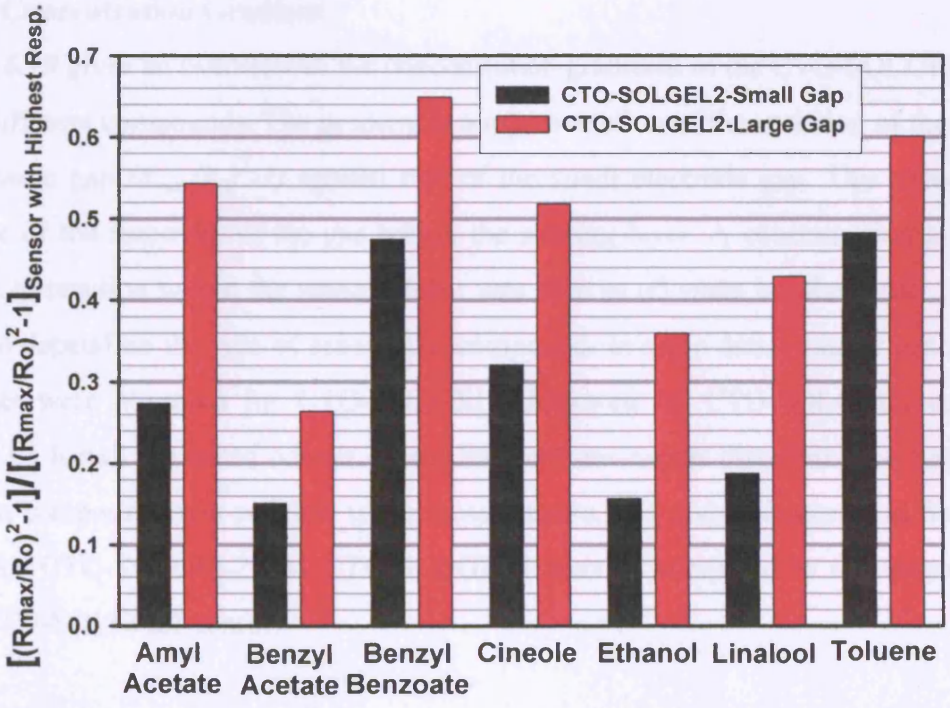

Figure 6.17 Overview of the relative amplitudes of response of CTO-SOLGEL2 sensor ($Cr_{1.95}Ti_{0.05}O_3$ (0.7 µm)) to different compounds

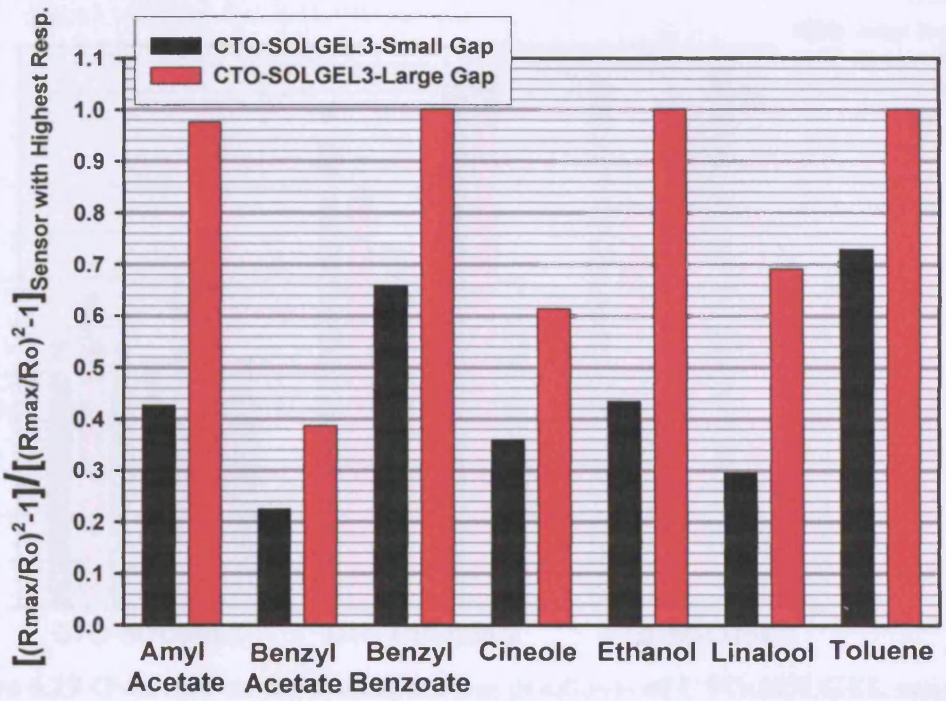

Figure 6.18 Overview of the relative amplitudes of response of CTO-SOLGEL3 sensor ($Cr_{1.9}Ti_{0.1}O_3$ (0.7 µm)) to different compounds

6.3.2.5 Concentration Gradient

Figure 6.19 gives an overview of the concentration gradients of the CTO-SOLGEL sensors to the different compounds. The gradient is a representation of the variation of the response of the large gap $(R_{max}/R_o)^2-1)$ against that of the small electrode gap. This value gives a measure of the reactivity of the gas within the sensing layer. A concentration gradient of gas due to reaction within the sensing layer was seen in all cases but the actual value was found to depend on the type of sensor and compound. In more detail, higher concentration gradients were observed for CTO-SOLGEL3 followed by CTO-SOLGEL2 and CTO-SOLGEL1 for all the tested odours. According to these results discrimination between the different compounds was possible using these sensors. The discrimination was found to be better for CTO-SOLGEL2 and CTO-SOLGEL3 sensors compared to the larger particle sized CTO-SOLGEL1 sensor.

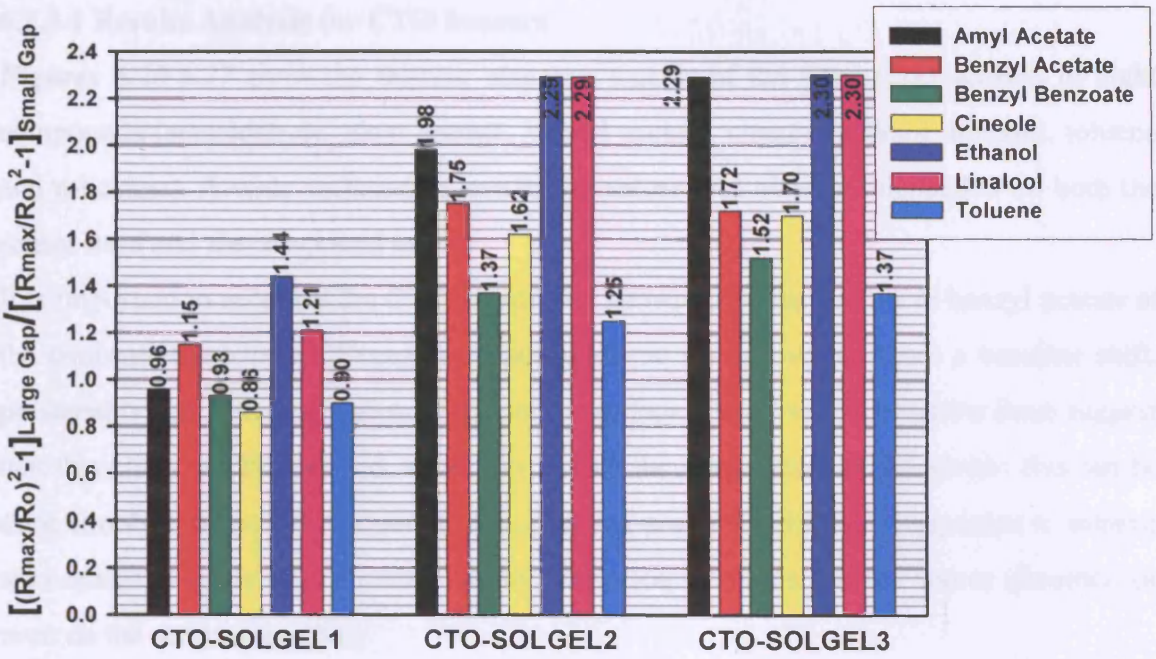

Figure 6.19 Overview of the concentration gradients of CTO-SOLGEL sensors to different volatile organic and flavour compounds
CTO-SOLGEL1: $Cr_{1.95}Ti_{0.05}O_3$ (2 µm), CTO-SOLGEL2: $Cr_{1.95}Ti_{0.05}O_3$ (0.7 µm)
CTO-SOLGEL3: $Cr_{1.9}Ti_{0.1}O_3$ (0.7 µm)

6.3.3 Experiments with CTO Sensors

Three different multi-electrode CTO sensor array devices were tested for their reactivity to seven different compounds.

The two CTO sensors (i.e. Capteur-CTO and CTO+Cr_2O_3) were supplied by 'Capteur Sensors and Analysers Ltd'. The other CTO sensor used (prepared at UCL) had the same nominal composition as the Capteur CTO sensors, but it was prepared with a different technique resulting in a finer microstructure. Details regarding the preparation of CTO sensor were given in Chapter 5. ***Table 6.2*** summarises the different CTO sensors used to perform the study described below.

Table 6.2 Summary of the prepared CTO sensors

CTO Sensor Name	Nominal Composition	Microstructure Particle Size (µm)
Capteur-CTO	$Cr_{1.95}Ti_{0.05}O_3$	1
CTO	$Cr_{1.95}Ti_{0.05}O_3$	0.5
CTO+Cr_2O_3	$Cr_{1.9}Ti_{0.1}O_3$ (Cr_2O_3 Layered on top)	1 for CTO and 0.7 for Cr_2O_3

6.3.3.1 Results Analysis for CTO Sensors

Figures 6.20-6.27 show the relative response signals of the three CTO sensors to eight compounds (acetaldehyde, amyl acetate, benzyl acetate, cineole, ethanol, linalool, toluene and n-hexane). A wide variation in sensitivity values was observed depended on both the sensor used and the compound tested.

It is important to note that the CTO sensor was shown to be insensitive to benzyl acetate at the concentrations tested. Exposure to acetaldehyde was shown to cause a baseline shift, presumably due to carboxylation of the sensor surface. However, experiments done suggest that this effect can be reversed, simply by raising the temperature of the sensor; this can be done simply and routinely as part of the operating protocol.[3] Similarly, exposure to toluene also causes baseline shift possibly due to adsorption of toluene on the sensor chamber, or even on the sensor mounting.

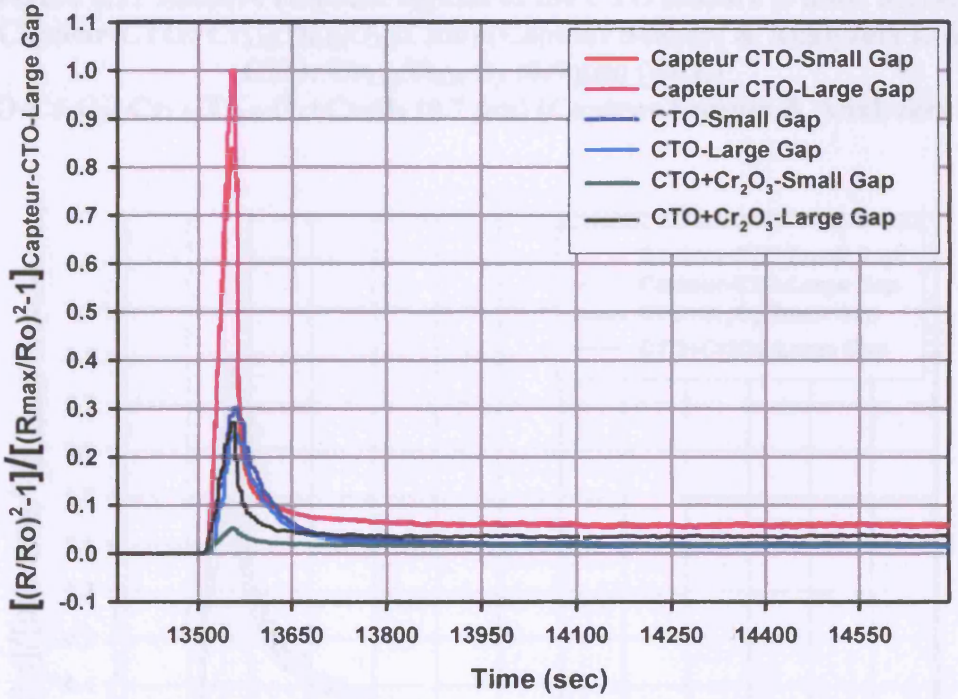

Figure 6.20 Relative response signals of the CTO sensors to acetaldehyde
Capteur-CTO: $Cr_{1.95}Ti_{0.05}O_3$ (1 µm) (Capteur Sensors & Analyzers Ltd)
CTO: $Cr_{1.95}Ti_{0.05}O_3$ (0.5 µm) (UCL)
CTO-Cr_2O_3: $Cr_{1.95}Ti_{0.05}O_3$+Cr_2O_3 (0.7 µm) (Capteur Sensors & Analyzers Ltd)

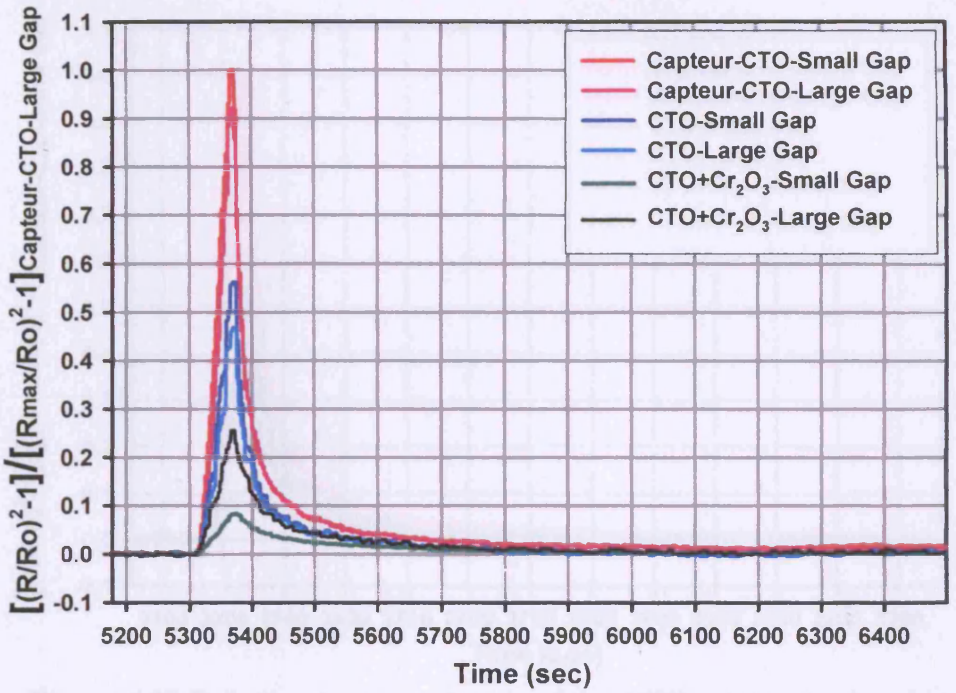

Figure 6.21 Relative response signals of the CTO sensors to amyl acetate
Capteur-CTO: $Cr_{1.95}Ti_{0.05}O_3$ (1 µm) (Capteur Sensors & Analyzers Ltd)
CTO: $Cr_{1.95}Ti_{0.05}O_3$ (0.5 µm) (UCL)
CTO-Cr_2O_3: $Cr_{1.95}Ti_{0.05}O_3$+Cr_2O_3 (0.7 µm) (Capteur Sensors & Analyzers Ltd)

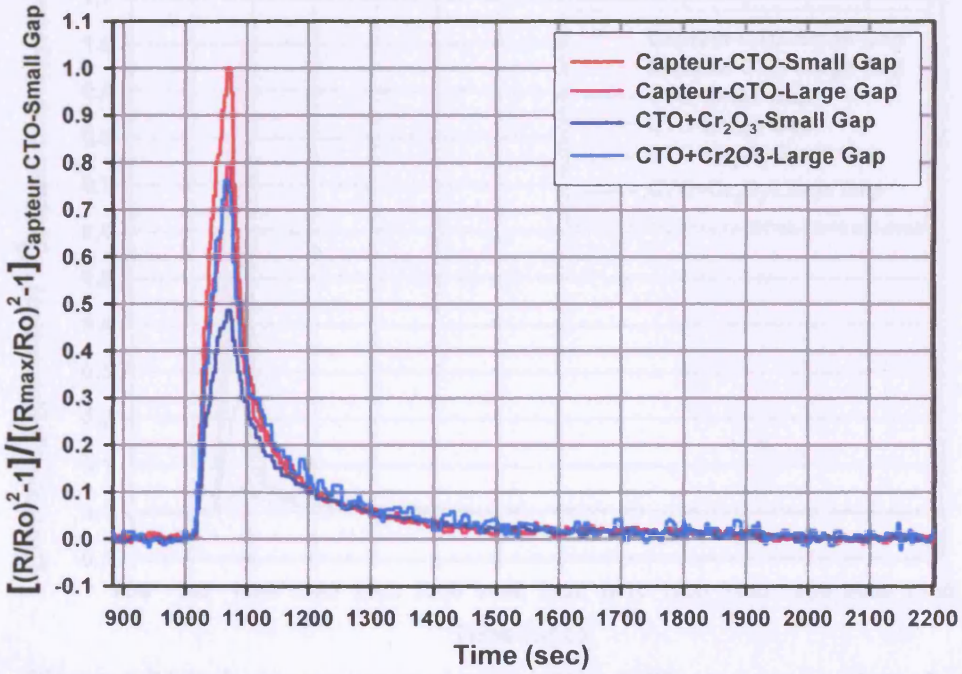

Figure 6.22 Relative response signals of the CTO sensors to benzyl acetate
Capteur-CTO: $Cr_{1.95}Ti_{0.05}O_3$ (1 µm) (Capteur Sensors & Analyzers Ltd)
CTO: $Cr_{1.95}Ti_{0.05}O_3$ (0.5 µm) (UCL)
CTO-Cr_2O_3: $Cr_{1.95}Ti_{0.05}O_3$+Cr_2O_3 (0.7 µm) (Capteur Sensors & Analyzers Ltd)

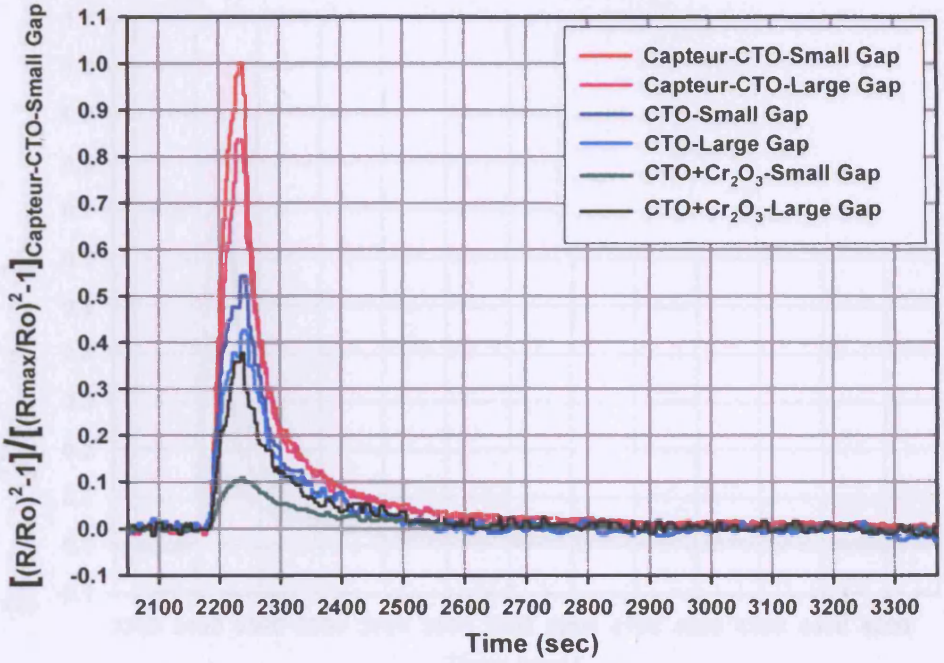

Figure 6.23 Relative response signals of the CTO sensors to cineole
Capteur-CTO: $Cr_{1.95}Ti_{0.05}O_3$ (1 µm) (Capteur Sensors & Analyzers Ltd)
CTO: $Cr_{1.95}Ti_{0.05}O_3$ (0.5 µm) (UCL)
CTO-Cr_2O_3: $Cr_{1.95}Ti_{0.05}O_3$ +Cr_2O_3 (0.7 µm) (Capteur Sensors & Analyzers Ltd)

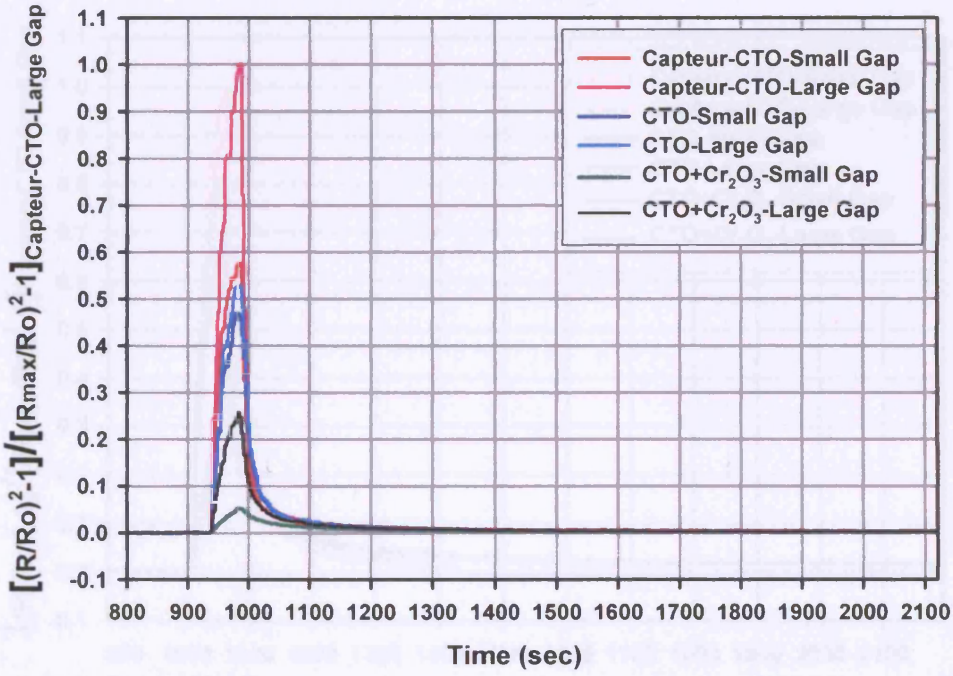

Figure 6.24 Relative response signals of the CTO sensors to ethanol
Capteur-CTO: $Cr_{1.95}Ti_{0.05}O_3$ (1 µm) (Capteur Sensors & Analyzers Ltd)
CTO: $Cr_{1.95}Ti_{0.05}O_3$ (0.5 µm) (UCL)
CTO-Cr_2O_3: $Cr_{1.95}Ti_{0.05}O_3$+Cr_2O_3 (0.7 µm) (Capteur Sensors & Analyzers Ltd)

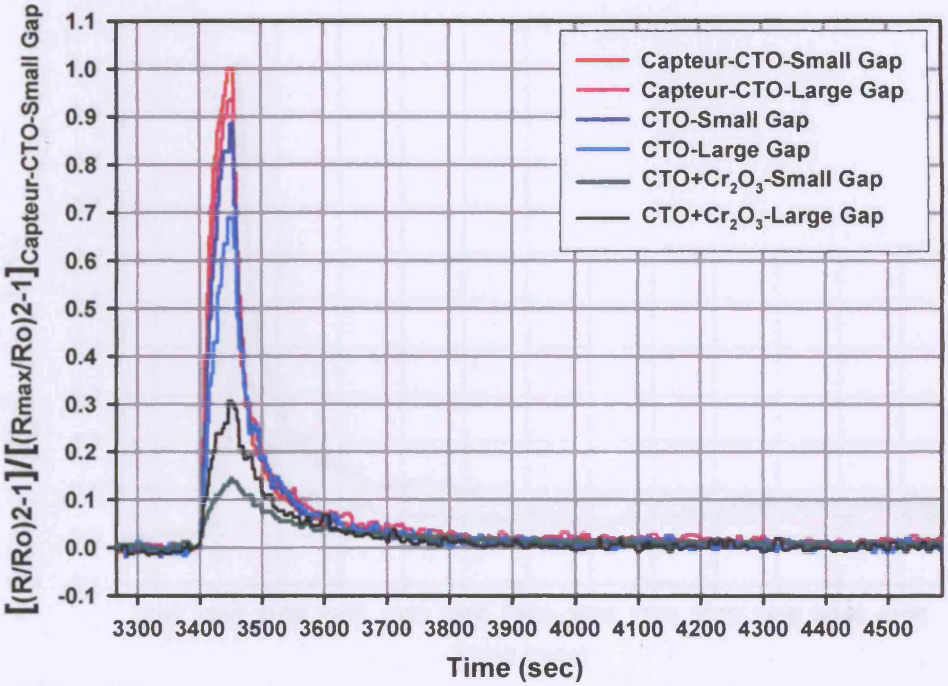

Figure 6.25 Relative response signals of the CTO sensors to linalool
Capteur-CTO: $Cr_{1.95}Ti_{0.05}O_3$ (1 µm) (Capteur Sensors & Analyzers Ltd)
CTO: $Cr_{1.95}Ti_{0.05}O_3$ (0.5 µm) (UCL)
CTO-Cr_2O_3: $Cr_{1.95}Ti_{0.05}O_3$+Cr_2O_3 (0.7 µm) (Capteur Sensors & Analyzers Ltd)

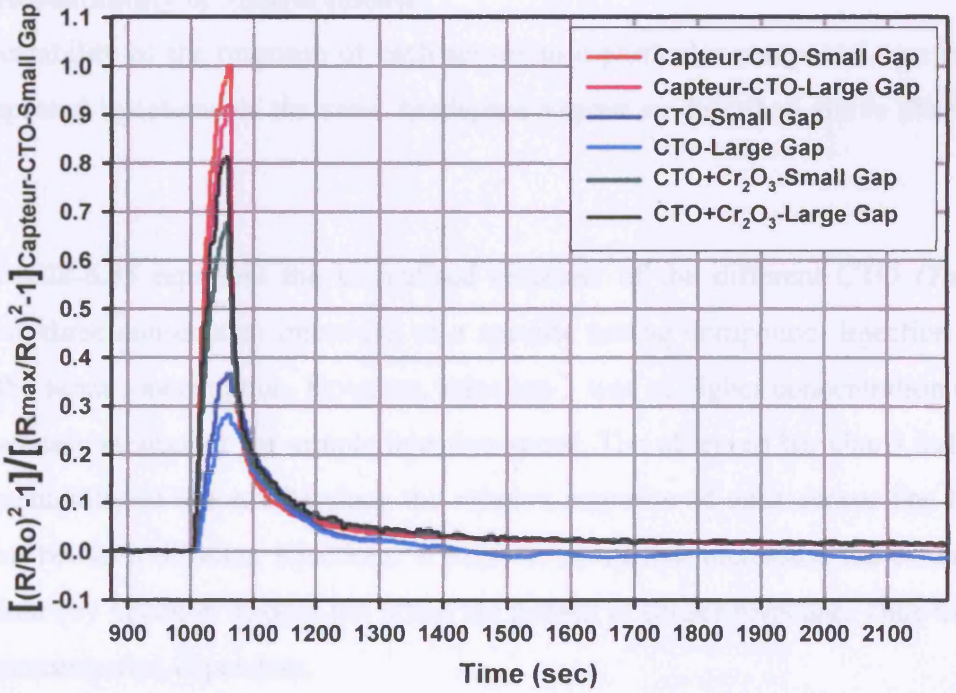

Figure 6.26 Relative response signals of the CTO sensors to n-hexane
Capteur-CTO: $Cr_{1.95}Ti_{0.05}O_3$ (1 µm) (Capteur Sensors & Analyzers Ltd)
CTO: $Cr_{1.95}Ti_{0.05}O_3$ (0.5 µm) (UCL)
CTO-Cr_2O_3: $Cr_{1.95}Ti_{0.05}O_3$+Cr_2O_3 (0.7 µm) (Capteur Sensors & Analyzers Ltd)

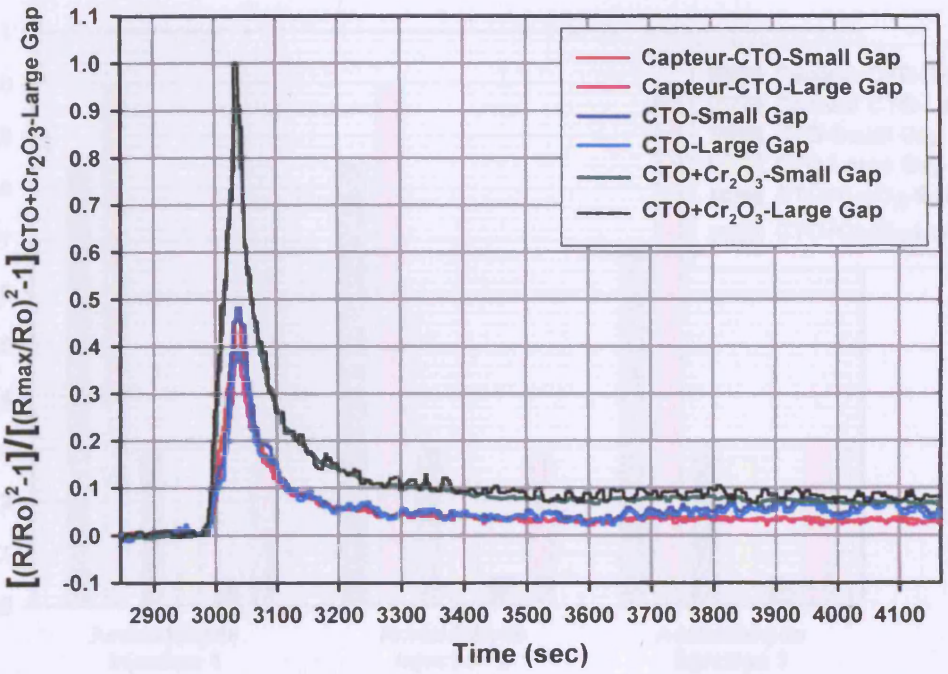

Figure 6.27 Relative response signals of the CTO sensors to toluene
Capteur-CTO: $Cr_{1.95}Ti_{0.05}O_3$ (1 µm) (Capteur Sensors & Analyzers Ltd)
CTO: $Cr_{1.95}Ti_{0.05}O_3$ (0.5 µm) (UCL)
CTO-Cr_2O_3: $Cr_{1.95}Ti_{0.05}O_3$+Cr_2O_3 (0.7 µm) (Capteur Sensors & Analyzers Ltd)

6.3.3.2 Repeatability of Measurements

The repeatability of the response of each sensor to a particular compound was examined using repeated injections of the same headspace vapour as described above ***(See Section 6.3.2.4)***.

Figures 6.28-6.35 represent the normalised response of the different CTO ***(Table 6.2)*** sensors to three consecutive injections of a specific testing compound. Injection 1 and 2 was of the same concentration. However, injection 3 was of higher concentration obtained by deliberately increasing the sample injection speed. The observed bar charts indicate the high repeatability of the results since the relative response of each sensor has the same behaviour between different injections. It must be noted that increasing the concentration of an odour (by injection 3) does not affect the pattern of sensor response. Thus the results are not concentration dependent.

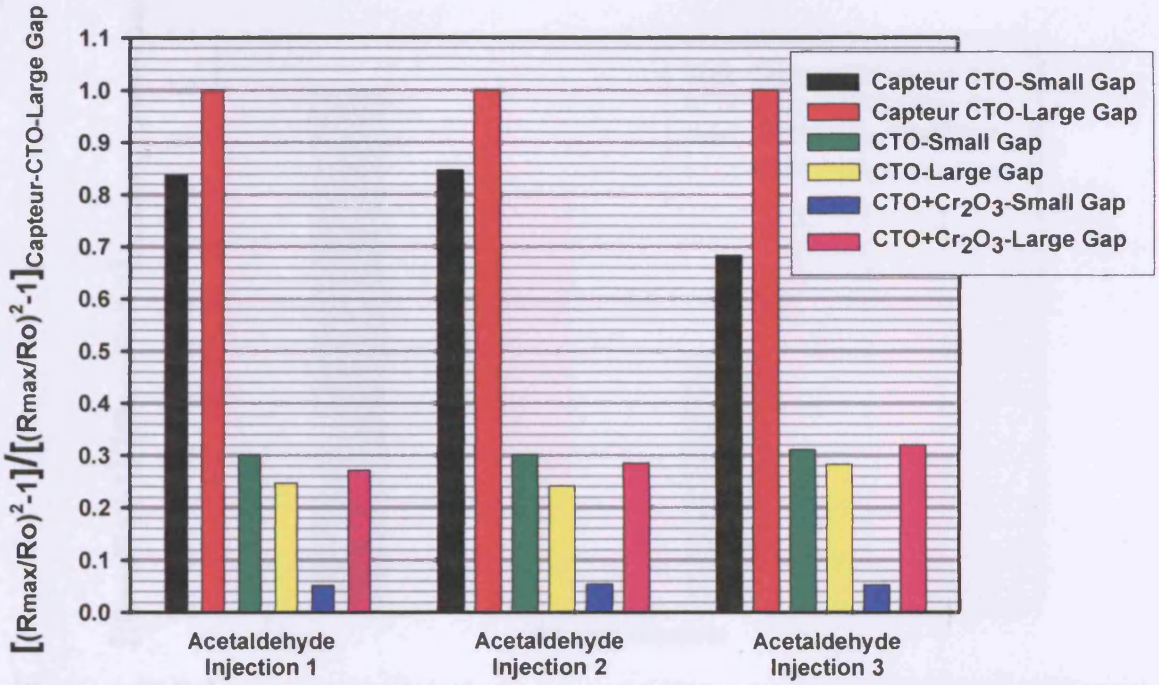

Figure 6.28 Relative amplitudes of response of CTO sensors to three consecutive injections of acetaldehyde
Capteur-CTO: $Cr_{1.95}Ti_{0.05}O_3$ (1 µm) (Capteur Sensors & Analyzers Ltd)
CTO: $Cr_{1.95}Ti_{0.05}O_3$ (0.5 µm) (UCL)
CTO-Cr_2O_3: $Cr_{1.95}Ti_{0.05}O_3$+Cr_2O_3 (0.7 µm) (Capteur Sensors & Analyzers Ltd)

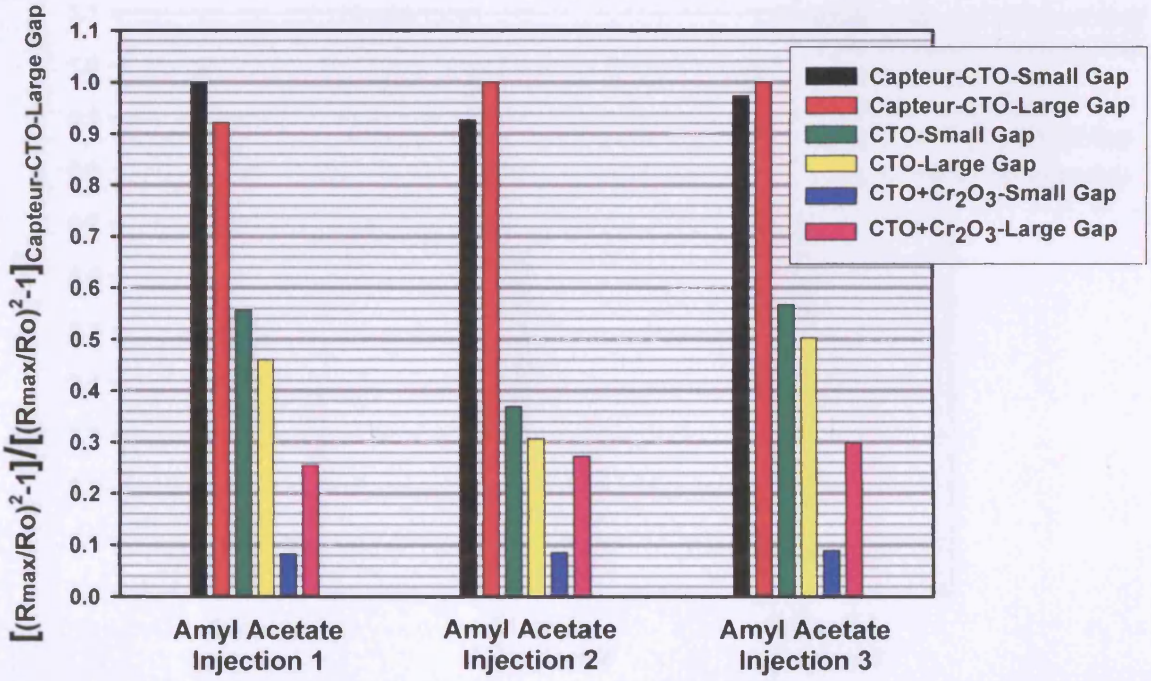

Figure 6.29 Relative amplitudes of response of CTO sensors to three consecutive injections of amyl acetate
Capteur-CTO: $Cr_{1.95}Ti_{0.05}O_3$ (1 µm) (Capteur Sensors & Analyzers Ltd)
CTO: $Cr_{1.95}Ti_{0.05}O_3$ (0.5 µm) (UCL)
CTO-Cr_2O_3: $Cr_{1.95}Ti_{0.05}O_3$+Cr_2O_3 (0.7 µm) (Capteur Sensors & Analyzers Ltd)

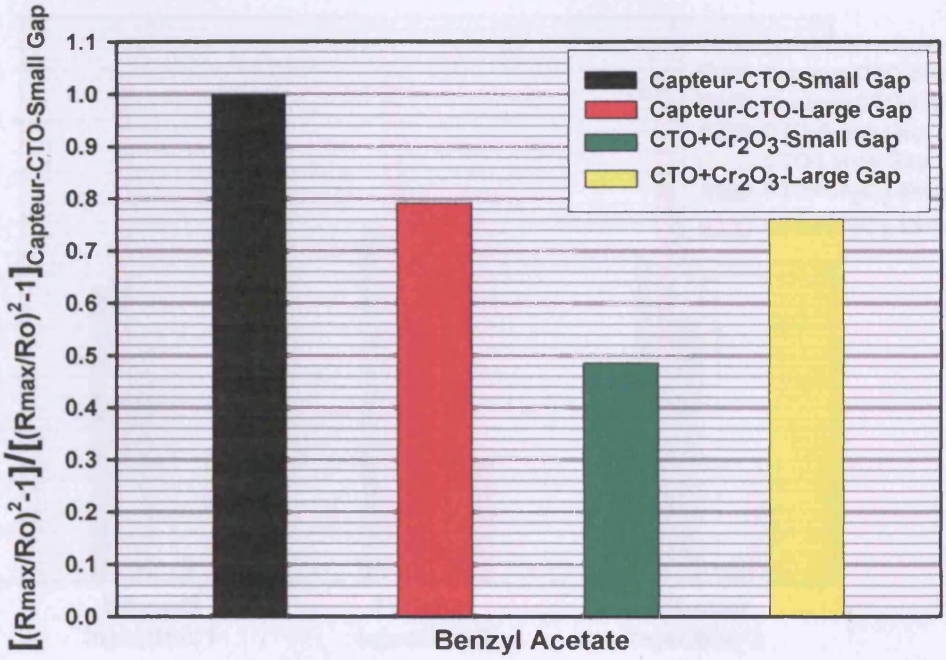

Figure 6.30 Relative amplitudes of response of CTO sensors to an injection of benzyl acetate
Capteur-CTO: $Cr_{1.95}Ti_{0.05}O_3$ (1 µm) (Capteur Sensors & Analyzers Ltd)
CTO: $Cr_{1.95}Ti_{0.05}O_3$ (0.5 µm) (UCL)
CTO-Cr_2O_3: $Cr_{1.95}Ti_{0.05}O_3$+Cr_2O_3 (0.7 µm) (Capteur Sensors & Analyzers Ltd)

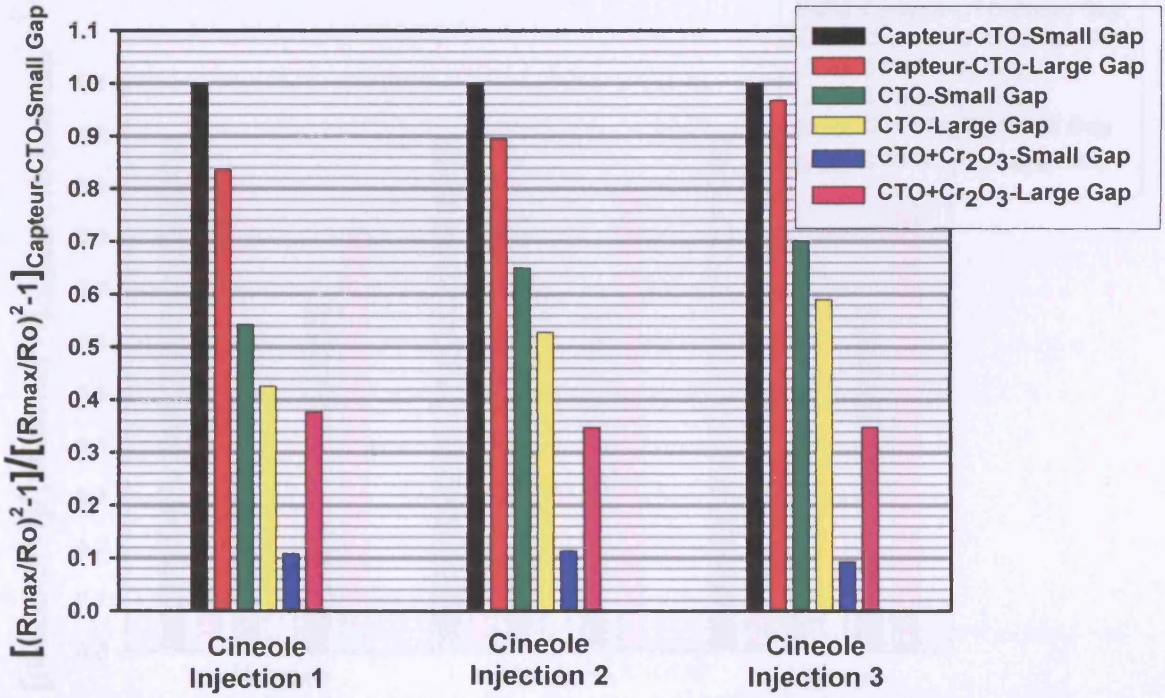

Figure 6.31 Relative amplitudes of response of CTO sensors to three consecutive injections of cineole
Capteur-CTO: $Cr_{1.95}Ti_{0.05}O_3$ (1 µm) (Capteur Sensors & Analyzers Ltd)
CTO: $Cr_{1.95}Ti_{0.05}O_3$ (0.5 µm) (UCL)
CTO-Cr_2O_3: $Cr_{1.95}Ti_{0.05}O_3$+Cr_2O_3 (0.7 µm) (Capteur Sensors & Analyzers Ltd)

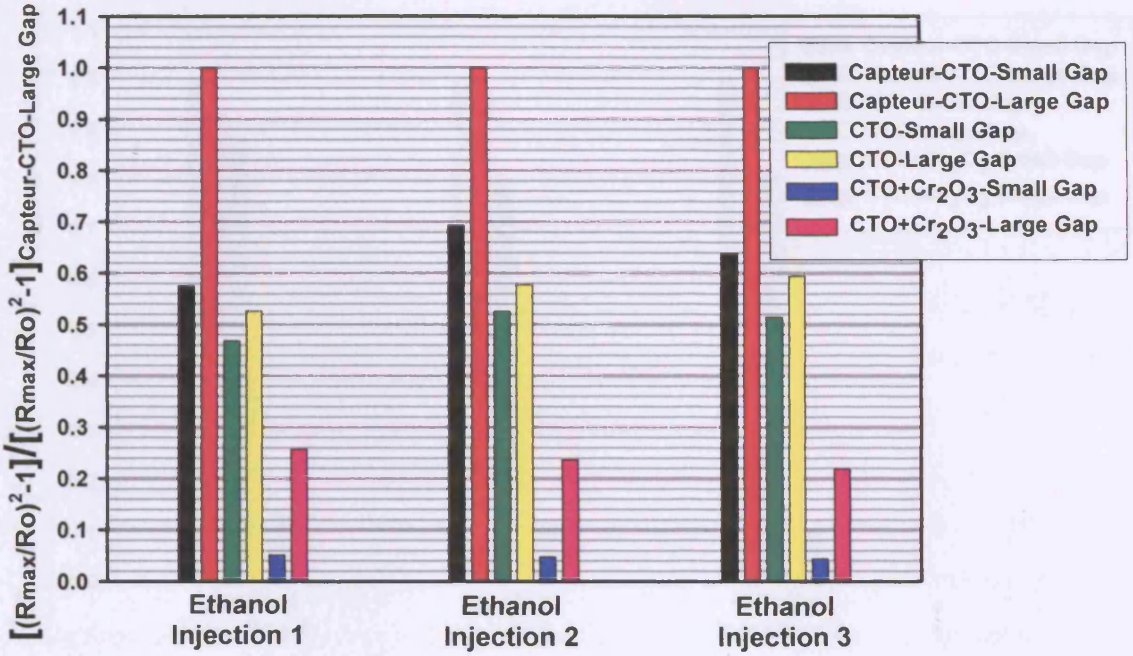

Figure 6.32 Relative amplitudes of response of CTO sensors to three consecutive injections of ethanol
Capteur-CTO: $Cr_{1.95}Ti_{0.05}O_3$ (1 µm) (Capteur Sensors & Analyzers Ltd)
CTO: $Cr_{1.95}Ti_{0.05}O_3$ (0.5 µm) (UCL)
CTO-Cr_2O_3: $Cr_{1.95}Ti_{0.05}O_3$+Cr_2O_3 (0.7 µm) (Capteur Sensors & Analyzers Ltd)

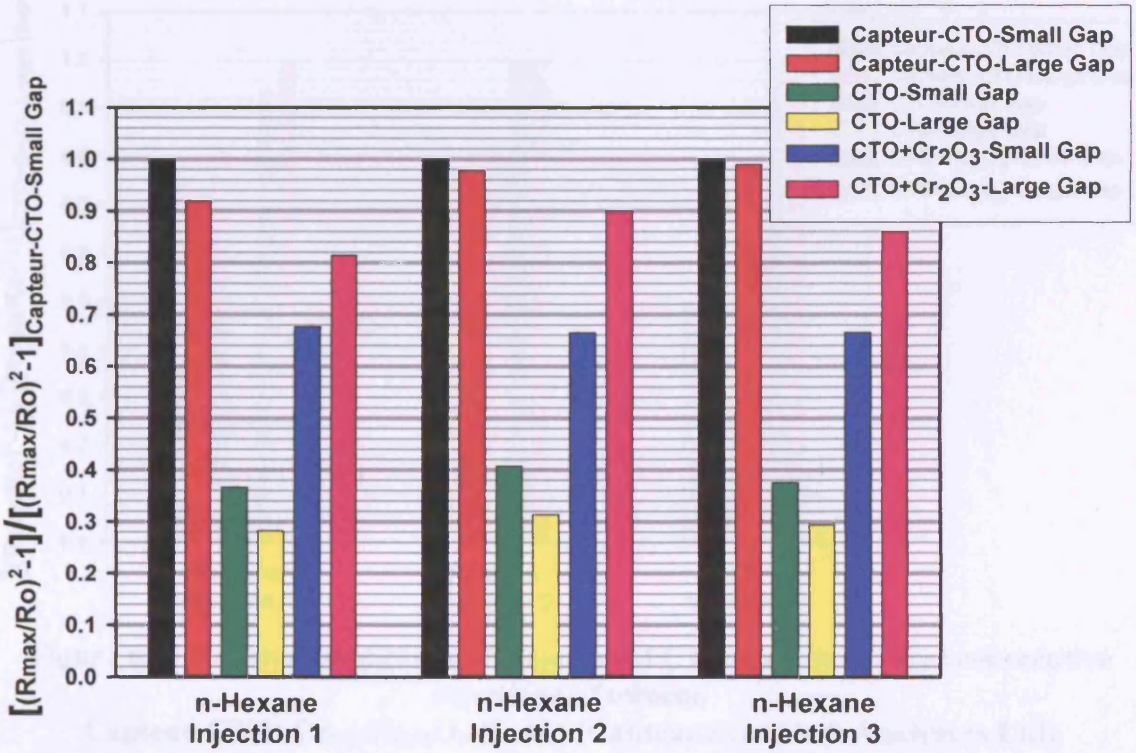

Figure 6.33 Relative amplitudes of response of CTO sensors to three consecutive injections of n-hexane
Capteur-CTO: $Cr_{1.95}Ti_{0.05}O_3$ (1 µm) (Capteur Sensors & Analyzers Ltd)
CTO: $Cr_{1.95}Ti_{0.05}O_3$ (0.5 µm) (UCL)
CTO-Cr_2O_3: $Cr_{1.95}Ti_{0.05}O_3$+Cr_2O_3 (0.7 µm) (Capteur Sensors & Analyzers Ltd)

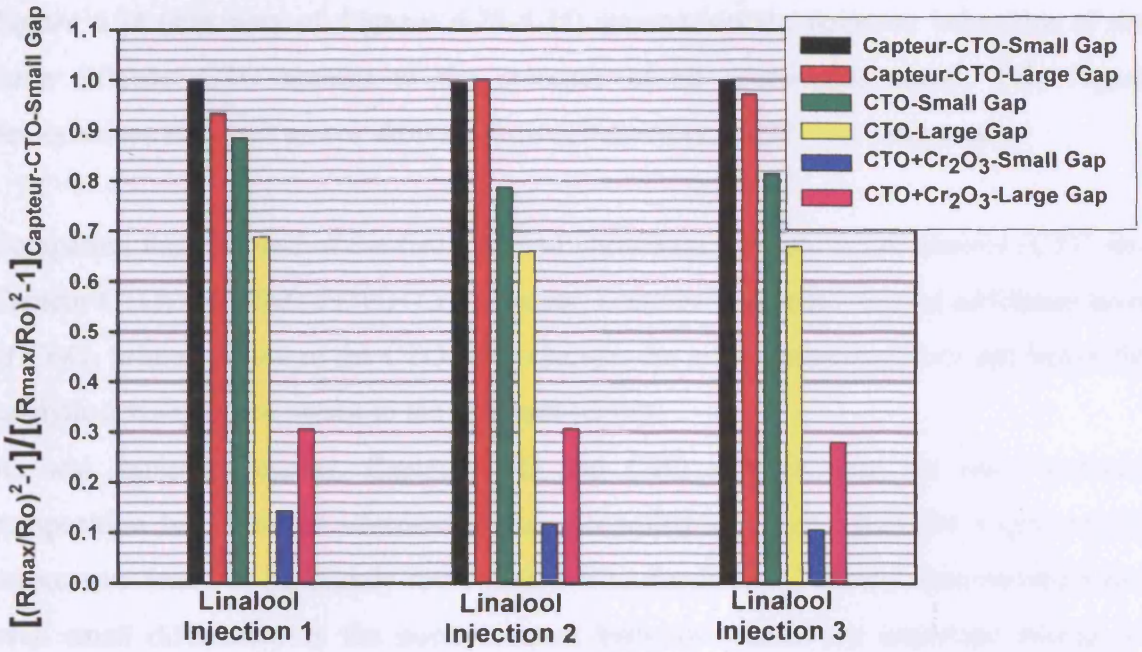

Figure 6.34 Relative amplitudes of response of CTO sensors to three consecutive injections of linalool
Capteur-CTO: $Cr_{1.95}Ti_{0.05}O_3$ (1 µm) (Capteur Sensors & Analyzers Ltd)
CTO: $Cr_{1.95}Ti_{0.05}O_3$ (0.5 µm) (UCL)
CTO-Cr_2O_3: $Cr_{1.95}Ti_{0.05}O_3$+Cr_2O_3 (0.7 µm) (Capteur Sensors & Analyzers Ltd)

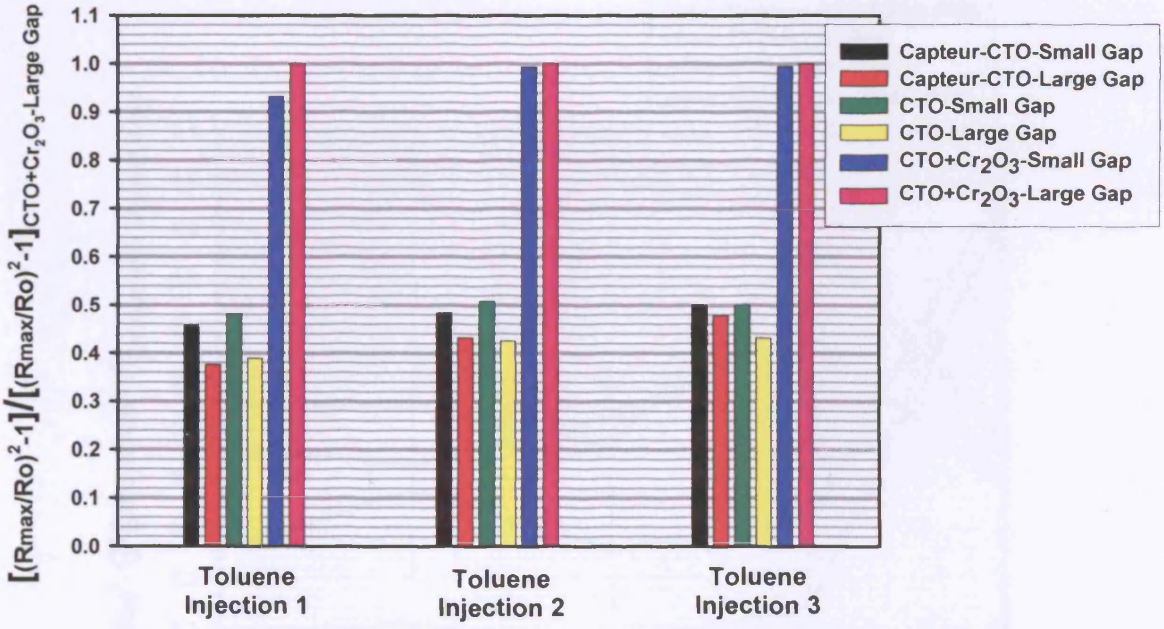

Figure 6.35 Relative amplitudes of response of CTO sensors to three consecutive injections of toluene
Capteur-CTO: $Cr_{1.95}Ti_{0.05}O_3$ (1 µm) (Capteur Sensors & Analyzers Ltd)
CTO: $Cr_{1.95}Ti_{0.05}O_3$ (0.5 µm) (UCL)
CTO-Cr_2O_3: $Cr_{1.95}Ti_{0.05}O_3$+Cr_2O_3 (0.7 µm) (Capteur Sensors & Analyzers Ltd)

Figure 6.36 (summary of ***Figures 6.28-6.35***) summarises the response behaviour of the three different CTO sensors to the presence of all compounds tested. This Figure demonstrates that each sensor shows a distinct behaviour to different compounds.

Comparing the response of the two standard chromium titanium oxide sensors (CTO and Capteur-CTO) with that of CTO+Cr_2O_3 sensor, it can be concluded that the additional layer of Cr_2O_3 printed on top of the CTO layer changes the sensor microstructure and hence the catalytic activity of the sensor to the different odours.

As was explained earlier, Capteur-CTO and CTO sensors have the same nominal composition but different microstructures. According to ***Figure 6.36*** the Capteur-CTO sensor was found to be slightly more sensitive to the different odours demonstrating that even small differences in the microstructure between sensors are important enough to produce different sensor responses. The Capteur-CTO sensor, followed by CTO, was found to have higher sensitivity to the majority of the tested compounds (with the exception of toluene and n-hexane).

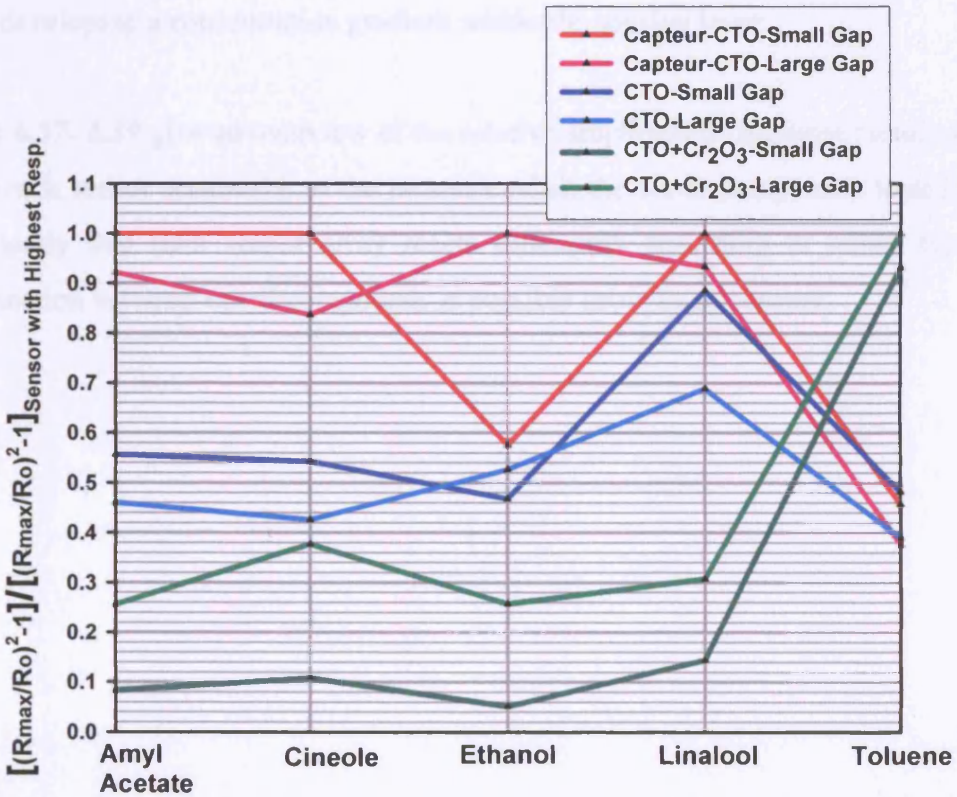

Figure 6.36 Overview of the relative amplitude of response of CTO sensors to different compounds
Capteur-CTO: $Cr_{1.95}Ti_{0.05}O_3$ (1 µm) (Capteur Sensors & Analyzers Ltd)
CTO: $Cr_{1.95}Ti_{0.05}O_3$ (0.5 µm) (UCL)
CTO-Cr_2O_3: $Cr_{1.95}Ti_{0.05}O_3$+Cr_2O_3 (0.7 µm) (Capteur Sensors & Analyzers Ltd)

From ***Figure 6.36*** it can be seen that in the presence of toluene, the CTO+Cr_2O_3 sensor was found to be the most sensitive one followed by Capteur-CTO and finally CTO, which both showed very similar sensitivities. A possible explanation for this behaviour is that the CTO+Cr_2O_3 sensor has oxidised toluene to CO to which this sensor is very sensitive to. In the case of n-hexane, Capteur-CTO sensor is the most sensitive followed by CTO+Cr_2O_3 and finally CTO.

It is important to acknowledge the observed inverse concentration gradient (i.e. small electrode gap > Large electrode gap) shown by both Capteur-CTO and CTO sensors for all the tested compounds, with ethanol as the only exception. What possibly happened is that these sensors chemically cracked the specific compounds to other by-products to which the sensors are more sensitive to, resulting in the observed enhancement in the response of the small gap relative to the large gap. However, in the presence of ethanol gas, the response of these sensors on the large electrode gap was found to be greater than that of the small electrode gap. This indicates that ethanol burns sufficiently and rapidly on the sensing surface developing a concentration gradient within the sensing layer.

Figures 6.37- 6.39 give an overview of the relative amplitude of response (small and large gap) of each sensor separately, to the presence of all the odour compounds tested. Figures show clearly that each sensor array reacts differently according to odour type. Thus discrimination between tested compounds is possible using these sensors.

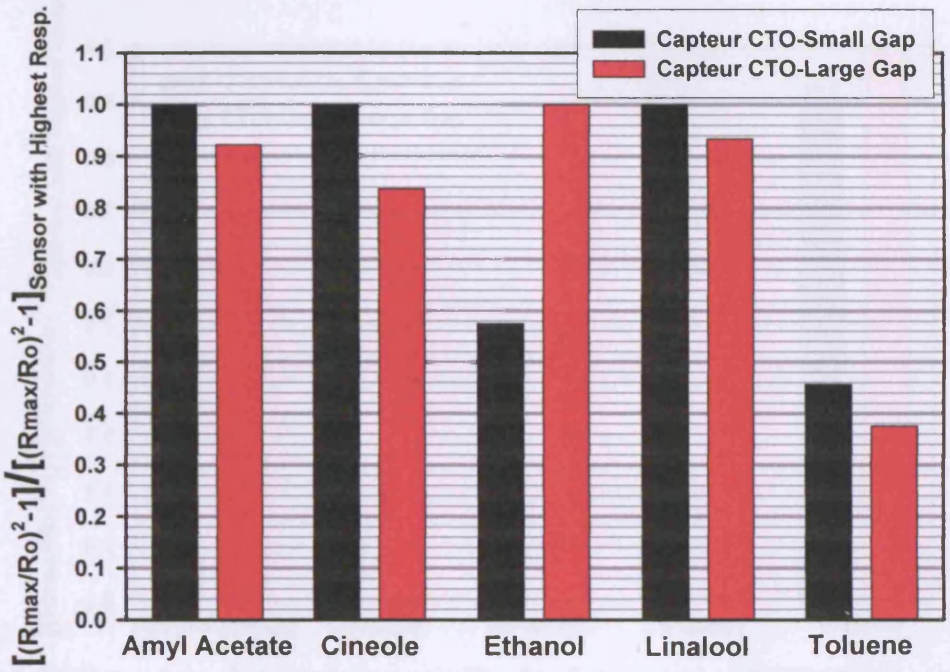

Figure 6.37 Overview of the relative amplitude of response of Capteur-CTO sensor (small and large gap) to different compounds
Capteur-CTO: $Cr_{1.95}Ti_{0.05}O_3$ (1 µm) (Capteur Sensors & Analyzers Ltd)

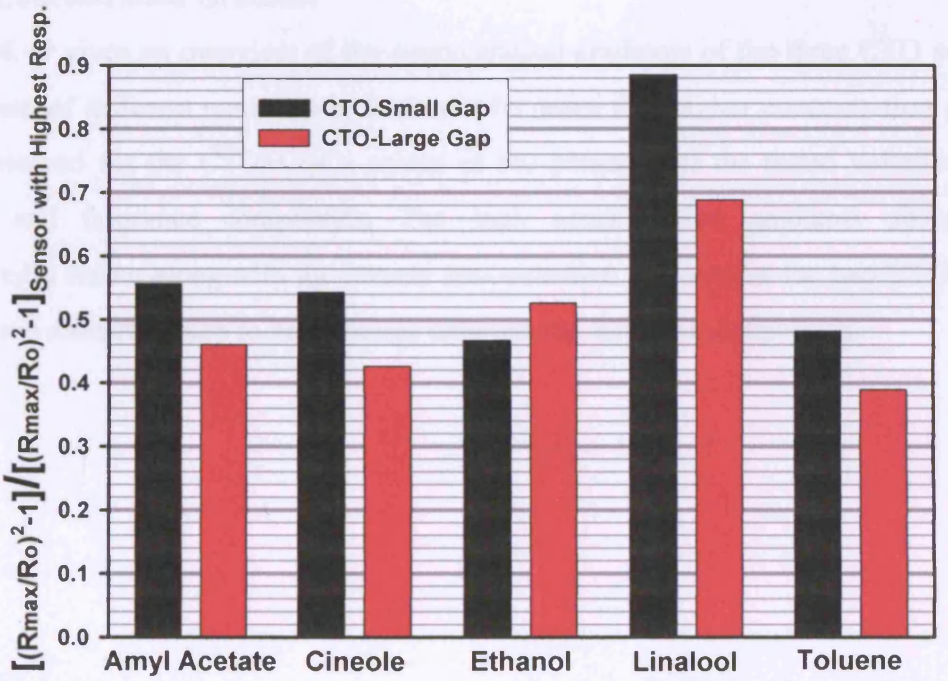

Figure 6.38 Overview of the relative amplitude of response of CTO sensor to different compounds
Capteur-CTO: $Cr_{1.95}Ti_{0.05}O_3$ (1 µm) (Capteur Sensors & Analyzers Ltd)

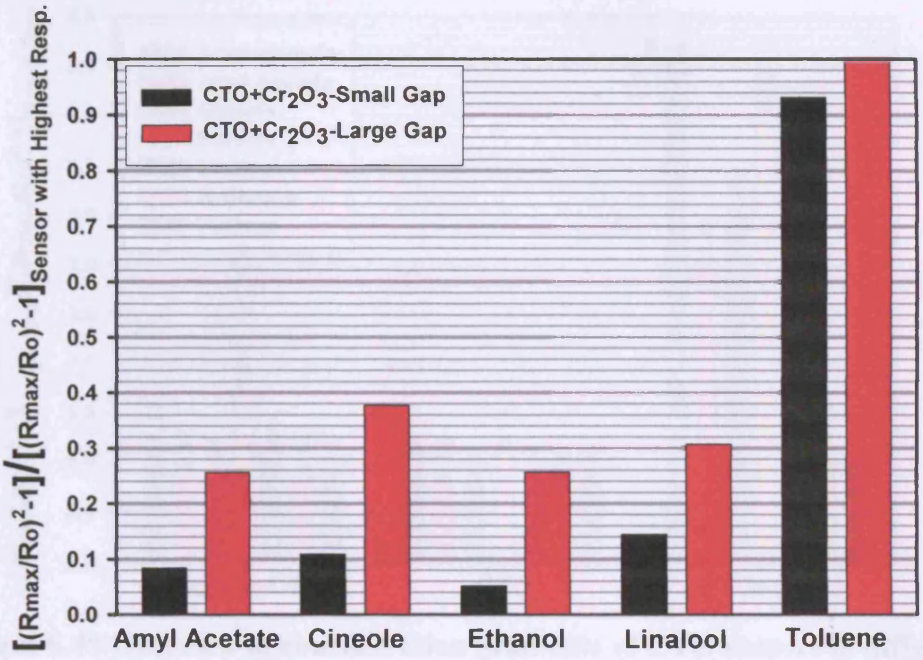

Figure 6.39 Overview of the relative amplitude of response of CTO+Cr_2O_3 sensor to different compounds
CTO-Cr_2O_3: $Cr_{1.95}Ti_{0.05}O_3$+Cr_2O_3 (0.7 µm) (Capteur Sensors & Analyzers Ltd)

6.3.3.3 Concentration Gradient

Figure 6.40 gives an overview of the concentration gradients of the three CTO sensors to the present of different compounds. It should be noted that higher concentration gradients were observed for the CTO+Cr_2O_3 sensor in the presence of the tested volatile organic, flavour and fragrance compounds. The high concentration gradients observed for CTO+Cr_2O_3 sensor along with the inverse concentration gradient for the two CTO sensors, allow good discrimination to be achieved between the different compounds.

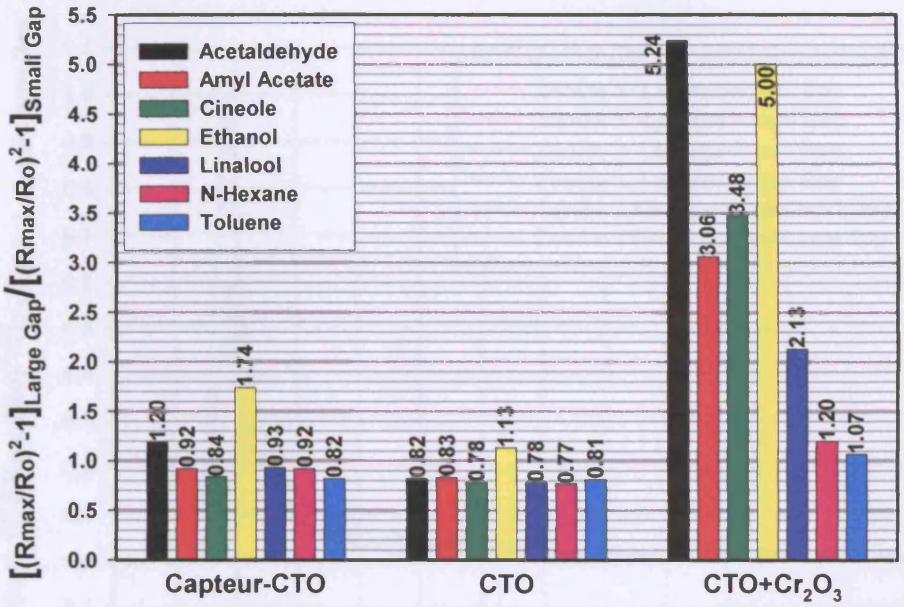

Figure 6.40 Overview of concentration gradients of CTO sensors to different compounds
Capteur-CTO: $Cr_{1.95}Ti_{0.05}O_3$ (1 µm) (Capteur Sensors & Analyzers Ltd)
CTO: $Cr_{1.95}Ti_{0.05}O_3$ (0.5 µm) (UCL)
CTO-Cr_2O_3: $Cr_{1.95}Ti_{0.05}O_3$+Cr_2O_3 (0.7 µm) (Capteur Sensors & Analyzers Ltd)

6.3.4 Experiments with Layered Zeolite Sensors

Three different zeolite multi-electrode sensor array devices with layered microstructure (that have a layer of either zeolite Y, zeolite β or zeolite ZSM-5 printed over the CTO sensing layer) were tested to the presence of different compounds. Details regarding the preparation of the layered zeolite CTO sensors were given in Chapter 5.

Table 6.3 summarises the different zeolite sensors produced.

Table 6.3 Zeolite CTO sensors with layered microstructure

Sensor Types
Zeolite Y-Layered
Zeolite β -Layered
Zeolite ZSM-5- Layered

6.3.4.1 Results and Analysis for Layered Zeolite Sensors

Figures 6.41-6.46 show the relative response signals of the three layered zeolite sensors to six compounds (amyl acetate, benzyl acetate, cineole, ethanol, linalool, and toluene). A wide variation in the response signals was observed for different sensors and different compounds.

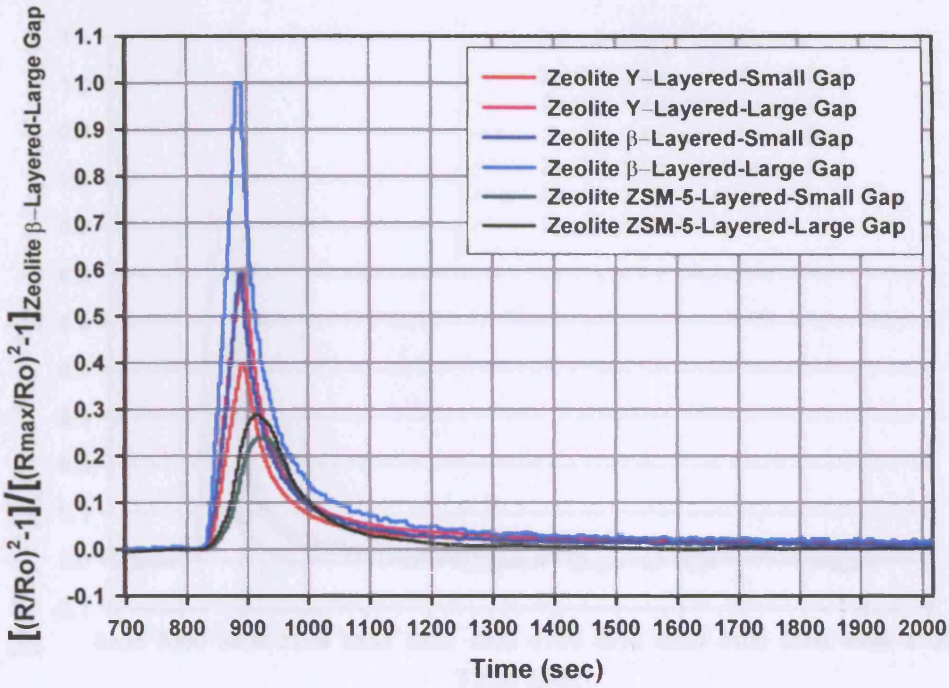

Figure 6.41 Relative response signals of Layered zeolite sensors to amyl acetate

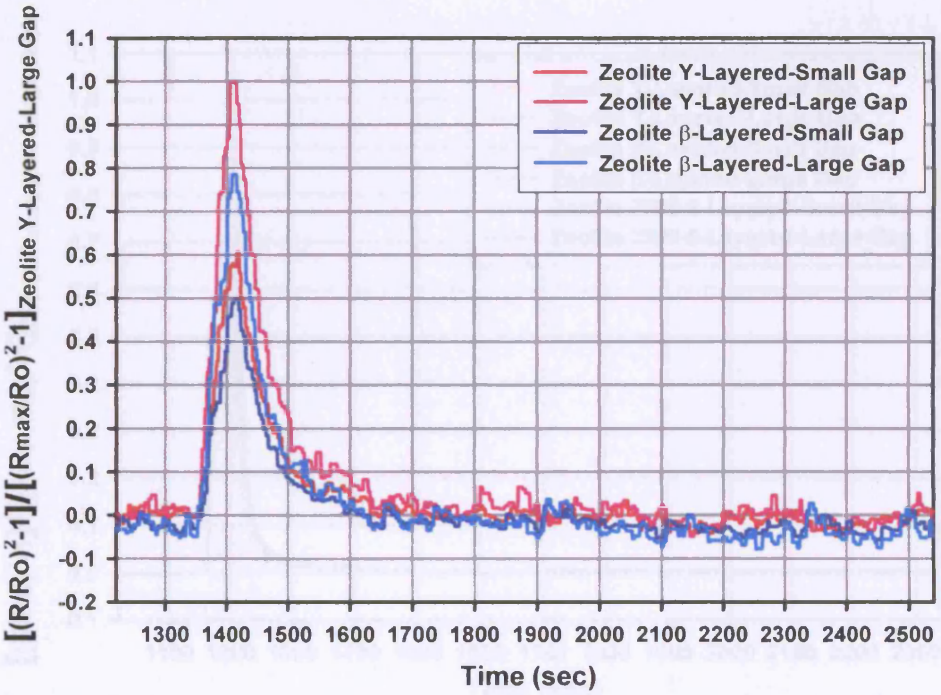

Figure 6.42 Relative response signals of Layered zeolite sensors to benzyl acetate

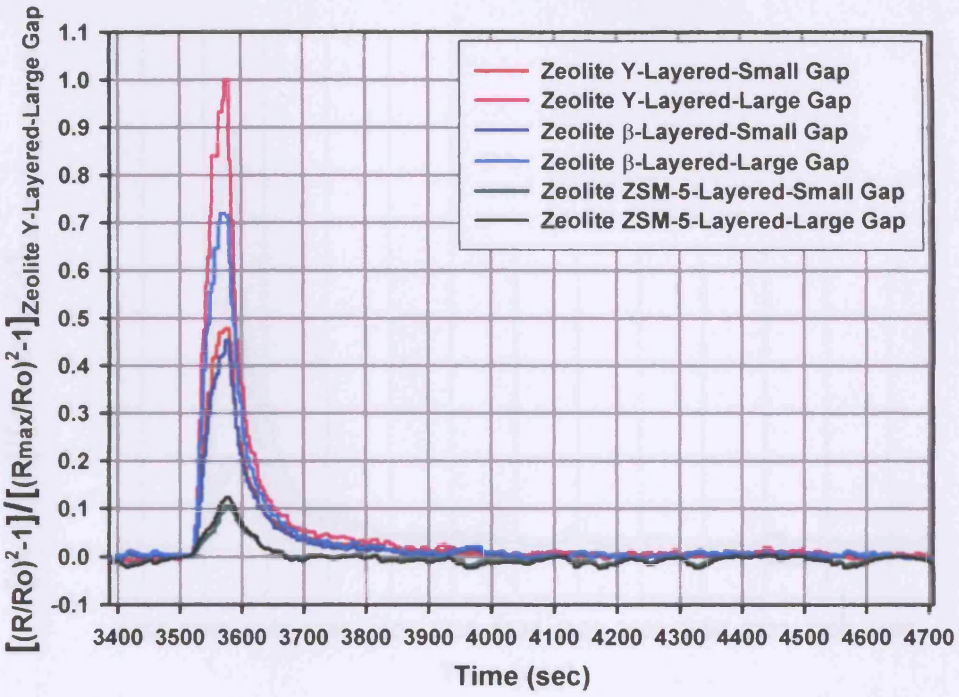

Figure 6.43 Relative response signals of Layered zeolite sensors to cineole

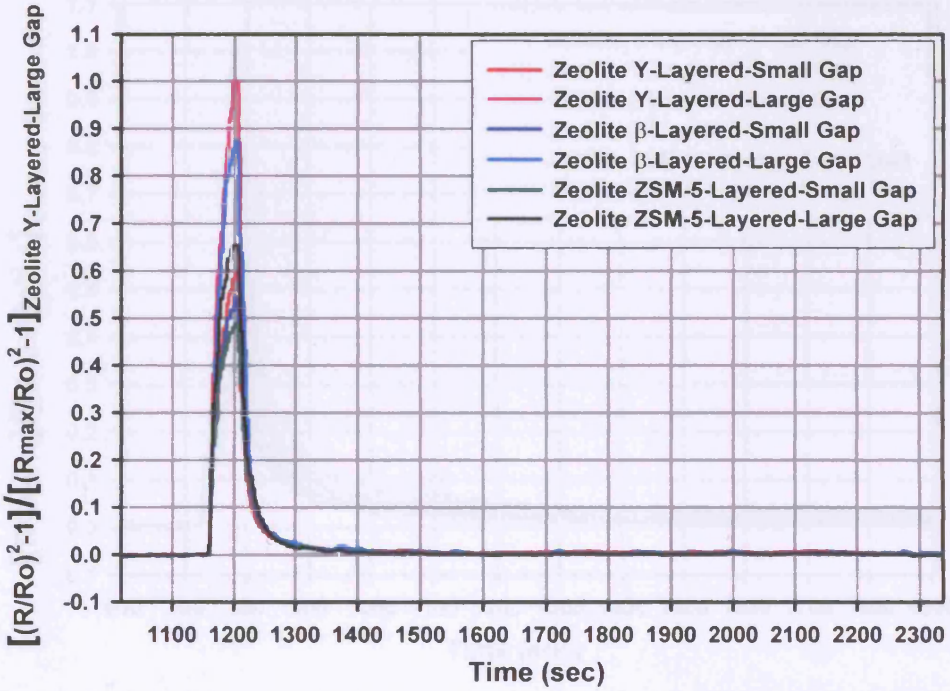

Figure 6.44 Relative response signals of Layered zeolite sensors to ethanol

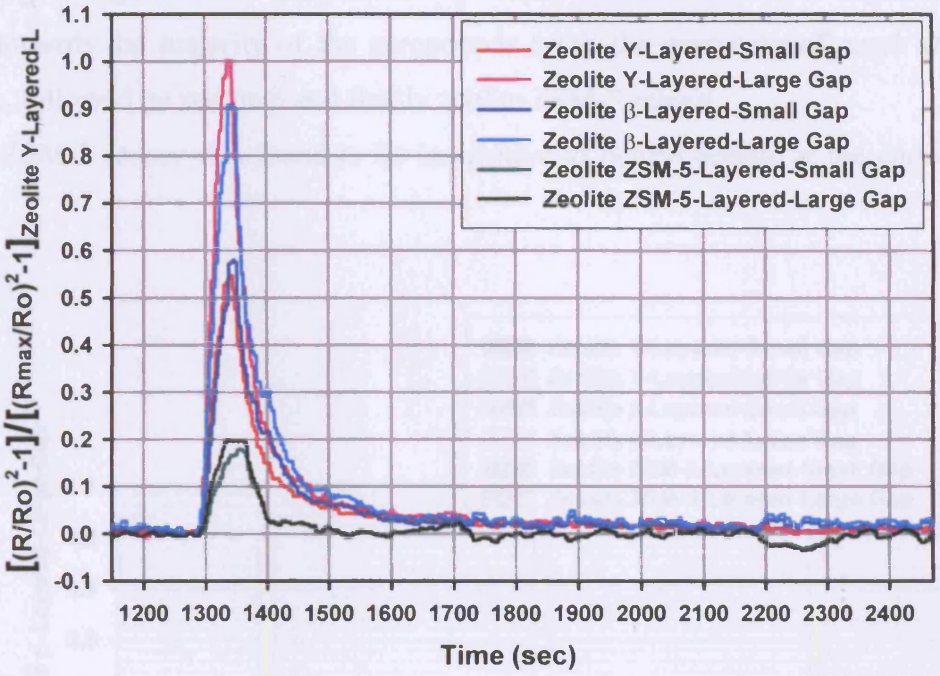

Figure 6.45 Relative response signals of Layered zeolite sensors to linalool

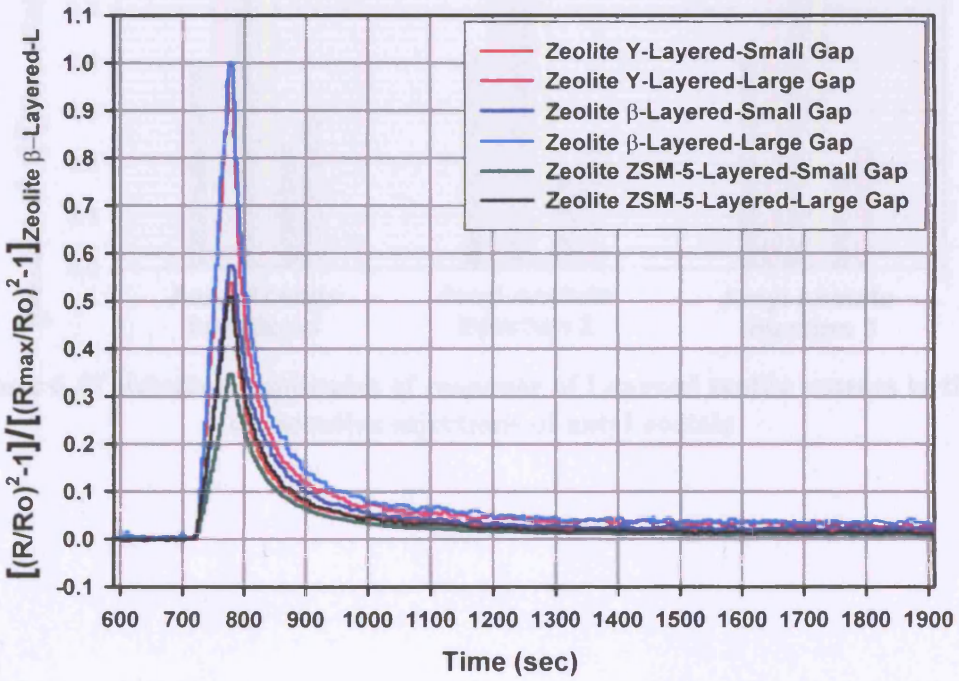

Figure 6.46 Relative response signals of Layered zeolite sensors to toluene

Figures 6.47-6.52 are bar charts showing the relative amplitudes of response of the three layered zeolite sensors to three consecutive injections of each compound. These Figures demonstrate that the results are highly reproducible and independent of the concentration of the compound.

According to ***Figures 6.47-6.52***, Zeolite Y sensor was found to have higher sensitivity values towards the majority of the compounds (with the exception of amyl acetate and toluene), followed by zeolite β and finally zeolite ZSM-5 sensor.

Zeolite ZSM-5 sensor was found to be insensitive to benzyl acetate at the concentrations tested.

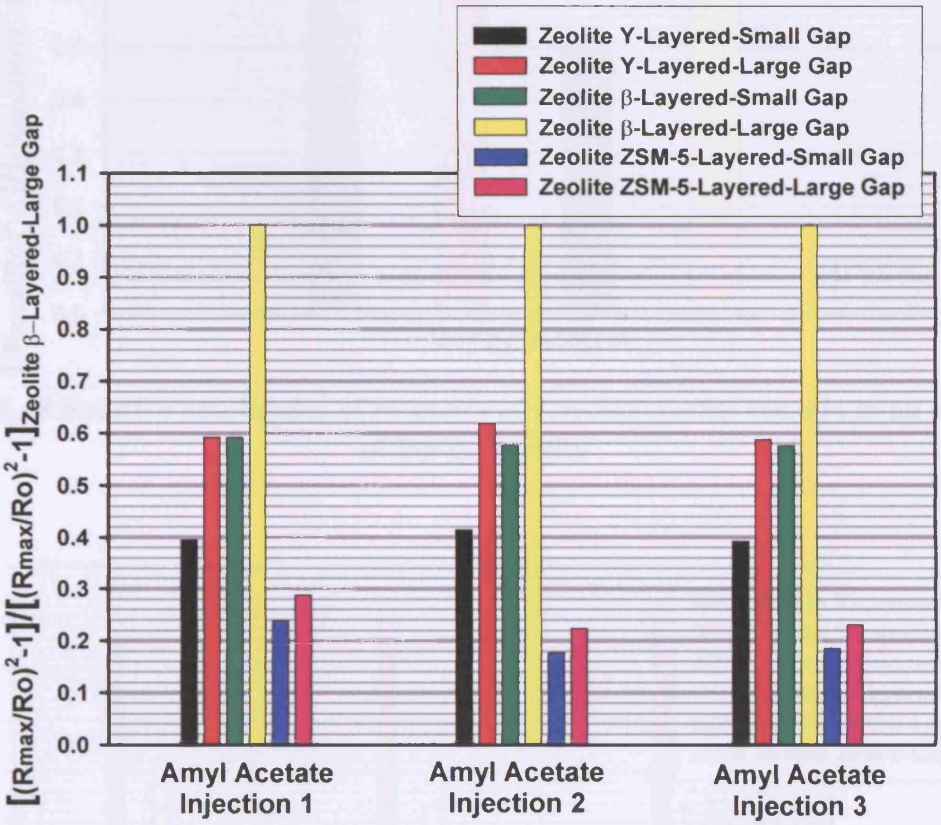

Figure 6.47 Relative amplitudes of response of Layered zeolite sensors to three consecutive injections of amyl acetate

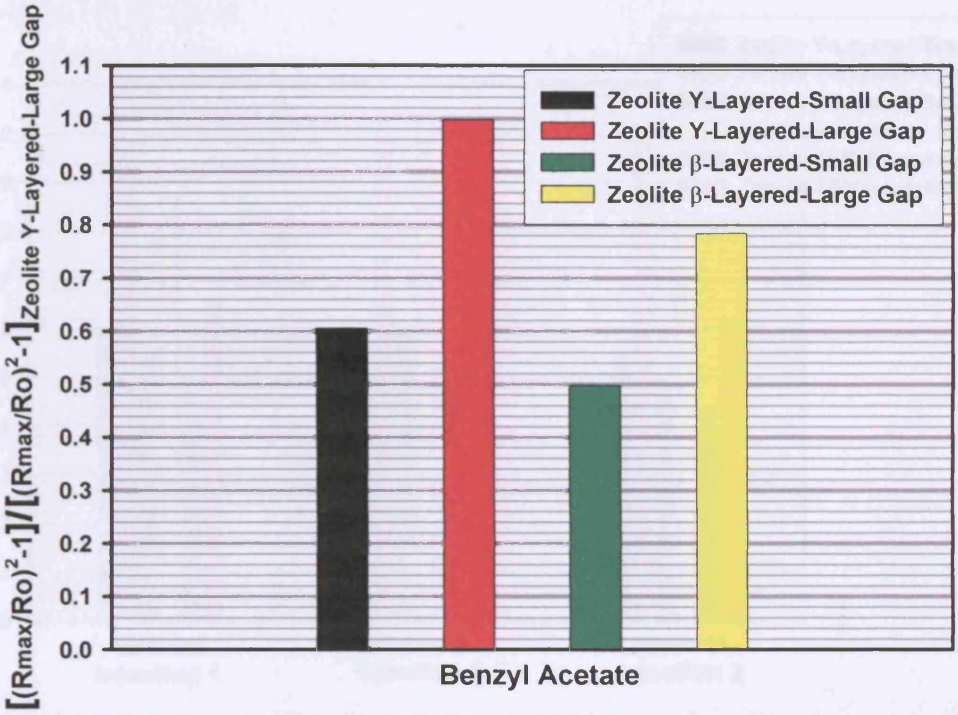

Figure 6.48 Relative amplitudes of response of Layered zeolite sensors to an injection of benzyl acetate

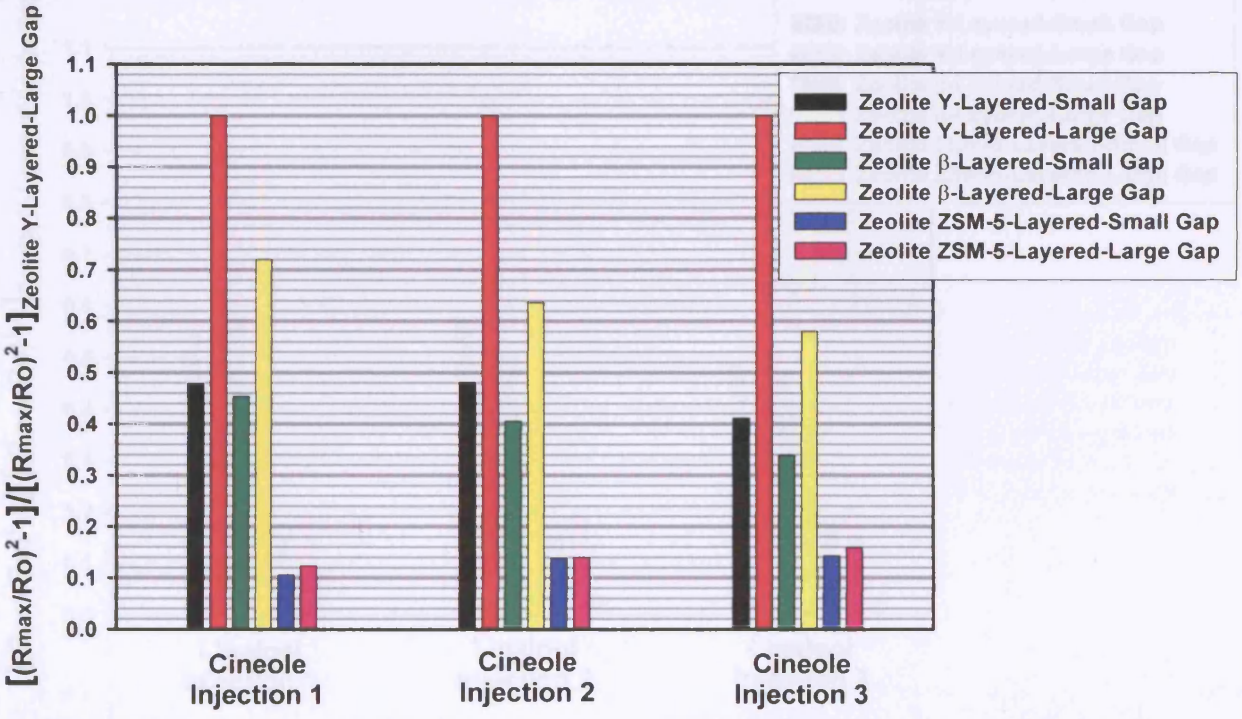

Figure 6.49 Relative amplitudes of response of Layered zeolite sensors to three consecutive injections of cineole

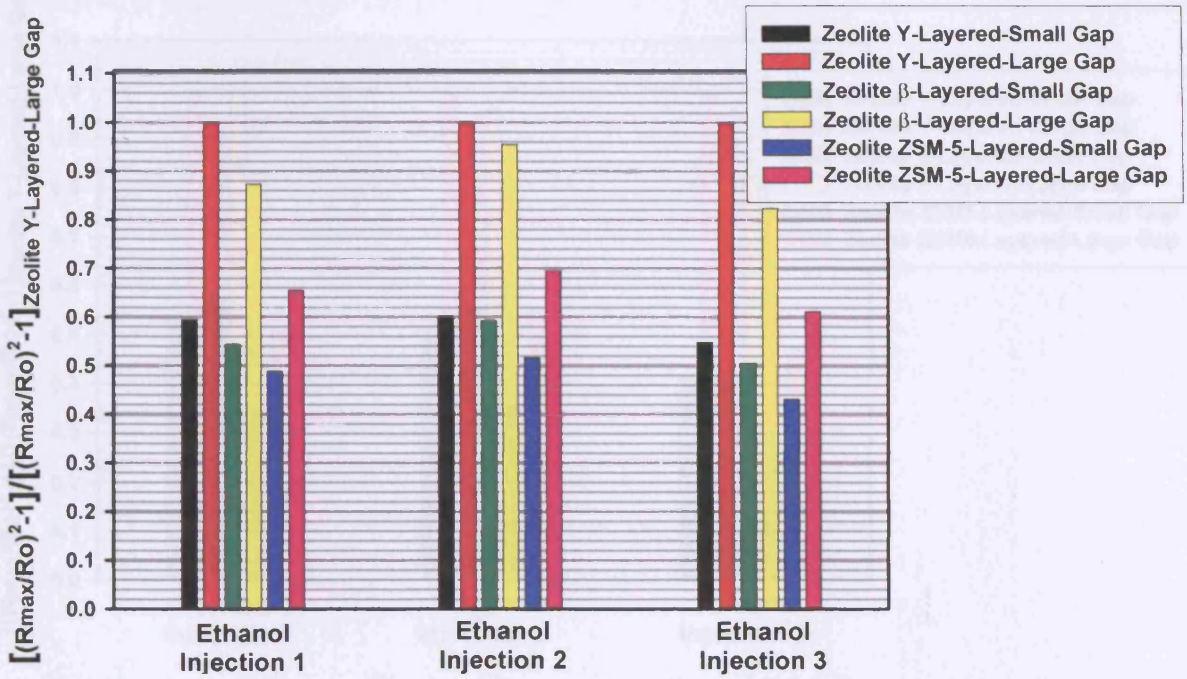

Figure 6.50 Relative amplitudes of response of Layered zeolite sensors to three consecutive injections of ethanol

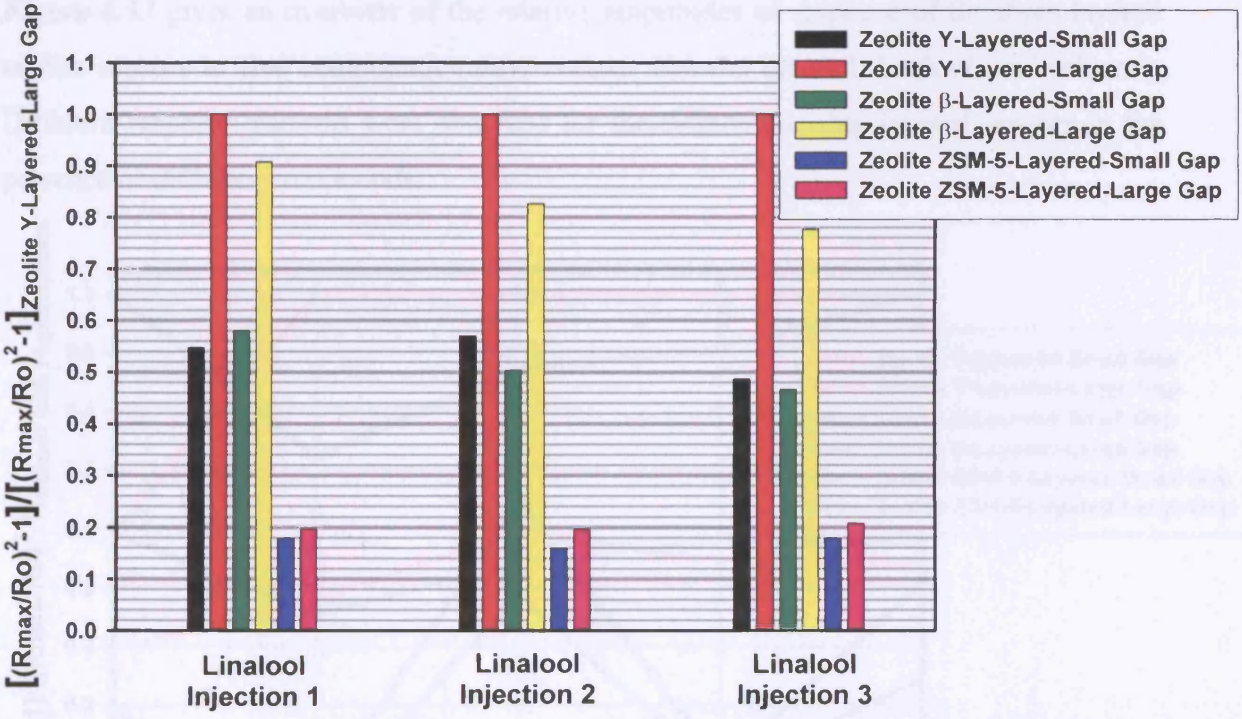

Figure 6.51 Relative amplitudes of response of Layered zeolite sensors to three consecutive injections of linalool

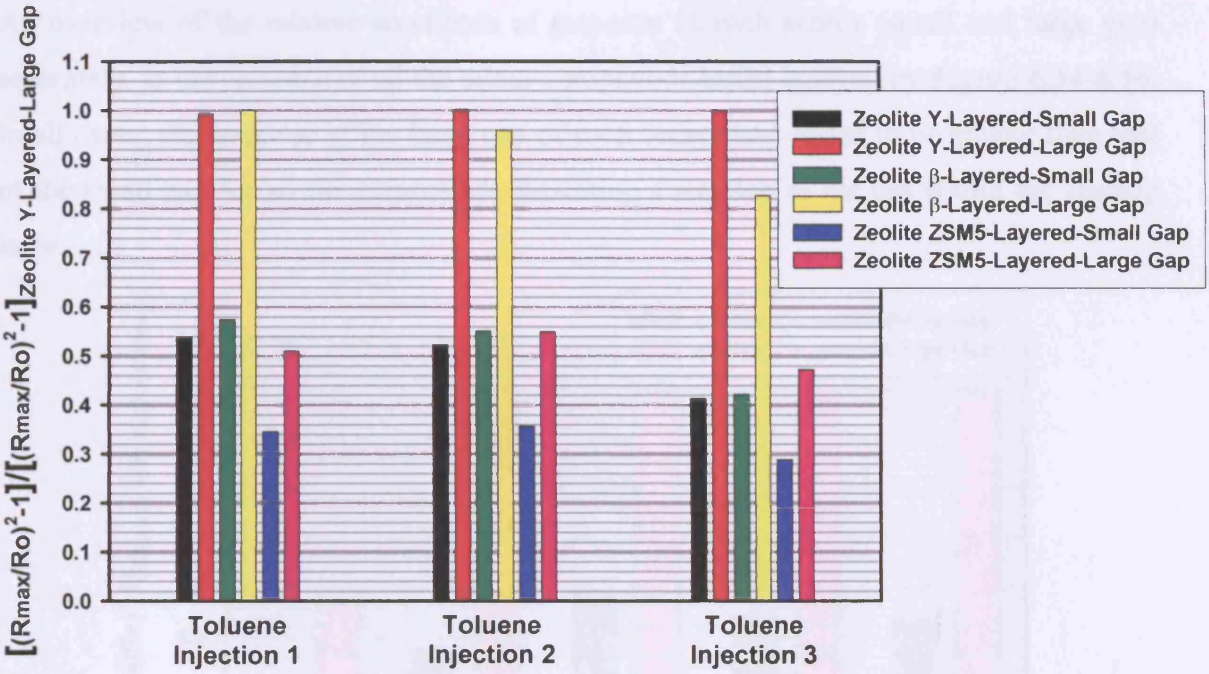

Figure 6.52 Relative amplitudes of response of Layered zeolite sensors to three consecutive injections of toluene

Figure 6.53 gives an overview of the relative amplitudes of response of the three layered zeolite sensors to five compounds (amyl acetate, cineole, ethanol, linalool, and toluene). Different response patterns were observed for the different zeolite layered sensors in the presence of different compounds.

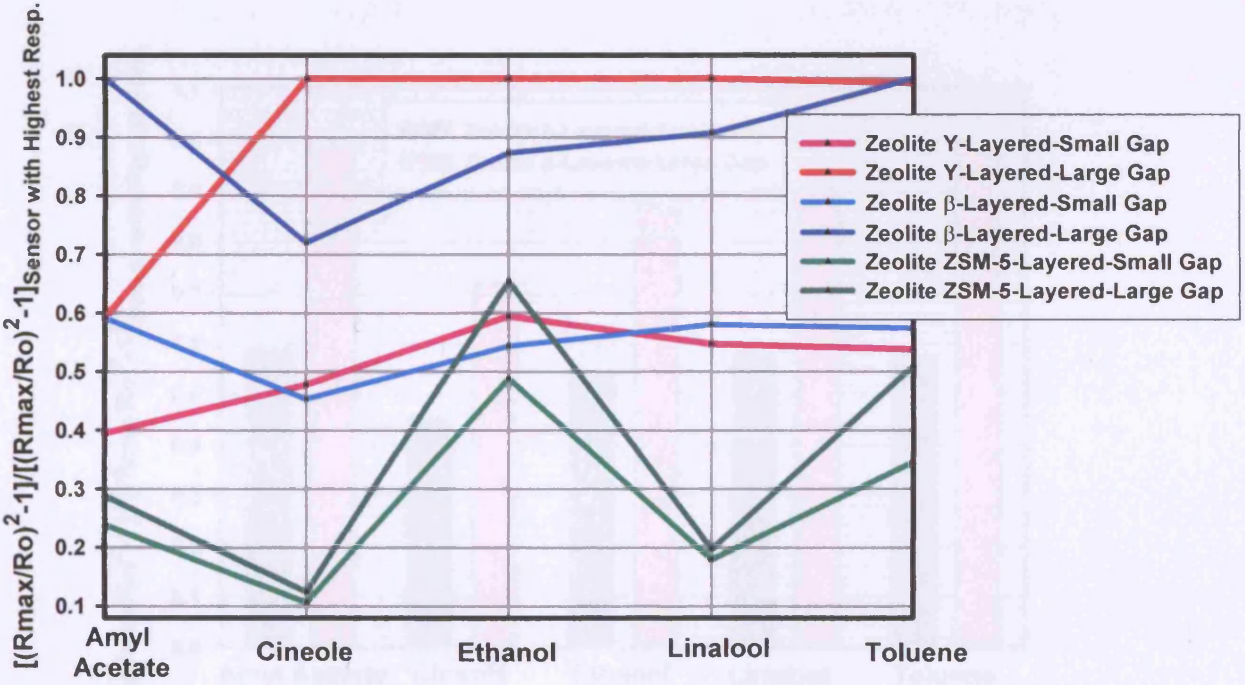

Figure 6.53 Overview of the relative amplitudes of response of the Layered zeolite sensors to different compounds

An overview of the relative amplitude of response of each sensor (small and large gap) separately, to the presence of all the odour compounds tested is given by ***Figure 6.54-6.56***. In all cases, the response of the large gap of each sensor was found to be greater than that of the small gap for all the compounds indicating a reaction of the gas within the sensing layer.

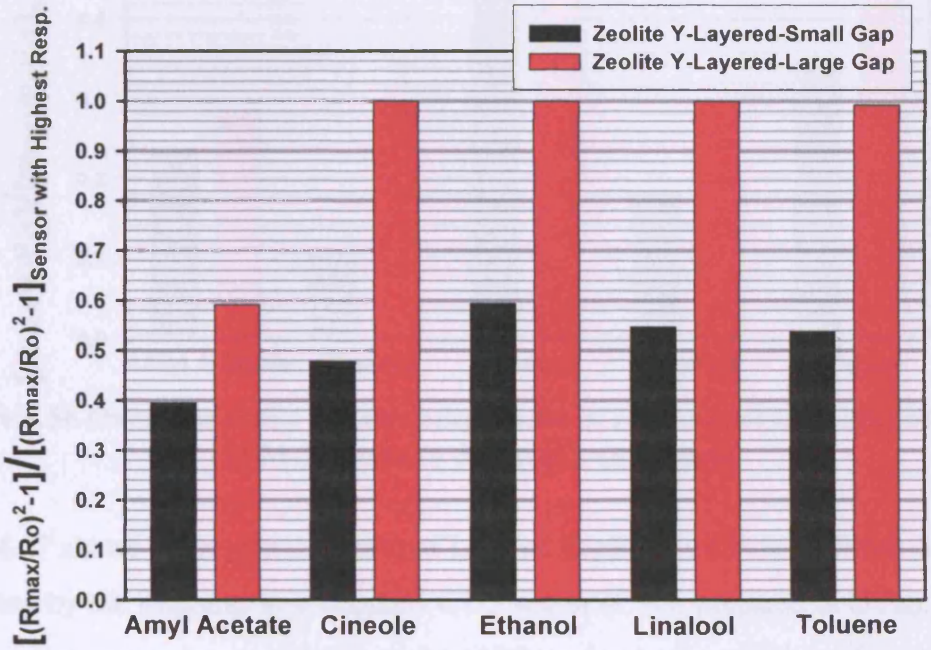

Figure 6.54 Overview of the relative amplitudes of response of the Layered zeolite Y sensor to different compounds

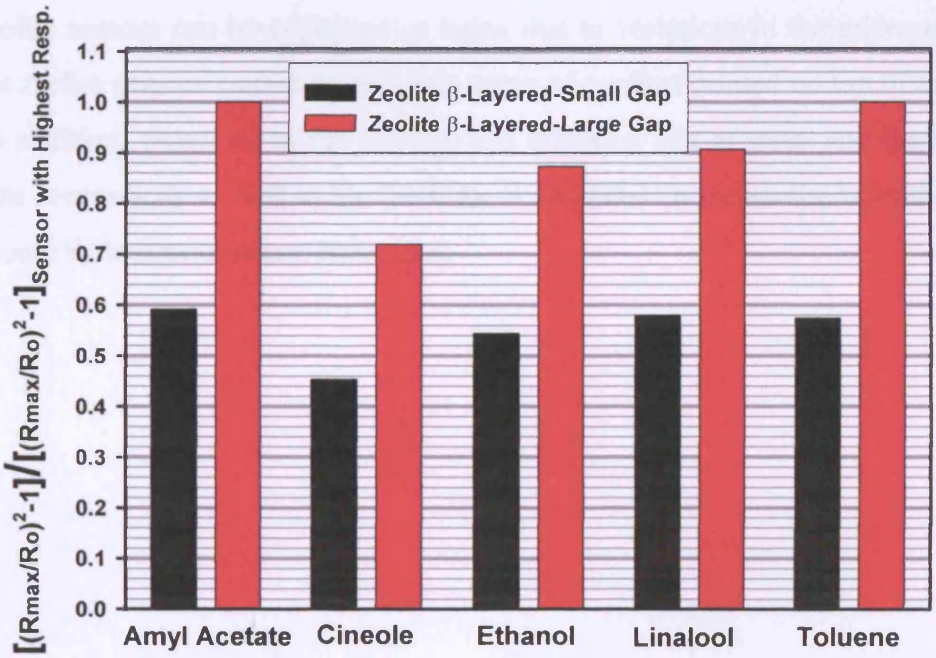

Figure 6.55 Overview of the relative amplitudes of response of the Layered zeolite β sensor to different compounds

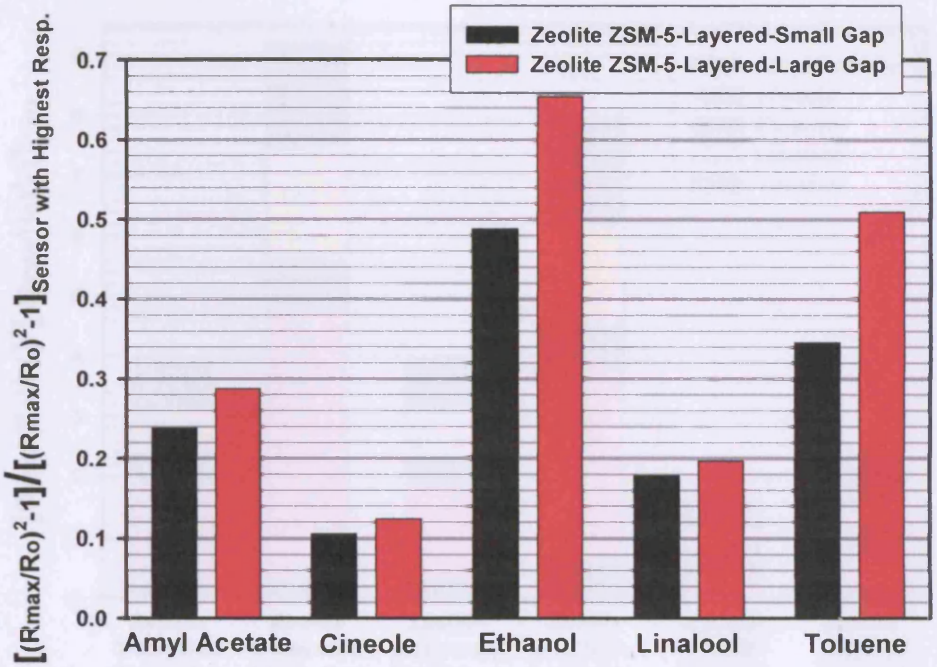

Figure 6.56 Overview of the relative amplitudes of response of the Layered zeolite ZSM-5 sensor to different compounds

Figure 6.57 shows the response pattern of Layered Zeolite sensors to different compounds normalised by the response to a standard CTO sensor (CTO, prepared at UCL). Since the difference between a layered zeolite and a CTO sensor is the addition of a zeolite layer over the sensing material, the sensor responses to different compounds were linearised to that of a standard CTO sensor. The differences in sensor responses observed between CTO-zeolite sensors can be explained as being due to variations in the microstructure of the three zeolite sensors caused by different types of zeolites printed on top of the sensing layer. In addition, variations in the reaction and diffusion rate of gases and their products within the sensor body as well as the cracking of the gases on the zeolite layer could result in additional variations in sensor behaviour.

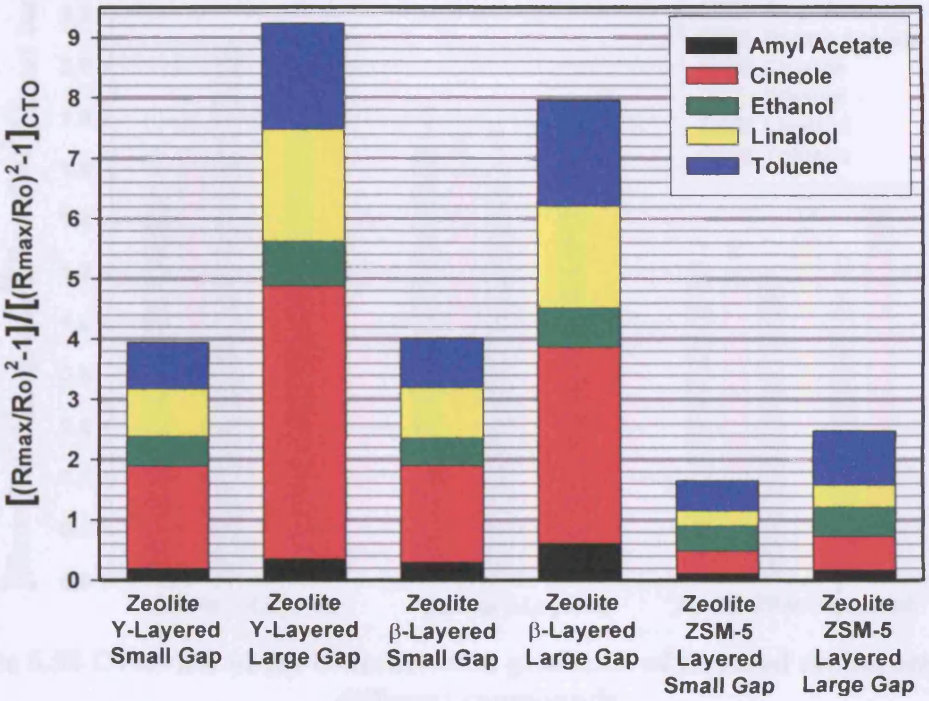

Figure 6.57 Response of the Layered zeolite sensors to different compounds normalised by the response to a standard CTO sensor

6.3.5 Concentration Gradient

Figure 6.58 gives an overview of concentration gradients of the layered zeolite sensors to different compounds. Zeolite Y sensor was found to have the highest concentration gradient in the presence of most of the tested compounds, followed by the smaller cavity size zeolite β. The different concentration gradients of these sensors to the presence of different compounds imply that a good discrimination can be achieved between different compounds using the new layered zeolite sensors. All layered zeolite sensors show considerable higher concentration gradients compared to standard CTO sensor ***(See Figure 6.40 and Figure 6.58)***.

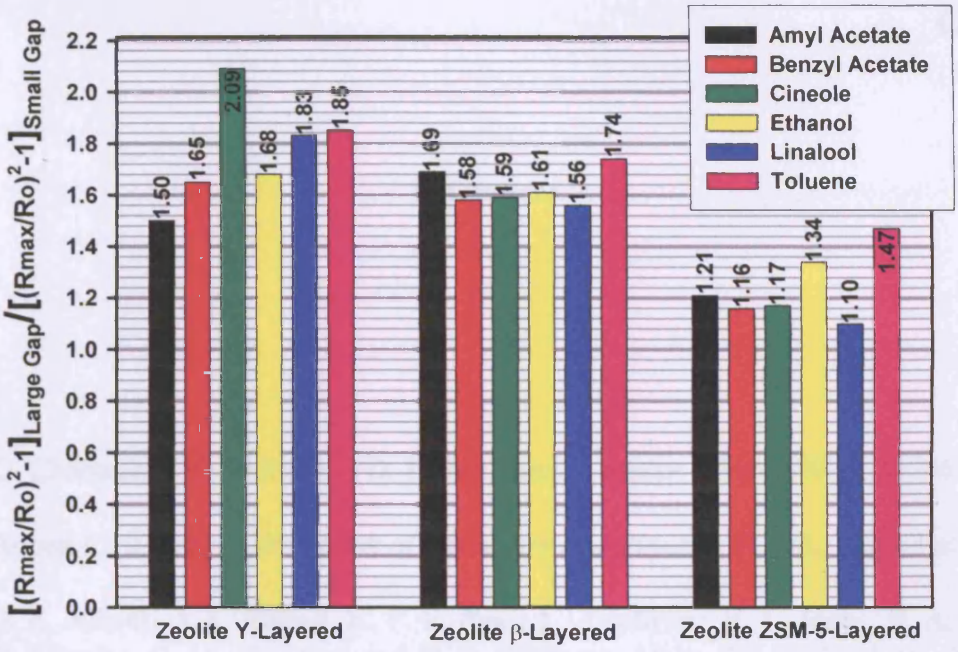

Figure 6.58 Overview of the concentration gradients of Layered zeolite sensors to different compounds

6.4 Conclusion

A variety of multi-electrode CTO sensors were studied in the presence of different volatile organic, flavour and fragrance compounds on a newly developed experimental rig. The repeatability of the results was demonstrated as well as the ability of the sensors to provide good discrimination between the tested compounds.

The newly developed zeolite-CTO multi-electrode array devices (produced with different zeolites types added as additional layers over the gas sensing material) demonstrated an increased selectivity to a range of compounds. Furthermore, these sensors proved to be successful in providing an improved discrimination between different compounds compared to standard CTO sensors.

Chapter 6

References

1. G. Chabanis, I. P. Parkin and D. E. Williams, *J. Mater. Chem.*, 2001, **11**, 1651.

2. Robert C. Weast, in *Handbook of Chemistry and Physics*, 51st ed., CRC Press.

3. S. R. Aliwell, J. F. Halsall, K. F. E. Pratt, J. O'Sullivan, R. L. Jones, R. A. Cox, S. R. Utembe, G. M. Hansford and D. E. Williams, *Meas. Sci. Technology.*, 2001, **12**, 684.

Chapter 7

A Study of the Response of Zeolite Sensors to Various Volatile Organic and Flavour Compounds Using Electronic Nose

7.1 Introduction

The objective of the work described in this Chapter was to demonstrate shape and size selectivity as well as enhanced catalytic activity of the newly developed zeolite multi-sensor array devices and their suitability for use in electronic nose applications.

7.2 Experimental Method

7.2.1 Chromium Modification of Zeolites

Chapters 5 and 6 described the preparation and testing of different types of zeolite sensors in the presence of target gases. These sensors were shown to exhibit filtering and catalytic effects. In this Chapter the various zeolites have been catalytically modified by the addition of chromium within the zeolite cavities in order to increase the reactivity of the zeolites for partial/complete oxidation of target gases and to enhance the discrimination between the target gases.

- Powdered zeolites were converted to the ammonium form after two ammonium exchanges at 60°C using ammonium chloride solution in water.
- Then the NH_4-zeolite was subjected to chromium exchange with chromium nanohydrate solution ($Cr(NO)_3.9.H2O$) as a form of chromium cations, at 60°C for 48h.
- The initial pH of the solution was adjusted to 4.0 by the addition of few drops of aqueous ammonium hydroxide.[1]
- After the chromium-exchanged process, the catalyst was washed with deionised and double distilled water, dried at 100°C and then calcined at 500°C for 12h with a heating ramp rate of 15°C min^{-1}.

7.2.2 Preparation of Layered Chromium Modified Zeolite Gas Sensor

- The newly prepared Cr-modified zeolite powder was transformed into an ink by mixing with a commercial dual component organic vehicle, ESL400 (supplied by Agmet ES Ltd) in appropriate ratios and then triple roll milled.
- The resulting ink was screen-printed onto SEMDEC alumina tiles onto which 8 layers of CTO gas-sensing material had first been printed.
- Either 4 (50 μm thick layer of zeolite) or 8 layers (100 μm thick layer of zeolite) of Cr-modified zeolite ink were printed on the CTO layer.
- The ink between each layer was dried by placing the sensor under an infra-red lamp for 15 minutes.
- Finally, the sensors were fired at 600°C for 30 minutes.

The following Cr-modified zeolite gas sensors were produced.

Table 7.1 Chromium modified zeolite sensors with layered microstructure

Sensor Types
Cr-Zeolite Y (8 Layers)
Cr- Zeolite β (8 Layers)
Cr- Zeolite ZSM-5 (8 Layers)
Cr- Zeolite Y (4 Layers)
Cr- Zeolite ZSM-5 (4 Layers)

7. 2.3 Development of Sensor Arrays for Use in the Electronic Nose

For a sensor array to be successful in providing a sufficiently large variance in behaviour of a set of sensors in response to a range of gases, a careful selection of gas sensors should be made. The sensor arrays developed for this research work always consisted of a standard CTO sensor (with no zeolite) in combination with a layered, mixed or Cr modified zeolite sensors. Such an arrangement was favourable because the difference between at least two sensor types increases the variance in the array, thereby assisting in the identification of the gases being sensed.

A significant additional benefit of the proposed array's arrangement was the use of the same sensing material (CTO) for all the sensors. Thus, the sensors were operated at the same temperatures producing signals of similar magnitudes. The desirable consequence

was that temperature and thus the performance of the array was not dominated by the response of a single sensor. Also, any long term drift or degradation of the sensors was likely to be similar and hence simpler to detect and/or compensate for.

It is important to note that the proposed arrays were multi-electrode array devices (i.e. gas sensors comprising arrays of differently spaced electrodes underneath the sensing layer creating a sensor array within a single device) instead of multi-sensor array devices resulting in the production of sensor arrays with small numbers of sensors (for example 4 or less).

Also, many operating problems such calibration stability, manufacturing reproducibility (due to the effects of microstructure on the response), selectivity, humidity dependency and poisoning of the devices by different species were resolved.

7.2.4 Experimental Set-Up

The Fox 2000 electronic nose (supplied by Alpha M.O.S.) ***(See Figure 7.1)*** has been used to evaluate the response of the newly developed sensors. In order to determine the shape and size selectivity of the sensors and their suitability for end users applications, a range of different volatile organic and flavour compounds were used ***(See Appendix A)***. The sensor chamber (consisting of 2 different cells) shown in ***Figure 7.2*** allowed the simultaneous testing of an array consisting of six multiple electrode SEMDEC sensors (each cell allowed the positioning of three SEMDEC sensors). Both sensor cells were equipped with a heater ***(See Figure 7.3)*** and were heated to a constant temperature to prevent the adsorption of the vapours onto the sensor chamber. The unit was automated to analyse a number of samples in a predetermined time cycle and method. Each sample was loaded in a 10 ml vial and then capped. A sampling method with all the required details for headspace generation (incubation temperature, agitation speed, injection volume, injection speed) was created for each sample using the αFox software. A static headspace autosampler (HS100) was used for headspace generation and injection into the instrument. Its principle of operation involved the transfer of each vial in turn to the autosampler's oven where it was heated and agitated in order to generate the required headspace. Finally, a certain quantity (according to the sampling method) of headspace was taken from the vial using a gas syringe (2.5 ml) and was injected into the carrier gas of the instrument.

It is important to note that certain testing procedures were strictly followed to ensure the accuracy and repeatability of the results,

- Firstly, the sampling conditions for each sample were optimised due to the wide range of volatilities and sensor sensitivities.
- The samples were heated to generate homogenous sample vapours and to ensure injection repeatability.
- For each vapour at least 4 repeated injections were performed to test the repeatability of the results.
- The gas syringe was heated above the sample temperature to avoid the condensation phenomenon.
- Between each sample, the gas syringe was flushed by carrier gas to avoid cross-contamination.
- A time delay (approximately 30 min) between the end of the acquisition and the beginning of a new one was necessary so that to allow the sensors to return to the baseline resistance.

Figure 7.1 The Fox 2000 electronic nose

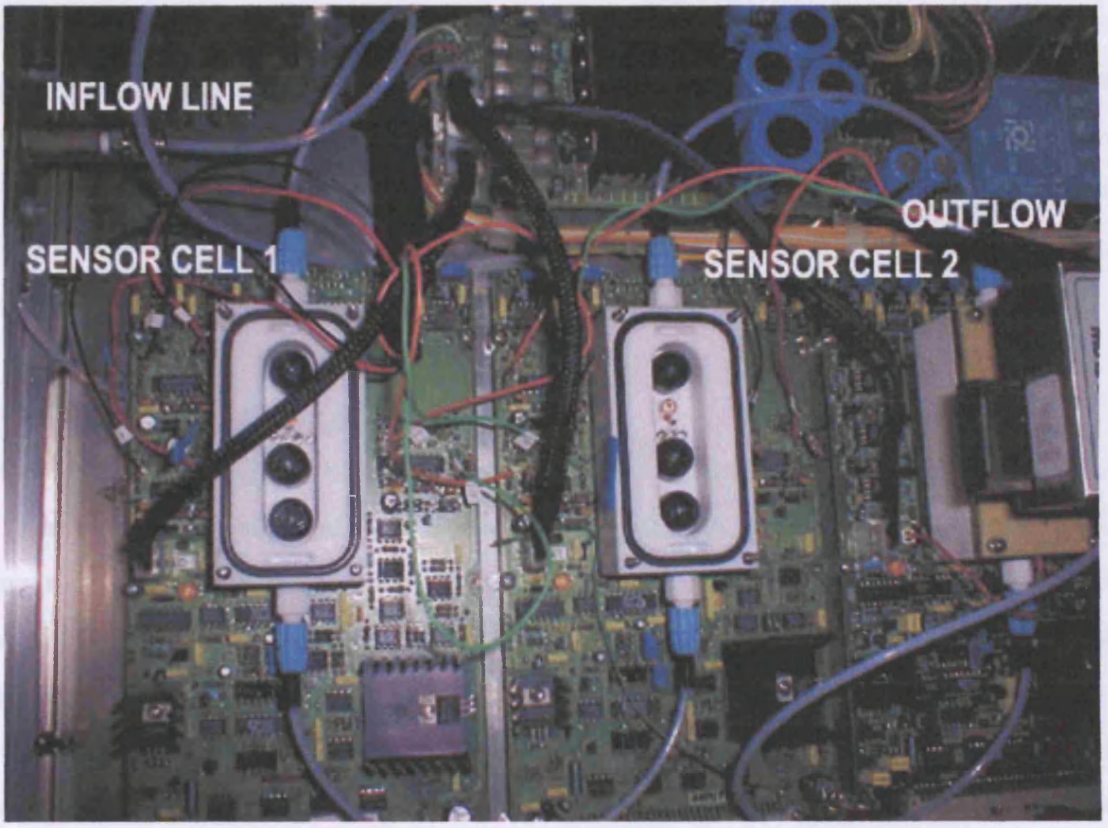

Figure 7.2 The sensor chamber of Fox2000 consisting of 2 different cells

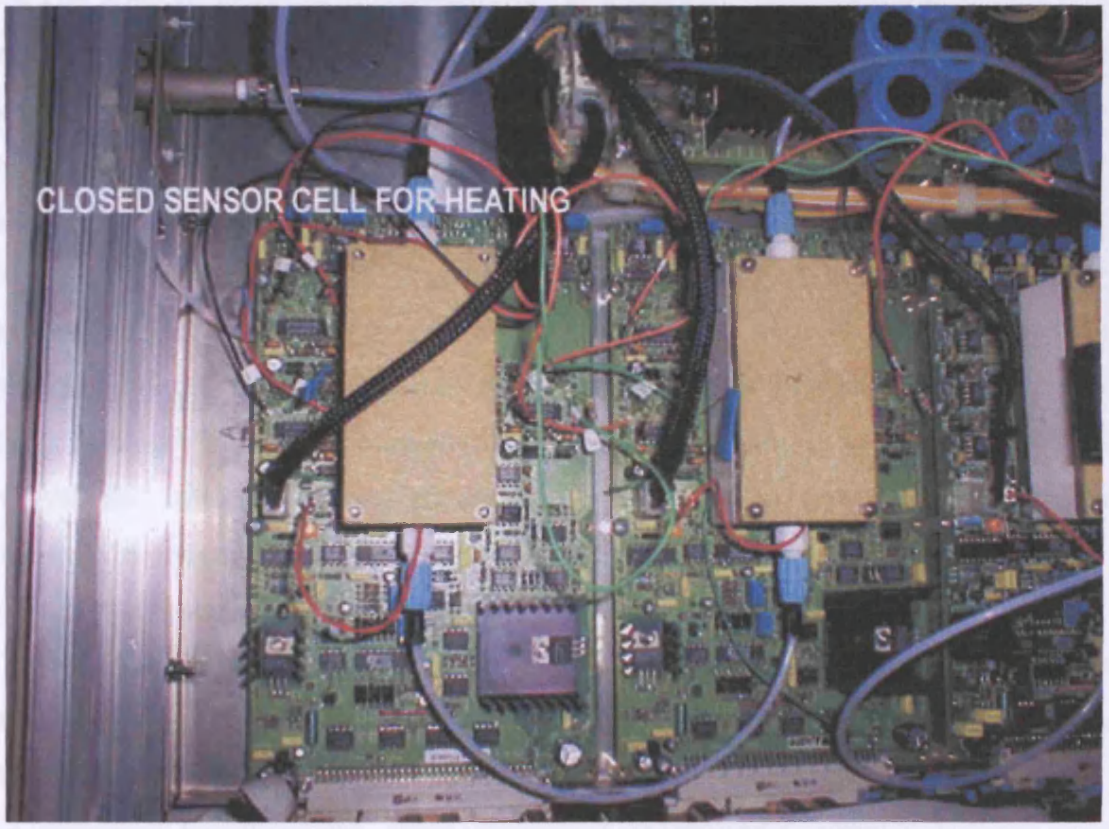

Figure 7.3 Sensor cells Fox2000 equipped with a heater

7.3 Experimental Results

To ensure the comprehensible examination of the sensor response different graphical representations such as scatter and line plots and vertical bar charts were used. Moreover, a statistical analysis namely, Principal Component Analysis (PCA) was used to get an overview of the pattern of response of a large number of sensors to a large number of target gases.

Principal Component Analysis (PCA) Plot

PCA is a multivariate technique in which a number of related variables are transformed to a smaller set of uncorrelated variables. PCA is mainly used to explore the data and to assess discrimination performances. In order to obtain discrimination (for two samples to be called different), we need to understand how large the differences in the individual sensor responses need to be.

PCA is recommended for use in this research work, since it is a more complex data analysis technique that compares data sets as a whole. This implies a reduction in the number of variables.

The Fox 2000 electronic nose was equipped with software (αFox) that allowed the quick comparison and identification of samples using automated pattern recognition algorithms. A more detailed explanation of PCA is given in ***Appendix B***.

7.3.1 Normalisation Method

Even small differences in the headspace concentration of a compound can be easily detected by the sensors, resulting in changes in their response pattern. Since the aim of this research work was to evaluate the pattern of response of the newly prepared sensors, it was important to correctly linearise the data to avoid confusion between any variations in headspace concentration and pattern of response. The response of each sensor was therefore linearised (converted to $(R/R_o)^2-1$) and then normalised to the response $((R/R_o)^2-1)$ of a standard CTO sensor operated at the same conditions.

This linearization/normalisation method offered the advantage of eliminating the effects of concentration variation between different injections of the same vapour, therefore obtaining repeatable results.

An additional benefit of the above mentioned normalisation method, was the better demonstration of the effects of the addition of different zeolite materials and the

chromium modification on CTO sensors. In more detail, the different response pattern of the newly prepared sensors (layered, mixed, Cr-zeolite) observed when normalised to the control sensor, allowed discrimination to be achieved by seeing the difference made by the different zeolite types (β, Y, ZSM-5), the different sensor microstructure (zeolite printed on top of the sensing layer or admix with it) and the effect of chromium catalysation.

7.3.2 Investigation of Possible Sensor Positioning Effect on the Sensor's Response

Preliminary experiments investigating the response of the different zeolite sensors to various organic species showed the desired variance in patterns of response between the tested sensors. To confirm that the achieved variance in sensors response was not due to the effect of positioning of the six tested sensors in the 2 cells, it was decided to further investigate the effect of the sensors position on the response. Unfortunately, this was not possible in the electronic nose since the αFox does not display the raw resistance value versus time. Instead, it displays the value of the relative resistance change.

Therefore, a data logger was connected to the electronic nose to record the variation of the sensor response with time –the transient effect- and thus to determine whether there was indeed an effect due to the positioning of the sensors. Experiments using six multi-electrode SEMDEC sensors and two different flow directions ***(See Figure 7.4)*** were performed in the presence of different gases. The time delay, the time required for each sensor to respond to a target gas, of each sensor was estimated relative to the first responding sensor. It should be noted that for the first sensor the time delay was zero seconds.

Figure 7.5 shows the response of six sensors to the presence of 2-methyl hexane with flow direction 1. As seen from these results, a time delay of few seconds was observed for all sensors compared to the first responding sensor (Zeolite β-Mixed). A small time delay was expected since the gas needs a few seconds to flow from sensor 3 (Zeolite β-Mixed) to sensor 6 (CTO-SOLGEL3) according to flow direction 1.

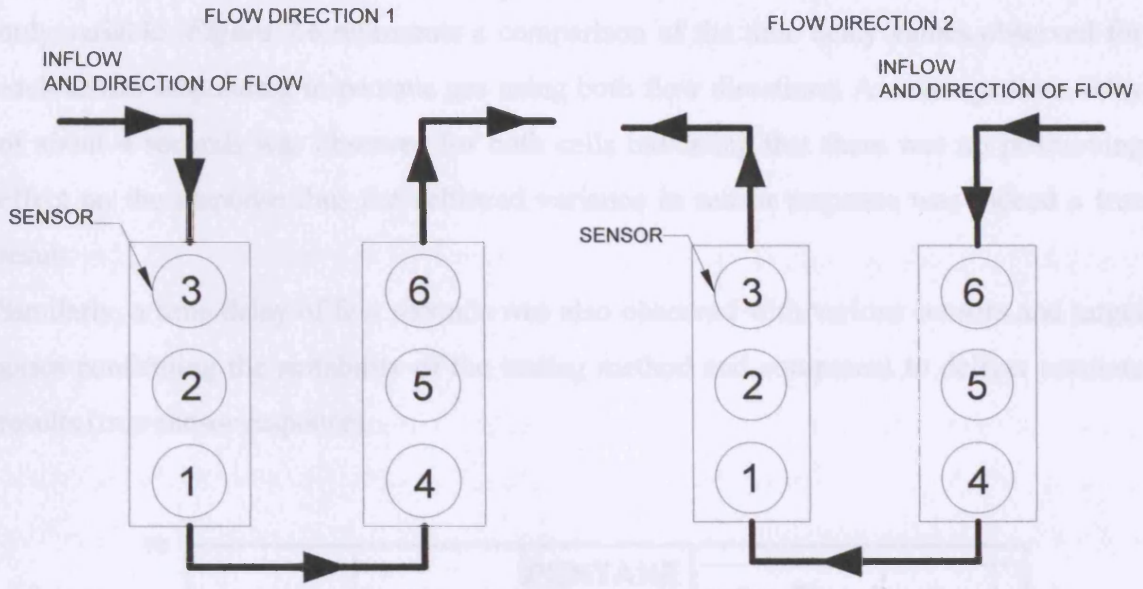

Figure 7.4 A representation of the two different flow directions used to investigate possible transient effect on sensors response

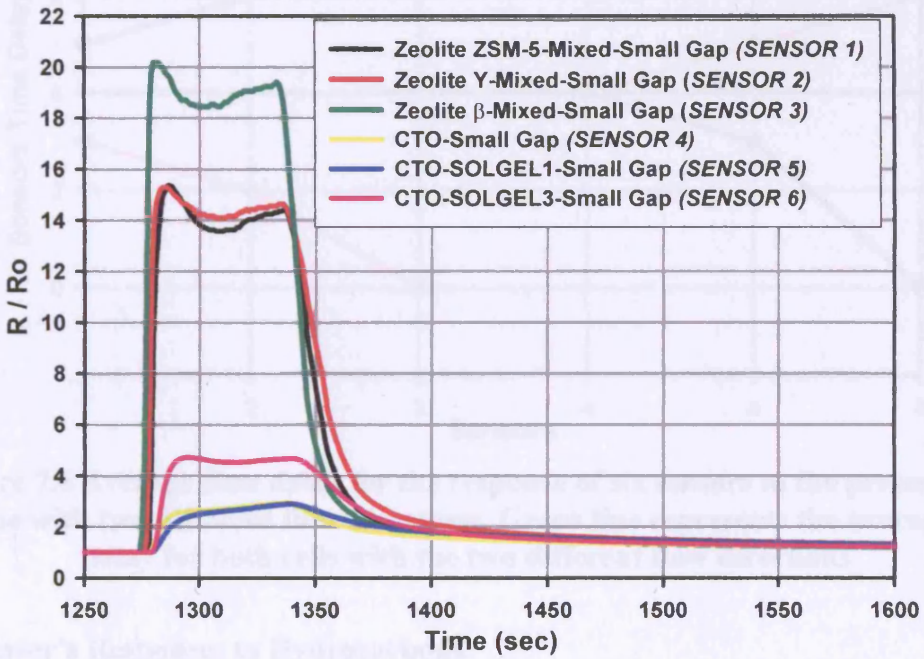

Figure 7.5 Response of six sensors to the presence of 2-methyl hexane with flow direction 1
CTO-SOLGEL1: $Cr_{1.95}Ti_{0.05}O_3$ (2 µm), CTO-SOLGEL3: $Cr_{1.9}Ti_{0.1}O_3$ (0.7 µm)
CTO: $Cr_{1.95}Ti_{0.05}O_3$ (0.5 µm) (UCL)

The next step in this investigation was to compare the response of the sensors to the presence of target gases using both flow direction 1 and 2. Thus, a series of experiments were performed using the same operating conditions (i.e. same concentration of tested

gases and sensors operating temperature) with the flow direction (either 1 or 2) being the only variable. ***Figure 7.6*** represents a comparison of the time delay values observed for each sensor responding to pentane gas using both flow directions. An average time delay of about 4 seconds was observed for both cells indicating that there was no positioning effect on the response thus the achieved variance in sensor response was indeed a true result.

Similarly, a time delay of few seconds was also observed with various sensors and target gases confirming the suitability of the testing method and equipment to deliver accurate results (true sensor response).

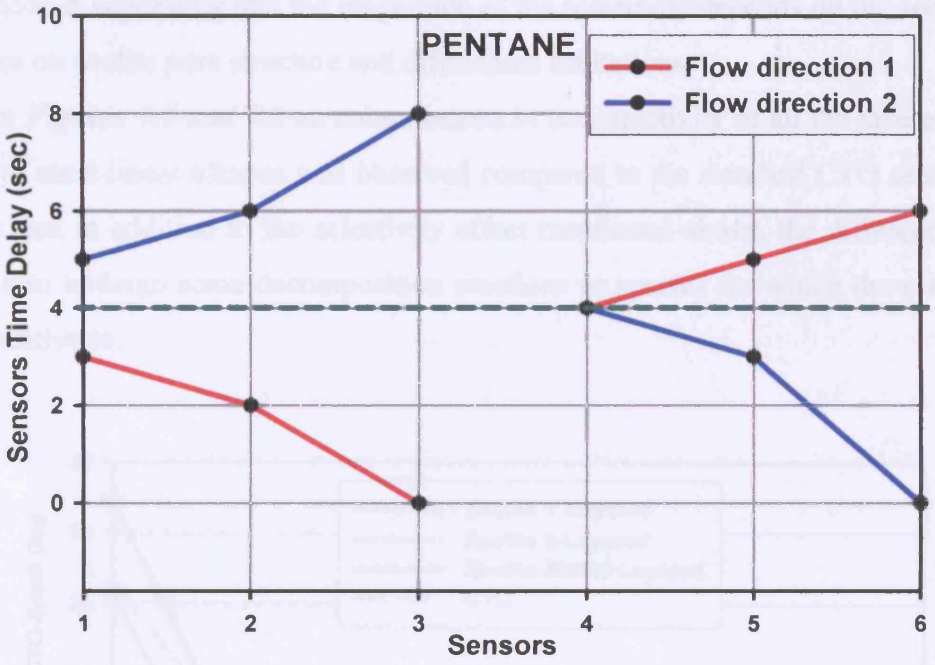

Figure 7.6 Average time delay for the response of six sensors to the presence of pentane with two different flow directions. Green line represents the average time delay for both cells with the two different flow directions

7.3.3 Sensor's Responses to Hydrocarbons

7.3.3.1 Linear Alkanes

The behaviour of layered zeolite sensors (that have a layer of either zeolite Y, zeolite β or zeolite ZSM-5 printed over the CTO sensing layer) and a standard CTO sensor to linear alkanes of varying carbon chain lengths (i.e. methane to dodecane) was studied at 400°C, with regards to small and large electrode gaps. All sensors were normalised to the response of a standard CTO sensor also being operated at 400°C so as to evaluate the

actual effect of the zeolite addition. According to ***Figures 7.7 and 7.8*** it was found that there was a decrease in the sensitivity of all zeolite sensors with increasing carbon chain length, for both small and large electrode gaps, relative to standard CTO sensor. This result was suggested to be due to an increase in the shape and size as well as diffusional limitations imposed by the zeolites with increasing carbon chain length.

All zeolite sensors showed a similar size selective effect, suggesting that the addition of zeolites over the top of the CTO sensing material lead to an increase in their size and shape selective properties as well as their discrimination ability for a range of linear alkanes, of different molecular size, compared to standard CTO sensor. However, slightly higher sensitivity was observed for layered zeolite Y sensor followed by β and finally by zeolite ZSM-5 suggesting that the magnitude of the selectivity depends on the zeolite type and hence on zeolite pore structure and diffusional limitations.

Based on ***Figures 7.7 and 7.8*** an enhancement in the sensitivity of all the layered zeolite sensors to most linear alkanes was observed compared to the standard CTO sensor. This suggests that in addition to the selectivity effect mentioned above, the different zeolites sensors also undergo some decomposition reactions to species for which the sensors are more sensitive to.

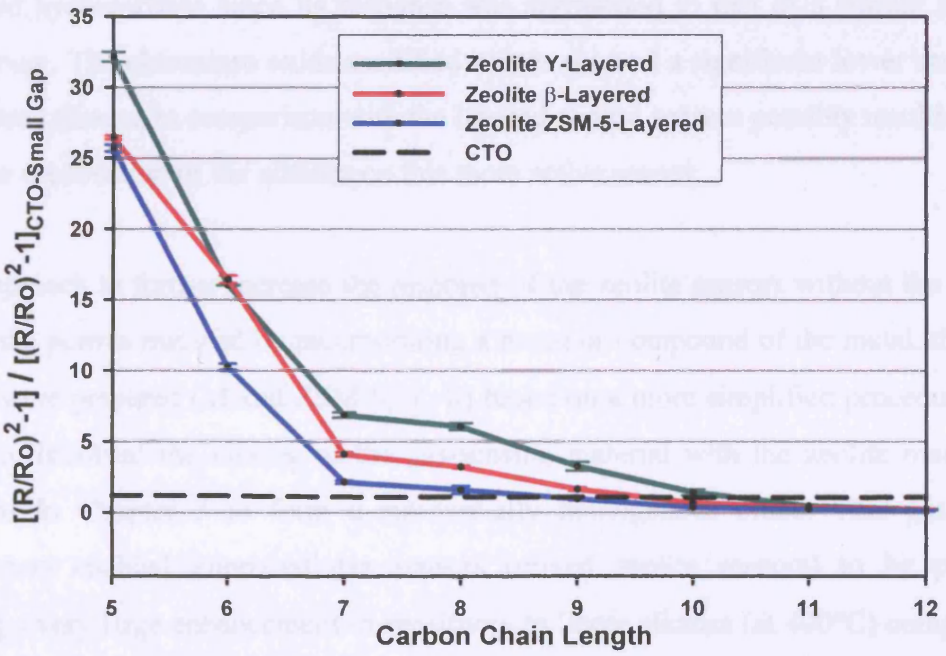

Figure 7.7 The normalised responses of layered zeolite sensors and a standard CTO sensor to various linear alkanes at 400°C with regards to small electrode gap CTO: $Cr_{1.95}Ti_{0.05}O_3$ (0.5 µm) (UCL)

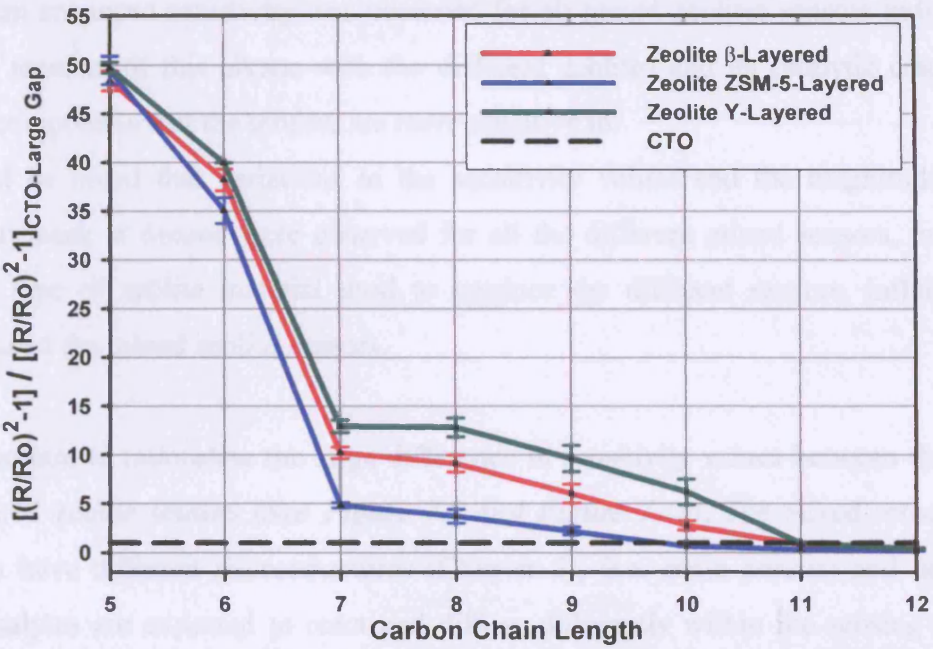

Figure 7.8 The normalised responses of layered zeolite sensors and a standard CTO sensor to various linear alkanes at 400°C with regards to large electrode gap CTO: $Cr_{1.95}Ti_{0.05}O_3$ (0.5 µm) (UCL)

Figure 7.9 represents the responses of the three layered zeolite sensors, a standard CTO sensor (Capteur-CTO) and a chromium oxide modified sensor (CTO+Cr_2O_3) with regards to their large electrode gap. As expected, the Capteur-CTO sensor showed no response to the tested hydrocarbons since its response was normalised to that of a similar standard CTO sensor. The chromium oxide modified sensor showed a significant lower sensitivity to all linear alkanes in comparison with the layered zeolite sensors possibly resulting from complete combustion of the alkanes on this more active sensor.

In an approach to further increase the response of the zeolite sensors without the need to modify the porous material by incorporating a metal or compound of the metal, three gas sensors were prepared (Mixed ZSM-5, Y, β) based on a more simplified procedure. This procedure involved the mixing of the gas-sensing material with the zeolite material as described in Chapter 5 to form a substantially homogenous blend. This gas sensor arrangement enabled improved gas sensors (mixed zeolite sensors) to be provided showing a very large enhancement in sensitivity to linear alkanes (at 400°C) compared to the layered and standard CTO sensors ***(See Figure 7.10)***. A similar filtering effect, as in the case of layered sensors, i.e. the sensor response decreases in relative sensitivity with increasing chain length, was also observed in the presence of most alkanes. However, at

decane, an enhanced sensitivity was observed for all mixed zeolites sensors indicating a possible reaction of this alkane with the different zeolites and its catalytic cracking to smaller compounds that the sensors are more sensitive to.

It should be noted that variations in the sensitivity values and the magnitude of the selectivity peak at decane were observed for all the different mixed sensors, indicating that the type of zeolite material used to produce the different sensors, influence the behaviour of the mixed zeolite sensors.

It is important to rationalise the large difference in sensitivity values between the mixed and layered zeolite sensors ***(See Figure 7.9 and Figure 7.10)***. The mixed sensors were found to have different microstructures (Chapter 5), (i.e. more porous) and hence the target analytes are expected to react and diffuse differently within the sensing material resulting in the observed different behaviour compared to the layered sensors.

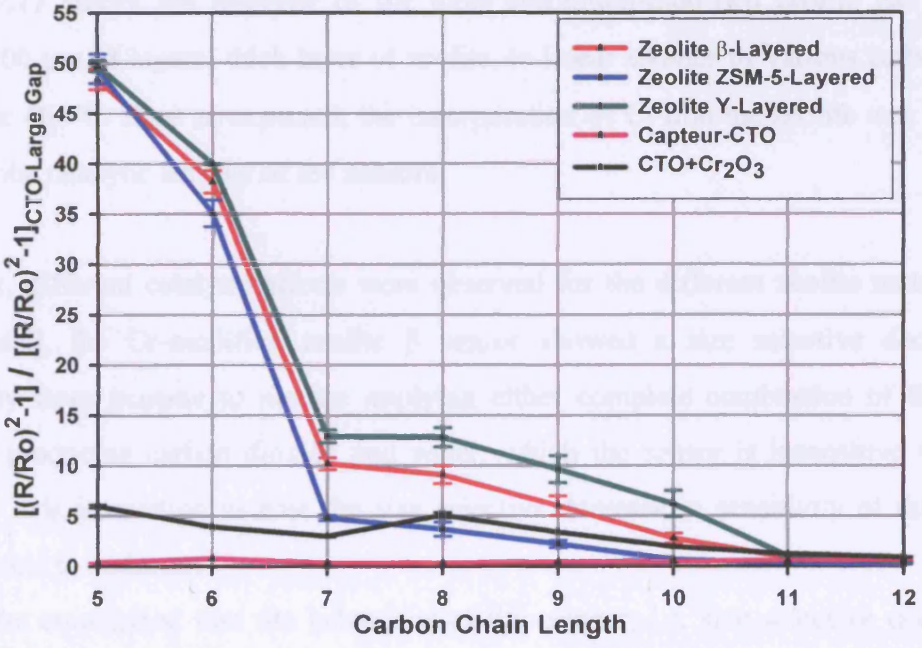

Figure 7.9 The normalised responses of layered zeolite sensors, Capteur CTO and a chromium oxide modified sensor to various linear alkanes at 400°C with regards to large electrode gap
Capteur-CTO: $Cr_{1.95}Ti_{0.05}O_3$ (1 µm) (Capteur Sensors & Analyzers Ltd)
CTO-Cr_2O_3: $Cr_{1.95}Ti_{0.05}O_3$ (0.7 µm) (Capteur Sensors & Analyzers Ltd)

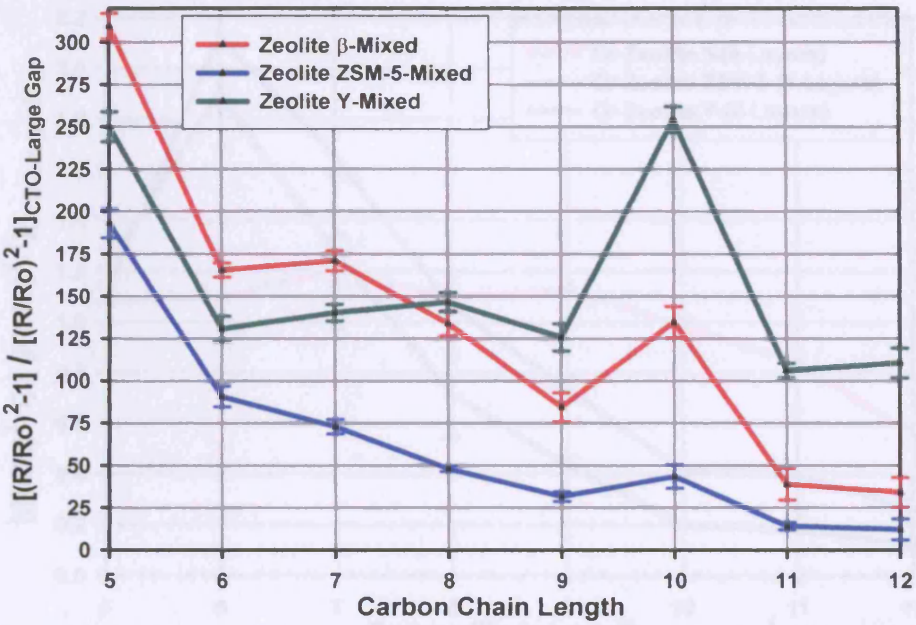

Figure 7.10 The normalised responses of mixed zeolite sensors to various linear alkanes operated at 400°C with regards to large electrode gap

Figure 7.11 shows the response of the three chromium-modified zeolite gas sensors, having 100 μm (8 layers) thick layer of zeolite, to linear alkanes of various carbon chain lengths at 400°C. Here as expected, the incorporation of Cr into the zeolite was found to increase the catalytic activity of the sensors.

However, different catalytic effects were observed for the different zeolite materials. In more detail, the Cr-modified zeolite β sensor showed a size selective decrease in sensitivity from pentane to nonane implying either complete combustion of the tested alkanes, producing carbon dioxide and water, which the sensor is insensitive to, or no reaction. It is interesting to note the size selective decrease in sensitivity of this sensor from decane to dodecane.

It must be emphisised that the behaviour of this sensor, i.e. size selective decrease in sensitivity for a range of alkanes, is very useful for discriminatory purposes when compared to other sensors.

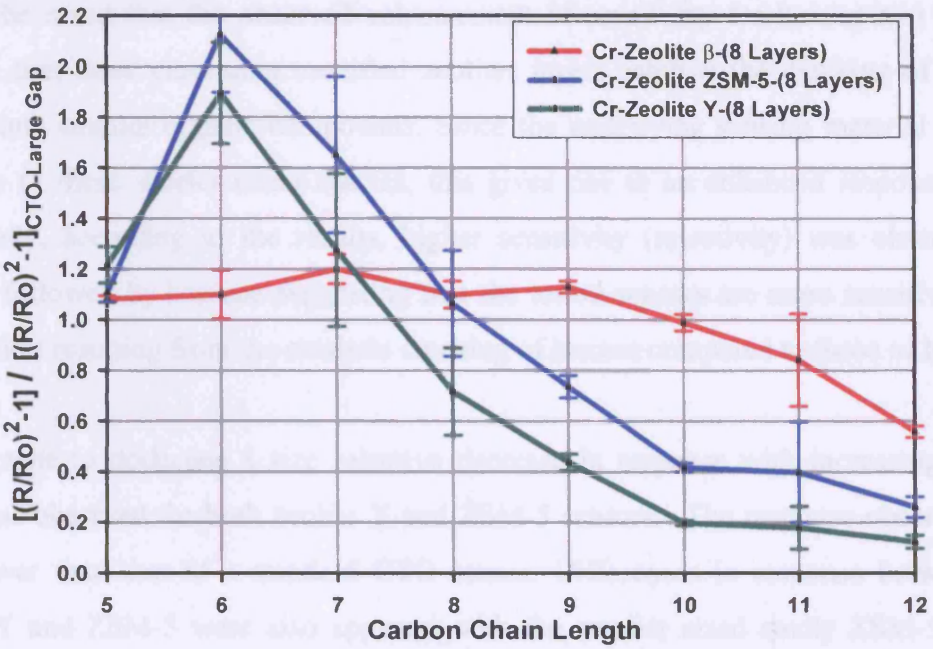

Figure 7.11 The normalised responses of layered chromium modified zeolite sensors to various linear alkanes operated at 400°C with regards to large electrode gap

Figure 7.11 also shows that an enhancement in sensitivity only for hydrocarbons with a narrow range of chain lengths can be obtained using Cr-modified zeolite Y and ZSM-5 gas sensors. In more detail, the chromium modification provided the porous material with the property of being able to selectively crack some of these organic species into smaller ones without resulting in complete conversion to carbon monoxide, carbon dioxide, hydrogen and water. Significant enhancement in sensitivity was only observed for hexane.

The narrow range of carbon chain lengths over which the effect was observed may in part be due to the fact that species significantly smaller than the zeolite cavity size (pentane) can pass though the cavity easily and thus have a lower residence time and hence lower probability of reaction. Hydrocarbons of slightly bigger size (hexane, and heptane for ZeoliteY) fit into the cavity but pass through the structure with more difficulty hence have a longer residence time and slightly higher probability of reaction. In contrast, species larger than the zeolite cavity (octane-dodecane) do not enter the zeolite cavity and hence they preferentially diffuse through the microstructure via the spaces in between the zeolite particles. Another possible explanation for the observed lower sensitivities of the larger hydrocarbons is that they get completely combusted on the tested sensors.

It must be noted that the observed enhancement of sensitivity for hexane and heptane suggests that these chromium modified zeolites layers catalyse the cracking of organic species into smaller organic compounds. Since the underlying sensing material is more sensitive to these shorter chain species, this gives rise to an enhanced response. More specifically, according to the results, higher sensitivity (selectivity) was observed for hexane, followed by heptane suggesting that the tested sensors are more sensitive to the by-products resulting from the catalytic cracking of hexane compared to those of heptane.

From octane to dodecane a size selective decrease in response with increasing carbon chain was observed for both zeolite Y and ZSM-5 sensors. The response observed was even lower than that of a standard CTO sensor. Differences in response between Cr-zeolite Y and ZSM-5 were also apparent with the smaller sized cavity ZSM-5 zeolite material showing slightly higher response compared to zeolite Y.

The thickness of the Cr-zeolite layer was also shown to affect the magnitude of sensor response. This is represented in ***Figure 7.12*** where a small variation in the sensitivity to linear alkanes was observed for Cr-zeolites ZSM-5 and Y sensors (operated at 400°C) with variation of the zeolite layer thickness (4 and 8 layers). However, it should be noted that the size selective enhancement in sensitivity at hexane was observed for both 4 and 8 layers.

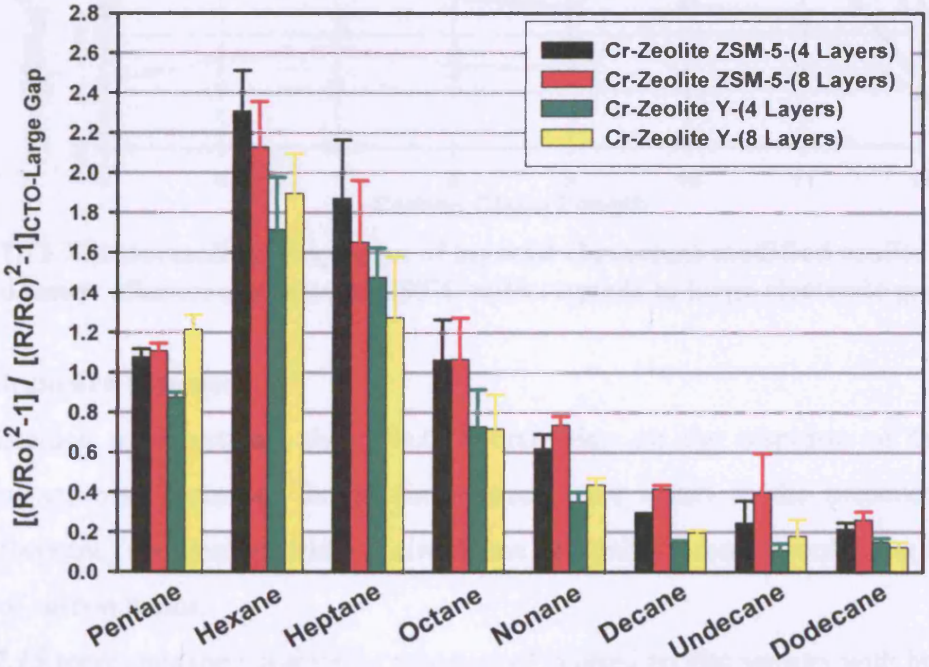

Figure 7.12 The normalised responses of layered chromium modified zeolite sensors (of different layer thickness) to linear alkanes operated at 400°C

Since the interactions of gases with the catalyst materials are temperature dependent, additional variance (different catalytic effects) and hence discrimination can be achieved by operating the same gas sensors at a multiplicity of temperatures. Thus, the responses of the three Cr-modified zeolite sensors (Y, β, ZSM-5) to alkanes of various carbon chain lengths were monitored at 350°C. ***Figure 7.13*** indicates that the Cr-modified zeolite sensors show different catalytic activity at this lower operating temperature. A size selective enhancement in the sensitivity was observed for all tested sensors compared to that obtained at 400°C. The magnitude of this effect was also found to be depended on zeolite type. A small variation in the sensitivities values with variation of zeolite layer thickness was also found at 350°C ***(Figure 7.14)***.

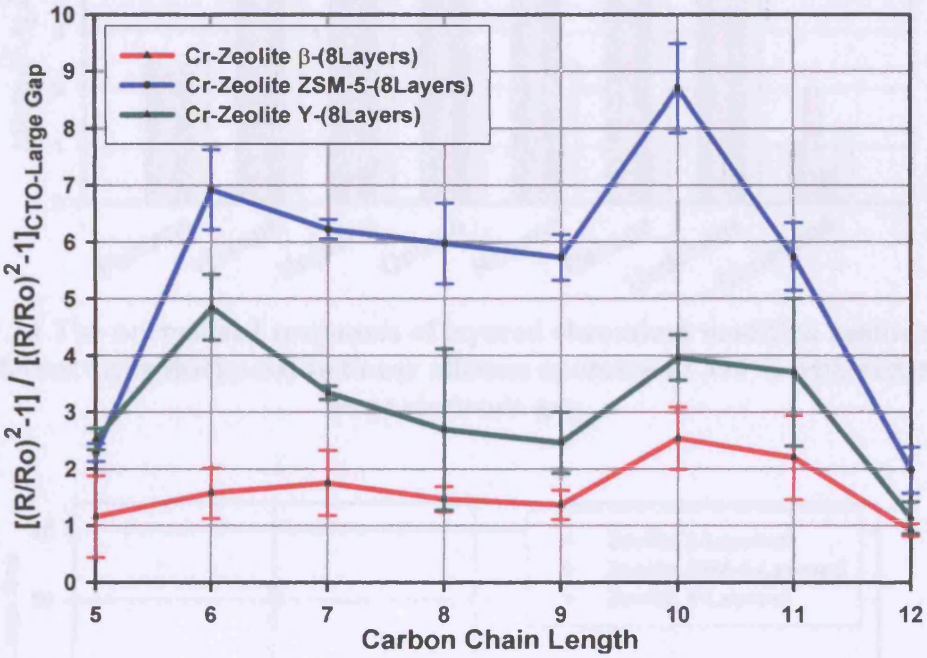

Figure 7.13 The normalised responses of layered chromium modified zeolite sensors to linear alkanes operated at 350°C with regards to large electrode gap

7.3.3.2 Branched Alkanes

It was decided to investigate the effect of branching on the response of the newly developed sensors. Therefore the zeolite sensors were tested in the presence of one straight (heptane) and one branched chain alkane (2-methyl hexane) containing the same number of carbon atoms.

Figure 7.15 represents the variation in response of layered zeolite sensors with branching. All layered zeolite sensors show an increase in response with increasing branching. In

more detail, all sensors were significantly found to be more sensitive to 2-methyl hexane compared to heptane. The examination was further extended using different zeolite types, where different sensitivities were observed.

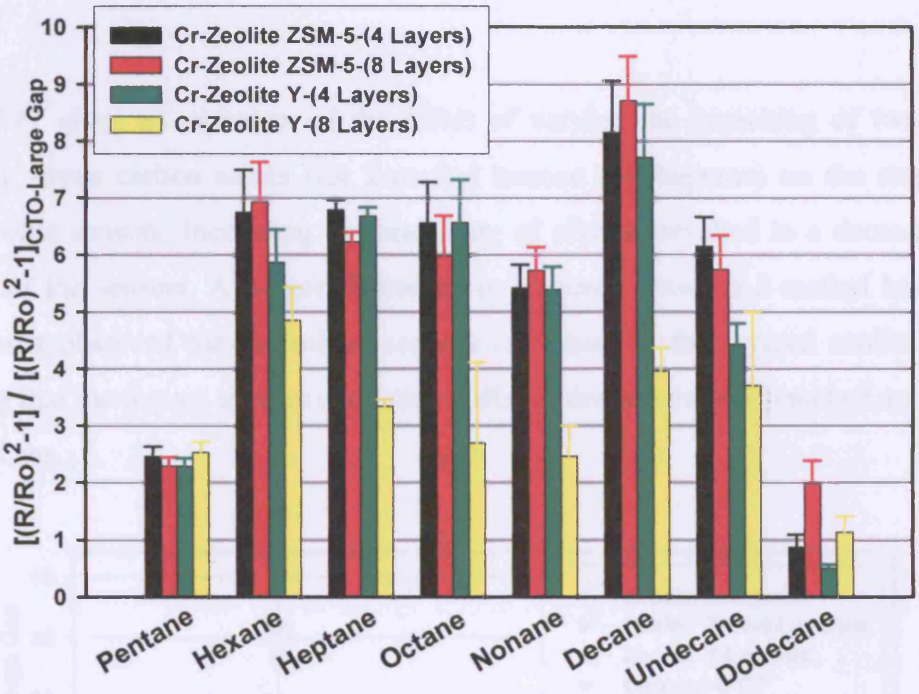

Figure 7.14 The normalised responses of layered chromium modified zeolite sensors (of different layer thickness) to linear alkanes operated at 350°C with regards to large electrode gap

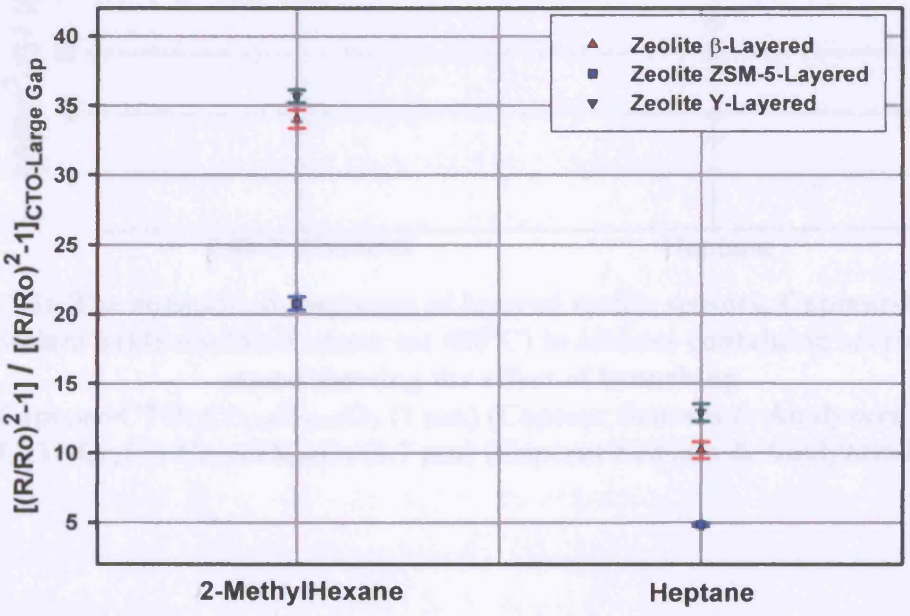

Figure 7.15 The normalised responses of layered zeolite sensors (at 400°C) to alkanes containing seven carbon atoms showing the effect of branching

Figure 7.16 compares the response behaviour of Capteur-CTO sensor, CTO+Cr_2O_3 and layered zeolite sensors to the presence of 2-methyl hexane and heptane. Both Capteur-CTO and CTO+Cr_2O_3 sensors seem to be unaffected by variations in branching in contrast to layered sensors. It must be said that these results are very useful for discrimination purposes.

Figure 7.17 gives an overview of the effect of varying the branching of two alkanes containing seven carbon atoms (for 2-methyl hexane and heptane) on the response of mixed zeolite sensors. Increasing the branching of alkanes resulted in a decrease in the response of the sensors. A bigger difference in response between 2-methyl hexane and heptane was observed for the mixed sensors compared to the layered zeolite sensors, indicating that the former sensors are better to discriminate between branched and straight chain alkanes.

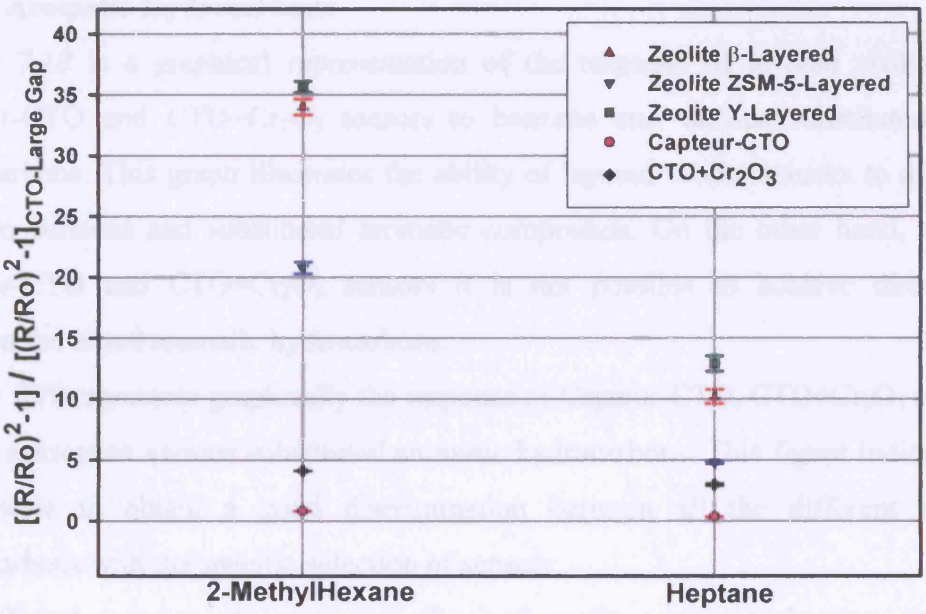

Figure 7.16 The normalised responses of layered zeolite sensors, Capteur-CTO and a chromium oxide modified sensor (at 400°C) to alkanes containing seven carbon atoms showing the effect of branching
Capteur-CTO: $Cr_{1.95}Ti_{0.05}O_3$ (1 µm) (Capteur Sensors & Analyzers Ltd)
CTO-Cr_2O_3: $Cr_{1.95}Ti_{0.05}O_3$ (0.7 µm) (Capteur Sensors & Analyzers Ltd)

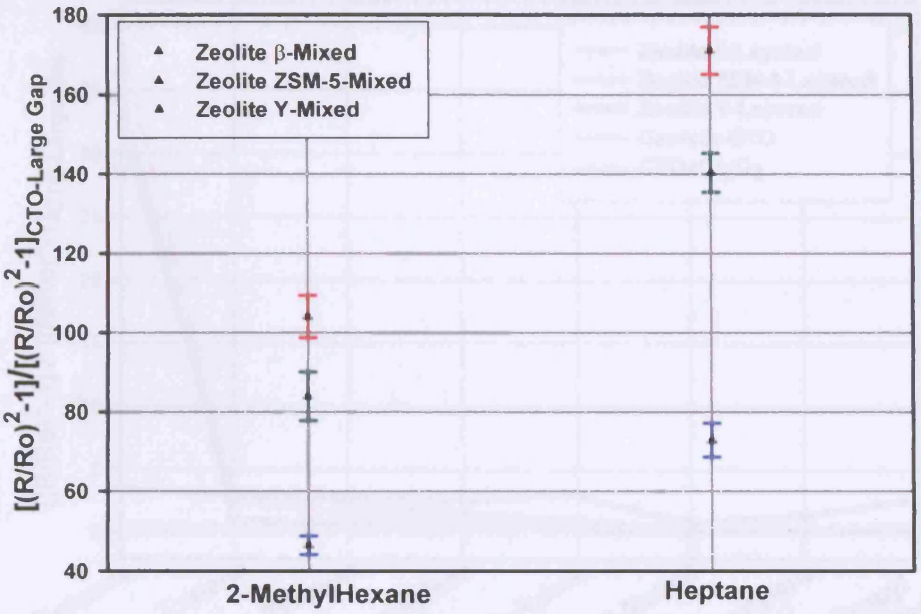

Figure 7.17 The normalised responses of mixed zeolite sensors (at 400°C) to alkanes containing seven carbon atoms showing the effect of branching

7.3.3.3 Aromatic Hydrocarbons

Figure 7.18 is a graphical representation of the response of layered zeolite sensors, Capteur-CTO and CTO+Cr_2O_3 sensors to benzene and various substituted aromatic hydrocarbons. This graph illustrates the ability of layered zeolite sensors to discriminate between benzene and substituted aromatic compounds. On the other hand, using only Capteur-CTO and CTO+Cr_2O_3 sensors it is not possible to achieve discrimination between the tested aromatic hydrocarbons.

Figure 7.19 represents graphically the response of Capteur-CTO, CTO+Cr_2O_3 and layered zeolite sensors to various substituted aromatic hydrocarbons. This figure indicates that it is possible to obtain a good discrimination between all the different substituted hydrocarbons with the specific selection of sensors.

The different response characteristics of mixed zeolite sensors to benzene and various substituted aromatic hydrocarbons are represented by ***Figure 7.20***. The very high sensitivities observed along with the wide variation in the responses, indicate the suitability of the mixed zeolite sensors to discriminate benzene, toluene, ethylbenzene and propylbenzene from each other and from the remaining hydrocarbons (m-xylene, p-xylene, 1,2,3-methyl benzene and mesitylene). Furthermore, according to ***Figure 7.21*** m-xylene and p-xylene can be discriminated from 1,2,3-methyl benzene and mesitylene using the same sensors.

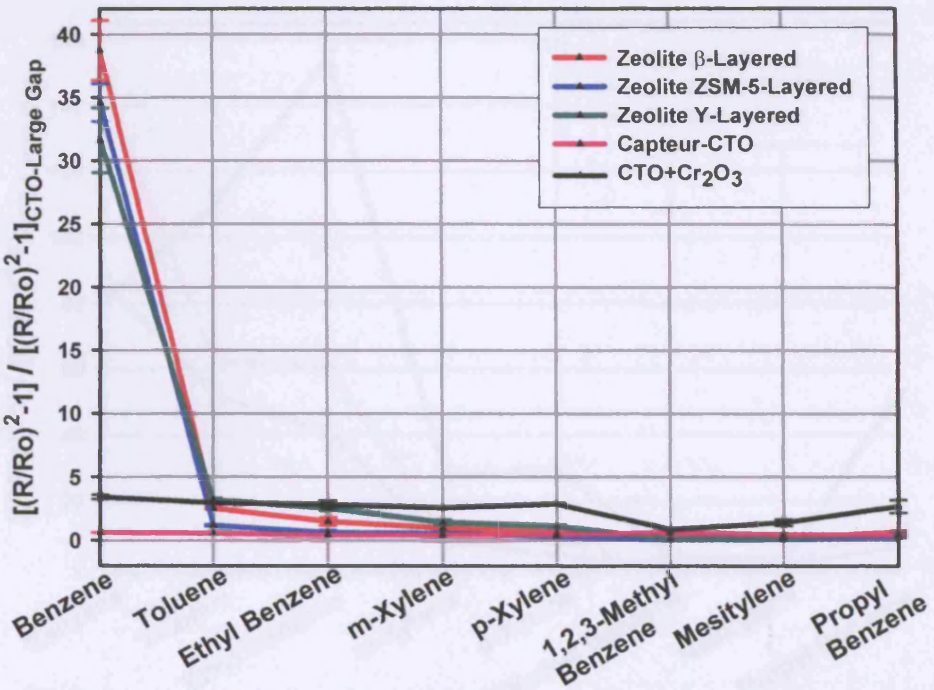

Figure 7.18 The normalised responses of layerd zeolite sensors, Capteur-CTO and a chromium oxide modified sensor (at 400°C) to benzene and substituted aromatic hydrocarbons with regards to large electrode gap
Capteur-CTO: $Cr_{1.95}Ti_{0.05}O_3$ (1 µm) (Capteur Sensors & Analyzers Ltd)
CTO-Cr_2O_3: $Cr_{1.95}Ti_{0.05}O_3$ (0.7 µm) (Capteur Sensors & Analyzers Ltd)

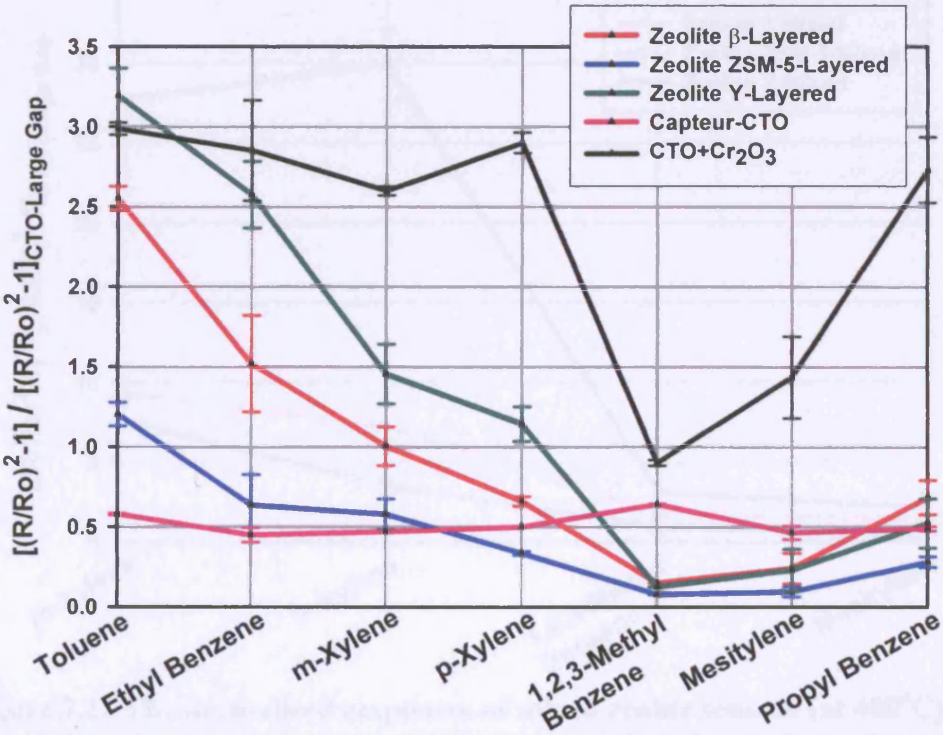

Figure 7.19 The normalised responses of layered zeolite sensors, Capteur-CTO and a chromium oxide modified sensor (at 400°C) to substituted aromatic hydrocarbons with regards to large electrode gap
Capteur-CTO: $Cr_{1.95}Ti_{0.05}O_3$ (1 µm) (Capteur Sensors & Analyzers Ltd)
CTO-Cr_2O_3: $Cr_{1.95}Ti_{0.05}O_3$ (0.7 µm) (Capteur Sensors & Analyzers Ltd)

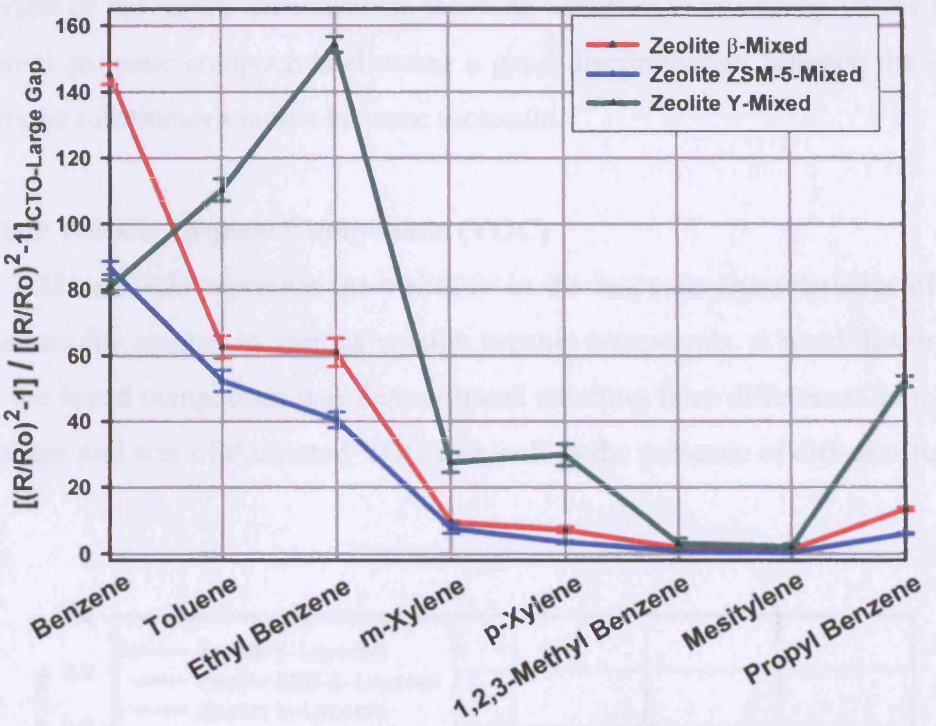

Figure 7.20 The normalised responses of mixed zeolite sensors (at 400°C) to benzene and substituted aromatic hydrocarbons with regards to large electrode gap

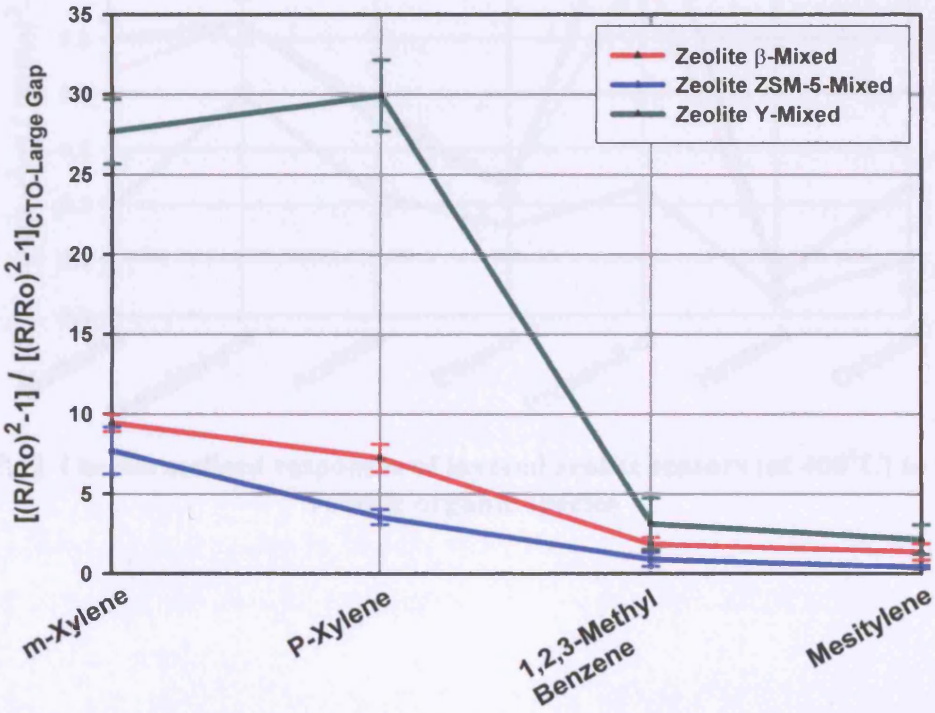

Figure 7.21 The normalised responses of mixed zeolite sensors (at 400°C) to substituted aromatic hydrocarbons with regards to large electrode gap

An overview of the results demonstrates the wide variation in sensitivity values between the different aromatic compounds allowing a good discrimination between the different hydrocarbons substitutions onto a benzene molecule.

7.3.4 Other Volatile Organic Compounds (VOC)

Figures 7.22 and 7.23 represent the variation in the response characteristics of layered and mixed zeolite sensors to various volatile organic compounds. A good discrimination between the tested compounds was demonstrated resulting from differences in molecular weight, shape and size of the tested VOC's as well as the presence of different functional groups.

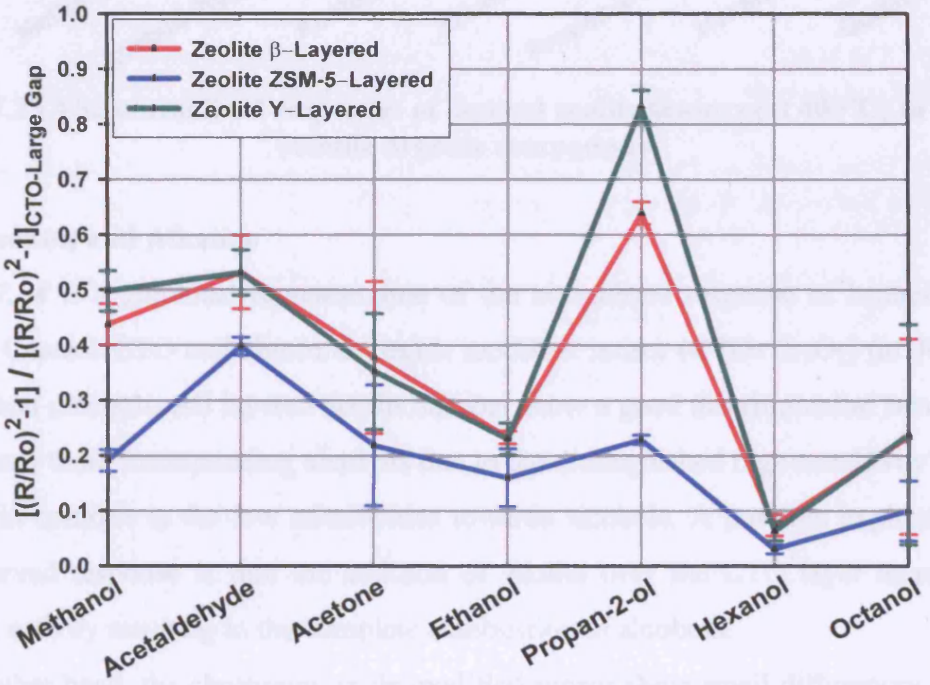

Figure 7.22 The normalised responses of layered zeolite sensors (at 400°C) to various volatile organic species

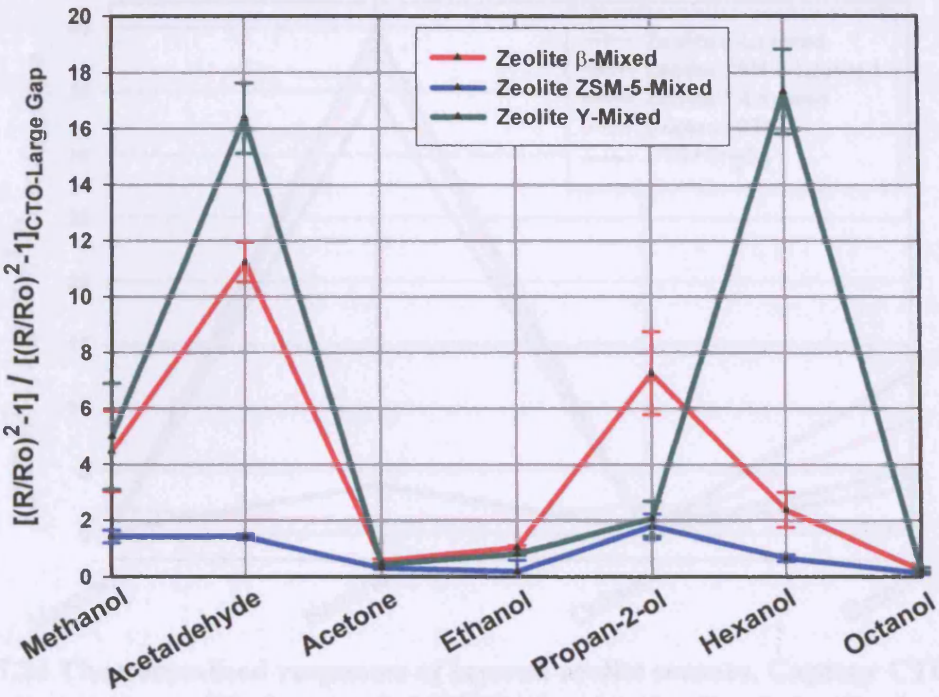

Figure 7.23 The normalised responses of layered zeolite sensors (at 400°C) to various volatile organic compounds

7.3.5 Alcohols and Alkanes

Figure 7.24 is a graphical representation of the normalised response of layered zeolite sensors, Capteur-CTO and chromium oxide modified sensor (CTO+Cr_2O_3) (at 400°C) to alkanes and alcohols. All layered zeolite sensors show a good discrimination between the alkanes and their corresponding alcohols due to the distinguished high sensitivity towards alkanes in contrast to the low sensitivities towards alcohols. A possible explanation for the observed response is that the addition of zeolite over the CTO layer increases its catalytic activity resulting in the complete combustion of alcohols.

On the other hand, the chromium oxide modified sensor show small differences between the two different functional groups (alkanes/alcohols). This can be explained by the fact that this sensor is not sensitive to alkanes and causes complete combustion of alcohols. Finally, ***Figure 7.24*** verifies that the Capteur-CTO sensor does not discriminate between the two different compounds.

Figure 7.25 represents the normalised response of mixed zeolite sensors to some alkanes and alcohols. The enhanced sensitivity observed for alkanes compared to alcohols demonstrate the suitability of mixed zeolite sensors to discriminate between the two different functional groups.

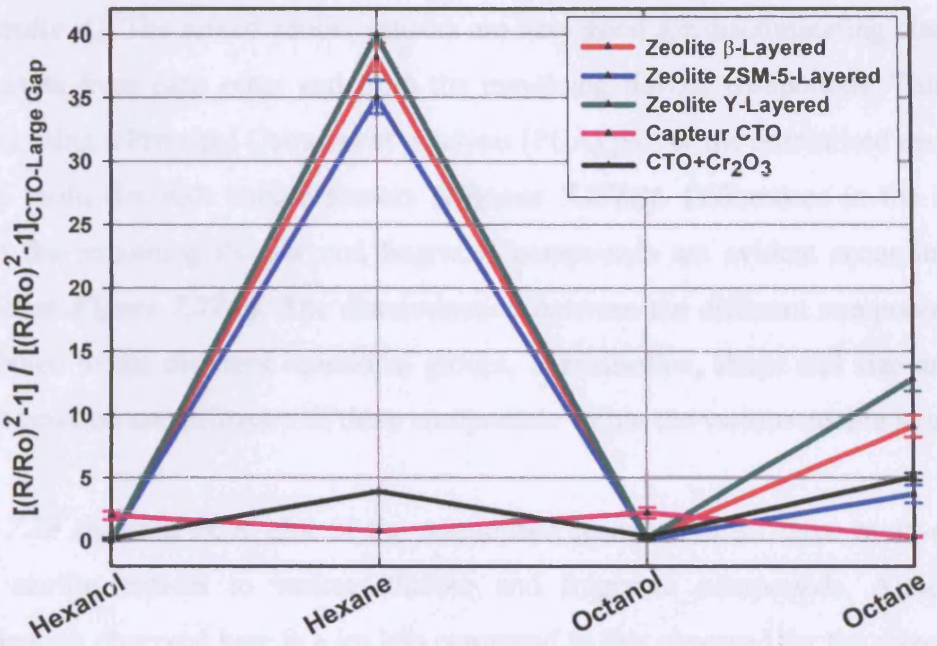

Figure 7.24 The normalised responses of layered zeolite sensors, Capteur CTO and a chromium oxide modified sensor (at 400°C) showing the discrimination between alkanes and their corresponding alcohols
Capteur-CTO: $Cr_{1.95}Ti_{0.05}O_3$ (1 µm) (Capteur Sensors & Analyzers Ltd)
CTO-Cr_2O_3: $Cr_{1.95}Ti_{0.05}O_3$ (0.7 µm) (Capteur Sensors & Analyzers Ltd)

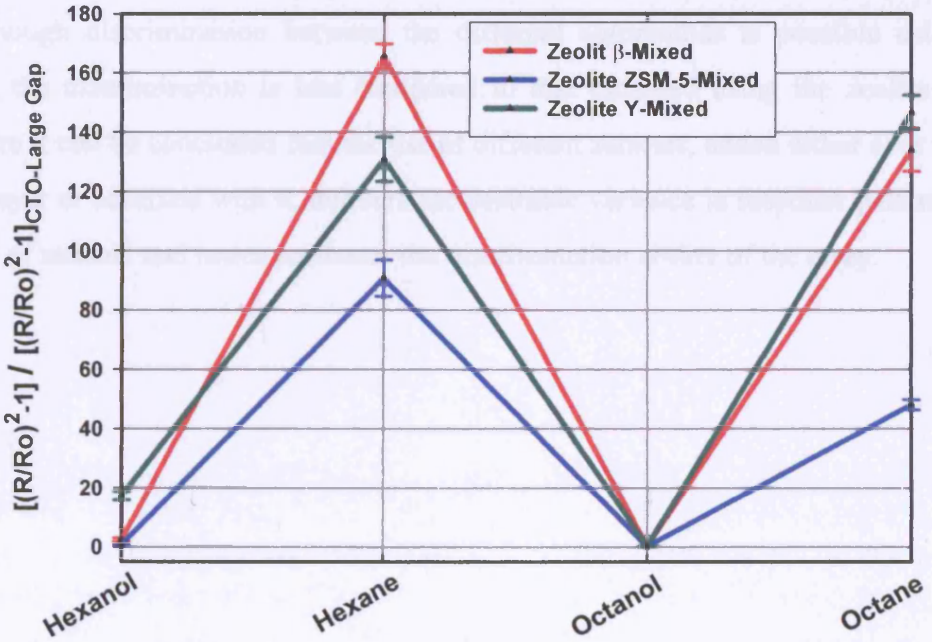

Figure 7.25 The normalised responses of mixed zeolite sensors at 400°C showing the discrimination between alkanes and their corresponding alcohols

7.3.6 Flavour and Fragrance Compounds

Figures 7.26 show the normalised response of mixed zeolite sensors to various flavour compounds (Details regarding the structure of the tested flavour compounds can be found

in ***Appendix A***). The mixed zeolite sensors are very good for discriminating cineole and amyl acetate from each other and from the remaining flavour compounds. This is also indicated using a Principal Component Analysis (PCA) plot of the normalised response of all three multi-electrode mixed sensors ***(Figures 7.27(a))***. Differences in the response between the remaining flavour and fragrance compounds are evident according to the PCA plot at ***Figure 7.27(b)***. The discrimination between the different compounds could be attributed to the different functional groups, hybridisation, shape and size and hence different reaction and diffusion of these compounds within the various zeolite structures.

Figure 7.28 shows a PCA plot of the normalised response of all three multi-electrode layered zeolite sensors to various flavour and fragrance compounds. Although the discrimination observed here is a lot less compared to that observed for the mixed zeolite sensors, all compounds are found to be well discriminated.

Finally, ***Figure 7.29*** shows a PCA plot for a range of flavour and fragrance compounds using standard CTO sensors (Capteur-CTO, CTO+Cr_2O_3 and CTO). It can be suggested that although discrimination between the different compounds is possible using these sensors, the discrimination is less compared to that obtained using the zeolite sensors. Therefore it can be concluded that the use of different zeolites, added either over the CTO sensor layer or admixed with it, delivers the desirable variance in response patterns across an array of sensors and hence increases the discrimination ability of the array.

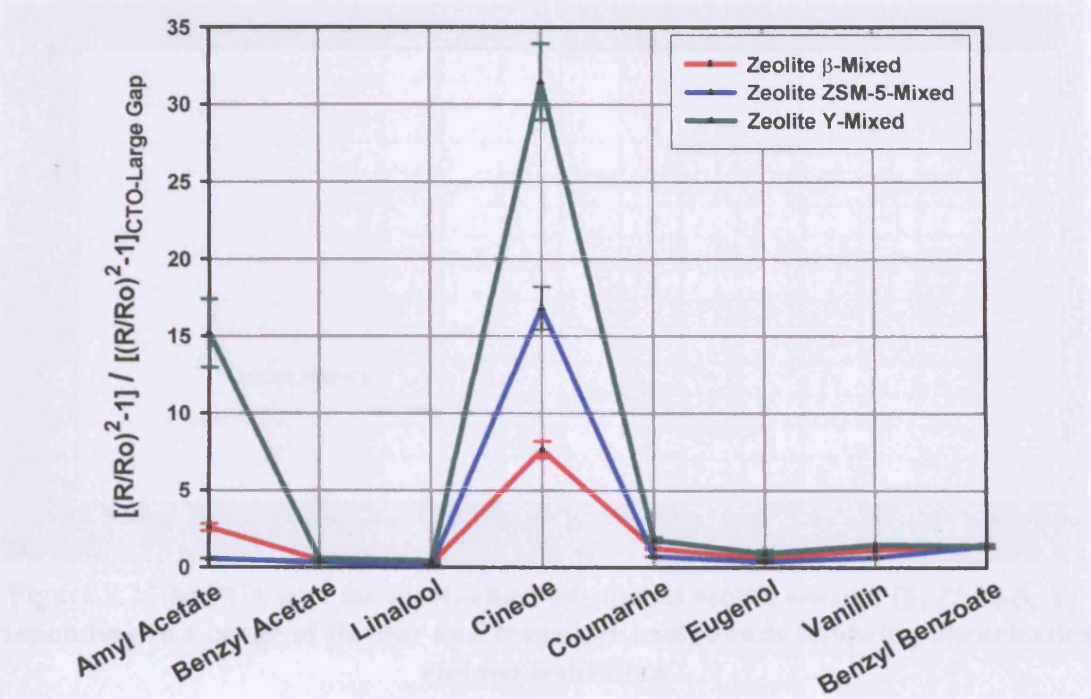

Figure 7.26 The normalised responses of mixed zeolite sensors at 400°C to various flavour compounds with regards to large electrode gap

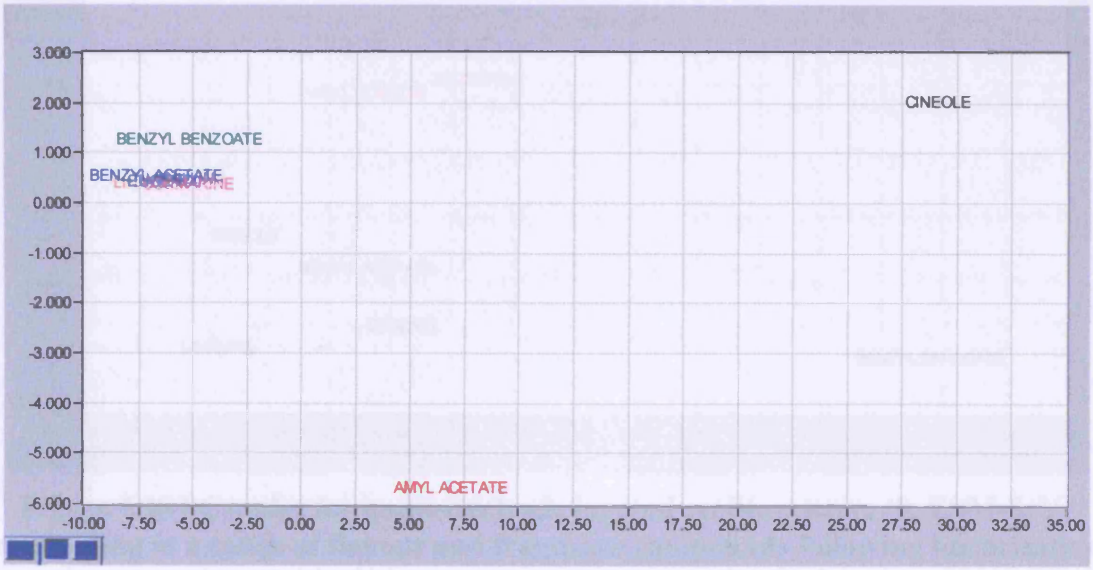

Figure 7.27(a) PCA plot for multi-electrode mixed zeolite sensors (β, ZSM-5, Y) responding to a range of flavour and fragrance compounds following linearisation and normalisation

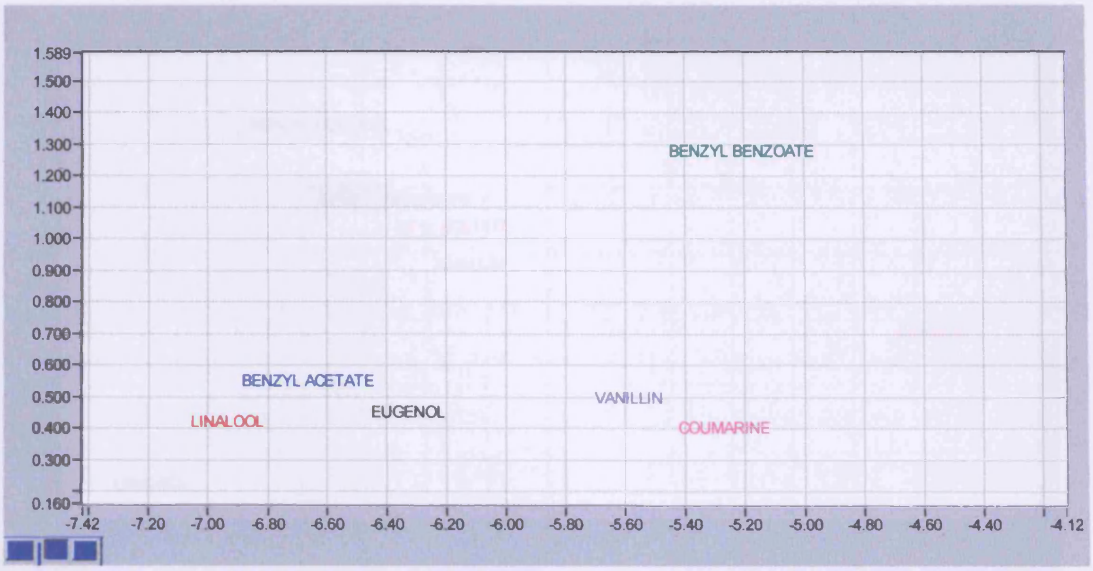

Figure 7.27(b) PCA plot for multi-electrode mixed zeolite sensors (β, ZSM-5, Y) responding to a range of flavour and fragrance compounds following linearisation and normalisation

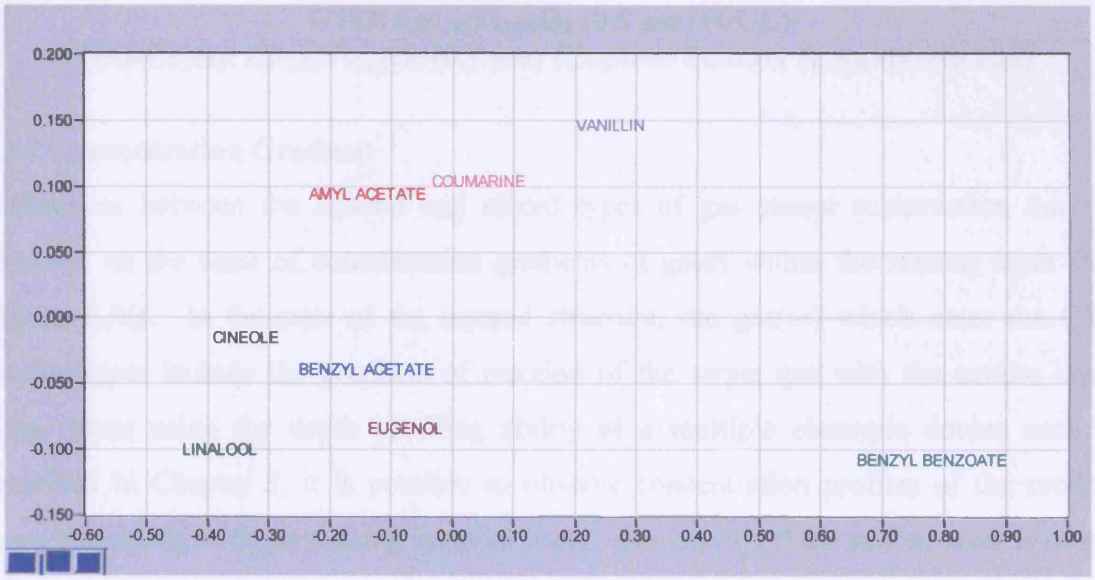

Figure 7.28 PCA plot for multi-electrode layered zeolite sensors (β, ZSM-5, Y) responding to a range of flavour and fragrance compounds following linearisation and normalisation

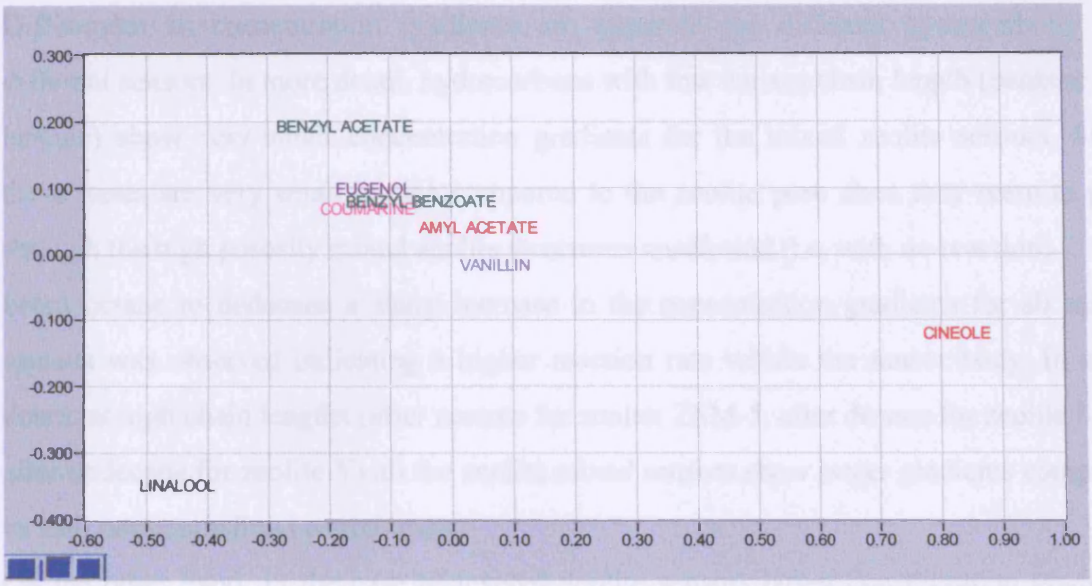

Figure 7.29 PCA plot for multi-electrode standard CTO sensors (Capteur-CTO, CTO+Cr_2O_3 and CTO) responding to a range of flavour and fragrance compounds following linearisation and normalisation
Capteur-CTO: $Cr_{1.95}Ti_{0.05}O_3$ (1 µm) (Capteur Sensors & Analyzers Ltd)
CTO: $Cr_{1.95}Ti_{0.05}O_3$ (0.5 µm) (UCL)
CTO-Cr_2O_3: $Cr_{1.95}Ti_{0.05}O_3$ (0.7 µm) (Capteur Sensors & Analyzers Ltd)

7.3.7 Concentration Gradient

Differences between the layered and mixed types of gas sensor construction may be observed on the basis of concentration gradients of gases within the sensing layer ***(See Figure 5.36)***. In the case of the layered structure, the gas(es) which enter the CTO sensing layer include the products of reaction of the target gas with the zeolite layer. Thus, when using the depth profiling ability of a multiple electrode device such as described in Chapter 3, it is possible to observe concentration profiles of the product gases interacting with the sensing material itself. Conversely, if the zeolite layer is mixed with the sensing material, then the depth profiling ability of the electrodes results in a measure of the concentration profiles of gases as they interact with the zeolite sensing material blend. This explains the enhanced concentration gradients usually observed for the mixed zeolite sensors compared to the layered ones.

Figure 7.30 shows the concentration gradients (ratio of response on a large electrode gap to that on a small electrode gap) of the layered and mixed zeolite sensors, a standard CTO sensor and a chromium oxide modified CTO sensor to a range of linear alkanes of varying carbon chain lengths.

Differences in concentration gradients are apparent for different hydrocarbons and different sensors. In more detail, hydrocarbons with low carbon chain length (pentane and hexane) show very small concentration gradients for the mixed zeolite sensors. Since these gases are very small in size compared to the zeolite pore sizes they seem to pass through the high porosity mixed zeolite structures unaffected (i.e. with no reaction).

From octane to dedecane a sharp increase in the concentration gradients for all mixed sensors was observed indicating a higher reaction rate within the sensor body. In more detail, at high chain lengths (after nonane for zeolite ZSM-5, after decane for zeolite β and after undecane for zeolite Y) all the zeolite mixed sensors show larger gradients compared to their corresponding layered ones.

On the other hand, in the case of layered zeolite sensors larger concentration gradients were observed for low carbon chain lengths hydrocarbons compared to their corresponding mixed sensors and smaller for high chain length.

The standard CTO sensor shows almost no concentration gradient for the tested hydrocarbons. However, the chromium modified CTO sensor show a small concentration gradient indicating little reaction.

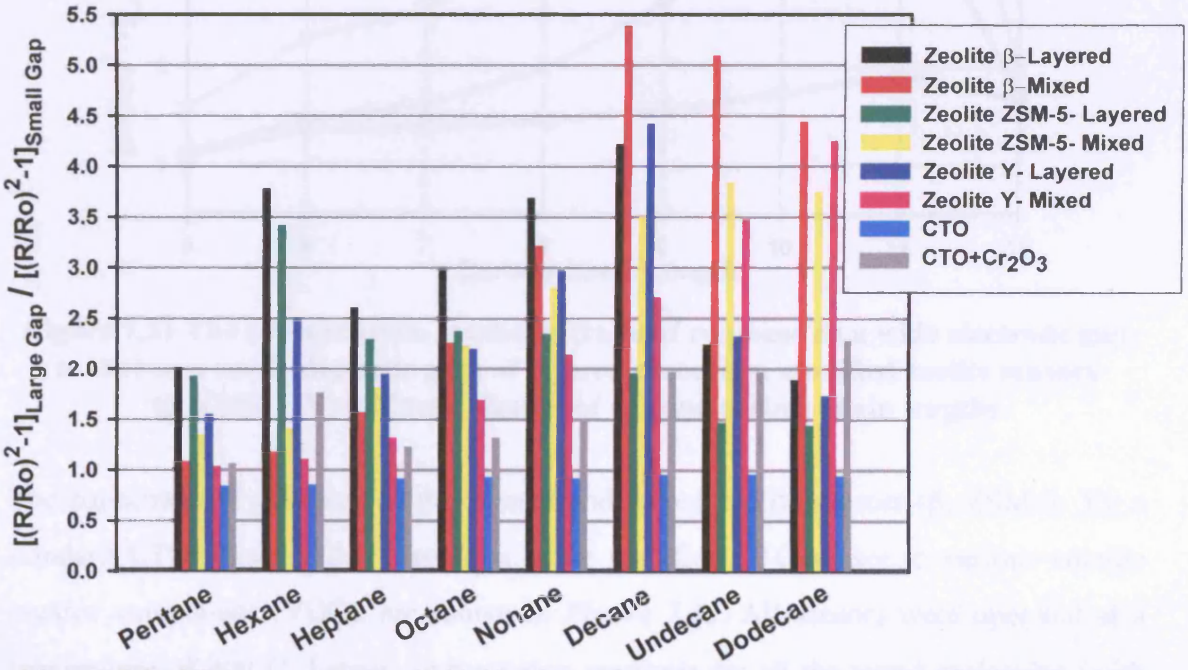

Figure 7.30 The concentration gradients (ratio of response on a wide electrode gap to that on a small electrode gap) of layered and mixed zeolite sensors (β, ZSM-5, Y), a standard CTO sensor and a chromium oxide modified CTO sensor to linear alkanes of varying carbon chain lengths
CTO: $Cr_{1.95}Ti_{0.05}O_3$ (0.5 μm) (UCL)
CTO-Cr_2O_3: $Cr_{1.95}Ti_{0.05}O_3$ (0.7 μm) (Capteur Sensors & Analyzers Ltd)

Figure 7.31 shows the concentration gradients of Cr-zeolite sensors (at 400°C) in the presence of linear alkanes of varying carbon chain length. A steady increase in concentration gradients with increasing carbon chain length was observed for both Cr-Zeolite Y and ZSM-5 up to undecane. For dodecane, a very small concentration gradient was observed comparable in magnitude to that obtained for pentane showing that these two alkanes are unaffected by the Cr-zeolite modification (almost unreactive). Cr-Zeolite β sensor show very small concentration gradient for all the tested alkanes, slightly increasing in magnitude with increasing carbon chain length. This suggests that this sensors is almost uncreative to the majority of alkanes tested.

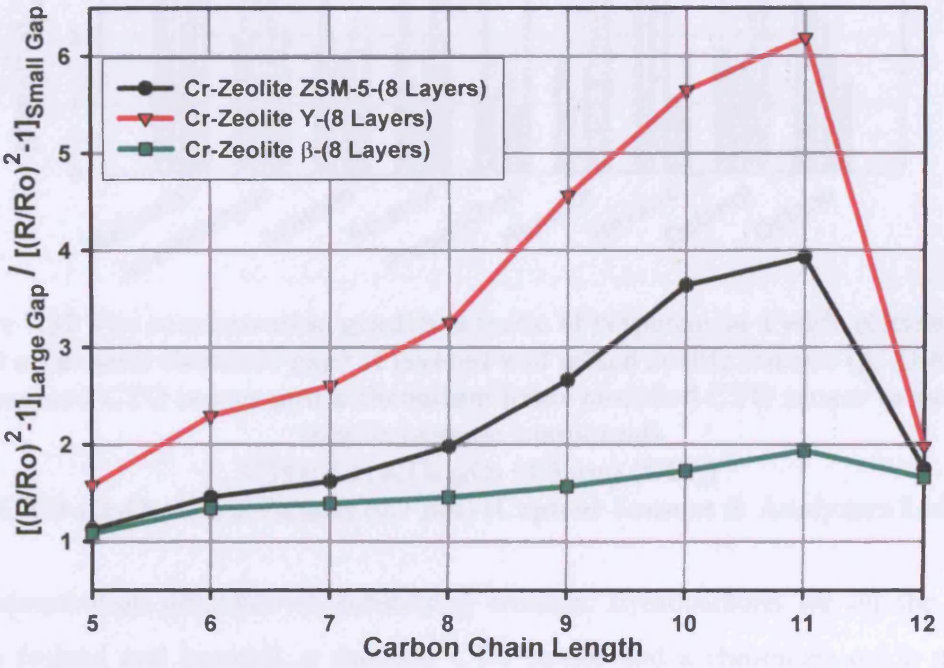

Figure 7.31 The concentration gradients (ratio of response on a wide electrode gap to that on a small electrode gap) of layered chromium modified zeolite sensors (β, ZSM-5, Y) to linear alkanes of varying carbon chain lengths

The concentration gradients of the layered and mixed zeolite sensors (β, ZSM-5, Y), a standard CTO sensor and a chromium oxide modified CTO sensor to various volatile organic compounds (VOC), are shown in ***Figure 7.32***. All sensors were operated at a temperature of 400°C. Larger concentration gradients for all the tested molecules (with the exception of hexane and octane) were observed on the mixed zeolite sensors compared with their corresponding layered zeolite sensors. The higher concentration

gradient of hexanol compared with hexane indicates a higher rate of combustion of this gas within the sensing layer.

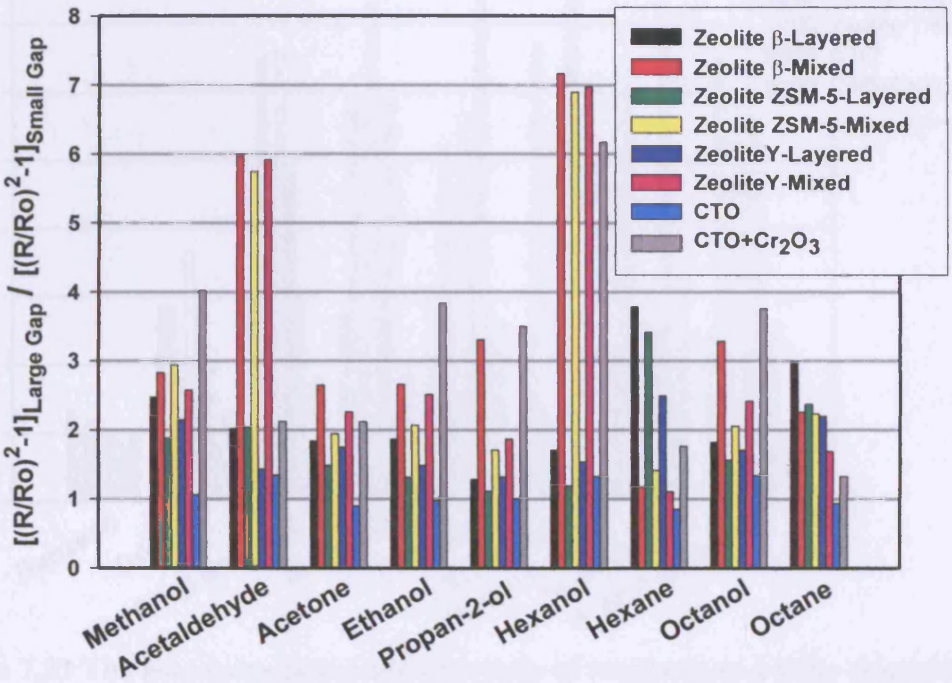

Figure 7.32 The concentration gradients (ratio of response on a wide electrode gap to that on a small electrode gap) of layered and mixed zeolite sensors (β, ZSM-5, Y), a standard CTO sensor and a chromium oxide modified CTO sensor to various volatile organic compounds
CTO: $Cr_{1.95}Ti_{0.05}O_3$ (0.5 µm) (UCL)
CTO-Cr_2O_3: $Cr_{1.95}Ti_{0.05}O_3$ (0.7 µm) (Capteur Sensors & Analyzers Ltd)

The concentration gradients of substituted aromatic hydrocarbons for all the zeolites sensors (mixed and layered), a standard CTO sensor and a chromium oxide modified CTO sensor, are shown in ***Figure 7.33***. The very low gradient observed for benzene along with the high gradients for the substituted benzenes allow a good discrimination to be achieved between them. In addition, the wide variation in the values of concentration gradients observed between the different aromatic compounds, show that discrimination can also be achieved between different hydrocarbons substitutions onto a benzene molecule using the tested gas sensors. It should be noted that higher concentration gradients were observed for all the mixed versus the layered and standard sensors according to ***Figure 7.33*** in the presence of a range of aromatic hydrocarbons with the exception of benzene, toluene and ethyl benzene.

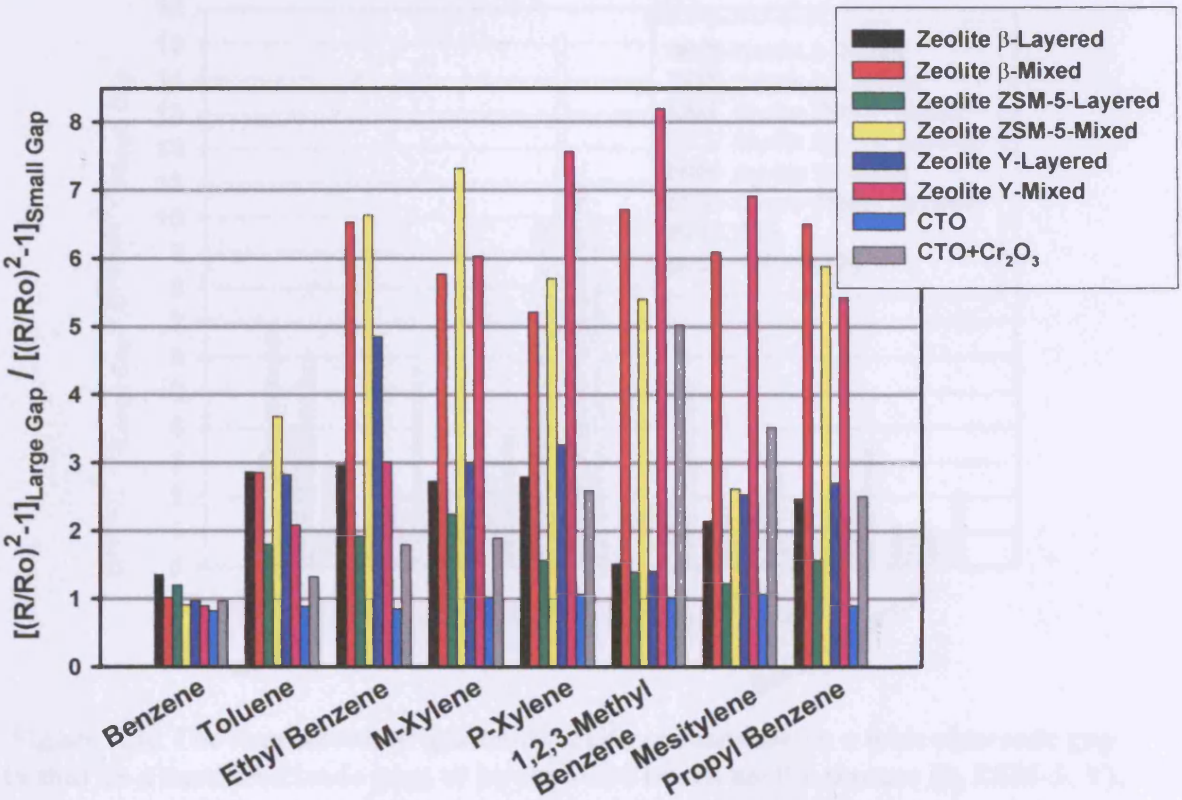

Figure 7.33 The concentration gradients (ratio of response on a wide electrode gap to that on a small electrode gap) of layered and mixed zeolite sensors (β, ZSM-5, Y), a standard CTO sensor and a chromium oxide modified CTO sensor to various aromatic compounds
CTO: $Cr_{1.95}Ti_{0.05}O_3$ (0.5 μm) (UCL)
CTO-Cr_2O_3: $Cr_{1.95}Ti_{0.05}O_3$ (0.7 μm) (Capteur Sensors & Analyzers Ltd)

Finally, ***Figure 7.34*** represents the response of the zeolite sensors (layered and mixed), a standard CTO sensor and a chromium oxide modified CTO sensor to the presence of different flavour and fragrance compounds. According to this figure, amyl acetate and cineole were shown to be well discriminated from each other and from the remaining flavours in terms of their reactivity within the sensor body.

Four PCA plots (***See Figure 7.35(a)-(d)***) are represented to demonstrate the discrimination ability (based on concentration gradient values) of the different multi-electrode zeolite sensor devices (layered, mixed, Cr-zeolite) to the present of a range of volatile organic, flavour and fragrance compounds. The results show a good discrimination resulting from differences in the reactivity of the different gases within the sensing layer of the tested sensors.

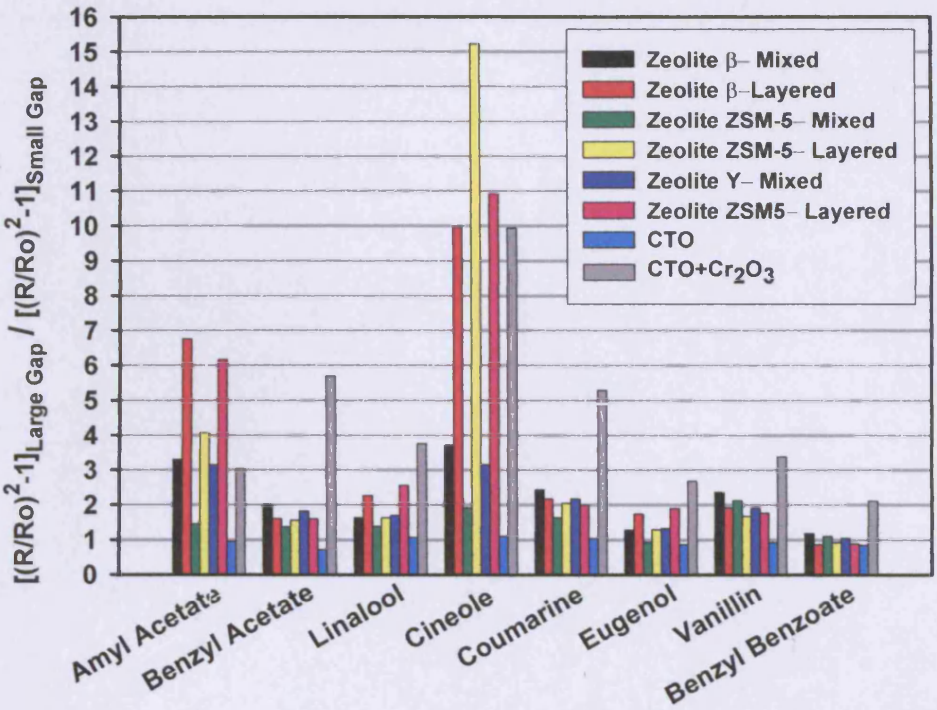

Figure 7.34 The concentration gradients (ratio of response on a wide electrode gap to that on a small electrode gap) of layered and mixed zeolite sensors (β, ZSM-5, Y), a standard CTO sensor and a chromium oxide modified CTO sensor to various flavour compounds
CTO: $Cr_{1.95}Ti_{0.05}O_3$ (0.5 µm) (UCL)
CTO-Cr_2O_3: $Cr_{1.95}Ti_{0.05}O_3$ (0.7 µm) (Capteur Sensors & Analyzers Ltd)

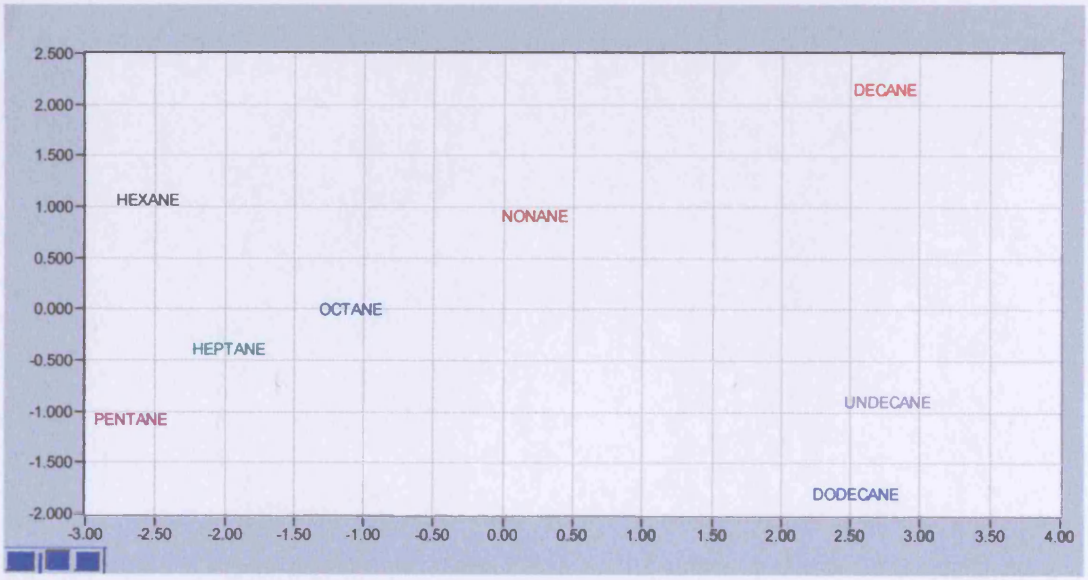

Figure 7.35(a) PCA plot of concentration gradients of multi-electrode layered and mixed zeolite sensors (β, ZSM-5, Y) responding to linear alkanes of varying carbon chain lengths following linearisation and normalisation

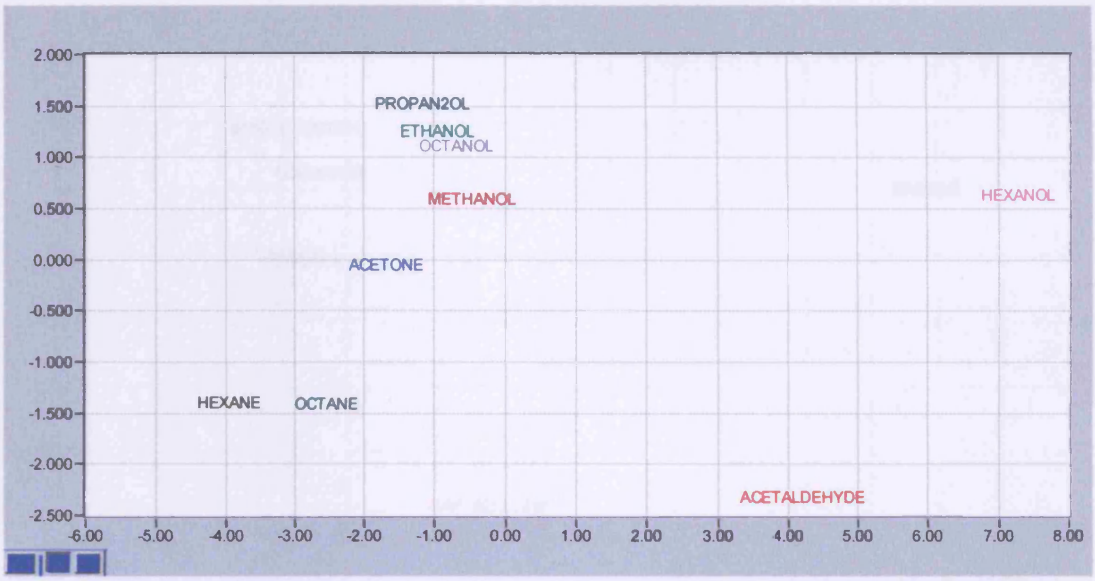

Figure 7.35(b) PCA plot of concentration gradients of multi-electrode layered and mixed zeolite sensors (β, ZSM-5, Y) to various volatile organic compounds following linearisation and normalisation

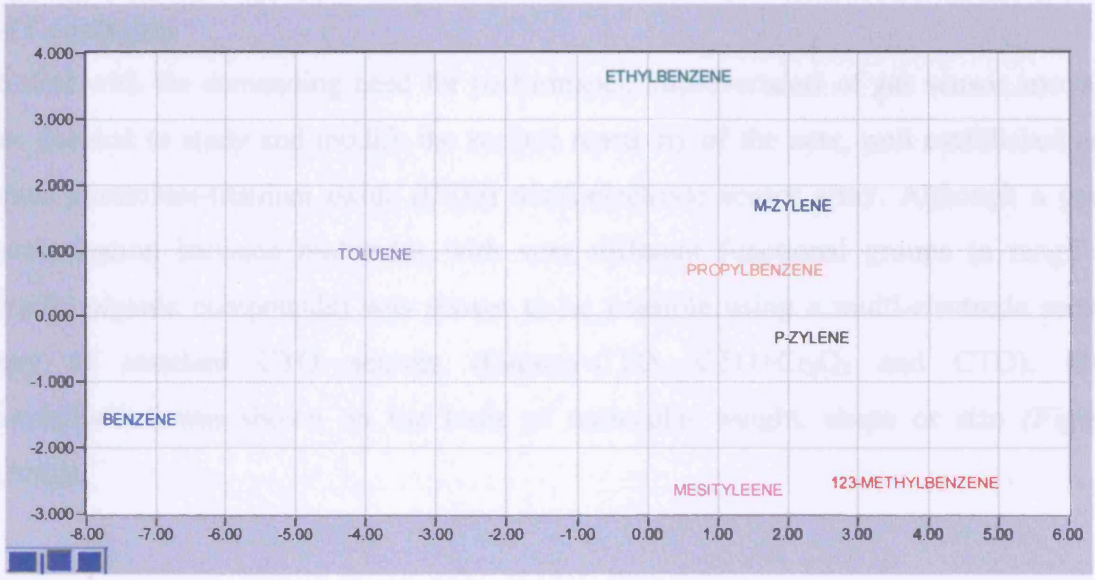

Figure 7.35(c) PCA plot of concentration gradients of multi-electrode layered and mixed zeolite sensors (β, ZSM-5, Y) to various aromatic compounds following linearisation and normalisation

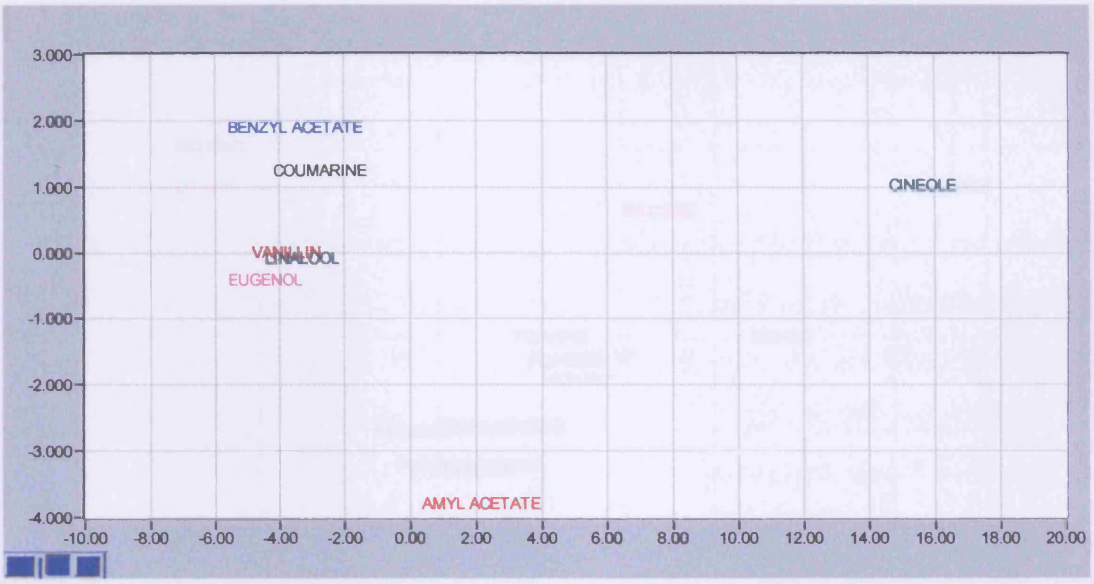

Figure 7.35(d) PCA plot of concentration gradients of multi-electrode layered and mixed zeolite sensors (β, ZSM-5, Y) to various flavour and fragrance compounds following linearisation and normalisation

7.4 Conclusion

To deal with the demanding need for performance improvements of gas sensor arrays it was decided to study and modify the surface reactivity of the new, well established and robust chromium-titanium oxide (CTO) multi-electrode sensor array. Although a good discrimination between molecules with very different functional groups (a range of volatile organic compounds) was shown to be possible using a multi-electrode sensor array of standard CTO sensors (Capteur-CTO, CTO+Cr_2O_3 and CTO), little discrimination was shown on the basis of molecular weight, shape or size ***(Figure 7.36(a))***.

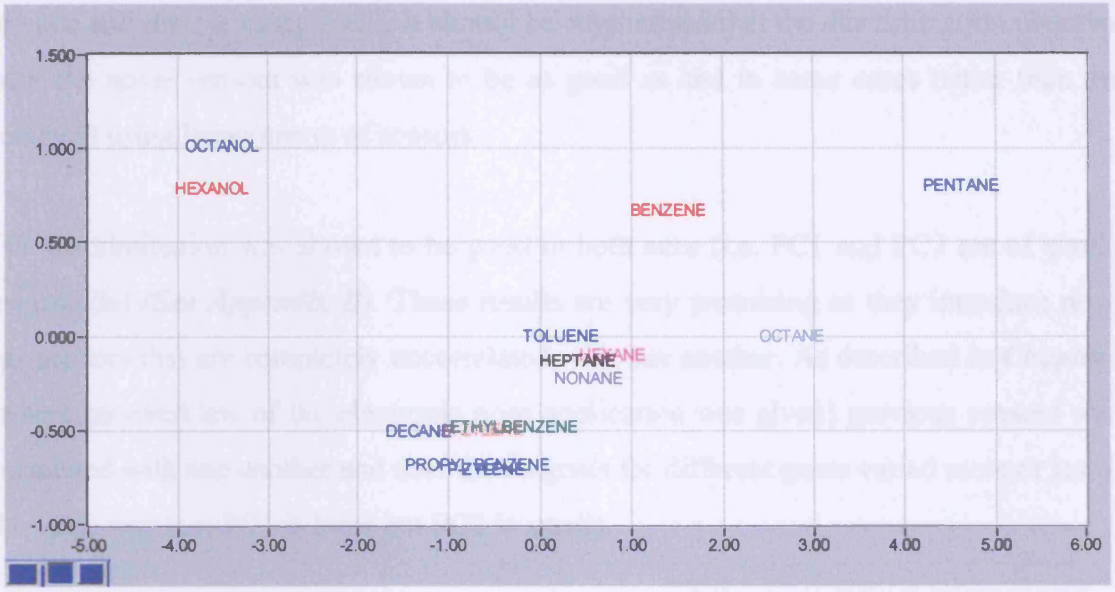

Figure 7.36(a) PCA plot for multi-electrode standard CTO sensors (Capteur-CTO, CTO+Cr_2O_3 and CTO) responding to a range of volatile organic compounds following linearisation and normalisation
Capteur-CTO: $Cr_{1.95}Ti_{0.05}O_3$ (1 µm) (Capteur Sensors & Analyzers Ltd)
CTO: $Cr_{1.95}Ti_{0.05}O_3$ (0.5 µm) (UCL)
CTO-Cr_2O_3: $Cr_{1.95}Ti_{0.05}O_3$ (0.7 µm) (Capteur Sensors & Analyzers Ltd)

To increase the variance of response patterns of CTO multi-electrode sensors, multiple-electrode sensor devices were fabricated using the chromium titanium oxide as a suitable generic sensing material, with additional zeolite layers either printed over the top of the sensing layer or admixed with it. Additional zeolite sensors were produced with chromium catalysation to enhance the catalytic properties of the sensors.

The sensors were tested in a commercial electronic nose (Fox 2000) with a range of volatile organic, flavour and fragrance compounds. The results showed a clear improvement in the discrimination between compounds when compared to standard CTO sensors. In addition, shape and size selectivity was achieved even with the use of only two multi-electrode zeolite sensor devices ***(Figures 7.36(b)-7.36(c))***.

Increasing the number of sensors in the array was shown to further increase its discrimination ability ***(Figures 7.36(d) and 7.36(e))***. An overview of the above study clearly indicates that a careful selection of gas sensors (i.e. a standard CTO sensor and at least one zeolite sensor) provides different patterns of response and therefore delivers a multi-sensor array with a small number of sensors able to discriminate a range of volatile

organic and flavour compounds. It should be emphasised that the discrimination observed with the novel sensors was shown to be as good as and in some cases better than that achieved using larger arrays of sensors.

The discrimination was shown to be good in both axes (i.e. PC1 and PC2 are of similar magnitude) ***(See Appendix B)***. These results are very promising as they introduce novel gas sensors that are completely uncorrelated with one another. As described in ***Chapter 2*** (where an overview of the electronic nose application was given) previous sensors were correlated with one another and thus their signals for different gases varied more or less in the same way (i.e. PC1 is large but PC2 is small).

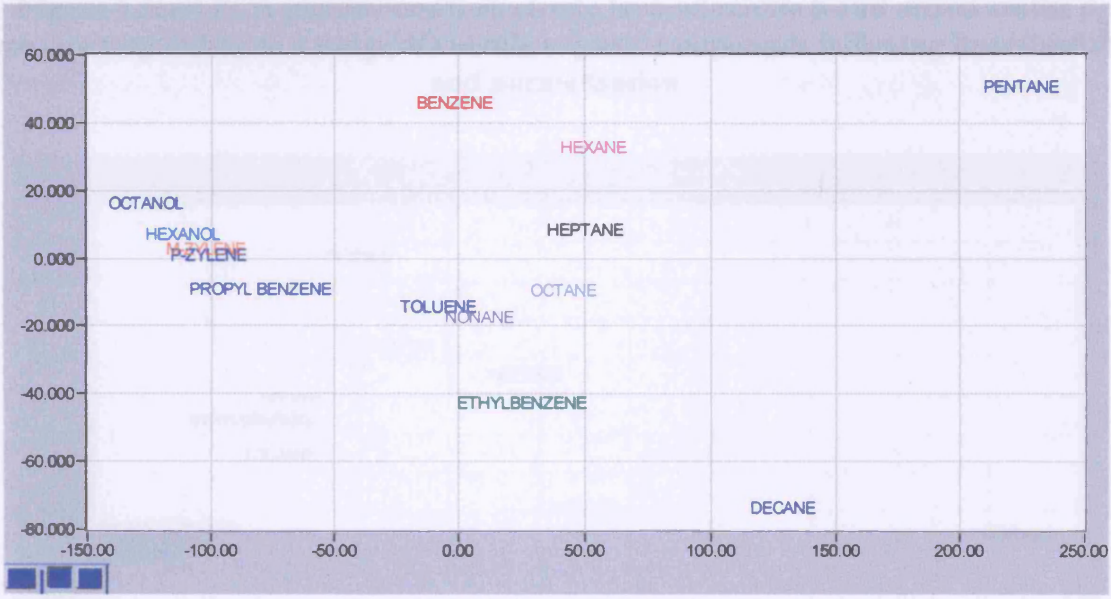

Figure 7.36(b) PCA plot for multi-electrode layered zeolite Y and mixed zeolite Y sensors responding to a range of volatile organic compounds following linearisation and normalisation

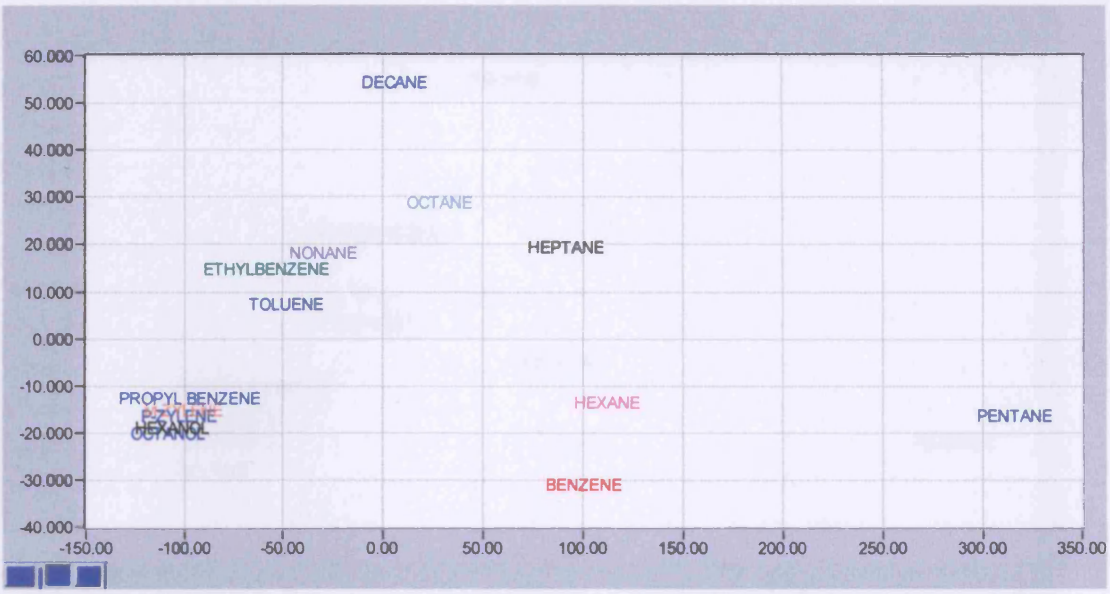

Figure 7.36(c) PCA plot for multi-electrode layered zeolite β and mixed zeolite β sensors responding to a range of volatile organic compounds following linearisation and normalisation

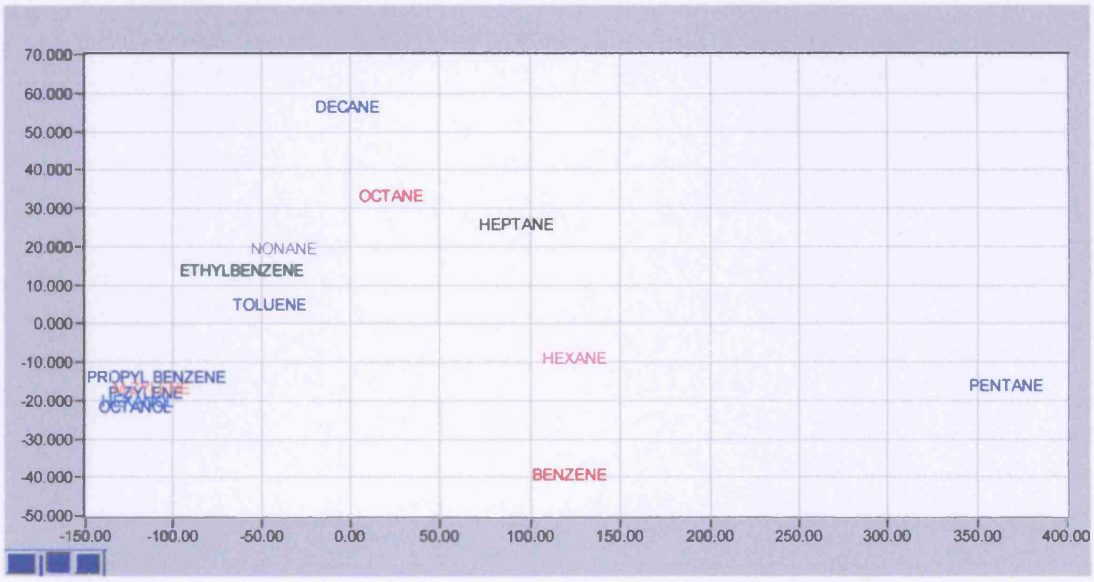

Figure 7.36(d) PCA plot for multi-electrode layered zeolite Y, mixed zeolite ZSM-5 and mixed β sensor responding to a range of volatile organic compounds following linearisation and normalisation

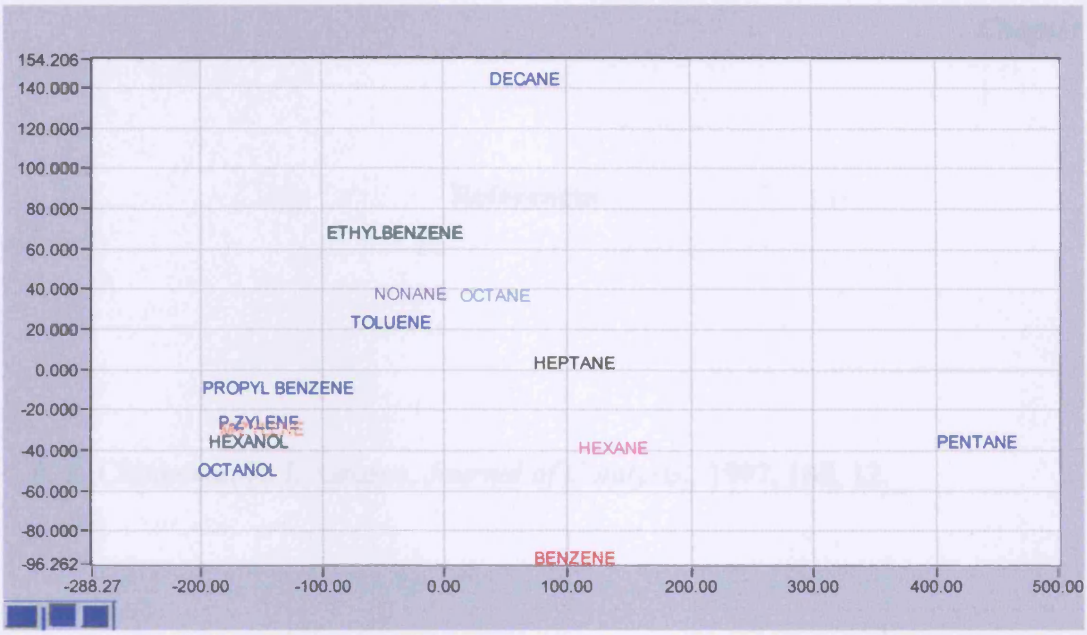

Figure 7.36(e) PCA plot for all multi-electrode layered and mixed zeolite sensors (β, ZSM-5, Y) responding to a range of volatile organic compounds following linearisation and normalisation

Chapter 7

References

1. P. S. Chintawar, H. L. Greene, *Journal of Catalysis.*, 1997, **165**, 12.

Chapter 8

Computational Study of Adsorption and Transport of Organic Species in Zeolites

8.1 Introduction

In recent years the application of molecular modelling techniques (computational simulations) for the study of the behaviour of organic molecules in zeolites has grown substantially. The stimulus for this growth stems from many sources; (a) the evolution of appropriate computational methods (b) the development of successful theoretical predictions (algorithms) (c) the importance of industrial zeolite applications and (d) the development of powerful computers which minimise the simulation time.

Computational simulations of the interactions of a range of volatile organic molecules with different zeolites were performed using a commercially available software *'Materials Studio'* by Accelrys.[1] The software is effectively a molecular mechanics modelling package, which allows structures of zeolites to be generated, and the strength of interactions between those and target molecules to be determined.

8.2. Aim of Computational Work

The aims of this computational work were to:

- Systematically assess the sieving of a range of volatile, flavour and fragrance compounds by different zeolite structures.
- Select promising zeolite catalyst materials for the construction of new sensors based on the results for selective interaction with target gases.
- Correlate the computational predictions with the experimental results as this could support the better understanding of the sensor response.

Below a more detailed description of the specific tasks of the computational work is given for a more clear understanding of the results analysis.

8.2.1 Specific Tasks of the Computational Work

More specifically, the tasks of the work were as follows:

- Assess which molecules can enter into the cavity of the different zeolite structures.
- Determine the binding energy and energy minimum positions in the zeolite cavity for molecules that can enter into the cavity.
- Investigate, whether there is a diffusion pathway for the compound through the specific zeolite structures, and if there is a barrier to diffusion through these structures.
- Determine whether there are differences in the diffusion process between the seven different host zeolites that were considered due to structural effects.
- Assess what cracking products may diffuse through the structure.

8.3. Description of Host Zeolite Structures

A range of zeolites were used for this study ranging from 8 to 12 member ring openings. These were specifically chosen, as it was believed that the molecules that were of interest to this project would show different behaviour in these zeolites. A description of the seven zeolite structures selected to perform the simulations is given below.

8.3.1 Zeolite ZSM-5

The 3-D structure of ZSM-5 is represented in ***Figures 8.1 and 8.2.*** ZSM-5 exhibits the MFI structure type. Rings of 10 oxygen atoms are evident from these figures; these are important because they provide openings in the structure, large enough for the passage of rather large molecules (e.g. big enough for 1,2-dimethyl benzene).

The 10 member ring channels in ZSM-5 provide access to a network of intersecting pores within the crystal. There are two pore systems in ZSM-5 as shown in ***Figures 8.3(a) and (b)***; a set of elliptical straight pores (5.3 Å x 5.6 Å) that are intersected by a set of perpendicular zig-zag pores, sinusoidal pores, (5.1 Å x 5.5 Å).

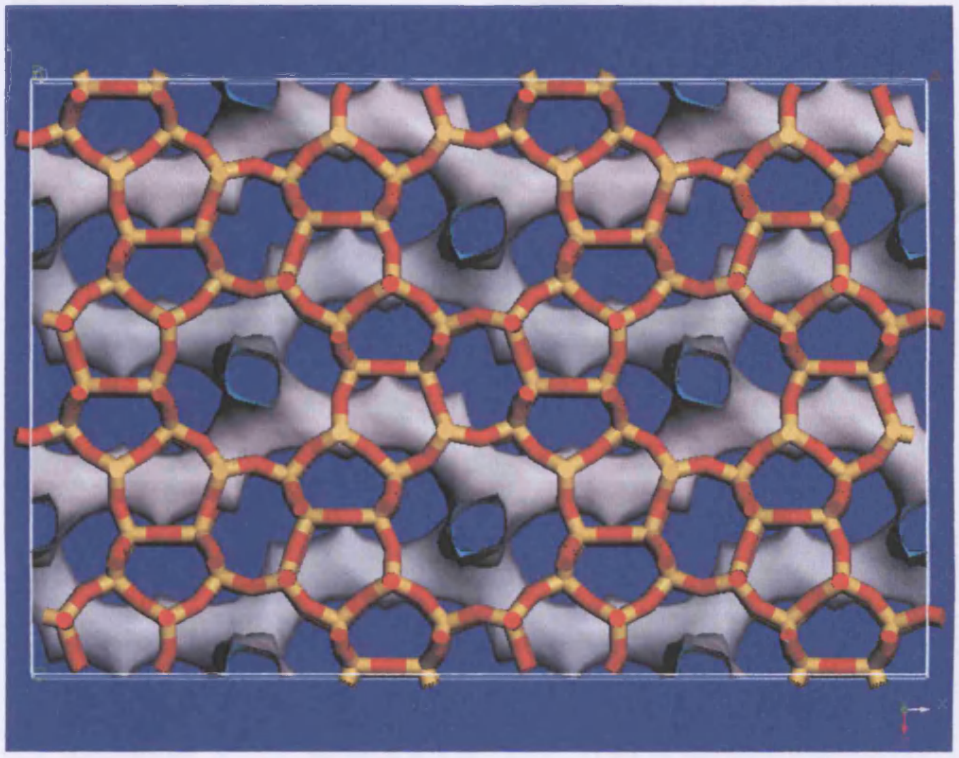

Figure 8.1 Straight 10 member ring channel of ZSM-5 framework viewed along [010]

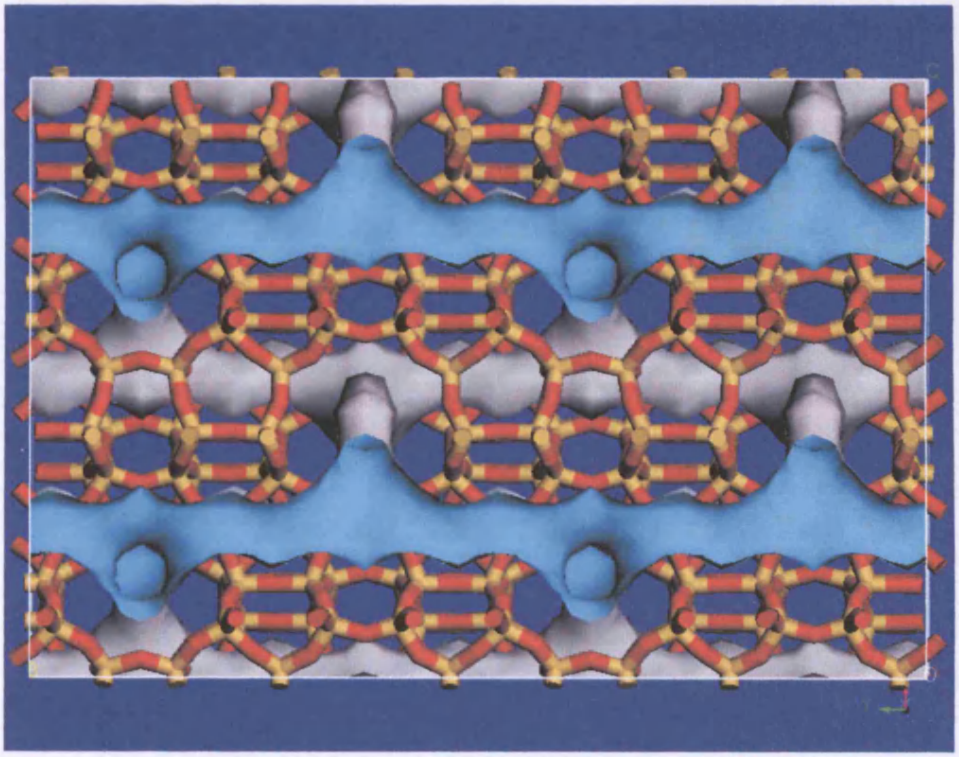

Figure 8.2 Sinusoidal 10 member ring channel of ZSM-5 framework viewed along [100]

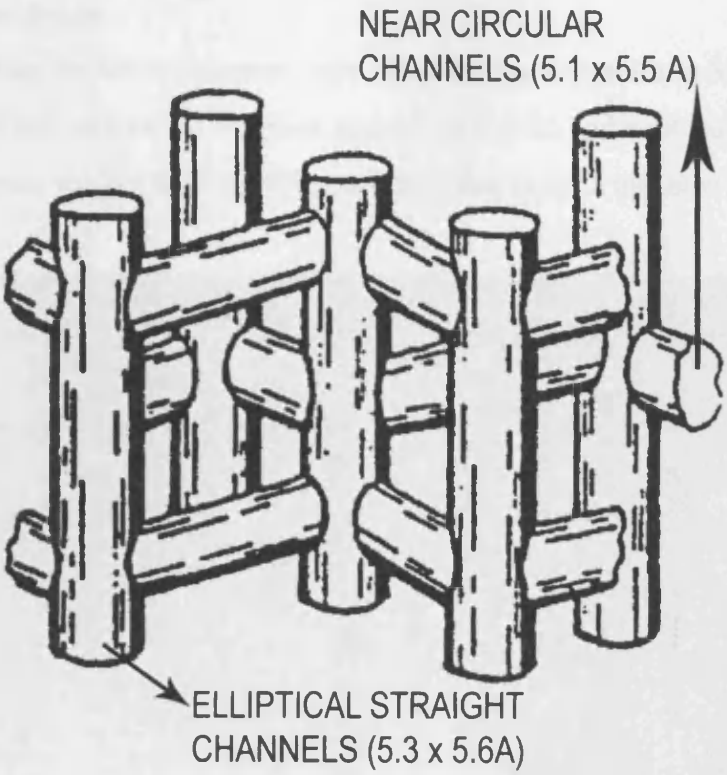

Figure 8.3 (a) Channel arrangements in ZSM-5

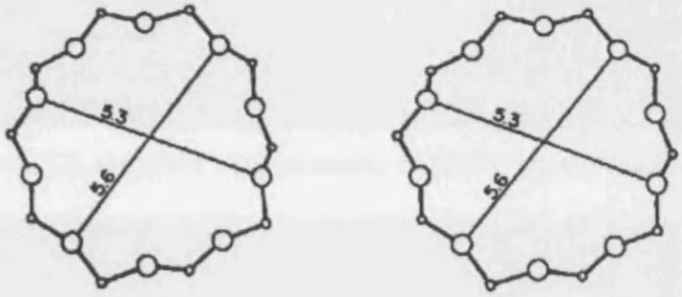

10-ring viewed along [010]
(straight channel)

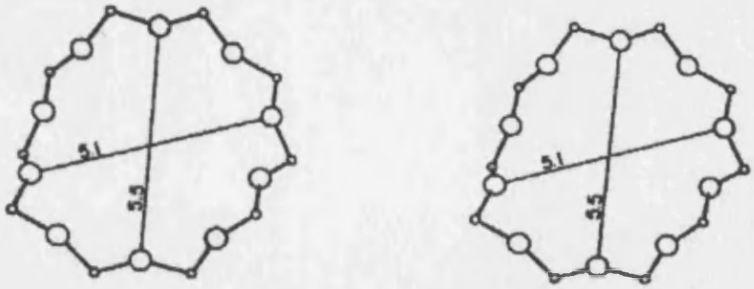

10-ring viewed along [100]
(sinusoidal channel)

Figure 8.3 (b) Dimensions of the two pore systems in ZSM-5

8.3.2 Zeolite Mordenite

Mordenite exhibits the MOR structure type. There are two channels in MOR as shown in ***Figures 8.4 and 8.5***; an oval 12 member ring (6.5 x 7.0 Å) and an 8 member ring (2.6 x 5.7 Å). The channel system here is effectively 1-D due to the small size of the 8 member ring.

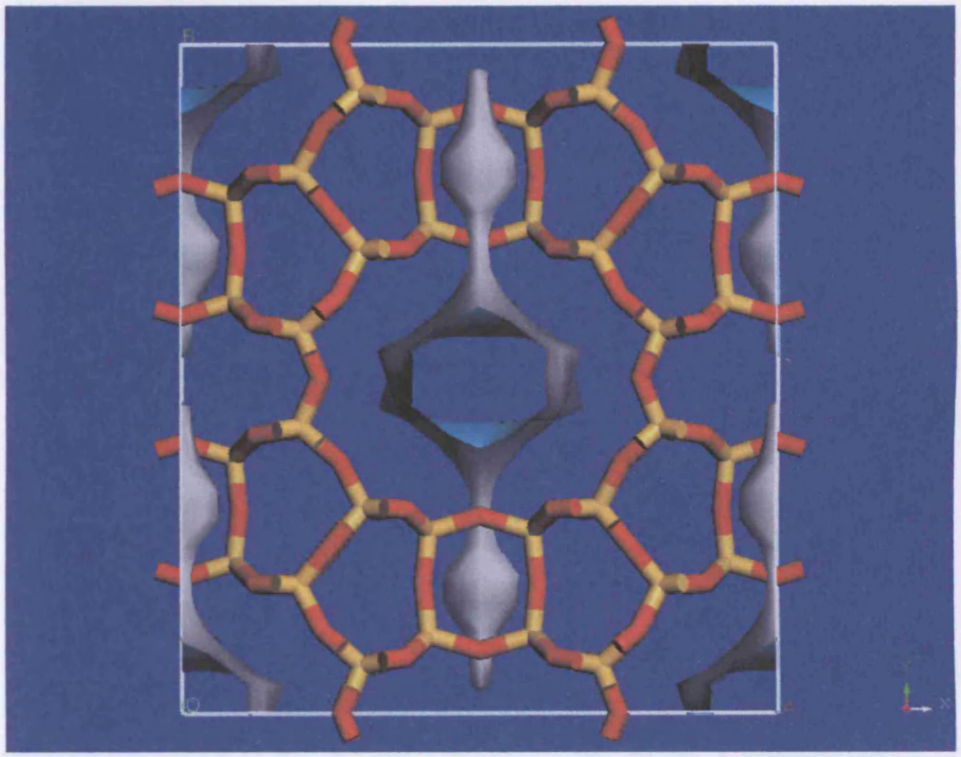

Figure 8.4 Twelve (12) member ring channel of MOR framework viewed along [001]

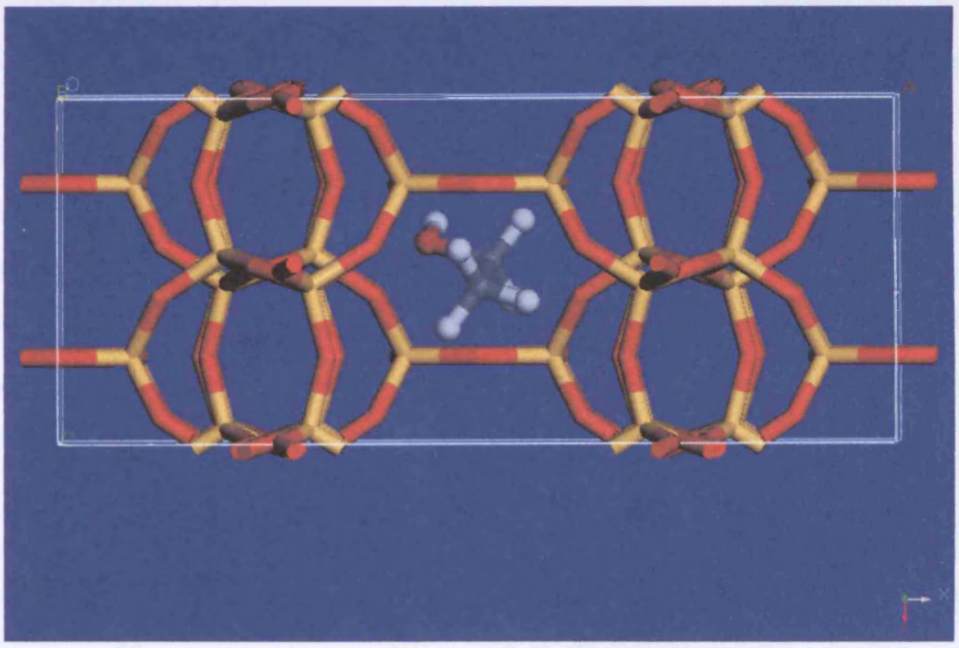

Figure 8.5 Complex 8 member ring channel of MOR framework viewed along [010], with ethanol molecule inside the pore

8.3.3 Zeolite Theta-1

Zeolite Theta-1 exhibits the TON structure type, which has the same basic structure as Mobil's ZSM-22. It consists of straight pores running in 1-D with 10 oxygen atoms around the circumference of the pore (known as a 10 member ring pore). Such a pore has a characteristic free aperture of about 5Å. The framework structure of TON is shown in ***Figure 8.6***.

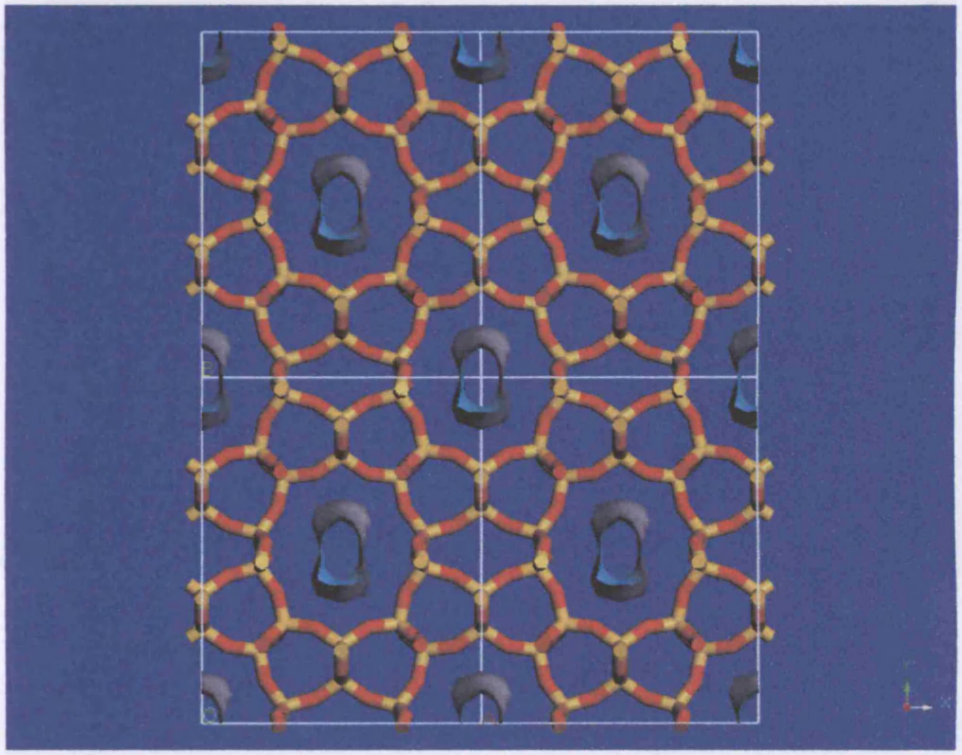

Figure 8.6 Ten (10) member ring channel of TON framework viewed along [001]

8.3.4 SSZ-24

The framework structure of SSZ-24 exhibits the AFI structure type and is the *siliceous* analogue of the well-known aluminophosphate $AlPO_5$, which is shown in ***Figure 8.7***. It consists of hexagonal arrangement of 12 member ring channels running in 1-D, with pore opening of 7.3Å. To simplify the simulations the *siliceous* form of the AFI structure (SSZ-24) was used.

8.3.5 Zeolite β

It must be noted that all zeolite β materials show extreme disorder. Zeolite β exhibits the BEA structure. The pore system in BEA is 3-D. It consists of 12 member rings in y direction with pore openings of 7.6 x 6.4Å ***(Figure 8.8)*** and two 12 member ring channels

in a direction perpendicular to y-direction with pores of 7.4 x 6.4Å and 5.5 x 5.5Å, respectively.

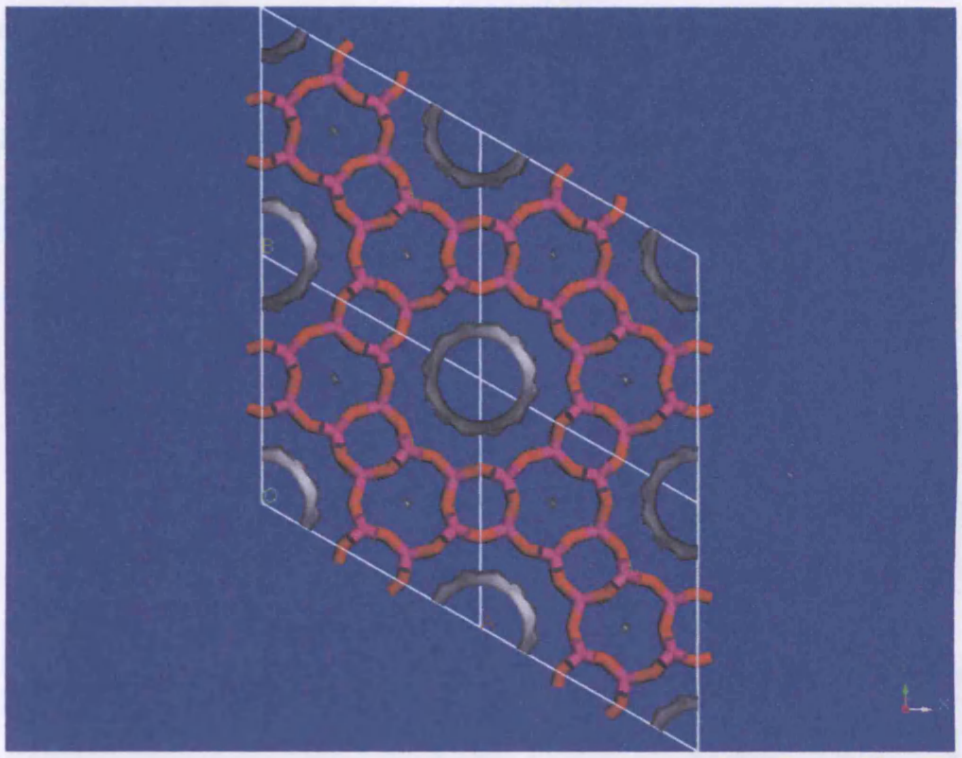

Figure 8.7 Twelve (12) member ring channel of AFI framework viewed along [001]

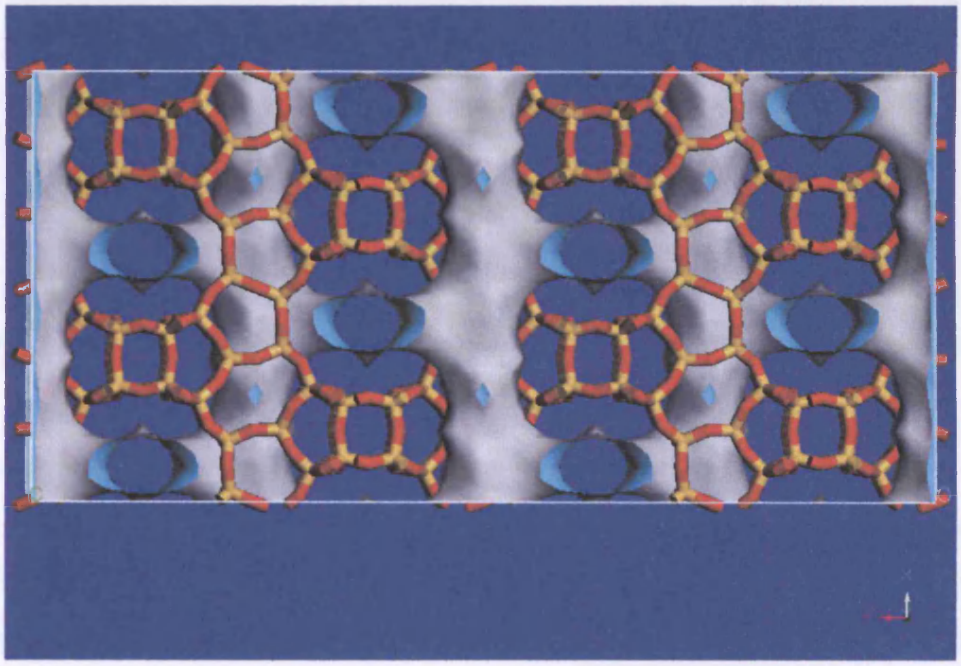

Figure 8.8 Twelve (12) member ring channel of BEA framework viewed along [010]

8.3.6 Zeolite Y

Zeolite Y exhibits the FAU (Faujasite) structure. It has a 3-D open channel system with pores running perpendicular to each other in the x, y, and z planes ***(Figure 8.9)***. The pore diameter is large at 7.4Å since the aperture is defined by a 12 member oxygen ring, and leads into a larger cavity of diameter 12Å. The cavity is surrounded by ten sodalite cages (truncated octahedral) connected on their hexagonal faces. To simplify the simulations the siliceous form of FAU structure was used in this computational work.

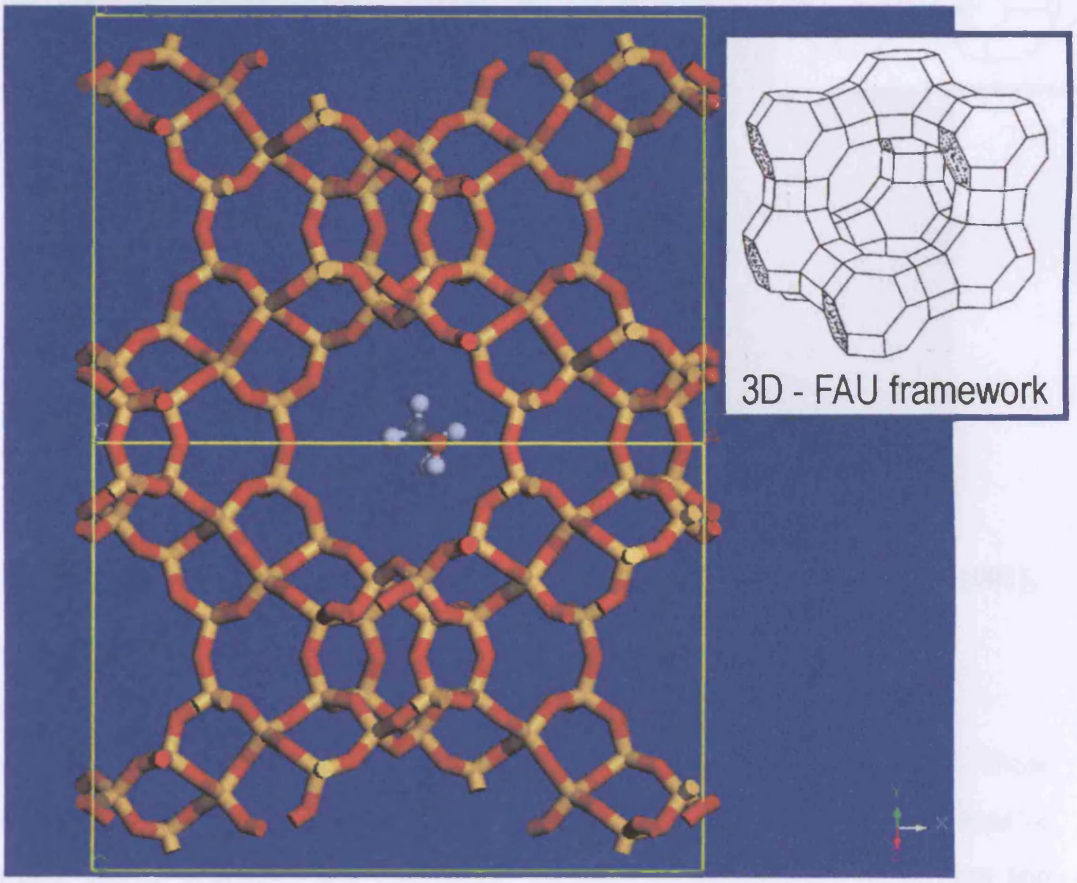

Figure 8.9 Twelve (12) member ring channel of FAU framework viewed along [111], with ethanol molecule inside the pore

8.3.7 Zeolite A

Zeolite A exhibits the LTA (Linde Type A) structure. It has a 3-D pore structure with pores running perpendicular to each other in the x, y, and z planes ***(Figure 8.10)***. The pore diameter is defined by an 8 member oxygen ring and is small at 4.1Å. This creates a larger cavity (an α-cage in the centre of the unit cell) of minimum free diameter 11.4Å. The cavity is surrounded by eight sodalite cages (truncated octahedral) connected by their

square faces in a cubic structure. To simplify the simulations the siliceous form of LTA structure was used in this computational work.

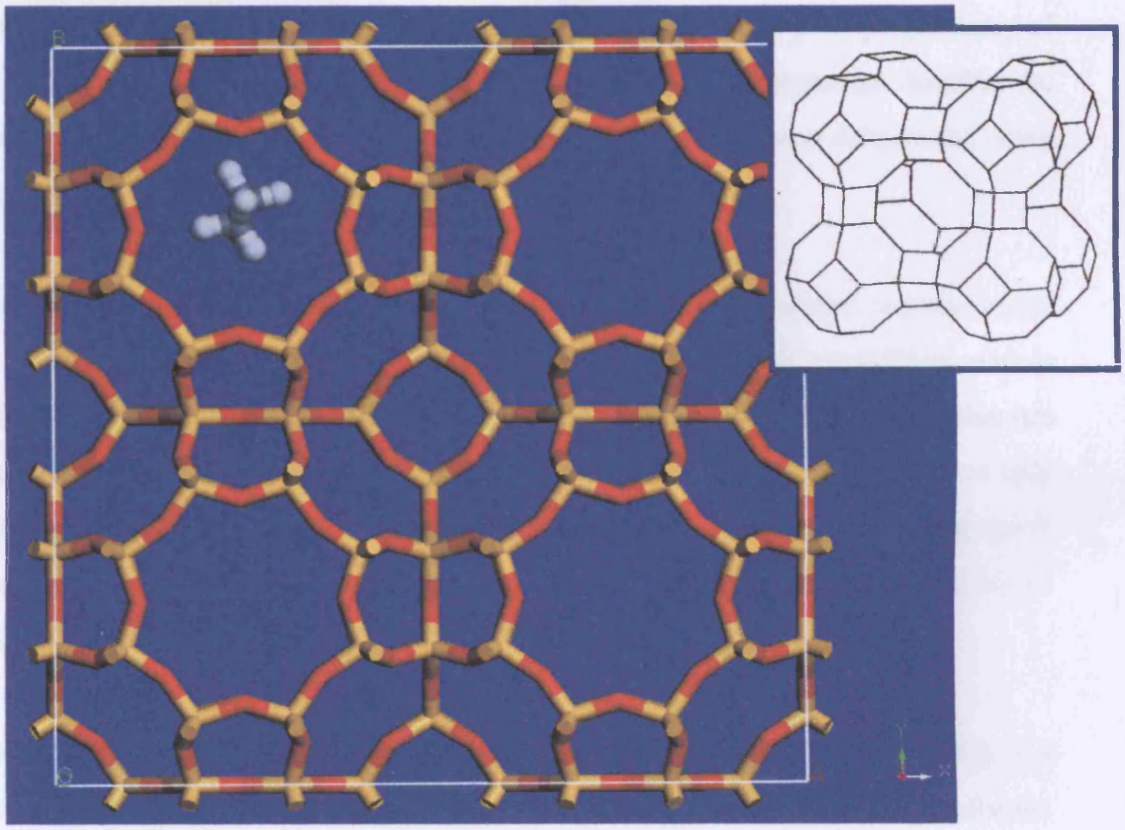

Figure 8.10 Eight (8) member ring channel of LTA framework viewed along [001], with ethanol molecule inside the pore

8.4 Introduction to Zeolite Theory and Computational Modelling

Various theoretical and computational approaches exist for the study of zeolites. These include methods to compute zeolite structure and stability, computer graphics to visualise the complex zeolite structures and calculation methods to simulate the adsorption and diffusion of small molecules in these materials[2].

The latest developments in the area of computational chemistry involve the use of novel algorithms, such as ab-initio Molecular Dynamics (MD) or novel Monte Carlo calculation techniques that allow the study of many more complicated problems in zeolite science. Molecular Dynamics is a simulation of the time-dependent behaviour of a molecular system, for example the diffusion of molecules within a zeolite structure[3,4]. This branch of chemistry offers an insight into the underlying molecular behaviour of a system as well as

probe the system under extreme conditions such as high pressure and temperature, which may not be obtained by any other method.

All Monte Carlo methods are based on a random sampling, which is simulated with a random-number-generating algorithm. The location, orientation, and perhaps geometry of a molecule or collection of molecules are chosen according to a statistical distribution. For example, the adsorption of long-chain alkanes in zeolites has been determined using configurational bias Monte Carlo methods[5].

The synthesis of many novel zeolites relies on the use of organic additives (templates). These 'template' molecules are occluded inside the zeolite as it crystallises and is subsequently removed via calcination. The aim of templating is to form a material that has specific structural features. Computer modelling techniques have been applied to not only advance our understanding of this phenomenon[6] but also to guide the synthesis of novel microporous and mesoporous materials through the use of computer-designed template molecules[7,8].

The computational work of this project was based on manual docking (or positioning) of a range of molecules in different zeolites using *'Materials Studio'* visualisation software. However, there have been applications[2] where the docking of template molecules in zeolites, to search for low energy adsorption sites for the molecules, has been automated. Lewis[6] and Boyett[9] used both manual and automatic approaches to locate template molecules. Their methods were shown to accurately produce structure and absorption trends in binding energies as well as being able to predict which template is most likely to form a given structure. Similarly, other works[10] verified that docking calculations can be used to identify low-energy configurations of templates within microporous structures.

Furthermore, adsorbates docking methods together with diffusion pathway simulations have been used to rationalise the high conversion of a mixture of butanes to iso-butene on DAF-1[11] and the diffusion of dimethyl benzenes in zeolites[12]. Molecular Dynamic methods were shown to be able to provide the detailed mechanism for the diffusion as well as a reaction highlight for the different diffusion properties of para and ortho xylenes in CIT-1[3].

Two calculation methods, quantum mechanics and force-field or inter-atomic potentials are employed to calculate the energy of the systems under study.[13] Whilst quantum mechanics is the more rigorous method it is restricted to small systems. Since zeolites can contain many hundreds of atoms, the force-field method was suggested to be a more appropriate technique to be used in this computational study.

8.5 Force-Field Methods

The force-field is a set of equations and parameters, which is used to describe the energy of the potential energy surface of the system under study as a function of its atomic coordinates. [14] In force-field methods the particles in the system are treated classically using the 'ball and spring' model whereby the atoms may be of different sizes and 'softness' and the bonds more or less 'stiff'. A force-field contains all the information required to conduct calculations on energy and force, including a list of atom types, a list of atomic charges, atom-typing rules, functional forms for each component of the energy expression and parameters for the functional terms. The force-field energy can be expressed as a sum of functional forms (a sum of valence or bond interactions, non-bond interactions and cross terms), each describing the energy required for distorting a molecule in a specific fashion:

$$E_{FF} = E_{str} + E_{bend} + E_{tors} + E_{vdw} + E_{el} + E_{cross} \qquad [8.1]$$

Where,

E_{FF} is the force-field energy

E_{str} is the energy function for stretching a bond between two atoms

E_{bend} represents the energy required for bending an angle

E_{tors} is the torsional energy for rotation around a bond

E_{vdw} is the Van der Waals energy describing the repulsion or attraction between atoms that are not directly bonded

E_{el} is the electrostatic energy between non-bonded atoms. The electrostatic term most often used is the Coulombs law term for the energy of attraction or repulsion between charged centres.

E_{cross} describes coupling between the first three bonded terms. Modern force-fields generally achieve higher accuracy by including cross terms to account for such factors as bond or angle distortions caused by nearby atoms. Cross terms can include the following: stretch-stretch, stretch-bend-stretch, bend-bend, torsion-stretch, torsion-bend-bend, bend-torsion-bend, and stretch-torsion-stretch.

Table 8.1 gives the mathematical representation of some common force-field terms: [15]

Table 8.1 Mathematical representation of force-fields terms

Description	Energy Term
Bond Stretch	$k\,(l-l_0)^2$
Angle Bend	$k\,(\theta-\theta_0)^2$
Torsion	$k\,[(1+\cos(\gamma\theta)]$
Van der Waals	$4k\,[(A/r)^{12}-(B/r)^{6}]$
Electrostatic	$(q_1q_2)\,/\,(4\pi\varepsilon_0 r)$

Where: l is the bond length, θ is the bond angle, k, A, B are constants particular to the elements in a certain hybridization state, γ is an integer, r is the non bonded distance and q is the charge of an atom.

8.5.1 Assigning Force-Field Types to a Structure

Force-field types need to be assigned to all atoms in a structure before any energy related calculation can take place. The force-field type assigned depends on the type and properties of the atom, such as its hybridization state and its micro chemical environment (for example, the number and nature of connected atoms).

Modern software usually have a graphical interface that allows the molecule simply to be drawn on the screen. The interface then automatically assigns suitable atom types based on the selected atomic symbols and the connectivity, and converts the drawing to Cartesian coordinates.

8.6 Simulation Methodology

Minimization of the potential energy, computed by a suitable energy function with respect to appropriately chosen variables, provides a means of optimizing zeolite structural models. Such procedures, which yield energy minimum (effectively zero Kelvin (0K)), have been successfully applied to zeolite framework structures, extra-framework cation positions, and modelling sorbate locations. Energy minimizations, based on efficient numerical procedures provide information on low energy sorption sites rather that probing the thermodynamic ensemble of states accessed under thermal conditions. However, minimization can probe favourable binding locations for guest molecules in systems whose size complicates more detailed calculations. The quality of all computational simulations is determined by the quality of the potential energy function employed.

8.6.1 Minimization Methods

Discover[16] is the *Materials Studio* 'simulation engine' (software used in the present computational work). The Discover minimization dialog allows the user to optimise a molecular structure with respect to the potential energy of the system being examined, such that its energy is at a minimum. Minimization is an iterative procedure in which the coordinates of the atoms and possibly the cell parameters, are adjusted so that the total energy of the structure is reduced to a minimum (on the potential energy surface). An energy minimization is needed due to the fact that there may be strains on the system as a result of inaccurate representation of the geometry. These strains could potentially affect the results of the molecular dynamics by producing unusually large forces for some of the atoms. Minimization results in a structural model, which closely resembles the experimentally observed structure. At the end of the minimisation process the conformation obtained is the one that is likely to be assumed at zero Kelvin (0 K).

The interactions between the atoms are represented by potentials. The potential energy (PE) of a system is used as a measure of the system's stability; the lower the PE the more stable the system will be. Therefore by monitoring the potential energy of the system it is possible to predict whether the system under inspection is a feasible structure.

8.6.2 Minimization Methods

The minimisation of a molecular structure can be regarded in mathematical terms as an optimization in a multi-dimensional space (the exact number of dimensions depending on the number of atoms and the periodicity of the system). There are several different minimization methods available in *Discover (Materials Studio)*. By default, the '*Smart Minimization*' option is used. This automatically combines appropriate features of the other available methods in a cascade. As every simulation package, *Materials Studio* offers a range of algorithms to carry out the minimization. The *Smart Minimizer* starts with the *Steepest Descent* method, followed by the *Conjugate Gradient* and ends with a *Newton-Raphson* method.

Below a brief description of the calculation methods of the *Smart Minimizer* is given.

8.6.2.1 Steepest Descent

Steepest Descent has the highest convergence capability, no matter what the function is or from where it begins. It will quickly reduce the energy of the structure during the first few iterations. However, convergence will slow down considerably as the gradient approaches zero. It should be used when the gradients are very large and the configurations are far from the minimum (typically for poorly refined crystallographic data, or for graphically built molecules).

8.6.2.2 Conjugate Gradient

This method improves the line search direction by storing information from the previous iteration. *Conjugate Gradient* is the method of choice for systems that are too large for storing and manipulating a second-derivative matrix. The time per iteration is longer than for *Steepest Descent*, but this is more than compensated for by efficient convergence. There is choice between two algorithms; *Fletcher-Reeves* and *Polak-Ribiere*. The two algorithms differ on the way that they represent the next new direction vector for the iteration process.

8.6.2.3 Newton-Raphson Method

Newton-Raphson method requires computation and storage of first and second derivatives and therefore is expensive in terms of computer resources. The *Newton-Raphson* method

is only recommended for systems with a maximum of 200 atoms. It has a small convergence radius but it is very efficient near the energy minimum.

8.6.3 The Steps Involved in Running a Discover Minimization Calculation with Materials Studio

1. The 3-D structure of the molecule to be tested was built using the available drawing tools.
2. The Zeolite host structure was imported from a database of crystallographic data supplied with *Materials Studio*.
3. The zeolite structure was modified as follows:
    - The zeolite structure was converted into a crystalline superstructure with P1 symmetry. This was done to avoid interaction between molecules in the next unit cell.
    - Each molecule interacts only with those molecules within a distance of half the cell size. Therefore, if the zeolite structure to be tested had channel dimensions smaller or in the range of a molecule (to avoid interaction between molecules within consecutive cells) the host zeolite structure was converted to a supercell along the necessary channels. ***Table 8.2*** below summarises the seven host zeolite structures with their supercells range and crystallographic dimensions. Thus, each molecule inserted into the zeolite, can be considered as interacting with the zeolite alone.
    - ***Table 8.2*** presents the zeolite structures and their supercell dimensions. In the case of AFI, LTA and FAU zeolites the structure was corrected so that to have an *all-silica* zeolite system. This was done in order to make these zeolites simpler to study.
    - The framework unit cell of the zeolite was fixed (atom; fix Cartesian position and lattice; fix lengths and angles) thus allowing only the guest molecule atoms to move. This decreases the computational expense of the calculations, since the interactions between fixed atoms are constant and can be ignored. Therefore, only interactions between moving and fixed atoms are calculated.
4. The guest molecule was energy minimized to obtain the most stable conformation.

5. The guest molecule was then placed at the centre of a zeolite channel and energy minimized.
6. Results were saved and then plotted accordingly for further analysis
7. Calculations were also performed with different conformations.

Table 8.2 Summary of the seven host zeolite structures

Zeolite Structure	Supercells Range	Crystallographic dimensions/ Å
MFI	(2, 2, 2)	(40, 39.8, 26.8)
MOR	(1, 2, 4)	(18.1, 41, 30.1)
TON	(1, 1, 7)	(13.9, 17.4, 35.3)
AFI	(2, 2, 4)	(27.5, 27.5, 33.9)
BEA	(2, 2, 1)	(25.3, 25.3, 26.4)
FAU	(1, 1, 1)	(25, 25, 25)
LTA	(1, 1, 1)	(24.6, 24.6, 24.6)

8.7 Binding Energy Calculation

After the minimization of different guest molecules in different zeolite host structures, a single point energy calculation was performed using the *Compass* force-field (Condesed-phase Optimised Molecular Potentials for Atomistic Simulation Studies).[17]

- The more stable minimized structure, from the above analysis, was used for the energy calculation. It must be noted that the constraints that were applied in the framework unit cell before the minimization, were removed before the energy calculation.
- The energy of the guest molecule at gas phase, the energy of the zeolite host and the energy of the zeolite with the guest molecule in its channel were calculated.
- Then, the binding energy of the guest molecule in the zeolite was calculated using the following equation **[8.2]**. This energy corresponds to the adsorption energy, (ΔH_{ads}), of a molecule in a specific zeolite structure.

$$-E_{BIND} = E\,(M\text{-}Z) - [E\,(Z) + E\,(M)] \qquad \textbf{[8.2]}$$

Where:

E_{BIND} Binding energy of guest molecule (KJ/mol)

E (M-Z) Energy of the guest molecule in zeolite

E (Z) Energy of zeolite

E (M) Energy of guest molecule in the gas phase

8.8 Adsorption and Diffusion in Zeolites

Heats of adsorption and diffusion rates are properties that depend strongly on zeolite structure. The void spaces in the crystalline structures of zeolites provide high capacity for adsorbates, referred to as 'guest' molecules. The sorption capacity is a conveniently measured property that is used to identify the zeolites. Adsorption in the pores cannot take place unless the guest molecules are small enough to fit through the apertures.

Given that catalysis takes place largely within zeolite frameworks, access to this environment is patently controlled by the oxygen windows. This is a diffusion-limited process showing that zeolites have very special advantages over the more traditional catalysts since they will admit only certain reactant molecules and this can be potentially tailored to produce selected products. This selectivity is known as shape selective catalysis and is controlled by configurational diffusion. Different sizes of channels and cages may therefore promote the diffusion of different reactants, products or transition-state species. Transport may be roughly described as the hopping of molecules from site to site over significant energy barriers.

In general, sorption characteristics depend upon the size of the pore openings and the void volume. Catalytic behaviour depends upon the pore openings, the dimensionality of the channel system, the cation sites, and the space available for reaction intermediates.

Various studies suggest that if a molecule is inserted in a zeolite whose diameter is larger than its pore, the diffusion is expected to decrease (and even drop down to zero) since it will be more difficult for this bigger molecule to go through the pore. Moreover, Yashonath and co-workers[18] also discovered that if the molecules are small compared to the window diameter the window is an energetic barrier. However, for molecules that have approximately the same diameter as the window, this energy barrier disappears and hence the diffusion is larger than one would expect. Considering further the effect of the window size on diffusion, the research group concluded that the larger the adsorbate the slower its diffusion through the window. However, when the size of the adsorbate and the window are comparable then the rate of diffusion is increased.[19] This effect is probably due to the particle gaining more favourable interactions with the atoms in the window due to their close proximity, the so called 'levitation' effect.

8.9 Binding Energy Calculations

8.9.1 Linear Alkanes

The adsorption and diffusion behaviour of straight chain alkanes, ranging from one to twelve carbon atoms (C1 to C12), in the seven host zeolite structures (listed in ***Section 8.3***) were computationally studied using the *Materials Studio* simulation code.

Each alkane was placed in a host zeolite structure where it was energy minimized and its binding energy was calculated. ***Figure 8.11*** gives an overview of the variation of binding energy of n-alkanes in the seven zeolites against the number of carbon atoms, which were presented in their alkane chain. The binding energy is defined so that higher values indicate stronger binding of the molecule within the structure. According to ***Figure 8.11*** it can be seen that the binding energy of n-alkanes in all the different zeolite host structures becomes steadily more favourable with increasing carbon length. This is simply due to steady increase in the zeolite/molecule interaction with increasing chain length. In other words each additional CH_2 group interacts favourably with the framework hence increases the binding energy.

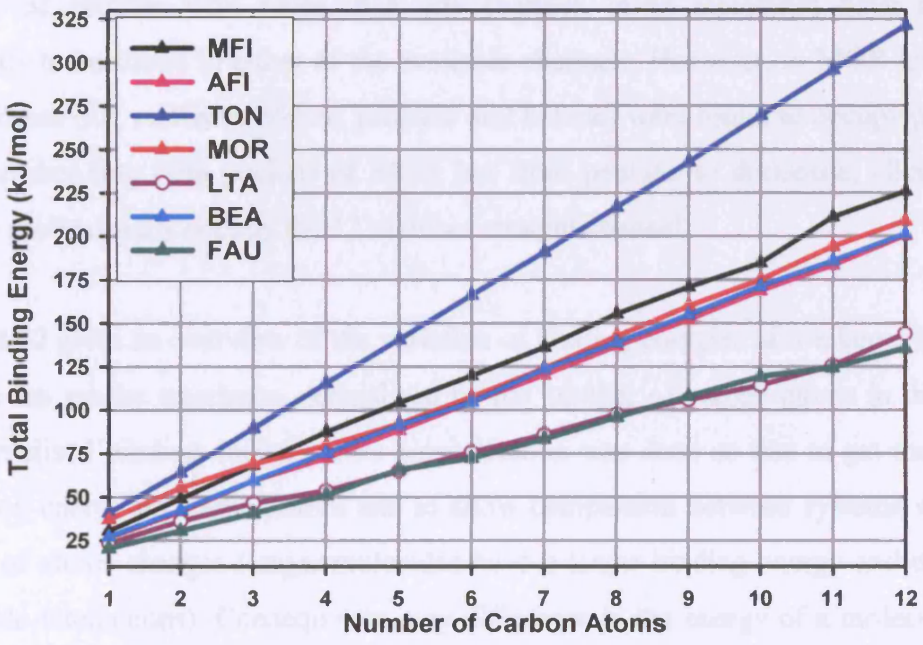

Figure 8.11 Binding energies for straight chain alkanes (C1 to C12 carbon atoms)

However, the value of binding energy for each molecule is different for different zeolite structural types. This implies that different hydrocarbons interact with their zeolite hosts

in different ways. This is because the sorption characteristics of zelolites depend upon the size of their pore openings and the void volume.

Stronger adsorption was observed on TON zeolite followed by MFI, AFI, MOR and BEA zeolites, which have very similar adsorption energies. Finally, all n-alkanes were found to be less strongly adsorbed on FAU and LTA, which again have very similar adsorption energies.

This trend can be directly correlated to their structure characteristics. For example, TON structure is 1-D with pore opening of 5Å, resulting in a tight fit of the tested molecules in its pore. Also, LTA and FAU have big curved inter walls so molecules are not so tight in the pore. All the other zeolites tested have bigger pores and thus molecules are relatively loose in them.

In the case of 3-D zeolite frameworks, where more than one zeolite channel is available for a guest molecule, simulations of the interactions of zeolite/molecule were performed in all different zeolite channels. Very similar values of energy were observed for all the different channels of each zeolite with the exception of MOR zeolite. This suggests that in the case of zeolites with more than one channel, guest molecules have the same probability to be found in either of the available channels. However, in MOR low carbon chain alkanes (i.e. methane, ethane, propane and butane) were found to occupy preferably the 8 member ring (site pocket) of MOR but from pentane to dodecane, alkanes were found to preferentially occupy the 12 member straight channel.

Figure 8.12 gives an overview of the variation of binding energies of n-alkanes (C1-C12) in the seven zeolite structures, normalised by the number of carbon atoms in their chain (i.e. normalised binding energy). This normalisation was done so that to get the average interaction energy per carbon atom and to allow comparison between systems where the number of atoms changes (larger molecules have a larger binding energy and thus more favourable interactions). Consequently, any difference in the energy of a molecule in the different zeolites, would suggest differences in the zeolite frameworks.

A decrease in the average interaction energy of n-alkanes from methane up to pentane was observed for all zeolites (***See Figure 8.12***). After that, the energy of the remaining alkanes (C6 to C12) was found to be very similar in magnitude for a given zeolite. Based on these

results, it was proved that discrimination is possible between low carbon chain alkanes (i.e. C1 to C4) and high carbon chain alkanes (i.e. C5 to C12) using any of the seven zeolites.

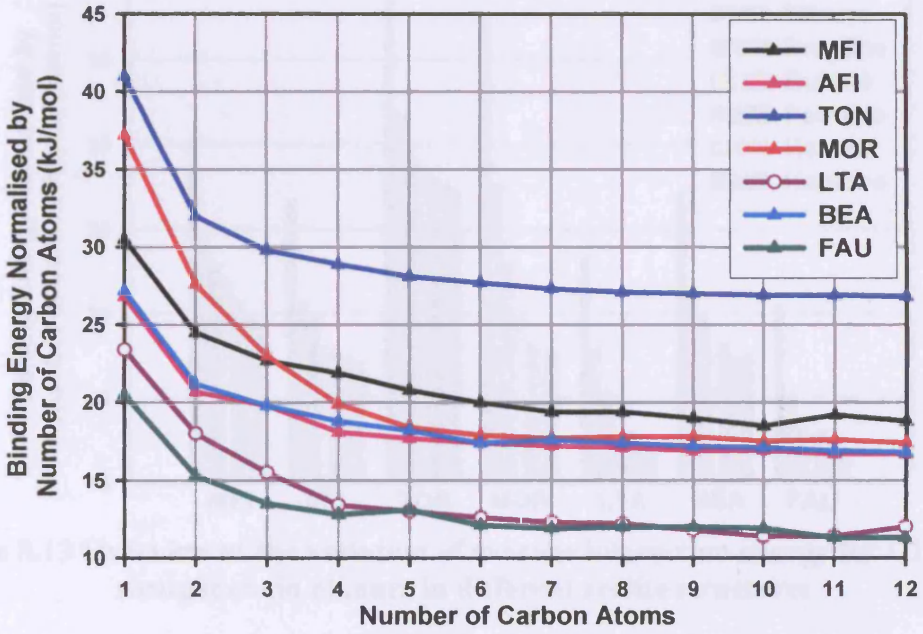

Figure 8.12 Average interaction energy for straight chain alkanes

As observed above, the adsorption capacity of the seven tested zeolites can be divided into three groups according to the magnitude of their binding energy. The first group is TON where all alkanes are more strongly bound to it, followed by MFI, MOR, AFI and BEA and finally, the third group that consists of LTA and FAU. Although the pattern of interaction observed was the same for all zeolite structural types, the three well separated groups (in terms of binding energy values), suggest that discrimination between the tested alkanes is possible and is due to the different zeolite structural types (having different adsorption and diffusion capabilities).

The bar chart shown in ***Figure 8.13*** represents the variation of the average interaction energy for C1 to C6 n-alkanes in all seven zeolites. In all cases, methane is more strongly bound to all zeolite structures compared to the remaining C2 to C6 alkanes.

MOR is probably the best zeolite to be used for discriminating between low (i.e. C1 to C4) and high carbon chain alkanes (C5 to C12). This is because as the molecule size increases the occupation of the 12 member ring channel over the 8 member ring side

pocket is dominated. Such discrimination is based on both the rate of adsorption and diffusion of the molecule in the particular zeolite.

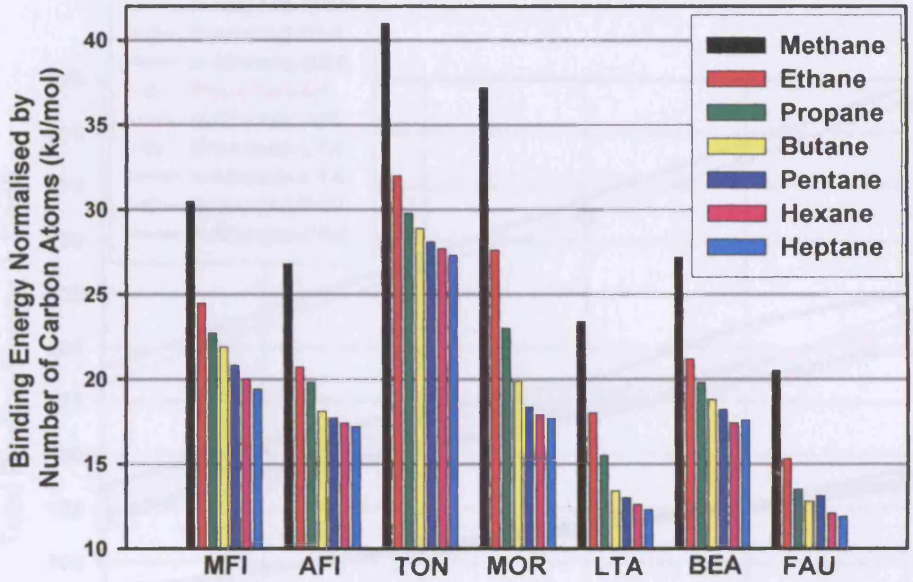

Figure 8.13 Overview of the variation of average interaction energy for C1 to C7 straight chain alkanes in different zeolite structures

8.9.2 Branched Compounds

8.9.2.1 Branched Alkanes

Figure 8.14 gives an overview of the variation of the binding energy of 2-methyl-isobranced alkanes and n-alkanes against the number of carbon atoms. Very similar behaviour, i.e. the molecule/zeolite interaction becomes steadily more favourable with increasing carbon length, was observed for branched compounds as in the case of n-alkanes. However, the average interaction energy for branched alkanes is slightly smaller in magnitude compared to n-alkanes (according to ***Figure 8.12*** and ***Figure 8.15***). The higher normalised binding energy values (stronger bonding with the zeolites), observed for n-alkanes, suggest that they have more favourable interactions with the zeolite hosts compared to branched alkanes. Hence, it can be suggested once again that n- and branched alkanes can be discriminated using the tested zeolites. In more detail, in the case of LTA zeolite branched molecules do not even enter the pore. This is because the size of the molecules tested is bigger than the LTA pore dimensions.

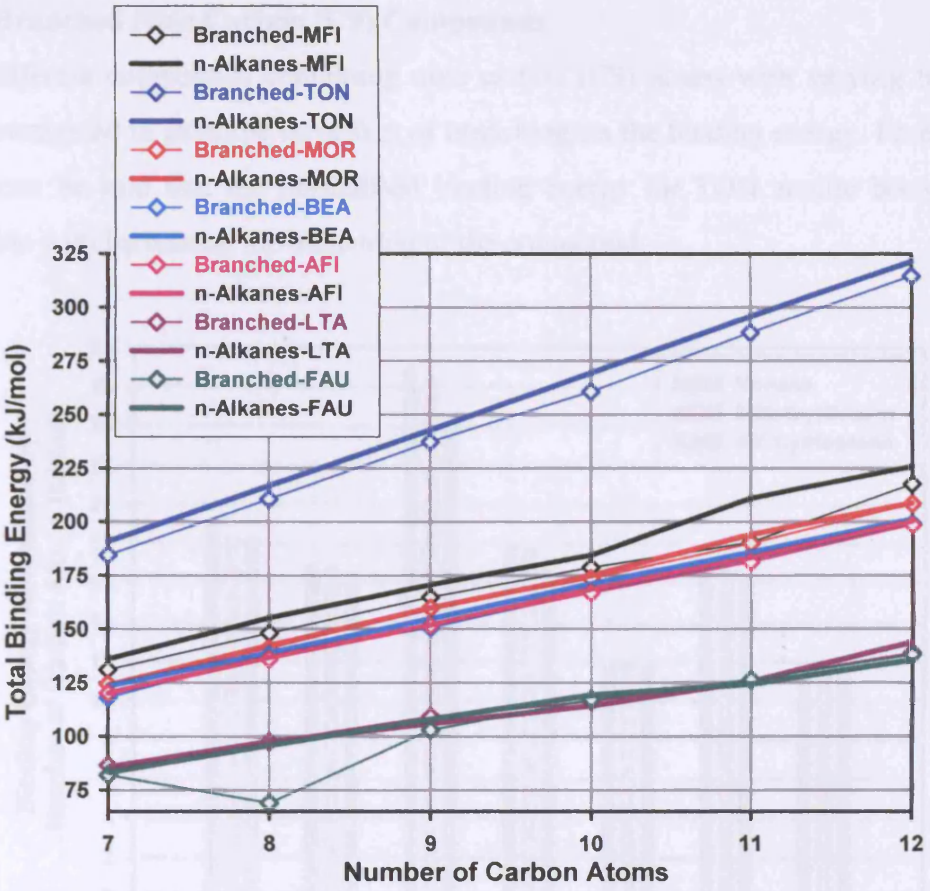

Figure 8.14 Comparison between binding energies for 2-Me-isobranched and n-alkanes

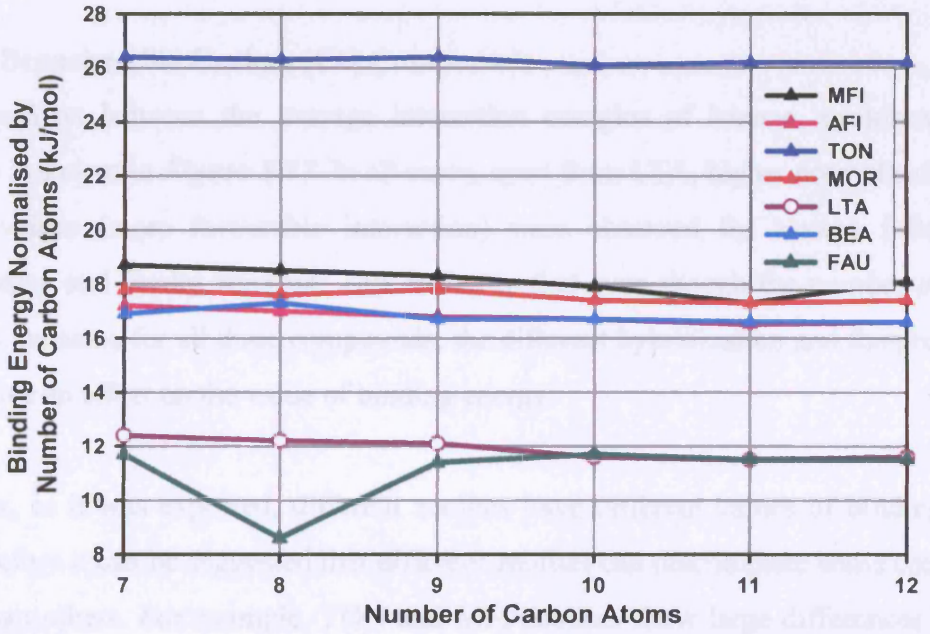

Figure 8.15 Average interaction energy for 2-Me-isobranched alkanes

8.9.2.2 Branched Nine Carbon (C9) Compounds

Three different compounds containing nine carbon (C9) atoms with varying branching were investigated to examine the effect of branching on the binding energy. From ***Figure 8.16*** it can be said that the normalised binding energy for TON zeolite becomes less favourable with increasing the branching of the compound.

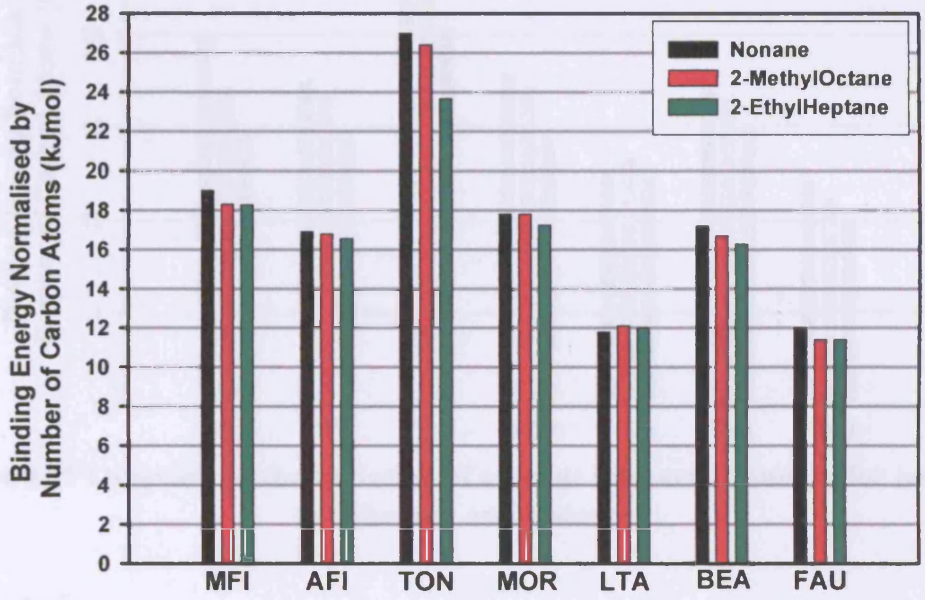

Figure 8.16 Overview of the variation of average interaction energy for branched and straight chain alkanes

8.9.2.3. Branched Six Carbon (C6) Compounds

A comparison between the average interaction energies of hexane, cyclohexane and benzene is shown in ***Figure 8.17***. In all cases, apart from LTA, higher normalised binding energy values (more favourable interaction) were observed for hexane followed by cyclohexane and finally benzene. This indicates that even though the number of carbon atoms is the same for all three compounds, the different hybridization and the presence of a ring have an effect on the value of binding energy.

However, as it was expected, different zeolites have different values of binding energy and therefore it can be suggested that different zeolites can discriminate some compounds better than others. For example, TON and MFI zeolites show large differences between the three C6 compounds compared to the other zeolites. All the tested aromatic

compounds are more strongly bound to TON zeolite followed by MFI, AFI, MOR, BEA and finally to LTA and FAU.

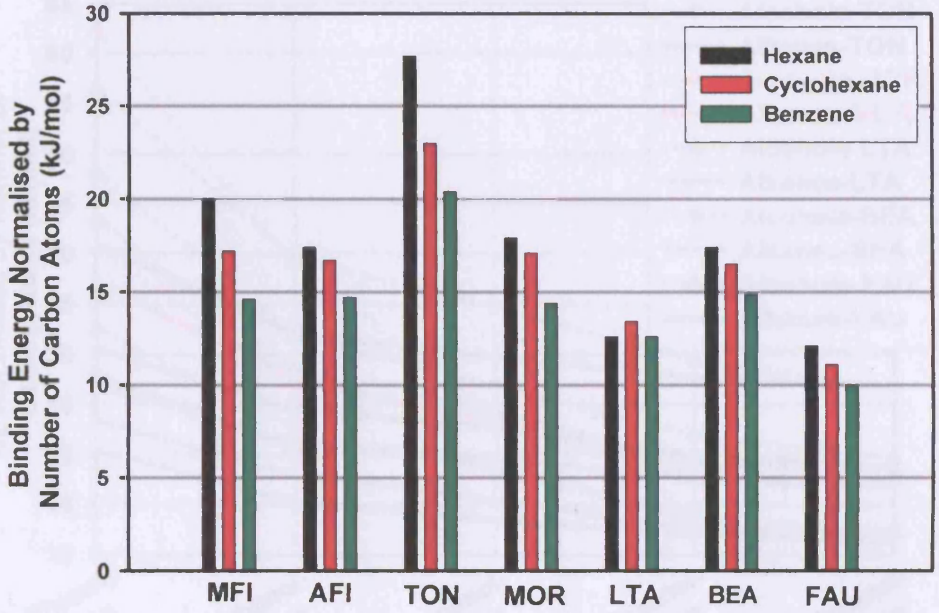

Figure 8.17 Overview of the variation of average interaction energy for hexane, cyclohexane and benzene

8.9.3 Alcohols

Figure 8.18 presents a comparison of the variation of the normalised binding energy of alcohols and n-alkanes against the number of carbon atoms. The pattern of interaction is very similar for both alcohols and alkanes i.e. the normalised binding energy becomes less favourable with increasing carbon chain. However, in all cases the alcohols are more strongly bound (i.e. have higher values of binding energy, stronger interaction) to the zeolite host structures compared to their corresponding same carbon number alkanes. The presence of the polar OH group in the alcohols results in more favourable interactions with the partly ionic zeolite framework.

It is interesting to note that a good discrimination can be observed between low (methanol, ethanol, propanol) and high (hexanol and dodecanol) carbon atom alcohols using any of the given zeolites. A better discrimination can be achieved using MOR and TON zeolites.

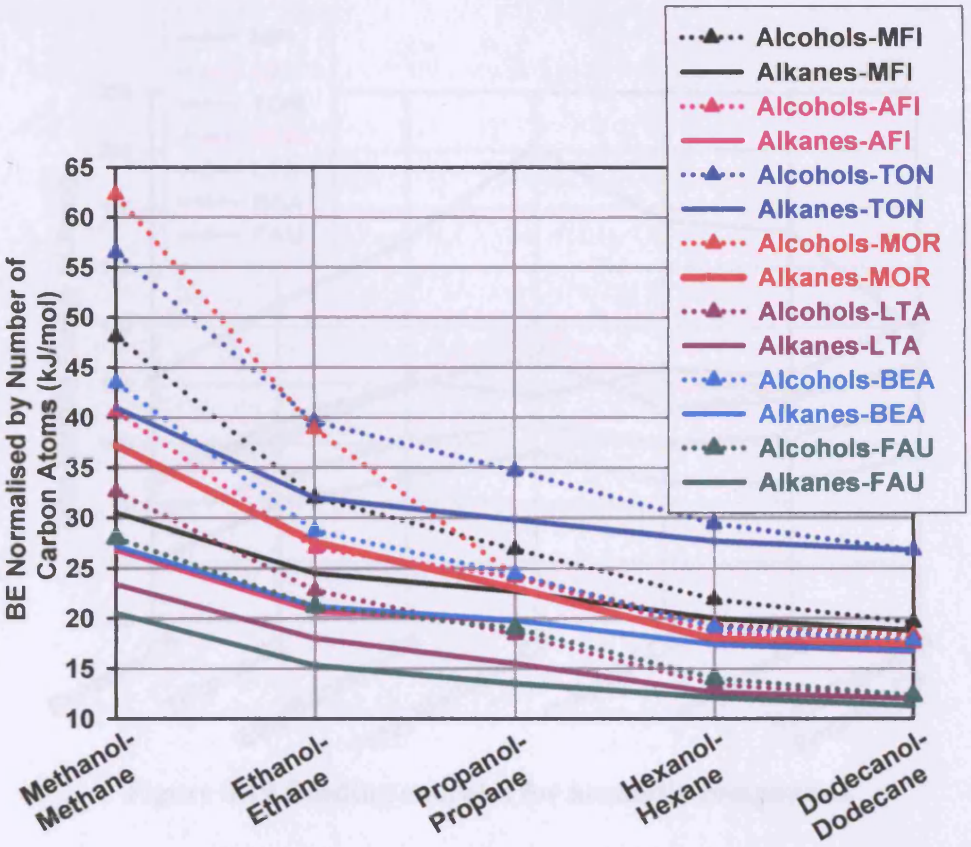

Figure 8.18 Overview of the variation of average interaction energy for alcohols and n-alkanes

8.9.4 Aromatic Compounds

Figure 8.19 is a representation of the variation of the binding energy of aromatic compounds in the seven zeolites against the number of carbon atoms. It can be seen that the binding energy becomes more favourable with increasing carbon chain, as in the case of n-alkanes. But, aromatic compounds are less strongly adsorbed on the tested zeolites compared to n-alkanes.

Figure 8.20 shows the variation of the average interaction energy of aromatic compounds in the seven zeolites against the number of carbon atoms. In general it can be said that there is little discrimination between the tested aromatics when only one zeolite is used. An exception is TON and MFI zeolites. The 1,3,5-trimethylbenzene can easily be discriminated from the remaining aromatics using TON zeolite. Similarly, using MFI zeolite, propylbenzene can be discriminated from the remaining aromatic compounds.

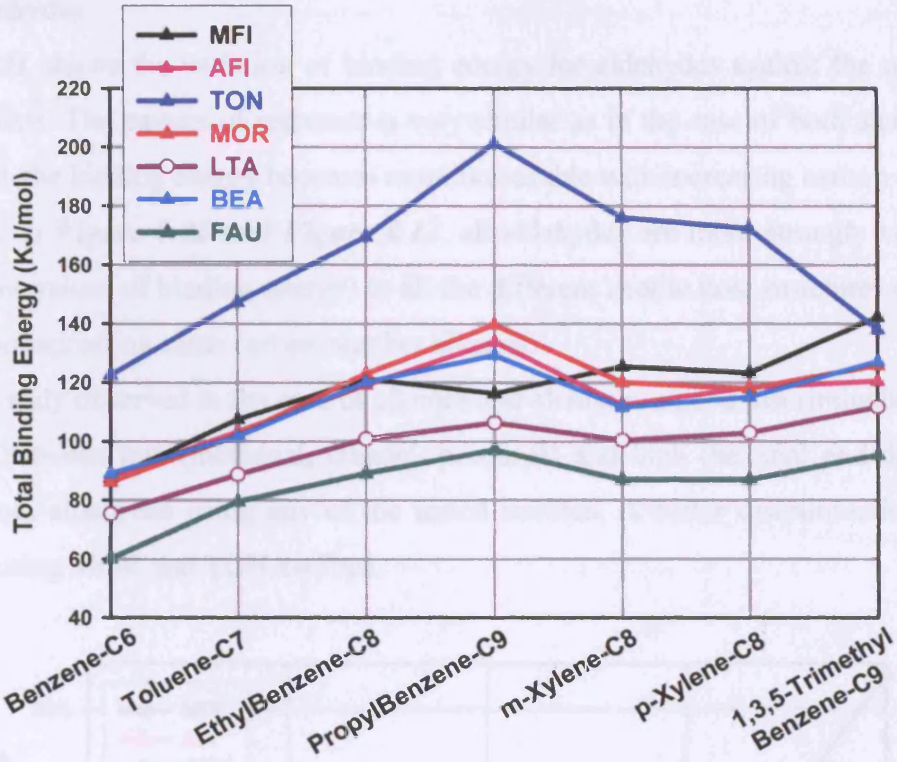

Figure 8.19 Binding energies for aromatic compounds

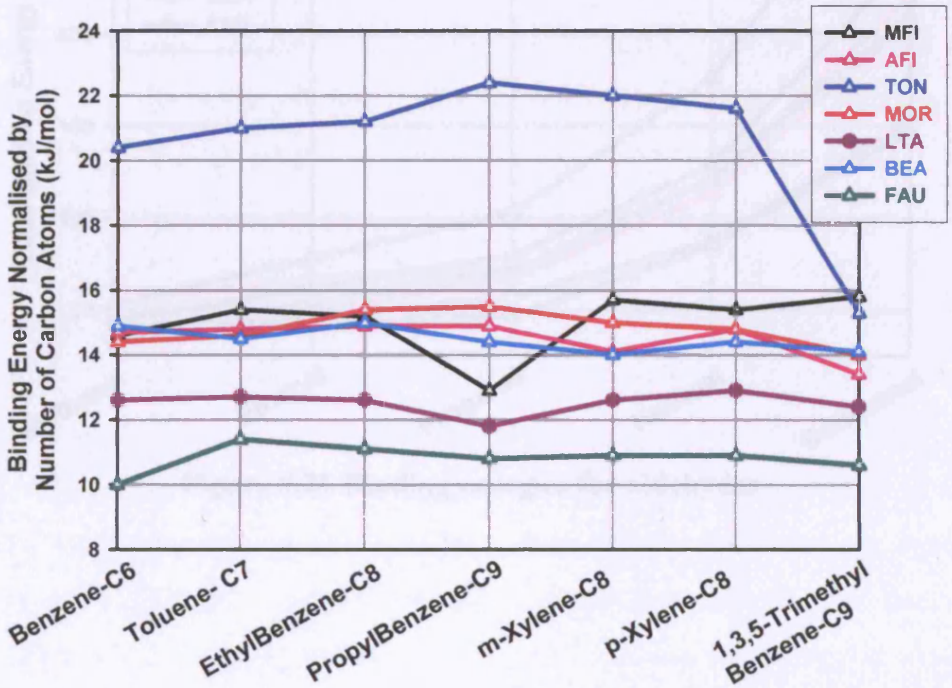

Figure 8.20 Average interaction energy for aromatic compounds

8.9.5 Aldehydes

Figure 8.21 shows the variation of binding energy for aldehydes against the number of carbon atoms. The pattern of response is very similar as in the case of both alcohols and alkanes i.e. the binding energy becomes more favourable with increasing carbon chain.

According to ***Figure 8.22 and Figure 8.12***, all aldehydes are more strongly bound (i.e. have higher values of binding energy) to all the different zeolite host structures compared to their corresponding same carbon number alkanes.

As was already observed in the case of alkanes and alcohols, a good discrimination can be observed between low (methanal, ethanal, propanal) and high (hexanal and dodecanal) carbon atom aldehydes using any of the tested zeolites. A better discrimination can be achieved using MOR and TON zeolites.

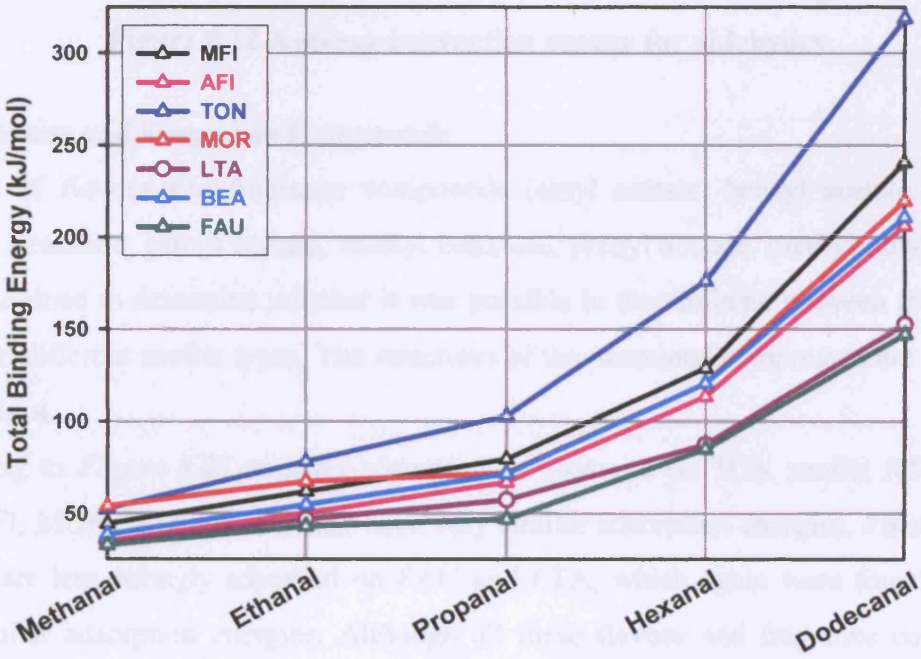

Figure 8.21 Binding energies for aldehydes

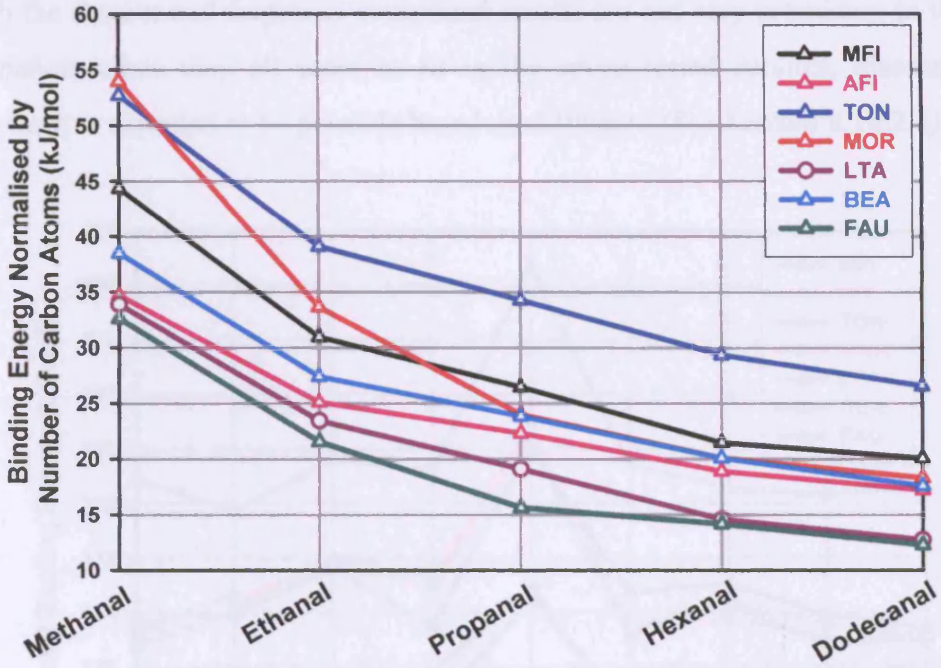

Figure 8.22 Average interaction energy for aldehydes

8.9.6 Flavour and Fragrance Compounds

A range of flavour and fragrance compounds (amyl acetate, benzyl acetate, linalool, cineole, farnesene, pentyl acetate, methyl benzoate, prenyl acetate, methyl butyl acetate) were examined to determine whether it was possible to discriminate between them using the seven different zeolite types. The structures of the examined compounds are shown in ***Appendix A***.

According to ***Figure 8.23*** stronger adsorption is observed on TON zeolite followed by MFI, AFI, MOR, BEA zeolites that have very similar adsorption energies. Finally, all n-alkanes are less strongly adsorbed on FAU and LTA, which again were found to have very similar adsorption energies. Although all these flavour and fragrance compounds have very different structures little discrimination was observed between them in terms of adsorption. An exception is farnesene, which is the most strongly bound compound from all the seven zeolites (i.e. have higher value of binding energy), and thus can be discriminated easily from the remaining compounds. Linalool can be well-discriminated from the other compounds using BEA zeolite. Furthermore, methyl benzoate can be well-discriminated using LTA zeolite since it cannot enter the small pore of LTA.

Although the flavour and fragrance compound results are not very promising in terms of discrimination, since they all seem to fit in the seven tested zeolites, discrimination between them is expected to be possible based on diffusion. ***(See Section* 8.10.2.5*)***

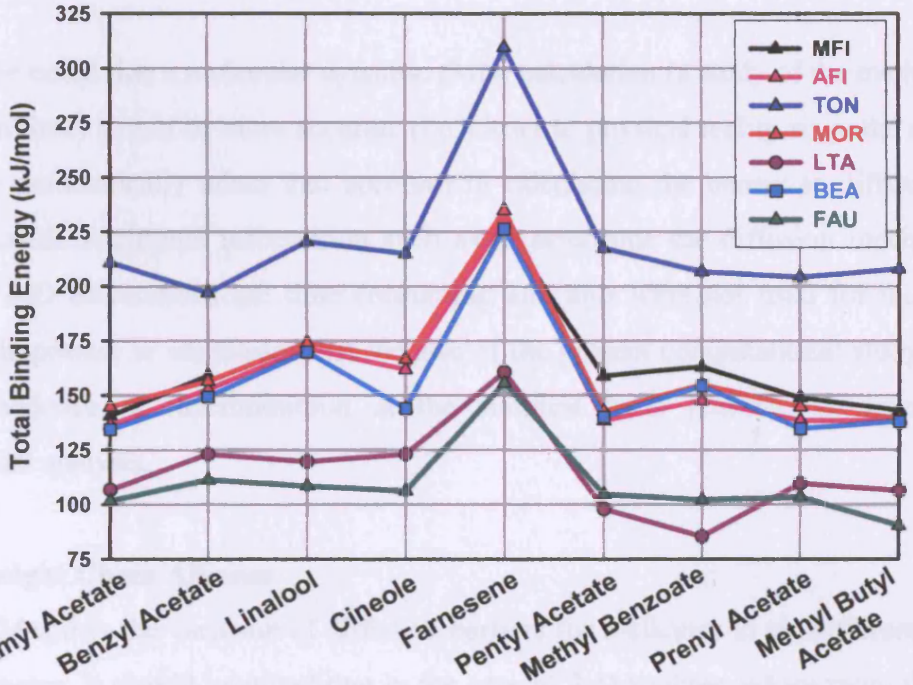

Figure 8.23 Binding energies for flavour and fragrance compounds

8.10 Diffusion Barrier Calculations

Diffusion calculations of selected molecules in different fixed host zeolite structures were performed in order to investigate the possible diffusion limitations imposed by zeolites for certain molecules.

The first step in conducting a diffusion barrier calculation was to carry out an energy minimization of the molecule of interest in a host zeolite structure. Details of the minimization process can be found in ***Section 8.6.3***. After the energy minimization, the molecule was manually moved along the channel with the cartesian position of one atom of a molecule (usually a hydrogen attached to the terminal carbon atom) fixed and then the molecule was energy minimized at each point. The difference between the maximum and the minimum potential energy was considered to correspond to the diffusion barrier of the molecule.

In general, it is expected that the greater the barrier to diffusion the slower the diffusion is. However, low diffusion barrier does not necessarily mean fast diffusion because the molecule might simply move about the pore, rather than being transported along the channel (as was found for CH_4 in AFI).

It should be noted that a molecular dynamic (MD) calculation (a study of the evolution of a system in time) would be more accurate (i.e. closer to physical reality since the entropic effects are automatically taken into account) in calculating the barrier to diffusion and able to provide additional information such as to determine the diffusion mechanisms. However, MD calculations are time consuming and thus were not used for this study. Here it is important to emphasise that the aim of the present computational study was to provide evidence of discrimination at the simplest level possible to support the experimental analysis.

8.10.1 Straight Chain Alkanes

Figure 8.24 shows the variation of diffusion barriers for n-alkanes in six different zeolite structural types. It should be noted that in the case of 3-D zeolites, where more than one channel is available for the guest molecule, the more stable case (i.e. the one with higher potential energy) was chosen for the diffusion barrier calculations.
Since MOR has a 1-D channel with side pockets (8 member ring) that can be entered from the main channel (12MR), the diffusion barrier can be considered to be the result of the difference in the total surface energy between the straight and the site pocket channel.

Figure 8.24 shows that n-alkanes diffuse in a similar manner in TON, AFI, MFI and BEA. It is important to note the wide variation in diffusion barrier for a range of n-alkanes in LTA and MOR. They both have higher diffusion barrier values compared to the other zeolites and different patterns of response. Thus, they can be characterised as good zeolite candidates to be used in conjunction with any of the other four zeolites, to discriminate between n-alkanes based on diffusion. In the case of MOR, it was found that the barrier to diffusion increases with increasing the number of carbon atoms from heptane to dodecane.
Although methane, ethane, propane and butane were found to interact more strongly with MOR compared to the remaining n-alkanes ***(See Figure 8.12)***, the lower diffusion barrier

observed for these molecules ***(See Figure 8.24)*** suggests that they will diffuse faster in MOR. However, butane being larger (i.e. similar in size to the channel) than the other molecules (methane, ethane and propane) it was found to have a lower diffusion barrier (faster diffusion).

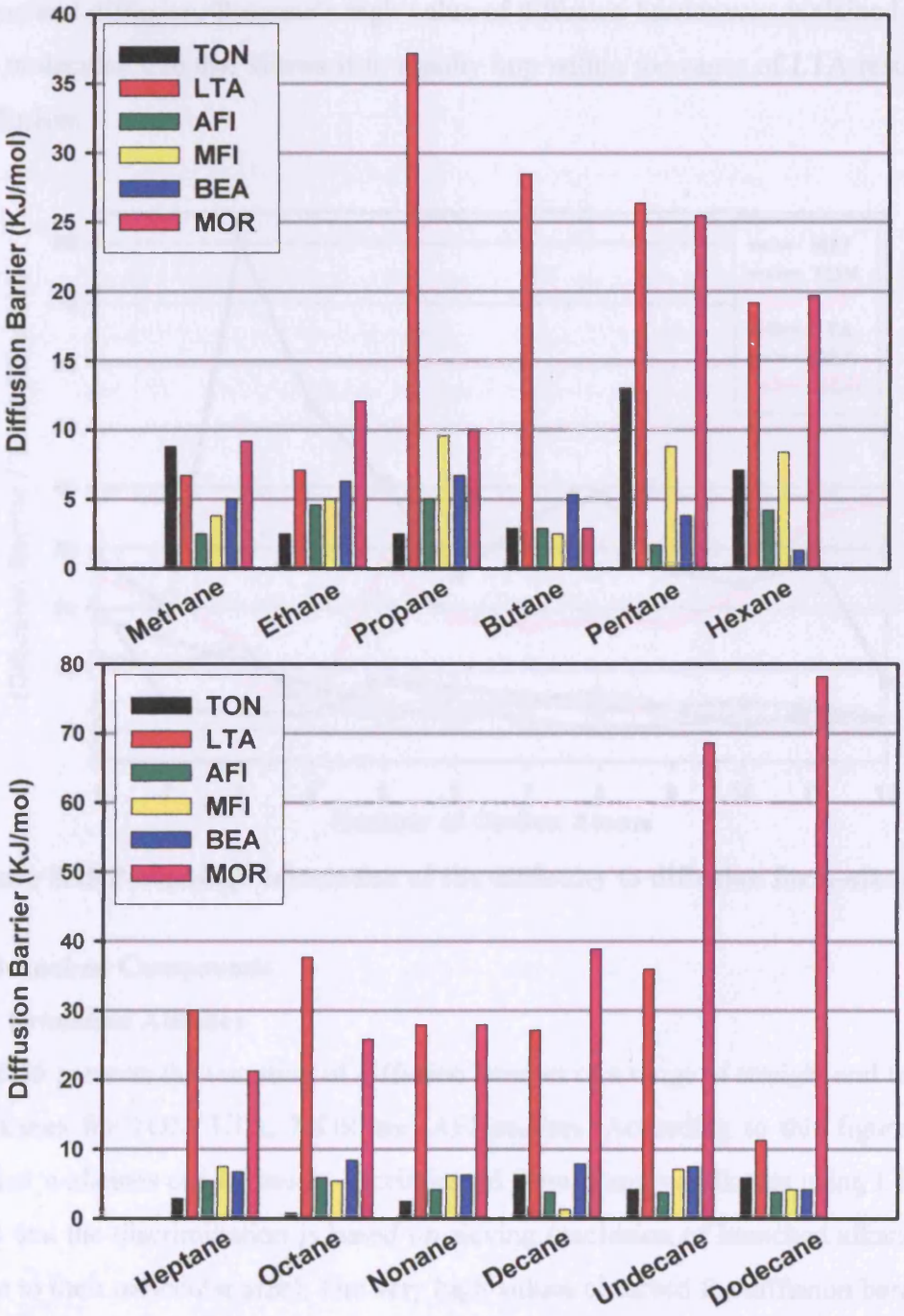

Figure 8.24 Diffusion barriers for n-alkanes

Figure 8.25 gives a 'measure of the probability to diffusion' for a range of n-alkanes. Here, the diffusion barrier value was divided by the total binding energy for a given molecule in a given zeolite. As discussed earlier, MOR and LTA were found to interact differently with the different alkanes and thus they can better discriminate between them, compared to other zeolites. It was suggested that the discrimination observed is based on adsorption and diffusion. Propane's high value of diffusion barrier was explained to arise from its molecular size that allows it to rapidly hop within the cages of LTA resulting in slow diffusion.

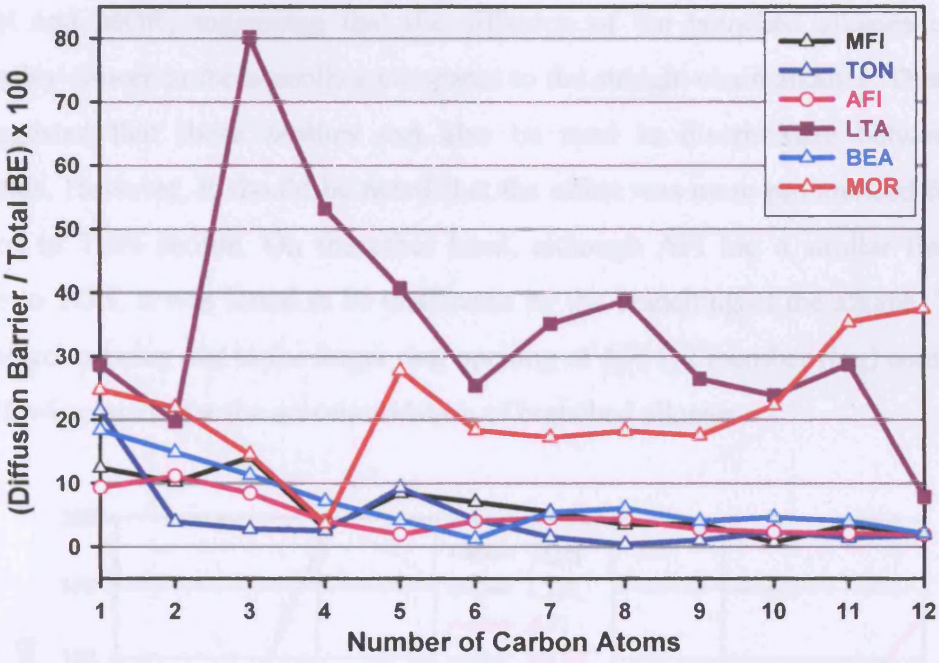

Figure 8.25 Percentage calculation of the difficulty to diffusion for n-alkanes

8.10.2 Branched Compounds

8.10.2.1 Branched Alkanes

Figure 8.26 presents the variation of diffusion barriers of a range of straight and branched chain alkanes for TON, LTA, MOR and AFI zeolites. According to this figure it was shown that n-alkanes can be easily discriminated from branched alkanes using LTA. It is believed that the discrimination is based on sieving (exclusion of branched alkanes from LTA due to their molecular size). The very high values observed for diffusion barriers for all branched alkanes suggest that they will not diffuse in the LTA zeolite (indeed they cannot even enter in the structure). This was also demonstrated in the literature,[20] where LTA was found to selectively exclude branched alkanes from entering the pore.

Figure 8.27 proposes an experiment (i.e. using gas chromatography) that can be used to discriminate straight and branched chain alkanes based on the results shown in ***Figure 8.26.*** If a mixture of 50% branched and 50% straight chain alkanes is passed over LTA, TON and AFI zeolites, discrimination between these alkanes will be observed based on diffusional constraints caused by the different framework structures of these zeolites.

Therefore, in the case of LTA, the branched alkanes will not enter this zeolite due to sieving control and thus, a 50% reduction in the signal will be observed. Moreover, smaller alkanes will diffuse faster than larger ones.

In the case of TON and AFI zeolites both branched and straight chain alkanes will enter the pores. Although both zeolites have 1-D structures, TON has a smaller pore compared to AFI and therefore a diffusional restriction is expected only for this zeolite. This will result in a faster diffusion of straight chain alkanes compared to the branched in AFI opposed to TON zeolite.

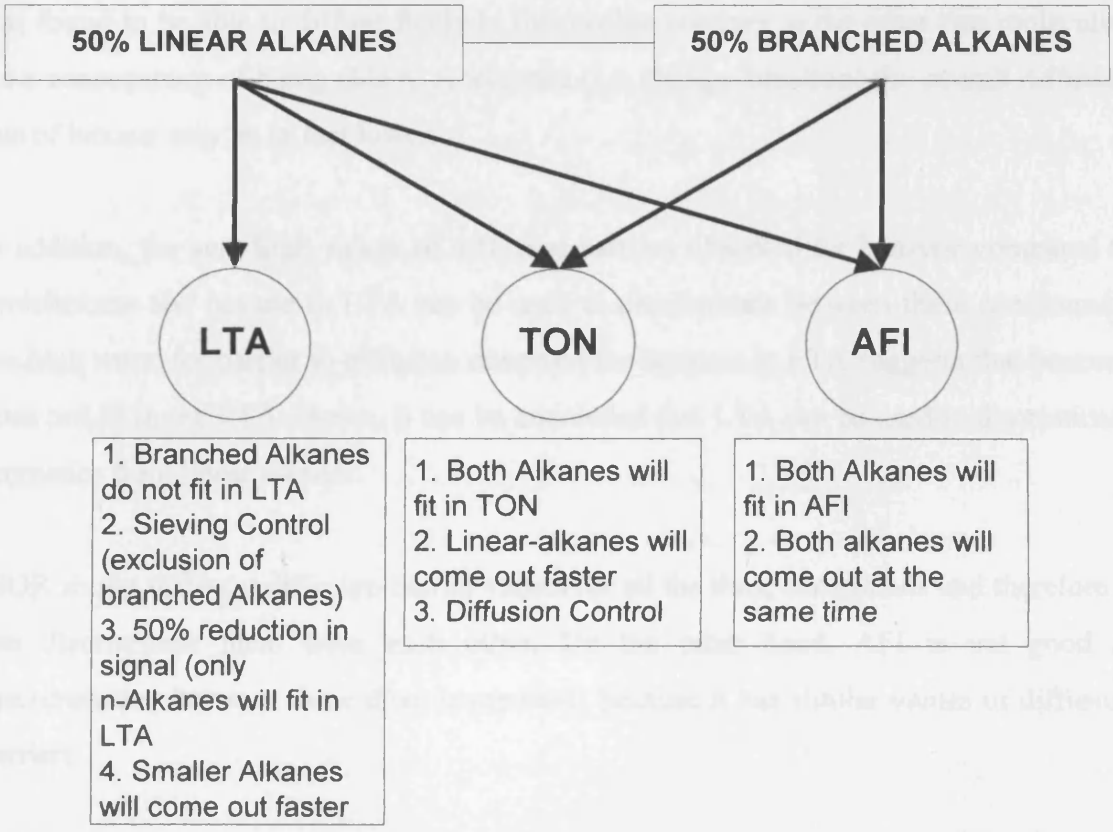

Figure 8.27 An experiment to separate n-alkanes and branched alkanes

8.10.2.2 Branched Six Carbon (C6) Compounds

Figure 8.28 presents the variation of diffusion barriers for six carbon atom containing compounds (hexane, cyclohexane, benzene) with a varying degree of branching. Based on ***Figure 8.28*** it can be emphasised that certain zeolites are best at discriminating different compounds. In particular, MFI, TON and BEA can be used to discriminate cyclohexane from hexane and benzene. A better discrimination between the tested compounds can be obtained using MFI zeolite, followed by TON and finally BEA.

Whilst cyclohexane and benzene molecules have sizes comparable to the pore size of MFI, the diffusion of these tight fitting molecules is expected to be fairly 'controlled' as the molecules may not be able to diffuse through all the pores and may have to re-orientate to do so. Since benzene is a rigid and planar molecule it may have to flip 90^{o} or spin in order to diffuse through the pore whilst the cyclohexane may have to change conformation. Hence, the lower value of diffusion barrier for benzene compared to cyclohexane suggested that benzene diffuses faster than cyclohexane. Since hexane is a lot smaller in size than benzene and cyclohexane as well as the pore of MFI, the molecule was found to be able to diffuse freely in this zeolite contrary to the other two molecules. As a consequence of being able to reorientate (i.e. change direction) the overall diffusion rate of hexane may be in fact lower.

In addition, the very high values of diffusion barriers observed for benzene compared to cyclohexane and hexane in LTA can be used to discriminate between these compounds; the high value for barrier to diffusion observed for benzene in LTA suggests that benzene does not fit in the LTA. Hence, it can be concluded that LTA can be used to discriminate aromatics from linear alkanes.

MOR shows different diffusion barrier values for all the three compounds and therefore it can discriminate them from each other. On the other hand, AFI is not good at discriminating between these three compounds because it has similar values of diffusion barriers.

8.10.2.4 Aromatic Compounds

Figure 8.31 shows the variation of diffusion barriers for some substituted aromatic compounds (benzene, propylbenzene, mesitylene (1,2,3-trimethylbenzene), p-xylene and m-xylene). The aim here was to assess how branching would lead to improved discrimination especially since many flavour and fragrance compounds, that are of interest to this project have branches.

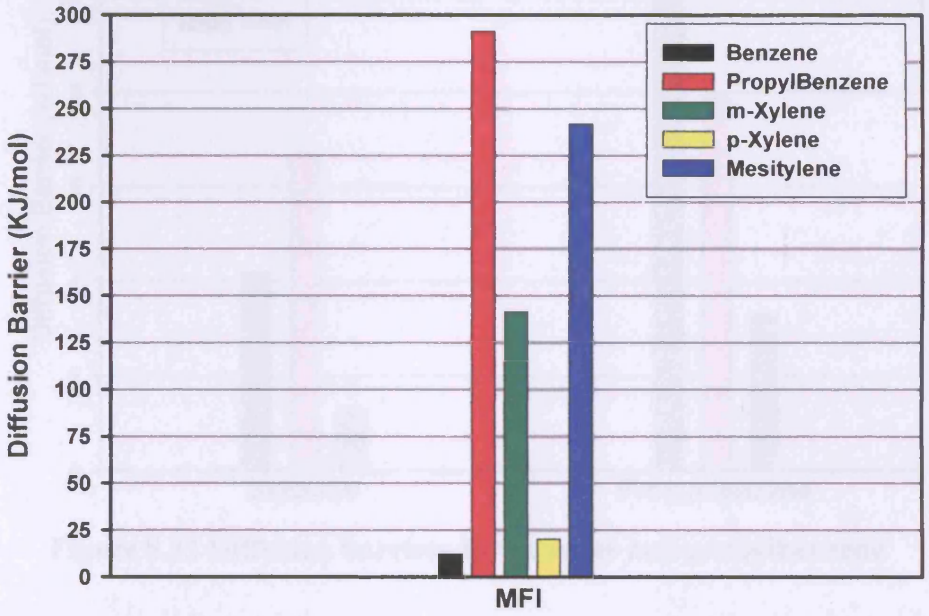

Figure 8.31 Diffusion barriers for aromatic compounds in MFI

MFI zeolite was chosen in favour of the remaining zeolites since it was expected to show a good discrimination between the chosen compounds. Moreover, ***Figure 8.31*** makes it clear that p-xylene and benzene can be well discriminated from the remaining substiututed benzenes. It is important to note that due to different values of diffusion barriers, it is possible to discriminate (based on diffusion constraints) propylbenzene, mesitylene and m-xylene. Propylbenzene diffuses slower in MFI followed by mesitylene, m-xylene, p-xylene and finally benzene. What is also interesting is the big difference in diffusion speed between m-xylene and p-xylene. P-xylene (1,4-dimethylbenzene) having the two methyl groups in para positions to each other, diffuses faster than m-xylene (1,3-dimethylbenzene) which has the two methyl groups in meta position to each other.

Figure 8.32 is an overview of the differences in diffusion barriers for benzene and propyl benzene in TON, AFI and BEA. It can be said that all compounds can be discriminated

adsorption energies of FAU (zeolite Y), MFI (zeolite ZSM-5) and BEA (zeolite β) were also found to be relatively close in magnitude.

Figure 7.24 gives an overview of the response of layered zeolite sensors to alcohols and alkanes. The low sensitivity of the different sensors to alcohols (resulting from complete combustion on the zeolite surface) along with the high sensitivity to alkanes demonstrate a good discrimination between these two compounds. Similarly, ***Figure 8.18*** shows that a good discrimination was observed between alcohols and alkanes due to more favourable interaction of alcohols with the zeolites.

Furthermore, ***Figure 7.18*** gives an overview of the response of layered zeolite sensors to aromatic compounds. The very high response to benzene relative to substituted benzenes suggests that a good discrimination is possible between these compounds. Similarly, ***Figures 8.19 and 8.32*** demonstrate that benzene can be well discriminated from substituted benzenes based on adsorption and diffusion within the different zeolite structures.

Generally, the results obtained through the computational and experimental studies undertaken in this project show the desirable correlation between them. Thus, it is suggested that the similar computational predictions could be used as a testing bed to further investigate other primising zeolites for a wide range of sensor applications.

8.12 Conclusion

Seven different zeolite structural types were used to perform computer simulations to predict the interactions between zeolites and various target compounds so as to enable suitable zeolite types to be identified as good candidates for the construction of new sensors. The results of the computational study proved that similar computational predictions could be used to propose new zeolite materials for sensor applications.

The results obtained proved the ability of this computational study to assess which compounds can enter into different zeolite structures. For those that can enter the pores, the binding energy and position in the zeolite cavity were determined.

In addition, barrier to diffusion values for various target compounds and zeolite structures were calculated. The results obtained showed that different sorbate compounds interact with their zeolite hosts in different ways (due to the nature of the host zeolite structures) and that different zeolites can be used to discriminate different compounds based on adsorption and diffusion.

In more detail, the computational study showed that some zeolites are more interesting than others in terms of discriminating different compounds. For example, TON, LTA and MOR can be said to be more ideal for introducing the required variance in response pattern across an array of sensors.

It can also be added that a combination of this study with the experimental results on sensors could help in the better understanding of sensor responses. Indeed, excellent correlation was found between the computational predictions and the observations made on the performance of the zeolite sensors ***(Chapter 7)***.

Finally, this computational study demonstrates the potential to develop a database where one could manually select a particular zeolite capable to either exclude completely one compound or provide a slow diffusion in order to discriminate between target compounds. This could be advantageous since the process of selecting appropriate zeolites for specific applications could be performed in minimum time with less cost and the sensor development time could be minimised significantly.

Chapter 8

References

1. http://www.accelrys.com

2. C. M. Freeman, C. R. A. Catlow and J. M. Thomas and S. Brode, *Chem. Phys. Lett.*, 1991, **186**(2), 137.

3. G. Sastre, N. Raj, C. R. A. Catlow, R. RoqueMalherbe and A. Corma, *J. Phys. Chem. B.*, 1998, **102**, 3198.

4. C. R. A. Catlow, R. A. Van Santen and B. Smith, in *Computer Modelling of Microporous Materials*, ed. Elsevier Academic Press., London, 2004.

5. T. J. H. Vlugt, R. Krishna and B. Smit, *J. Phys. Chem. B.*, 1999, **103**, 1102.

6. D. W. Lewis, C. M. Freeman and C. R. A. Catlow, *J. Phys. Chem.*, 1995, **99**, 11194.

7. D. W. Lewis, D. J. Willock, C. R. A. Catlow, J. M. Thomas and G. J. Hutchings, *Nature.*, **1996**, *382*, 604.

8. D. W. Lewis, G. Sankar, J. Wyles, J. M. Thomas, C. R. A. Catlow and D. J. Willock, *Angew. Chemie.*, 1997, **36**, 2675.

9. R. E. Boyett, A. P. Stevens, M. G. Ford and P. A. Cox, *Zeolites.*, 1996, **17**, 508.

10. A. P. Stevens, A, M. Gorman, C. M. Freeman and P. A. Cox, *J. Chem. Soc., Fraday Trans.*, 1996, **92**, 2065.

11. R. G. Bell, D.W. Lewis, P. Voigt, C. M. Freeman, J. M. Thomas and C. R. A. Catlow, *Stud. Surf. Sci. Catal.*, 1994, **84**, 2075.

12. C. M. Freeman, D. W. Lewis, T.V. Harris, A.K. Cheetham, N.J. Henson. P.A. Cox, A. M. Gorman, S. M. Levine, J. M. Newsam, E. Hernandez and C. R. A. Catlow, in *Computer-aided Molecular Design, ACS Symposium Series,* ed. C. H. Reynolds, M. K. Holloway and H. K. Cox., 589: 326-340, 1995.

13. G. H. Grant and W. G. Richards, in *Computational Chemistry*, ed. OUP., 1998.

14. www.materials-studio.com

15. D. C. Young, in *Computational Chemistry, A Practical Guide for Applying Techniques to Real –World Problems*, ed. John Wiley & Sons, Inc., New York, 2001.

16. http://www.msi.com

17. P. Ren and J. R. Fried, *Comp. and Theor. Polymer Science.*, 1998, **8**(1), 229.

18. Yashonath and P. Santikary, *J. Phys. Chem.*, 1994, **98**, 6368.

19. Yashonath and P. Santikary, *J. Phys. Chem.*, 1994, **98**, 9252.

20. Bruce C. Gates, in *Catalytic Chemistry*, ed. John Wiley and Sons, Inc., New York, 1992.

Chapter 9

Conclusions

9.1 Fabrication of Gas Sensors

Sensors were successfully fabricated using chromium titanium oxide (CTO) as a suitable gas-sensing material, with additional shape and size selective catalysts afforded by zeolites (ZSM-5, β and Y) either printed over the top of the sensing layer (layered microstructure) or admixed with it (mixed microstructure). Additional sensors were produced where the three different zeolite types were catalytically modified (ion exchanged) by the controlled addition of chromium catalysts to promote selective catalytic activity. It must be noted that multiple electrode SEMDEC substrates were used for all fabricated sensor devices as these allow discrimination of gases on the basis of their reactivity with the catalyst material.

9.2 Experimental Study of Sensors in the Presence of Ethanol and Carbon Monoxide

The behaviour of layered and mixed sensors prepared using three different zeolite types and a standard CTO sensor (no zeolite) to the presence of different concentrations of carbon monoxide and ethanol was evaluated using a custom built testing rig.

The results clearly suggested that the addition of zeolites over the top of the CTO sensing material or admixed with it, drastically change the sensor behaviour.

It should be emphasised that due to the complexity of the devices, a number of parameters was found to influence the sensor behaviour. These involve changes in the microstructure of the sensing material as well as effects due to differences in the reaction and diffusion rate of the target gases and its reaction products within the sensing material.

It must be emphasised that the type of zeolite used was also shown to affect the behaviour of such devices for a particular gas since different zeolite structures show different shape and size as well as diffusional limitations for various gases.

9.2.1 Ethanol Experiments

In the presence of ethanol different values for the response exponent (β) were observed for the mixed zeolite sensors compared to the layered and CTO sensors, illustrating the different microstructure of the mixed sensors. In more detail, it was found that the addition of zeolites to the CTO sensing-material caused an increase in the effective porosity of the CTO material.

Moreover, differences in the sensitivities (A_g) were observed for the different sensors (mixed, layered, CTO) in the presence of ethanol. Differences in A_g indicate variations in the sensitivities of the sensors resulting from changes of the microstructure and differences in the decomposition and diffusion of the gas within the sensing material. Lower values of A_g were observed for the mixed sensors followed by the layered and finally by the CTO sensors suggesting that ethanol burns on the mixed sensors at a relatively higher rate. This result was consistent with the concentration gradient results (ratio of response on a large electrode gap to that on a small electrode gap), which demonstrated that the mixed sensors have the highest gradients. This was expected as the concentration gradient of mixed sensors is directly affected by the zeolite since the gas is reacting with the zeolite as it passes through the sensing material.

In more detail, the mixed sensors have a shorter residence time for reaction products before they are detected, resulting in the observed different behaviour of small and large electrode gaps since these probe different parts of the reaction layer. This is in contrast with the layered and standard CTO sensors where only the CTO sensing material is probed.

Therefore, it can be said that the observed smaller concentration gradient of layered sensors is due to the interaction of the gas solely with the CTO sensing material. However, it must be noted that the composition of the gas at the sensing layer may be different since it has previously passed through the zeolite layer.

9.2.2 Carbon Monoxide Experiments

It is important to note the inverse concentration gradient (i.e. <1) observed for all zeolite devices in the presence of carbon monoxide. This effect has also been demonstrated by other researchers and it was found to be due to the interaction of the metal oxide layer with electrodes. Furthermore, very similar values of concentration gradients were observed for all zeolite sensors in the presence of CO, suggesting that there is no reaction between this gas and the sensors.

The different microstructures of the mixed compared to layered sensors, along with the wide variability in concentration gradients of ethanol and carbon monoxide gases demonstrated the ability of the new CTO-zeolite sensors to show good discrimination between the two gases. This discrimination was shown to be better than that obtained with a standard CTO sensor indicating a significant advance in selectivity enhancement for metal oxide based sensors.

9.3 Experimental Study of Sensors in the Presence of VOC and Flavour Compounds Using a Newly Developed Testing Rig

Subsequently, experiments were performed with a number of volatile organic (VOC), flavour and fragrance compounds using a newly developed testing rig.

Initially, a range of standard CTO sensors (made using a sol-gel method, a conventional ceramic preparation and ammonium dichromate method), having different microstructures, were tested to determine the performance of the specific sensors and to compare their behaviour with that of the newly developed layered zeolite-CTO sensors.

It was demonstrated that different sensors showed better discrimination between the tested compounds than others and this was explained to be due to the different microstructures of the sensors and/or the addition of different catalysts over the sensing material (i.e. addition of different zeolite types and addition of chromium oxide).

Since the zeolite-CTO sensors were proved to provide the desirable increased discrimination when compared to standard CTO sensors (prepared with the same method) it was decided to further investigate their behaviour using a wider range of compounds.

9.4 Experimental Study of Sensors in the Presence of VOC, Flavour and Fragrance Compounds Using a Commercially Available Electronic Nose

Following the interesting experimental results, all zeolite-CTO sensors (layered and mixed) and a standard CTO sensor were incorporated into a commercial electronic nose and tested in the presence of a range of volatile organic (hydrocarbons, alcohols, esters, aromatics), flavour and fragrance compounds.

The shape and size selectivity of the zeolite sensors was demonstrated by their ability to discriminate a wide range of organic species of different molecular size and shape.

Furthermore, improvements in the discrimination of target analytes (VOC and flavour compounds) were indicated compared to the standard CTO sensor.

Finally, three chromium modified sensors (of different zeolite types) were tested in the electronic nose in the presence of the same compounds. The results suggested that the modification of the zeolites with chromium increased the catalytic activity of the sensors in a controlled way by selectively cracking longer species into smaller ones without resulting in complete conversion to carbon monoxide, carbon dioxide, hydrogen and water. This resulted in different patterns of response for different compounds and thus an enhancement in the discrimination ability of the array of sensors.

Further investigation of different parameters, which affect the behaviour of sensors in a well-defined way (i.e. changes in the chromium loading of the zeolites, the thickness of the zeolite layer, the fabrication of the sensors and the sensor operating temperature) was performed. The results demonstrated the possibilities for further improvements in the discrimination between the different tested compounds for the different sensor arrays.

9.5 An Overview of the Experimental Results and Analysis

Following the thorough experimental analysis of the tested sensors in the presence of a wide range of volatile organic and flavour compounds it was demonstrated that the different zeolite sensors (layered, mixed, Cr-modified) were shown to be as good, and in some cases better in terms of discrimination than a larger array of standard CTO sensors prepared in the same way.

An overview of the experimental results obtained through this research work clearly indicates that a careful selection of a set of gas sensors (i.e. a standard CTO sensor and at least one zeolite sensor) could provide different patterns of response and therefore delivers a multi-sensor array, for electronic nose applications, with small number of sensors and a sufficiently large variance in the response for reliable and repeatable discrimination of gases.

An advantage of this gas-sensing array is that the gas sensors are made of the same sensing material and hence may operate at the same, or similar, temperatures, hence producing signals of similar magnitudes, with the desirable consequence that the

performance of the array is not dominated by a single sensor and also any long term drift or degradation of the sensors is likely to be similar and hence simpler to detect and/or compensate for.

According to the experimental results it is suggested that the newly developed sensors are capable to replace problematic large arrays of sensors used in complex electronic nose applications.

9.6 Computational Results

Computational simulations of the interactions of a range of volatile organic, flavour and fragrance compounds with different zeolites were performed using a commercially available software package to select promising zeolite catalyst materials for the construction of new sensors. The computational study identified a number of favourable zeolite types (such as TON, LTA and MOR), which can be added to those already studied as potential selectivity modifiers. These zeolites were shown to provide good discrimination between the target analytes.

Finally, the computational results were compared with the experimental and were shown to be well correlated, demonstrating the potential of similar computations to be used as a selection tool for potential zeolite materials in sensing technology.

9.7 Suggestions for Future Work

Following the experimental analysis demonstrating that different microporous solids (zeolites) added to CTO sensing material can generate characteristic behaviour for specific analytes, the primary suggestion for future work is a further experimental investigation of other suitable zeolite structures such as the mesoporous MCM-41 and ZSM-22 and the zeolites types proposed through the computational study.

Furthermore, it is suggested to examine the use of other metals (such as molybdenum and tunsten) for chemical modification of the zeolite cavities as well as different metal loadings to change the catalytic behaviour and cracking patterns of the sensors.

A further experimental investigation of the variations in the thickness of the sensing and zeolite layers as well as operating the sensor at a multiplicity of temperatures could also lead to important findings such as additional variance and hence discrimination.

APPENDIX B

References

1. H. Hotelling, *J. Educ. Phychol.*, 1993, **24**,417,498.

2. J. Edward Jackson, in *A User's Guide to Principal Components*, ed. John Wiley and Sons, INC., New York, 1991.

3. T. W. Anderson, in *An Introduction to Multivariate Analysis*, ed. John Wiley and Sons, Inc., New York, 1984.

4. M. S. Aldenderfer and R. K. Blashfield, in *Cluster Analysis*, ed. Sage Publications, Inc., Beverly Hills, Calif, 1984.